COMPARATIVE ANALYSIS OF OXYGEN TRANSFER IN FULL LIFT AND
DOWNFLOW BUBBLE CONTACT HYPOLIMNETIC AERATORS

By

KENNETH IAN ASHLEY

B.Sc. The University of British Columbia, 1976
M.Sc. The University of British Columbia, 1981
M.A.Sc. The University of British Columbia, 1989

A THESIS SUBMITTED IN PARTIAL FULFILLMENT OF

THE REQUIREMENTS FOR THE DEGREE OF

DOCTOR OF PHILOSOPHY

in

THE FACULTY OF GRADUATE STUDIES

(Department of Civil Engineering)

We accept this thesis as conforming
to the required standard

THE UNIVERSITY OF BRITISH COLUMBIA

March, 2002

ABSTRACT

This research conducted a detailed analysis of design factors influencing the oxygen transfer capabilities of two types of hypolimnetic aerators: full lift and Speece Cone, utilising non steady-state gas transfer methodology in a laboratory scale system. Full lift hypolimnetic aerators use the airlift pump principle to circulate water from the hypolimnion to the surface and return oxygenated water to the hypolimnion. Speece Cones use the Downflow Bubble Contact Aeration (DBCA) principle to oxygenate hypolimnetic water at depth using mechanical pumps to circulate water through the aeration chamber. Four standard units of measure were used to quantify oxygen transfer: (a) K_La_{20} (hr^{-1}), the oxygen transfer coefficient at 20 ^{o}C; (b) SOTR (g $O_2 hr^{-1}$), the Standard Oxygen Transfer Rate; (c) SAE (g $O_2 kWhr^{-1}$), the Standard Aeration Efficiency and (d) SOTE (%), the Standard Oxygen Transfer Efficiency. The design factors examined in the full lift experiments were: the effect of diffuser orifice pore diameter (140 μ, 400 μ and 800 μ), diffuser submergence (1.5 and 2.9 m), gas flow rate (10, 20, 30 and 40 l min^{-1}), oxygen partial pressure (air and Pressure Swing Adsorption generated oxygen) and four *in situ* modifications (floating surface cover in the separator box, mid-depth inlet tube bubble screens, counter-rotating blades and DBCA) in the outlet tube. In the full lift experiments, diffuser submergence positively influenced K_La_{20}, SOTR, SAE and SOTE and water velocity. Higher gas flow rates increased water velocity, K_La_{20} and SOTR but decreased SAE and SOTE. Oxygen partial pressure treatment exerted a significant positive effect on K_La_{20}, SOTR and SOTE, whereas SAE response decreased on PSA oxygen. Smaller orifice diameters exerted a significant positive effect on K_La_{20}, SOTR, SAE and SOTE. The *in situ* modifications exerted a significant negative effect on K_La_{20}, SOTR, SAE and SOTE. The DBCA treatment generated the smallest bubble sizes. The design factors examined in the Speece Cone experiments were

the effect of oxygen flow rate (1, 2 and 3 l min^{-1}) and outlet port discharge water velocity (20, 30, 40, 50, 60 and 70 cm sec^{-1}) on K_La_{20}, SOTR, SAE and SOTE. The inlet water velocity was insufficient to create an efficient gas transfer environment in the Speece Cone experiments. Oxygen flow rate and discharge velocity treatments exerted a significant positive effect on K_La_{20} and SOTR. SAE increased with oxygen flow rates but discharge velocity had no effect on SAE. SOTE increased with water discharge velocity but responded negatively to increasing oxygen flow, suggesting that oxygen flow rates > 1 l min^{-1} were not being fully dissolved inside the Speece Cone. A precipitous decline in SOTE at low oxygen flow rates and discharge velocities > 50 cm sec^{-1} was due to a destabilisation of the bubble swarm in the Speece Cone. The Speece Cone, at oxygen flow rates between 1 and 3 l min^{-1}, delivered K_La_{20} and SOTR performance comparable to the full lift system at 10 l min^{-1} on oxygen, and outstanding SOTE performance. The DBCA counter-current flow principle of the Speece Cone provides a superior gas transfer environment to the full lift design by positively influencing the fundamental aspects of gas transfer (i.e., a, K_L and C_i-C_L). The efficiency of the Pressure Swing Adsorption (PSA) generating units increases with unit capacity, as smaller PSA units are not designed solely for optimum oxygen recovery efficiency; improvements in SAE could be achieved by using lower pressure PSA generators. The relative magnitude of the effects from this study should be transferable to full-scale application, within reasonable limits. Further lab testing, comparative field studies, development of predictive models, reporting in engineering journals and case study reviews of specific installations will assist in resolving the engineering aspects of system selection. The Speece Cone and PSA oxygen generating systems represent the most significant advances in hypolimnetic aeration since their inception over half a century ago. Civil engineers should consider hypolimnetic aeration as a proven technique, which can significantly improve raw

water quality, and serve as an integral component of an overall watershed management program.

TABLE OF CONTENTS

LIST OF TABLES

LIST OF FIGURES

xx

NOMENCLATURE

A   Interfacial or absorbing surface area of air (m^2)

AE   Field Aeration Efficiency (g O_2 kWhr^{-1})

ASCE   American Society of Civil Engineers

A/V   a = the interfacial surface area of the air through which diffusion can occur generated by the particular aeration system per unit volume of water (m^2 m^{-3})

BOD   Biochemical Oxygen Demand (mg l^{-1})

BP   Barometric pressure (mm Hg)

BS   Bubble screen treatment (Group 9 and 10)

C_1 Dissolved oxygen concentration at time t_1 (mg l^{-1})

C_2 Dissolved oxygen concentration at time t_2 (mg l^{-1})

C_i Saturation value of dissolved oxygen at the interface between liquid and air bubble (mg l^{-1})

C_L Average concentration of dissolved oxygen in the bulk liquid (mg l^{-1})

C_m^* Measured dissolved oxygen air-solubility value (mg l^{-1}) for the ambient barometric pressure, temperature and vapor pressure of water

C_s^* Dissolved oxygen air-solubility value (mg l^{-1}) for the ambient barometric pressure, temperature and vapor pressure of water

$C_s^*_{760}$ Dissolved oxygen air-solubility value (mg l^{-1}) for the barometric pressure equal to 760.0 mm Hg and ambient temperature

CEME   Civil Engineering-Mechanical Engineering, UBC

CRB   Counter-rotating blades treatment (Group 13 and 14)

CSV   Comma Separated Variable format for data transmission/storage

d_b Mean bubble diameter

D_L Diffusion coefficient for oxygen (m^2 hr^{-1})

DBCA	Downflow Bubble Contact Aeration
DOBI	Deep Oxygen Bubble Injection
e	Compressor efficiency = 0.80 in adiabatic compression formula
EQD	Equivalent Bubble Diameter (mm)
ER	Extended run treatment (Group Misc. 2)
FPA	Fixed Point Averaging program for flow meter
g	Acceleration due to gravity (980 cm sec^{-2})
G_s^n	Gas flow rate
GLM	General Linear Model in SYSTAT™
GVRD	Greater Vancouver Regional District
ID	Inside diameter (cm)
k	Unit (1.395) for air (and oxygen) in adiabatic compression formula
K_L	Liquid film coefficient (m hr^{-1})
$K_L a$	Overall oxygen transfer coefficient (hr^{-1})
$K_L a_{20}$	Oxygen transfer coefficient at 20 ^oC (hr^{-1})
$K_L a_T$	Oxygen transfer coefficient at temperature T ^oC (hr^{-1})
kW	Unit of power measurement
l^2	Liquid film thickness (m^2)
n	(k-1)/k = 0.283 for air (and oxygen) in adiabatic compression formula
Nm^3 min^{-1}	Normal cubic meters per minute; metric unit measurement of gas flow @ 1 atmosphere pressure, 0% relative humidity and 0.0 ^oC
OTEC	Ocean Thermal Energy Conversion
p_1	Absolute inlet pressure before compression (kg cm^{-2})
p_2	Absolute inlet pressure after compression (kg cm^{-2})

P_{H2O}	Vapor pressure of water for the ambient temperature (mm Hg)
psig	Pounds per square inch gauge (lb in^{-2})
P_w	Power input (kW)
PSA	Pressure Swing Adsorption
r	Rate of renewal of liquid film (hr^{-1})
r^2	Correlation coefficient
r_e	Equivalent bubble radius (cm)
R	Engineering gas constant for air = 8.314 kJ/k mol ^{o}K
SAE	Standard Aeration Efficiency (g O$_2$ kWhr^{-1})
SC	Surface cover treatment (Group 11 and 12)
SCFM	Standard cubic feet per minute; American unit measurement of gas flow @ 1 atmosphere pressure, 0% relative humidity and 21.1 ^{o}C
SE	Standard error
SEM	Scanning Electron Micrograph
SOTE	Standard oxygen transfer efficiency (%)
SOTR	Standard Oxygen Transfer Rate (g O$_2$ hr^{-1})
t_1	Time at point 1 on the semi-logarithmic plot (hr)
t_2	Time at point 2 on the semi-logarithmic plot (hr)
T_1	Absolute inlet temperature before compression (^{o}K)
TE	Field Oxygen Transfer Efficiency (%)
u	Bubble terminal rise velocity (cm sec^{-1})
UBC	University of British Columbia
V	Volume of the liquid (m^3)
w	Weight of air flow (kg s^{-1}) (i.e., 1.2927 g l^{-1})

W_{O2} Mass flow rate of oxygen in the gas flow stream (g O_2 hr^{-1})

$W_{O2\ air}$ Mass flow rate of oxygen in air in the gas flow stream (g O_2 hr^{-1})

$W_{O2\ PSA}$ Mass flow rate of oxygen in PSA oxygen the gas flow stream (g O_2 hr^{-1})

ACKNOWLEDGMENTS

CHAPTER 1: INTRODUCTION

1.1 Introduction

Hypolimnetic aeration has developed into an important, but infrequently used, water quality improvement technique, due to its ability to selectively oxygenate the hypolimnion of stratified lakes and reservoirs *in situ,* while maintaining thermal stratification. This ability has important applications in civil engineering, limnology and inland fisheries management. For example, within the field of lake restoration (i.e., applied limnology), hypolimnetic aeration is often the only feasible water quality improvement option due to the cost and logistical difficulties of controlling point and non-point source nutrient loading. Even if nutrient abatement measures are to be implemented as part of a comprehensive watershed nutrient management plan, several years of monitoring, planning and construction are often required to complete the task. Hypolimnetic aeration can be used as an interim measure that can be rapidly deployed to improve water quality, while longer-term restorative works are being completed. Hypolimnetic aeration can be used to increase the effectiveness of alternative lake restoration techniques, such as enhancing the distribution of liquid alum applied to co-precipitate phosphorus (Soltero et al., 1994).

For fisheries management purposes, hypolimnetic aeration is critically important for restoring cold water fish habitat, as artificial circulation (i.e., destratification) during summer months typically elevates hypolimnetic temperatures above the preferred temperature range for salmonids and eliminates their thermal refuge. An aerobic hypolimnion permits the existence of "two story" fisheries, where the epilimnion is inhabited by warm water fish species (e.g., centrarchids) and salmonids inhabit the hypolimnion. Public surveys have consistently indi-

cated strong support for this type of multi-species fishery throughout temperate regions of North America. The presence of an aerobic hypolimnion allows re-colonization of the profundal sediments by benthic macroinvertebrates and provides a refuge for planktonic macrozooplankton, both of which provide an additional food supply for fish and increase the invertebrate species diversity of the water body.

In British Columbia, approx. 30 lakes in the Southern Interior Plateau region have been artificially circulated during the winter to provide an ice fishery and prevent overwinter mortality of trout (Ashley et al., 1992). Artificial circulation via destratification has been the preferred approach (Ashley and Nordin, 1999). However, a recent ruling in 1998 by the B.C. Attorney General's Ministry has interpreted the Criminal Code of Canada (Section 263) to indicate that it is illegal to modify the natural integrity of an ice surface during winter months without 100% fencing of the open ice area created by the destratification process:

Criminal Code of Canada, Section 263: "Duty to safeguard opening in ice – Excavations on land – Offences: 263 (1) Everyone who makes or causes to be made an opening in ice that is open to or frequented by the public is under legal duty to guard it in a manner that is adequate to prevent persons by falling in by accident and is adequate to warn them that the opening exists."

"Every one who fails to perform duty imposed by subsection (1) is guilty of manslaughter, if the death of any person results therefrom; (b) an offence under Section 269, if bodily harm to any person results therefrom."

This interpretation has lead to the partial cancellation of B.C.'s winter aeration program, which has been in existence since the mid 1960's (Halsey, 1968), due to the cost/safety/logistical impracticalities of installing and dismantling temporary barrier fences annually on approx. 25 rural and semi-wilderness lakes.

An alternative technology is required that will provide the oxygenation equivalent of artificial circulation without modifying the integrity of the ice surface. Hypolimnetic aeration, due to its selective circulation ability, does not create polynas as the bubble-water plume is contained with a floating or submerged aeration chamber. However, the oxygen transfer efficiency of the hypolimnetic aerator must be considerably higher than the destratification systems, as the large open ice area for gas transfer is replaced by a much smaller surface exchange area within the inlet tube and aeration chamber. Hypolimnetic aeration, with compressed air, may not have sufficient oxygenation capacity to cost-effectively meet overwinter oxygen demands, which can be as high as 0.1 mg L^{-1} d^{-1} in the Southern Interior Plateau limnological zone (Ashley et al., 1992). Hence, a high efficiency hypolimnetic aeration system has the potential to re-establish B.C.'s winter lake aeration program.

From a civil engineering perspective, oxygenation of anoxic or anaerobic hypolimnetic water from eutrophic lakes and reservoirs can significantly improve domestic and industrial water quality by venting reduced gases (e.g., H_2S), oxidizing reduced metals (e.g., Fe^{+2}, Mn^{+2}), and establishing a positive oxidation-reduction (i.e., redox) potential in the hypolimnion (Speece, 1971). The presence of an oxidizing environment in the hypolimnion is one of the most critical factors in determining lake or reservoir water quality due to the overriding influence of redox potential on water chemistry. Hypolimnetic aeration can be used as a potable water pre-treatment in combination with existing civil engineering works to provide improved water quality at a fraction of the cost of upgrading or expanding conventional water treatment plants. Hypolimnetic aeration can also be used to selectively oxygenate hypolimnetic releases from stratified eutrophic reservoirs, such that the downstream environment does not experience depressed oxygen concentrations from anoxic water releases.

CHAPTER 2: LITERATURE REVIEW

2.1   Literature Review

<u>2.1.1   History of Hypolimnetic aeration</u>

Hypolimnetic aeration was initially developed in post-war Switzerland as an innovative process
to improve the water quality of Lake Bret, which is the water supply for Lausanne (Mercier and
Perret, 1949). Water was mechanically pumped to a shore based splash basin where it was
aerated and allowed to return by gravity flow through a pipe to the hypolimnion. The concept
generated little interest for nearly twenty years, then re-emerged in the 1960's due to the pio-
neering research efforts of Heniz Bernhardt in West Germany, and Richard Speece and Arlo
Fast in the USA. In these systems, water was airlifted to the surface and oxygenated water
returned to the hypolimnion via return tubes. Reports on the selective aeration capabilities of
hypolimnetic aeration were published in the primary literature (Bernhardt, 1967; Speece, 1971;
Fast, 1971) and the process attracted attention from various professional disciplines. The
interdisciplinary nature of hypolimnetic aeration was clearly demonstrated in these initial
studies. Bernhardt's (1967) interest was in improving potable water quality in eutrophic reser-
voirs, whereas Speece (1971) focused on innovative engineering designs for oxygenating water
for lakes, reservoirs and fish hatcheries. In contrast, Fast (1971) emphasised the restoration of
eutrophic lakes for fisheries management purposes, and stressed the importance of understand-
ing the ecological effects of hypolimnetic aeration.

Following the limiting aquatic nutrient controversy of the late 1960's, attention in the 1970's
focused on reducing nutrient inputs and developing methods for rehabilitating culturally eutro-
phied lakes and reservoirs. Many of these water bodies experienced degraded water quality

during the prolonged period of economic activity and population growth that followed World War II. Cultural eutrophication is caused by excessive addition of nutrients such as nitrogen and phosphorus to lakes, rivers, reservoirs, estuaries and coastal waters (Wetzel, 1975). Excessive nutrient loading typically results in increased aquatic plant growth, undesirable changes in species composition, oxygen depletions, fish kills, and decreased water quality for domestic, recreational, and industrial use (Lee, 1970).

As a result, the interdisciplinary field of lake restoration blossomed in the 1970's as limnologists and engineers developed new methods for restoring eutrophic lakes and reservoirs. Lake restoration refers to "… the manipulation of a lake ecosystem to effect an in-lake improvement in degraded, or undesirable conditions." (Dunst et al., 1974). Coincidentally, hypolimnetic aeration had matured to a stage where it was viewed as suitable technology for the rapidly developing field of lake restoration. Hypolimnetic aeration systems were soon installed in several Western European countries (Bernhardt, 1974; Verner, 1984; Steinberg and Arzet, 1984; Jaeger, 1990; Lappalainen, 1994), in Canada (Taggart and McQueen, 1981; Ashley, 1983; McQueen and Lean, 1983; McQueen and Lean, 1984; Taggart, 1984; Ashley, 1985; McQueen and Lean, 1986; Ashley, 1987) and the United States (Fast, 1973; Fast et al., 1973; Fast et al., 1975; Wirth et al., 1975; Fast, 1975; Smith et al. 1975; Fast and Lorenzen, 1976; Fast et al., 1976; Garrell et al., 1977; Labaugh, 1980; Fast, 1981). By the late 1980's, hypolimnetic aeration was recognized by perceptive environmental engineers and limnologists as a valuable, multi-purpose water quality restoration technique.

In the late 1980's and 1990's, research efforts on hypolimnetic aeration had progressed beyond reporting on individual installations, and tended to focus on four general areas of interest: (1)

examining the ecological effects of hypolimnetic aeration with liquid oxygen or Pressure Swing

Adsorption (i.e., PSA) generation of oxygen (Prepas et al., 1990; Prepas et al., 1997; Prepas and

Burke, 1997; Dinsmore and Prepas, 1997a; Dinsmore and Prepas, 1997b; Field and Prepas,

1997; Webb et al., 1997; Lawrence et al., 1997 and Gemza, 1997); (2) developing mathematical

models to predict oxygen transfer rates and aerator performance (Little, 1995); (3) full scale

testing of innovative designs e.g., Downflow Bubble Contact Aeration systems (i.e., DBCA or

"Speece Cone") (Thomas et al., 1994; Doke et al., 1995) and (4) engineering studies of factors

influencing oxygen transfer in full lift hypolimnetic aerators (Ashley and Hall, 1990; Ashley et

al., 1990).

For the purposes of this discussion, hypolimnetic aeration systems are grouped into three

general categories: (1) full or partial lift with compressed air; (2) full or partial lift with pure

oxygen or oxygen supplementation and (3) DBCA or Speece Cone aerators.

2.1.2   Types of Hypolimnetic Aerators

2.1.2.1   Full or Partial Lift Hypolimnetic Aeration with Compressed Air

A variety of hypolimnetic aerators designs have been proposed and at least 13 designs subjected

to full scale testing (Fast and Lorenzen, 1976). However, the conventional full lift "Bernhardt"

hypolimnetic aerator (Figure 2.1) has emerged as one of the more widely used designs due to its

relatively simple design and availability of published data on site specific oxygen transfer and

energy efficiency (Lorenzen and Fast, 1977; Taggart and McQueen, 1982; Ashley, 1985;

Ashley et al., 1987; Little, 1995). Several design improvements have been suggested for full lift

aerators (Lorenzen and Fast, 1977; Taggart and McQueen, 1982; Ashley, 1989), however,

relatively few have been subject to thorough laboratory and field testing.
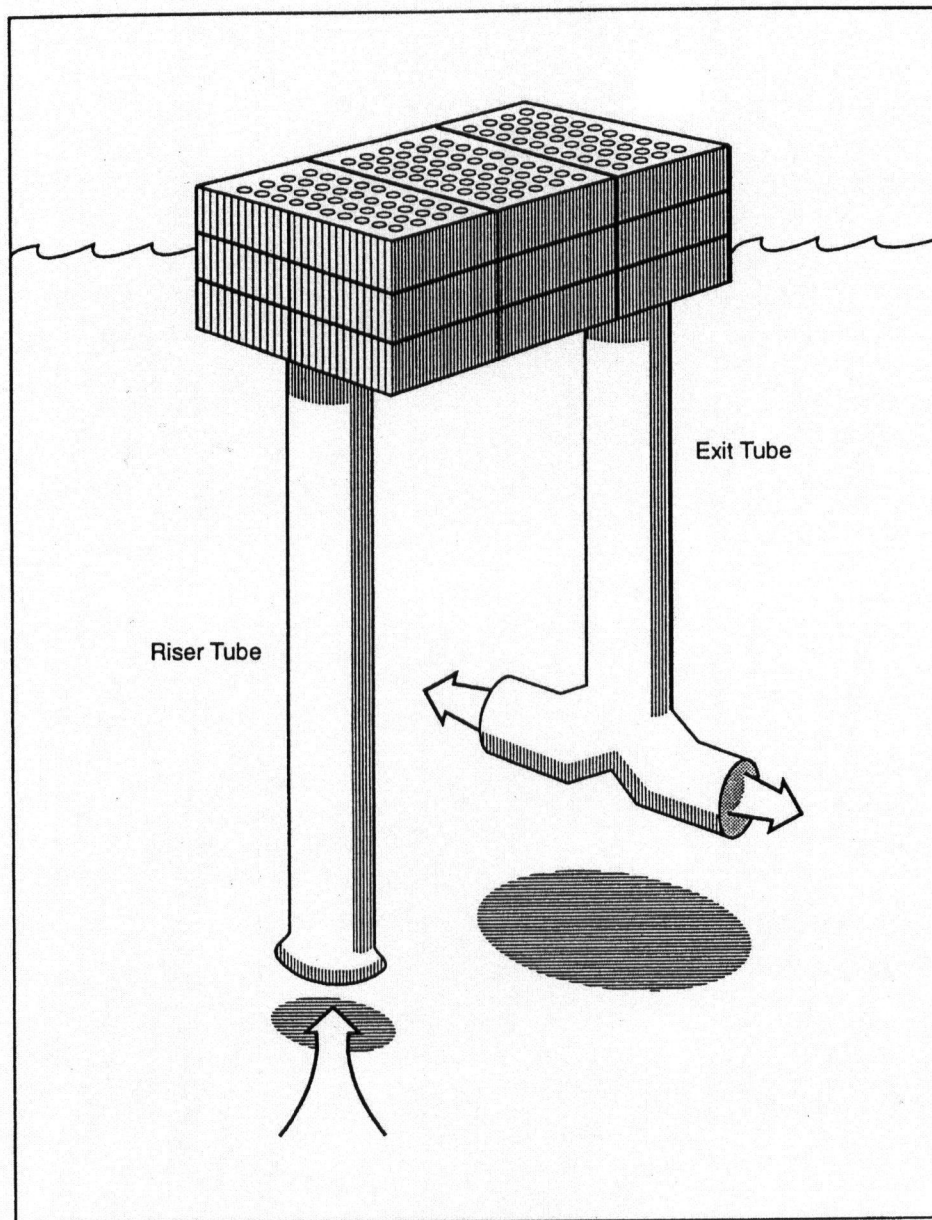
Figure 2.1. **Full lift "Bernhardt" type of hypolimnetic aerator (from Soltero et al., 1994)**

Three design parameters relevant to full lift designs that have undergone limited laboratory and field trials include (1) depth of air injection; (2) separator box surface exchange area and (3) diffuser orifice diameter. Varying the surface exchange area of the separator box was found to have no effect on induced water velocity, oxygen input, daily O_2 load, aeration efficiency (AE; g $O_2 \cdot kWh^{-1}$) and oxygen transfer efficiency (TE; %) (Ashley and Hall, 1990). The effect of diffuser depth on oxygen input was significant, however the effect was less than expected; but orifice diameter did exert a significant influence on oxygen input, daily oxygen load, TE and AE (Ashley et al., 1990). The importance of diffuser design was clearly demonstrated by a diffuser retrofit on a large Bernhardt style full lift hypolimnetic aerator, where the original 3,175 μ diameter diffusers were replaced with 140 μ diameter fine bubble silica glass diffusers. This increased the overall average daily oxygen input to St. Mary Lake (Saltspring Island, B.C.) from 311 kg·day^{-1} to 512 kg·day^{-1} with no corresponding increase in operational costs (Ashley et al., 1990).

Partial lift hypolimnetic aerators have not experienced the widespread application of full lift systems, although the concept is technically sound (Figure 2.2). One reason may be the "over-selling" of their capabilities relative to other designs of hypolimnetic aerators. The submerged design approach is particularly useful in high boat traffic areas and ice-prone regions, but it is more difficult to conduct routine inspections and performance monitoring. In extreme cases, undersized partial lift systems may have to be replaced, as they are less amenable to retrofitting than full lift designs. This was the unfortunate situation in Medical Lake, Washington where a partial lift hypolimnetic aeration system, with a coarse bubble diffuser, was unable to meet the hypolimnetic oxygen demand. After retrofitting with a smaller 600 μ orifice diameter diffuser and a higher output compressor, the partial lift unit was still undersized and
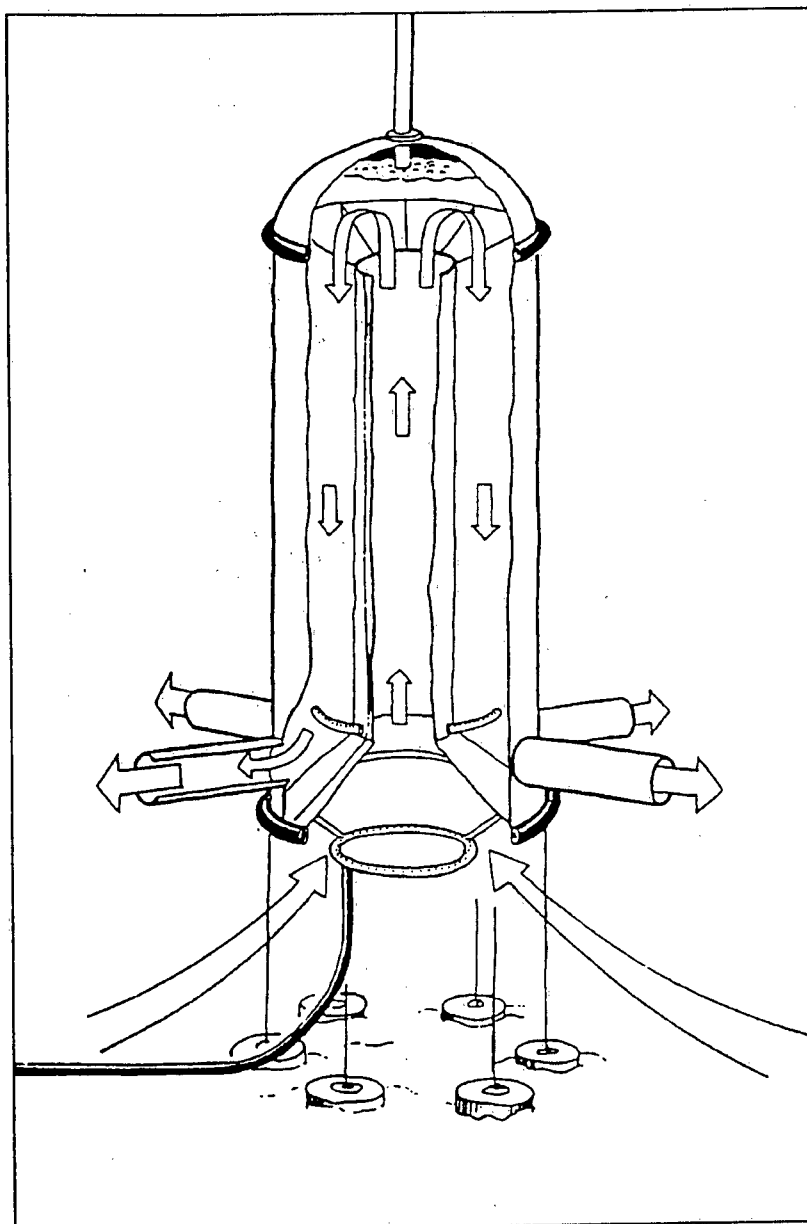
Figure 2.2.   **Partial lift hypolimnetic aerator (from Soltero et al., 1994)**

then experienced complete structural failure. It was replaced with two Bernhardt style full lift

hypolimnetic aerators, which successfully oxygenated the hypolimnion and significantly

improved the water quality of Medical Lake (Soltero et al., 1994).

2.1.2.2   Full or Partial Lift Hypolimnetic Aeration with Pure Oxygen or Oxygen Supplementation

Pure oxygen has been used in several installations to increase the amount of oxygen transferred

to the hypolimnion of eutrophic lakes and reservoirs. Although technically classified as a

mechanical pump design of hypolimnetic aeration, Fast and Lorenzen (1976) describe two

examples of side stream pumping (SSP) where pure oxygen was added to water pumped from a

quarry lake and returned to the hypolimnion via a high pressure discharge line. This method

increased the hypolimnetic oxygen concentration in Ottoville Quarry, Ohio to 21.5 $mg \cdot L^{-1}$

which was the highest hypolimnetic oxygen concentration recorded to date in a stratified water

body (Fast et al., 1977). Smith et al., (1975) used supplemental oxygen in Mirror Lake, Wis-

consin to overcome the high rate of hypolimnetic oxygen demand, and measured oxygen

concentrations in the full lift separator box of 13.4 $mg \cdot L^{-1}$ on pure oxygen and 8.6 $mg \cdot L^{-1}$, using

a blend of 0.45 $m^3 \cdot min^{-1}$ compressed air and 0.16 $m^3 \cdot min^{-1}$ liquid oxygen.

Prepas et al., (1997) successfully used liquid oxygen to oxygenate the north basin of naturally

eutrophic Amisk Lake, Alberta using a Deep Oxygen Bubble Injection (DOBI) system origi-

nally proposed by Speece (1971). This system injected up to 1.3 $t \cdot day^{-1}$ of fine oxygen bubbles

(20-1,500 μ diameter) at 33 m and was able to maintain hypolimnetic oxygen concentrations

>1.7 $mg \cdot L^{-1}$ in summer and >5 $mg \cdot L^{-1}$ in winter. Gemza (1997) used an innovative full lift

aerator design with an electric impeller in the separator box to increase water flow and oxygen

transfer. Using Pressure Swing Adsorption (i.e., PSA) generated oxygen, this design oxygenated anoxic hypolimnetic water up to 8.0 - 11.5 mg·L^{-1}, and was instrumental in improving the water quality in Heart Lake and Whittaker Lake in Southern Ontario. The main limitations and concerns with the use of liquid oxygen are the high operating costs (Fast et al., 1976), availability in remote locations, and site storage/security issues. However, the development of PSA oxygen generation has changed the economics and storage/security issues of using oxygen, and increased the opportunities for innovative application in hypolimnetic aeration (Speece et al., 1990).

2.1.2.3 Downflow Bubble Contact Aeration

A promising new type of hypolimnetic aerator is the "Speece Cone" design (Figure 2.3). This concept was originally proposed in 1971 as a Downflow Bubble Contact Aerator (DBCA) with an open cone (Speece, 1971), then re-designed in 1990-91 with a closed cone and field tested for the first time in 1992 in Newman Lake, Washington (Doke et al., 1995). An innovative design of hypolimnetic aerator was necessary as Newman Lake is large (490 ha) but quite shallow, with a maximum depth of 9.1 m and a mean depth of only 5.8 m, which was too shallow for conventional partial or full lift hypolimnetic aerator designs. The Speece Cone installed in Newman Lake was 2.8 m in diameter, 5.5 m tall, with a 45 kW submerged axial flow pump for water circulation and two 37 kW air compressors supplying compressed air to two Pressure Swing Adsorption (PSA) on-site oxygen generation units. The system was designed to supply 1,360 kg·d^{-1} of oxygen to the hypolimnion through a specially designed diffuser to avoid unintentional destratification and sediment disturbance (pers. comm., G. Lawrence, UBC, Vancouver, B.C.).
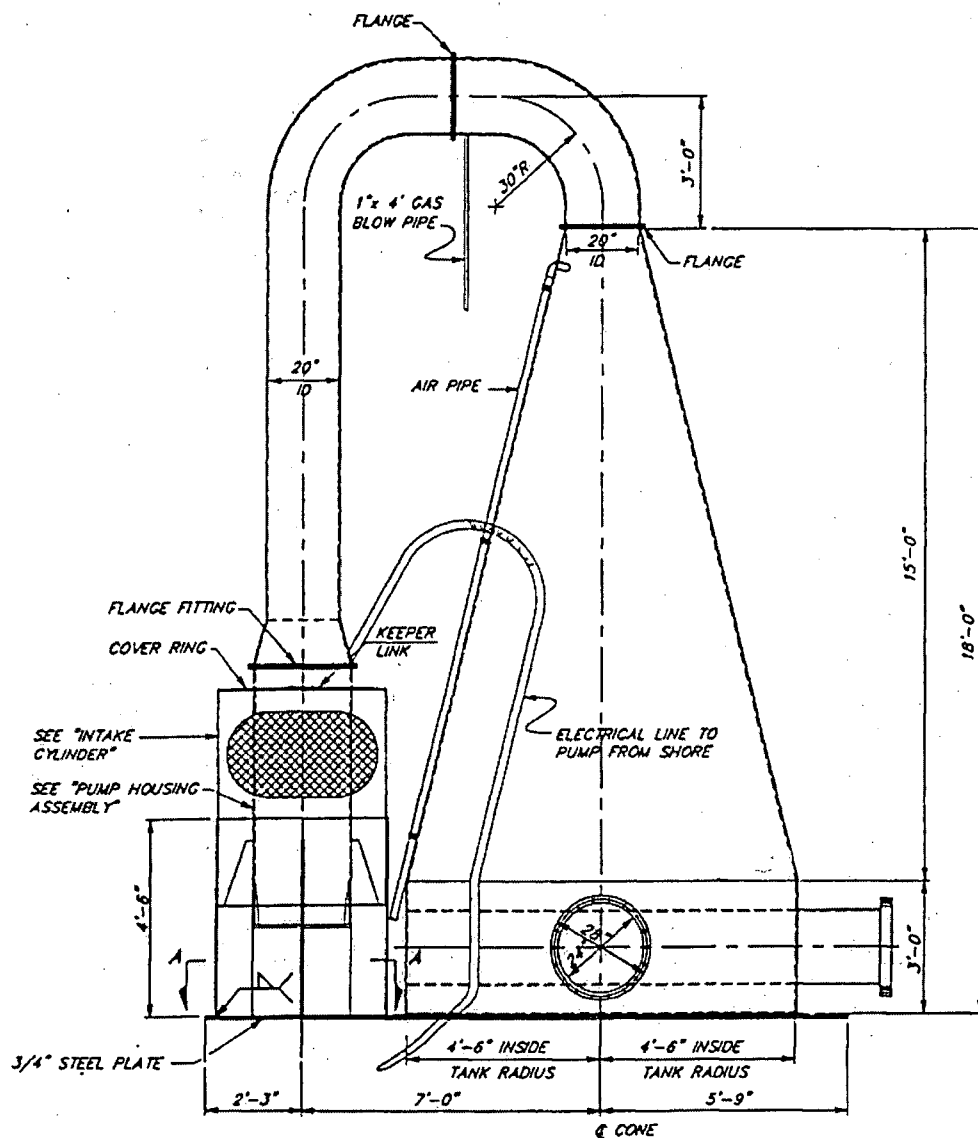
Figure 2.3   Downflow Bubble Contact Aerator "Speece Cone" hypolimnetic aerator

The system has performed extraordinarily well to date, with measured oxygen concentrations in the outlet pipe >30 mg·L^{-1} despite being located in only 8.7 m of water. The system increased average summer hypolimnetic oxygen concentrations to 5.5 mg·L^{-1} in 1992; however, thermal stratification was less stable due to two severe storm events (Thomas et al., 1994). An even larger Speece Cone (7 m in height), capable of supplying 8,000 kg·d^{-1} of oxygen, was installed and operated in Camanche Reservoir, California in 1993 and 1994 to improve water quality and prevent periodic fish kills in a salmonid hatchery that was relying on hypolimnetic water discharged from the anoxic hypolimnion. Unpublished reports indicate this system has also performed extremely well to date (pers. comm., A. Horne, U. California at Berkeley).

2.2   Rationale for Current Research

After nearly 50 years of extensive testing and reporting, hypolimnetic aeration is still infrequently used by civil engineers to improve potable water quality in eutrophic lakes and reservoirs. This seems paradoxical in light of evolving regulatory requirements for higher quality raw water supplies and the well documented capabilities of hypolimnetic aeration for improving water quality while maintaining thermal stratification. I believe this situation is partially a result of the interdisciplinary nature of hypolimnetic aeration, where much of the research and reporting has been conducted by limnologists and fisheries biologists. In addition, the conservative tendency for most civil engineers has been to address raw water quality concerns through conventional and updated water treatment facilities, rather than accept risks with less certain "ecological engineering" approaches in lakes or reservoirs. However, with increasingly stringent regulations for permissible concentrations of disinfection by-products eliminating such traditional practices as chlorine pre-treatment and pre-oxidation, it is inevitable that water utilities will adopt more pro-active watershed management strategies for their raw water sup-

plies. This can be achieved through strict control of watershed land use, implementing storm-water best management practices, and by using in-lake techniques such as hypolimnetic aeration to improve and/or maintain high-quality, raw water.

Since hypolimnetic aeration is one of the most effective in-lake water quality improvement techniques, it is necessary to provide updated information to water treatment engineers so that hypolimnetic aeration can be integrated into current and future water quality management strategies. An afternoon session at the 1998 American Water Works Association Water Quality Technology Conference in San Diego was organised on this theme, and several papers were presented reviewing the various methods available for hypolimnetic aeration and the resultant improvements in raw water quality. Unfortunately, only abstracts of these papers were ever published in the conference handbook.

To date, a detailed analysis of design factors influencing the oxygen transfer efficiency of conventional and innovative hypolimnetic aerators has not been conducted. Neither has an economic and engineering analysis been attempted comparing different designs of hypolimnetic aerators and alternate sources of oxygen (e.g., compressed air, liquid oxygen and Pressure Swing Adsorption oxygen) to determine which is the most cost effective type of aerator and source of oxygen. Given the variable cost of electricity in the Pacific Northwest and California markets, it is imperative that energy costs be factored into any potential in-lake water quality improvement strategy, as the cumulative operational and maintenance costs of large electric pumps and compressor motors can be substantial. To their credit, Fast and Lorenzen (1976) and Fast et al., (1976) initiated a comparative analysis in the mid 1970's; however, an update is

required given the development of PSA technology as an alternative to cryogenic oxygen and the recent, full-scale tests of the Speece Cone in Newman lake and Camanche Reservoir.

At present, there are at least three areas of study that require additional information in order to expand the knowledge base for hypolimnetic aeration: (1) optimising oxygen transfer with compressed air; (2) examining the use of PSA generated oxygen, and (3) understanding the oxygenation characteristics of the Downflow Bubble Contact Aerator i.e., the "Speece Cone". In addition, Ashley (1989) suggested three areas of research that may improve the performance of conventional full lift hypolimnetic aeration systems. These involved (1) installing bubble screens in the inlet tube in an attempt to fragment coalesced bubbles in the rising air:water plume; (2) increasing bubble:water contact time in the inlet tube through the use of deflectors or vanes and (3) using counter-current air or oxygen injection in the outlet tube, in conjunction with co-current upflow in the inlet tube to increase oxygen transfer per unit energy input.

Accordingly, this current research effort conducted a detailed analysis of design factors influencing the oxygen transfer capabilities of two different designs of hypolimnetic aerators: full lift and Speece Cone. The experiments utilised non steady-state gas transfer methodology in a laboratory scale system. Specifically, the research examined the effect of several engineering design factors on oxygen transfer using four standard units of measure for quantifying oxygen transfer: (a) K_La_{20} (hr^{-1}), the oxygen transfer coefficient at 20 °C; (b) SOTR (g O_2 hr^{-1}), the Standard Oxygen Transfer Rate; (c) SAE (g O_2 kWhr^{-1}), the Standard Aeration Efficiency and (d) SOTE (%), the Standard Oxygen Transfer Efficiency:

The design factors examined in the full lift experiments were as follows:

1. the effect of diffuser orifice pore diameter (140 μ, 400 μ and 800 μ) on K_La_{20}, SOTR, SAE and SOTE;

2. the effect of diffuser submergence (1.5 and 2.9 m) on K_La_{20}, SOTR, SAE and SOTE;

3. the effect of gas flow rate (10, 20, 30 and 40 l min^{-1}) on K_La_{20}, SOTR, SAE and SOTE;

4. the effect of oxygen partial pressure (air and PSA generated oxygen) on K_La_{20}, SOTR, SAE and SOTE ;

5. the effect of a floating surface cover in the separator box (present or absent) on K_La_{20}, SOTR, SAE and SOTE;

6. the effect of a mid-depth inlet tube bubble screen (i.e., fine strand stainless steel mesh screen of 0.64 cm square openings to fragment rising bubbles) on K_La_{20}, SOTR, SAE and SOTE;

7. the effect of mid-depth inlet tube counter-rotating blades (i.e., mechanical propeller blades that rotated with the upwelling water velocity and fragmented rising bubbles) on K_La_{20}, SOTR, SAE and SOTE;

8. the effect of Downflow Bubble Contact Aeration (DBCA) in the outlet tube in combination with co-current upflow in the inlet tube on K_La_{20}, SOTR, SAE and SOTE.

The design factors examined in the Speece Cone experiments were as follows:

1. the effect of oxygen flow rate (1, 2 and 3 l min^{-1}) on K_La_{20}, SOTR, SAE and SOTE;

2. the effect of outlet port discharge water velocity (20, 30, 40, 50, 60 and 70 cm sec^{-1}) on K_La_{20}, SOTR, SAE and SOTE.

The purpose of this research was to determine the effect of several key design factors on oxygen transfer, and determine which combination(s) of design factors was most effective at dissolving oxygen into water under laboratory test conditions. The immediate goal of this research is to provide the necessary engineering design analysis, such that practising engineers and applied limnologists can confidently design and construct cost effective and energy efficient full scale hypolimnetic aeration systems. The ultimate goal is to protect and improve raw water quality in stratified lakes and reservoirs.

CHAPTER 3: METHODS

3.1 System Design

The entire aeration test facility was custom fabricated as there were no existing facilities in the

Civil Engineering-Mechanical Engineering (CEME) laboratory, at the University of British

Columbia (UBC), suitable for bench-scale, non steady-state aeration studies.

3.1.1 Aeration Tank

The vessel used for the experiments was a custom fibreglass tank built by Condor Engineering

Ltd. (Surrey, BC). The tank dimensions were 0.92 m wide x 0.47 m deep x 3.25 m high (exte-

rior dimensions) and 0.905 m x 0.425 m x 3.205 m (interior dimensions). The tank was filled to

a depth of 3.105 m for the tests; hence the operational volume of the tank was 1,194 litres. The

tank was equipped with a single 2.54 cm drain valve near the bottom on one side, while the

other side was fitted with a 16 cm self-sealing inspection port that could be opened from the

exterior when the tank was empty. The tank was designed around two custom cast pieces (300

cm x 30 cm x 25.4 mm) of clear acrylic polymer (Reynolds Polymer Technology Inc., Grand

Junction, CO) on the front panel to allow viewing of the tank interior (Figure 3.1).

The tank developed a noticeable deflection when filled to capacity; hence a steel I-beam (7 mm

thickness) was attached to the front of the tank to reduce deflection of the front panel. During

initial test fill/drain cycling, the lateral tank deflection was still sufficient to cause a major leak

at an acrylic panel seal. Therefore, a pair of flat steel bars (12 mm thickness) was attached to

the sides of the tank at heights of 82 cm and 174 cm and connected by 8 mm diameter threaded

steel rods to prevent lateral deflection of the tank sidewalls. In addition, a 5 cm wide nylon
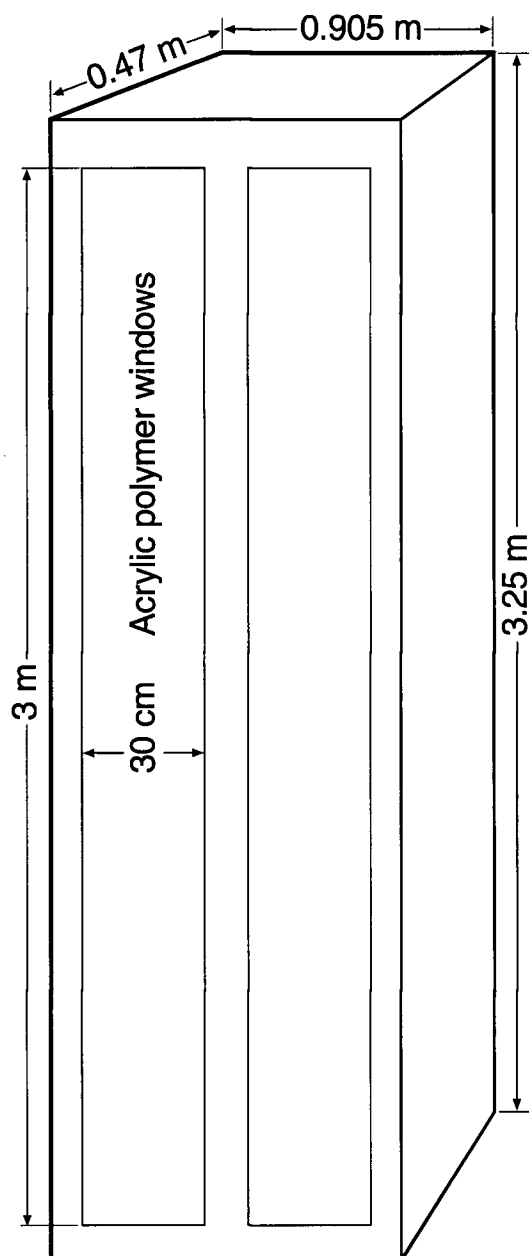
Figure 3.1   Schematic diagram of aeration tank

strap was placed around the entire tank at 1.5 m and tightened as much as possible with a cam ratchet in an attempt to minimize tank deflection.

3.1.2   Water Supply

The water used in the tests was taken directly from the water supply system in the CEME laboratory, which is usually Capilano Reservoir water delivered by the Greater Vancouver Regional District (GVRD) distribution system to UBC. Capilano Reservoir water is low in total dissolved solids (22 mg l^{-1}), slightly acidic (mean pH of 6.1), and typically of high quality, except during high rainfall events when the water can become turbid due to landslides or deltaic erosion in the upper reaches of Capilano Reservoir (Perrin et al., 2000). No significant turbidity events occurred during the test period.

3.1.3   Air Supply

A 44.74 kW Quincy rotary screw compressor (Model QNW 260-D) rated at 6,800 l min^{-1} (240 Standard Cubic Feet per Minute; SCFM) supplied compressed air. A nominal efficiency filter and water-cooled aftercooler was fitted to the discharge end of the compressor. The compressor was located in the basement of the CEME laboratory, and air was available throughout the CEME laboratory at several distribution points. The connection to the experimental manifold was via ~10 m of 1.9 cm ID compressed air hose at the nearest distribution point. The compressor was regulated to maintain line pressure at 7.03 kg cm^{-2} (100 pounds per square inch gauge; psig), and a pressure switch would activate the compressor when line pressure decreased below 6.3 kg cm^{-2} (90 psig), and shut off when line pressure reached 7.7 kg cm^{-2} (110 psig).

3.1.4   Oxygen Supply

Oxygen gas for the experiments was produced by an AS-20 PSA oxygen generator, manufactured by the AirSep Corporation (Buffalo, New York). The PSA generator separates oxygen from air using the Pressure Swing Adsorption (PSA) air separation process. The PSA process uses packed beds of a molecular sieve (synthetic zeolite) which attracts (adsorbs) nitrogen at high pressure and releases (desorbs) it at low pressure. The unit has two adsorbent beds, and a set of pressure activated solenoids which cycles the two adsorbent beds between high and low pressure so that as one bed is producing oxygen, the other one is regenerating by releasing nitrogen to the atmosphere. The beds are completely regenerative under normal conditions and will last indefinitely.

The factory specifications for the AS-20 indicate it requires a minimum air pressure and flow of 6.3 kg cm^{-2} (90 psig) and 0.14 Normal cubic meters per minute; Nm^3 min^{-1} (5.3 SCFM) respectively (see Nomenclature for SCFM and Nm^3 min^{-1} definitions), and will deliver 0.0088 Nm^3 min^{-1} (0.33 SCFM) at 3.2 kg cm^{-2} (45 psig). A 227 l storage receiver was connected to the AirSep unit to allow it to temporarily deliver oxygen in excess of 0.0088 Nm^3 min^{-1} (0.33 SCFM). The purity of oxygen generated ranges from 90 to 95%. A reference cylinder of certified oxygen gas (> 99.99 % oxygen), obtained from Air Liquide Canada, was used to calibrate the oxygen gas probe (i.e., Probe 7) and continuously monitor the purity of the oxygen generated by the AirSep unit.

3.1.5   Gas Delivery and Flow Measurement

Point Four Systems Inc. manufactured a custom designed manifold board to distribute and regulate the flow and delivery pressure of the various gases being tested (Figure 3.2).
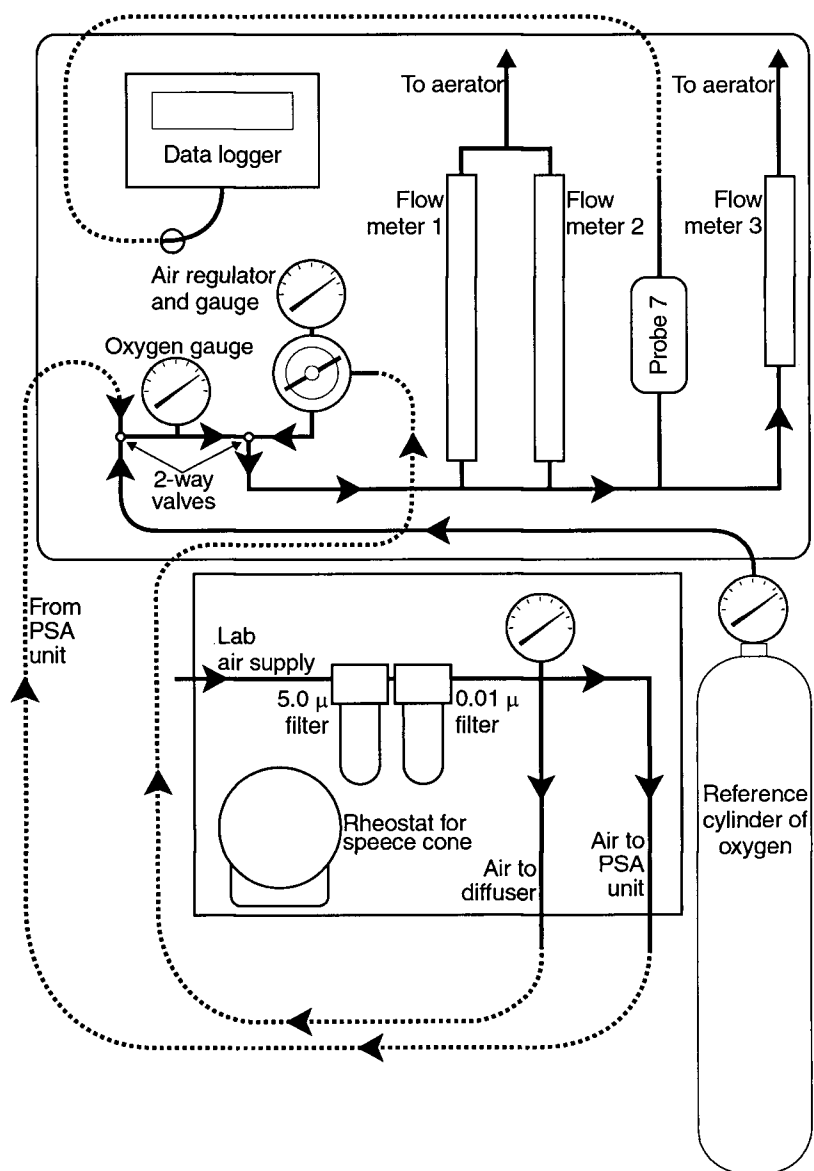
Figure 3.2. **Schematic diagram of manifold board with data logger and flow meters**

Inflowing compressed air from the CEME laboratory supply was passed through a Wilkerson 5.0 μ particulate and oil/water filter, then a 0.01 μ particulate filter and oil/water filter. PSA molecular sieves are very sensitive to contamination so it was imperative that no moisture, particulates or compressor oil reached the synthetic zeolite adsorbent beds. Filtered air was then routed to the PSA unit or straight to the manifold via a pair of on-off ball valves. The filtered gas (air or oxygen) was then routed via separate regulators to an array of three mechanical flow indicators, which could be operated independently, or in any combination. Pressure gauges were fitted to each regulator (air or oxygen) on the manifold, on a single stage regulator fitted to the PSA oxygen receiver and on a two stage regulator fitted to the reference cylinder of high purity compressed oxygen.

The coarse scale flow meter was a Brooks Sho-rate flow indicator with 150 mm scale, 2 to 46 l min^{-1}; the medium scale meter was a Brooks Sho-rate flow indicator with 150 mm scale, 2 to 12 l min^{-1}; and the fine scale meter was a Key Instruments flow indicator with 80 mm scale, 0 to 3.5 l min^{-1}. The Brooks flow indicators were designed to operate at 3.2 kg cm^{-2} (45 psig), and the Key Instruments flow indicator was designed for 3.5 kg cm^{-2} (50 psig), although it was operated at 3.2 kg cm^{-2}. Pressure regulation for the various gases was achieved by adjusting the compressed air regulator on the manifold board, a single stage regulator on the discharge side of the AirSep oxygen receiver, or a two-stage regulator on the reference oxygen cylinder.

Flow meter readings were corrected by a specific density correction factor (i.e., $\sqrt{1.105/1.0}$) when operated on compressed air. The Key Instruments meter was corrected by a pressure correction factor (i.e., $\sqrt{59.7/64.7}$) to compensate for the lower operating pressure (i.e., 3.2 vs.

3.5 kg cm^{-2}). All of the flow meters were calibrated for 21 °C; hence no temperature correction factor was required.

The manifold board was fitted with two 2-way ball valves so that compressed air, PSA oxygen, or high purity reference oxygen could be delivered to the diffusers. The gas supply for the % volume probe cup (i.e., Probe 7) was located downstream of the three flow indicators, however, the volumetric flow rate of gas to the probe cup was so low that it did not introduce a bias to the various flow meter readings. The gas exiting the probe cup was vented into an 11 cm water filled cylinder so that the gas flow could be directly observed in a bubble stream and adjusted to maintain a low, but constant discharge rate (Figure 3.2).

3.1.6   Water Velocity Measurement

Water velocity was measured by a Marsh McBirney Model 2000 flow meter. Since fluid dynamics around the sensor electrodes caused some variation in readings, a Fixed Point Averaging (FPA) program in the Model 2000 software dampened the output display. This program calculated an average of velocities recorded over a fixed period of time. A time duration of 120 seconds was used for the averaging period, as this was the maximum time duration available in the meter.

3.1.7   Data Logger

An eight channel microprocessor based PT4 Monitor (Point Four Systems Inc., Richmond, B.C.) was used to record and log data collected during the experiments. The unit was configured with 6 channels for measuring dissolved oxygen in water (Ch. 1-6), one % oxygen channel (Ch. 7) for measuring the purity of the oxygen gas and one temperature channel (Ch. 8). The

PT4 Monitor included a communications package enabling RS 232 connectivity to a portable computer for viewing and downloading data from the PT4's internal non-volatile memory. Data transmission is via ASCII Comma Separated Variable (CSV) format.

Data logging for all active channels was selectable from 4 seconds to 18 hours, with a maximum capacity of 8,044 samples. Since the unit was equipped with 8 probes (plus time stamp), the maximum memory capacity was 8,044/9 = 894 readings. The PT4 monitor read the channel values and updated the display at 1.5-2.0 second intervals. During the first half of each scan cycle Channels 1-4 were simultaneously read, and Channels 5-8 were read during the second half of the scan cycle. The PT4 Monitor included user defined sample averaging time and log interval settings. The sample averaging time is the period in which channel values are read, accumulated in the internal memory, and the average value taken. The log interval is the time interval between one set of channel values being logged and the next set.

The PT4 monitor was programmed for the first set of experiments with the full lift hypolimnetic aerator (Groups 1-6) to average readings for 10 seconds, and log the averaged values at 20 second intervals, so that 3 readings per minute were recorded. This allowed 5 hours of data logging capability, which was required when measuring low air flow rates with 800 μ diffusers at the 1.5 m depth. In the second set of experiments with the full lift aerator (Group 7-14) and the Speece Cone (Group 15-21), the averaging time and log interval was reduced by 50% to 5 and 10 seconds, respectively, so that 6 readings per minute were taken. This decreased the maximum logging period to 2.5 hours which was adequate for this phase of the experiments.

Data values were logged until at least 60 % saturation had been reached at the intake sampling probe (i.e., Probe 1) during the full lift experiments, and at least 65 % saturation was reached at the intake sampling probe (i.e., Probe 5) in the Speece Cone experiments. Continuous visual checks were made during each test to ensure the upstream gas pressure remained constant at 3.2 kg cm^{-2}, and that gas flow remained at the desired delivery rate.

3.1.8   OxyGuard Probe Design

The PT4 monitor was supplied with seven OxyGuard probes; with six probes measuring dissolved oxygen in the water and one measuring the % oxygen volume of the inlet gas (air, PSA oxygen, or calibration oxygen). The OxyGuard design is a membrane covered self polarizing galvanic measuring element with built-in temperature compensation. The probes produce a millivolt output in direct proportion to the amount of oxygen present in the medium in which they are placed. Oxygen diffuses through the membrane onto a silver cathode where it reacts chemically and then combines with a zinc anode. This chemical process produces an electrical current which flows through a built in resistor that converts the current (microamps) into millivolts, which is then transmitted via a two conductor cable to the data logger (Point Four Systems, 1997). The minimum current speed required across the membrane for the in-water probes is 2.5 cm s^{-1}.

3.1.9   Probe Membrane

Preliminary tests with higher oxygen flows and fine pore diffusers revealed that dissolved oxygen concentrations in the water were changing too quickly to register with the mg l^{-1} membranes. Therefore, the Oxyguard probes were configured to measure dissolved oxygen in %

saturation, rather than mg l^{-1}, as the % saturation probe membranes were 50% thinner than the mg l^{-1} membranes, resulting in a faster probe response time.

3.1.10   Water Temperature

Water temperature was measured with a dedicated stainless steel thermister probe (Channel 8) on the PT4 Monitor, and a temperature probe on the YSI meter. Both probes were typically within ~0.2 °C, and the PT4 temperature reading was used for the probe calibration procedure. The PT4 temperature probe was checked in an ice bath (0 °C) and room temperature (20 °C) water as determined by a mercury calibration thermometer, and found to be accurate within 0.5 °C.

3.2   Test Procedure

The test procedure started each morning by draining and refilling the tank with clean water from the CEME laboratory supply line. Two Little Giant 5-MSP submersible mixing pumps rated at 4,500 l hr^{-1} (1,200 gallon hr^{-1} each at 0.3 m head) located in diagonal corners on the tank floor, were then turned on and allowed to circulate the tank water for 5-6 minutes. Red food coloring dye was added to the tank on several occasions to examine circulation patterns and determine if any stagnant zones existed. The 1,200 litres of water in the tank was well mixed within an average of 2 minutes, thus confirming initial observations that complete mixing was quickly achieved.

The monitoring/data logging equipment was then activated. This included the PT4 data logger and Oxyguard probes, a YSI 57 digital dissolved oxygen-temperature meter, and a Toshiba laptop computer for data transfer and storage. An electronic balance for weighing deoxygena-

tion chemicals was activated on the same circuit. The PSA unit was pressurized with compressed air from the CEME laboratory supply line to full operating pressure (7.03 kg cm^{-2}, 100 psig) and allowed to cycle for several minutes, to pressurize the PSA storage receiver to maximum pressure (4.2 kg cm^{-2}, 60 psig).

3.2.1 Oxygen Probe Calibration

Two replicate samples of water were then collected from the tank surface in 300 ml BOD bottles, and analyzed in the Environmental Engineering laboratory for dissolved oxygen, using the Winkler titration procedure (Azide modification; Lind, 1979). The two Winkler readings were then averaged to provide the reference oxygen concentration to calibrate the PT4 unit and probes for the day. The YSI meter was calibrated in mg l^{-1} to the average of the two Winkler readings.

3.2.2 Calculation of Daily Oxygen Saturation

The percent saturation for dissolved oxygen on each test day was calculated according to Colt (1984):

(3.1) $\qquad C_s^* = C_s{^*}_{760} \, (BP - P_{H2O}) \, / \, (760.0 - P_{H2O})$

where:

C_s^* = the dissolved oxygen air-solubility value (mg l^{-1}) for the ambient barometric pressure, temperature and vapor pressure of water;

$C_s{^*}_{760}$ = the dissolved oxygen air-solubility value (mg l^{-1}) for the barometric pressure equal to 760.0 mm Hg and ambient temperature;

BP = barometric pressure in mm Hg;

P_{H2O} = vapor pressure of water in mm Hg for the ambient temperature.

Values for C_s*_{760} and P_{H2O} were taken from reference tables in Colt (1984), and the barometric

pressure for each test day was taken from the Vancouver weather station on the Environment

Canada WebPage at www.weatheroffice.com.

The % oxygen saturation of the test water was then determined by dividing the average dis-

solved oxygen concentration from the Winkler titrations by the calculated oxygen saturation

(i.e., C_s*) on each day:

$$(3.2) \qquad \frac{(\text{Winkler 1 (mg l}^{-1}) + \text{Winkler 2 (mg l}^{-1}))/2}{C_s* \text{ (mg l}^{-1})} \times 100 = \% \text{ oxygen saturation}$$

The PT4 Monitor was then calibrated with this value using the single point calibration proce-

dure outlined in the PT4 software (Point Four Systems, 1997). The probe response was exam-

ined from 0 % saturation (sulfite bath) to 100 % saturation (AirLiquide certified > 99.99%

oxygen gas) and found to be essentially linear, hence this calibration procedure was satisfactory.

Once calibrated, the probes were quite stable, and would remain accurate for several days,

although they were re-calibrated on each test day to ensure adjustment was made for daily

variations in barometric pressure and water temperature.

The purity of the oxygen gas (% volume) produced by the PSA unit was monitored by a dedi-

cated probe (Ch 7) in the PT4 Monitor. This probe was calibrated daily using the reference

cylinder of certified oxygen gas (> 99.99 % oxygen). The experimental manifold contained a 2

way valve and a cup into which the Channel 7 probe was inserted. The valve was set to allow

the reference oxygen to flow to probe 7 for several minutes each day while the test tank was

mixing. The probe was then calibrated to this reference standard using the single point calibra-

tion procedure in the PT4 software (Point Four Systems, 1997). When the PSA unit became pressurized to its maximum operating pressure (4.2 kg cm^{-2}, 60 psig), the 2 way valve was turned to allow PSA oxygen to flow to Probe 7, and the % volume oxygen reading was continuously recorded during each reaeration test using PSA gas. The probe also monitored the oxygen concentration in air when tests were being conducted on compressed air.

3.2.3   Deoxygenation Procedure

The deoxygenation-oxygenation procedure used was the nonsteady-state reaeration test (ASCE, 1992; Boyd and Watten, 1989). The test water was deoxygenated with 0.1 mg l^{-1} of cobalt chloride (Certified Grade of CoCl$_2$·6H$_2$O) and 10.0 mg l^{-1} of sodium sulfite (Sulftech Catalyzed Na$_2$SO$_3$; Code 098-3393) for each 1.0 mg l^{-1} of dissolved oxygen present in the water (Boyd, 1986) plus an additional 10% weight of Na$_2$SO$_3$ to ensure rapid deoxygenation at the colder test temperatures. The cobalt chloride was dissolved in a 1 l flask, added to the tank and allowed to mix into the test water. Sodium sulfite was then mixed into a slurry in a 1 l flask, added to the tank water and thoroughly mixed by the two submersible pumps. Theoretically only 7.9 mg l^{-1} of sodium sulfite is required for each mg l^{-1} of dissolved oxygen; however, due to partial oxidation during mixing, it is necessary to add up to 1.5 times the stoichiometric amount (Beak, 1977).

The PT4 Monitor low level alarm lighting system was set to activate at 1.0 % saturation, hence it was possible to detect at a distance when probes 1-6 decreased below 1.0 % saturation. A stopwatch was started as soon as the sodium sulfite slurry was added. The YSI meter and PT4 monitor confirmed that the tank water was rapidly deoxygenated, as the % oxygen saturation invariably declined to < 1.0 % within 2 minutes (full lift experiments) and 2.5 minutes (Speece

Cone) respectively. The tank was allow to mix for 6 minutes (full lift experiments) and 8 minutes (Speece Cone) respectively, before reaeration treatments were initiated.

Since the oxygen differential between the inlet and outlet of the Speece Cone was often quite large, the oxygen flow was terminated when the % saturation at the intake port (i.e., Probe 5) reached 65 % saturation; however, the mixing pumps remained operating. This allowed the pumps to continue circulating water within the tank and displace oxygenated water out of the Speece Cone into the bulk water. The % saturation recorded at Probe 5 (see Speece Cone schematic) following 2 minutes of circulation with zero oxygen flow was then used to represent the terminal % oxygen saturation for the experiment. The 2 minute period following termination of oxygen flow was not included in the various oxygen transfer calculations as no "new" oxygen was added during this procedure, only redistribution of existing oxygen within the Speece Cone and tank.

A maximum of six test runs was conducted on each tank of water, to minimise interference from sodium sulfite accumulation (ASCE, 1992; Beak, 1977). The tank was then drained, refilled, and the procedure was repeated. The tank required approx. 40 minutes to drain, and 45 minutes to refill. Since the TDS of the Capilano Reservoir water supply was so low (i.e., 22 mg l^{-1}), the addition of sodium sulfite did not result in a decrease in oxygen saturation due to increased salinity. For example, the greatest amount of Na_2SO_3 was added during the Speece Cone tests, which resulted in a total addition of 635 g (Group 15), and 626 g (Group 17). This increased the total dissolved solids concentration of the test water by 529 and 521 mg l^{-1} respectively during the Group 15 and 17 tests, well below the 1,000 mg l^{-1} negligible effect concentration noted by Beak (1977). The sodium sulfite imparted a slight brownish tint to the water, which increased

with each successive addition of Na_2SO_3. There was no foaming of the water, or any other noticeable changes in the test water. A description of the test procedure used for the full lift and Speece Cone experiments is listed in Appendix 1 and Appendix 2 respectively.

3.3   Full Lift Hypolimnetic Aerator

3.3.1   Aerator Dimensions

The full lift hypolimnetic aerator was based on a modified Bernhardt (1974) design, as described in Ashley (1988). The unit was constructed of clear acrylic, and consisted of an open separator box fitted with inlet and outlet tubes (Figure 3.3). The separator box was 82 cm (l) x 36 cm (w) x 28 cm (h) (outside dimensions). The sides of the box were 6.3 mm thick and the bottom section was 9.15 mm. The inlet and outlet tubes were 282.2 cm in length, with an inside diameter of 19.5 cm, and wall thickness of 3 mm. The tube entrance and exit were cut at 90°, as there was insufficient space in the aeration tank to attach an intake flare or discharge elbow. The tubes were located on the centre-line long axis of the separator box, with a 2 cm setback from the endwalls. The separator box was equipped with adjustable supports to suspend it in the tank. The supports were adjusted so that 8 cm of water was present in the separator box with the air flow turned off. The total operating depth of the system was therefore 8 cm + 282.2 cm (tube length) + 0.9 cm (box bottom section thickness) = 291.1 cm. Since the box was filled to a depth of 310.5 cm, there was 19.4 cm clearance between the bottom of the inlet/outlet tubes and the tank floor.

A divider was inserted into the tank between the inlet and outlet tubes to prevent short-circuiting from the outlet tube immediately back into the inlet tube. The divider was constructed of clear 6 mm acrylic, and was 200 cm high and 38 cm in width. The divider rested on the tank floor, so
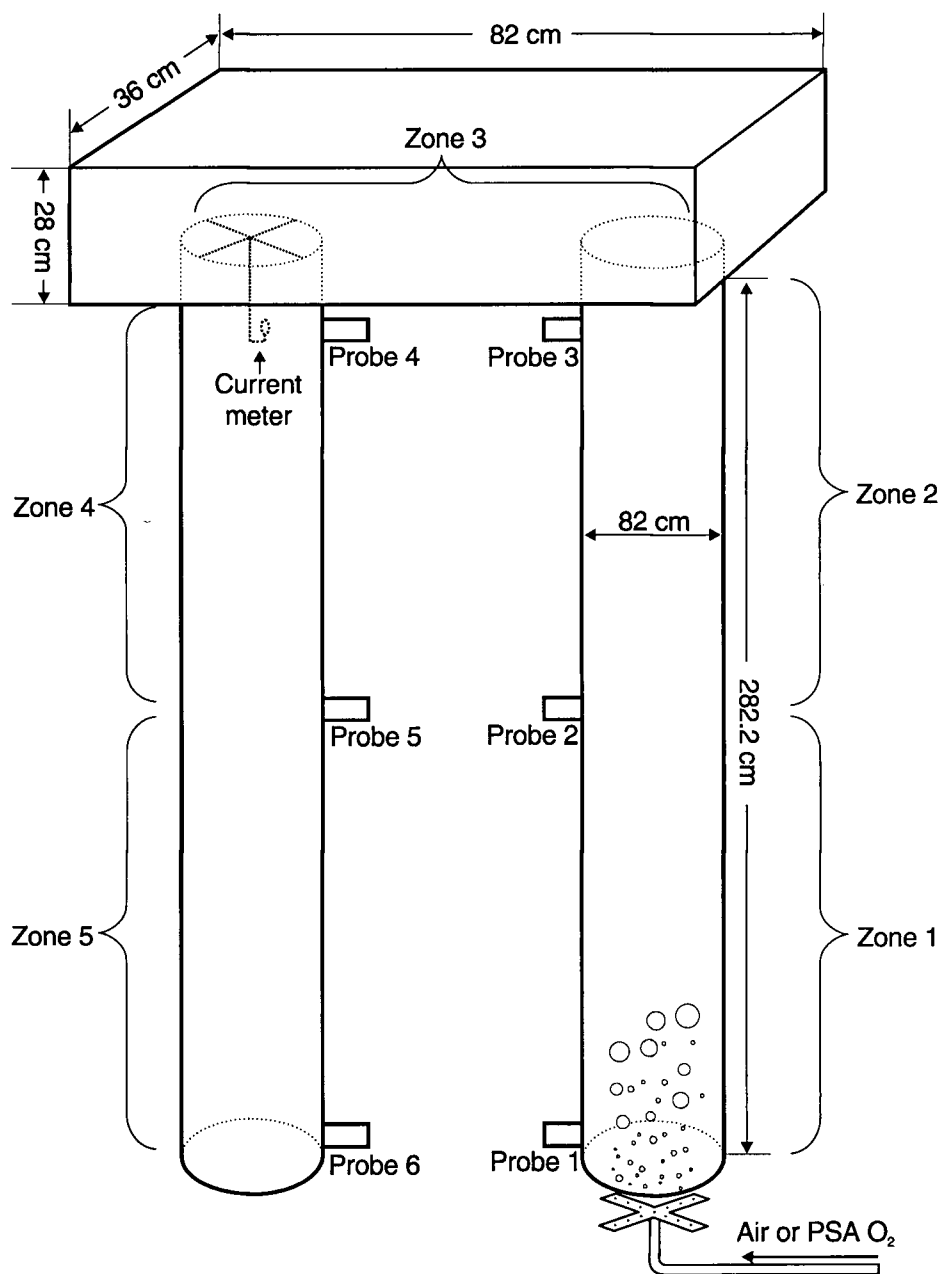
Figure 3.3. Schematic diagram of full lift aerator with probe location and aeration zones

the two tubes were effectively separated for a vertical distance of 200 cm, leaving 110.5 cm for

water exchange over the top of the divider. Dye tests indicated that the divider was an effective

barrier to short circuiting, as introduced dye could be seen travelling across the separator box,

down the outlet tube, then mixing around the bottom of the tank on the outlet tube side of the

tank as the dye was discharged into the bulk liquid. The dye would then move upwards over the

top of the divider, and flow towards the entrance of the inlet tube and into the inflow tube. The

oxygen probes confirmed the visual mixing pattern as the two submersible mixing pumps

(4,500 l hr^{-1}), located in diagonal corners on the tank floor, completely mixed the tank to < 1%

saturation, within an average of 2 minutes during actual tests (which was the same time period

observed to completely disperse the dye).

3.3.2   Probe Locations

The tubes were fitted with oxygen probe insertion ports near both ends of the tubes, and at the

mid-point of each tube. The probes were numbered according to their position in the aerator

(see Figure 3.3):

Probe 1 – 8 cm from the inlet of the inflow tube, operating depth – 283 cm

Probe 2 - midpoint of the inflow tube, operating depth – 150 cm

Probe 3 - 8 cm from the outlet of the inflow tube, operating depth – 17 cm

Probe 4 - 8 cm from the inlet of the outflow tube, operating depth – 17 cm

Probe 5 – midpoint of the outflow tube, operating depth – 150 cm

Probe 6 - 8 cm from the outlet of the outflow tube, operating depth – 283 cm

Probe 7 was the % vol/vol probe, located in a probe cup on the manifold board (see Figure 3.2)

and Probe 8 was the temperature probe located at a depth of 3.0 m. The velocity sensor was

suspended on a wire frame in the centre of the downflow tube, 28 cm from the junction with the floor of the separator box (see Figure 3.3).

3.3.3   Diffuser Description

Four different diffusers were used in the full lift experiments. The fine pore diffusers were made of fused silica glass with a rated maximum orifice diameter of 140 μ (Model AS-8, Aquatic Ecosystems Inc., Apopka, FL) or 2 μ (Model MBD 600, Point Four Systems Inc., Richmond, B.C.) (Figure 3.4). Scanning electron micrographs (SEMs) of the diffusers confirmed the maximum pore size was in the stated size range (Ashley et. al., 1991). The external dimensions of the 140 μ diffusers were 7.6 cm L x 3.8 cm W x 3.8 cm D. Each diffuser weighed 0.18 kg and was fitted with a 6.4 mm hose nipple. The 2 μ diffuser was 70 cm L x 8.3 cm W x 2.8 cm D, and weighed 2.3 kg.

Two sizes of coarse bubble diffusers were used: 397 μ (0.4 mm) and 794 μ (0.8 mm) diameter pore size. The diffusers were made of 12.7 mm I.D. white Sch. 40 PVC pipe. The diffusers were cross-shaped, with four arms joining into a common center (Figure 3.5). The center was fitted with a 6.4 mm diameter nipple for attaching a 6.4 mm vinyl tubing airline. The outside diameter of the diffusers was 19 cm, and they fit within the inflow tube with 0.3 mm clearance on either side. The diffusers were suspended in the centre of the inflow tube with a 0.45 kg weight, to counter their positive buoyancy and to minimize their movement when discharging gas. Since the surface area of a circle increases four fold as the diameter is doubled, the number of orifices required in each diffuser to maintain an equivalent cross-sectional orifice discharge area was as follows:

Figure 3.4   **Photograph of 140 μ fine pore diffusers**
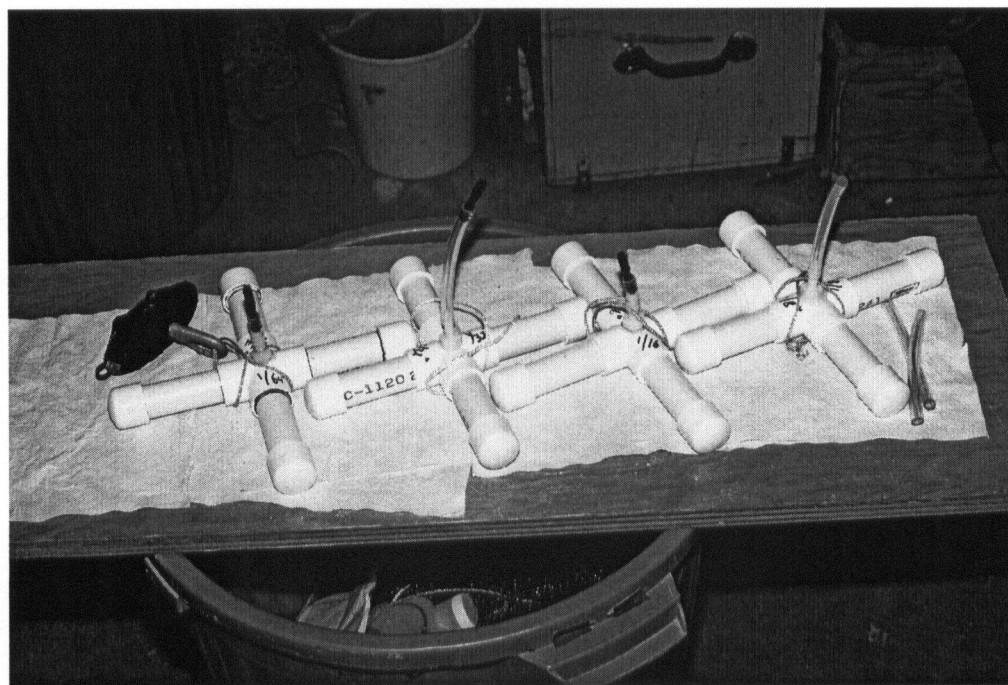
Figure 3.5.   **Photograph of 400 μ and 800 μ coarse bubble diffusers**

397 μ (0.4 mm) = 64 orifices (16 on each arm);

794 μ (0.8 mm) = 16 orifices (4 on each arm).

All three diffusers (140 μ, 397 μ and 800 μ) were suspended at two depths during the experiments: 1.5 m and 2.9 m. The 2 μ diffuser was positioned on the floor of the separator box, at a depth of 11 cm during the experiments, to introduce gas bubbles into the return flow of the outlet tube by the circulating water.

3.4   Experimental Design

The treatments examined in the full lift experiments were as follows:

1.   the effect of orifice pore diameter (140 μ, 400 μ and 800 μ);

2.   the effect of diffuser depth (1.5 and 2.9 m);

3.   the effect of gas flow rate (10, 20, 30 and 40) l min^{-1};

4.   the effect of oxygen partial pressure (air and PSA oxygen);

5.   the effect of a surface cover in the separator box (present or absent);

6.   the effect of a mid-depth inlet tube bubble screen (i.e., fine strand stainless steel mesh screen of 0.64 cm opening);

7.   the effect of mid-depth inlet tube counter-rotating blades (i.e., mechanical propeller blades that rotated with the upwelling water velocity);

8.   the effect of Downflow Bubble Contact Aeration (DBCA) in the outlet tube.

This resulted in a large number of possible treatment combinations. In order to examine all of the various combinations in a realistic time frame, the treatments were sub-divided into14 experimental groups; Group 1-6 being the "base case" study group where diffuser pore diameter, diffuser depth, gas flow rate and gas composition were examined. Groups 7-14 were variations on the "base case" conditions where various hypothesised "enhancements" (i.e.,

bubble screen, counter-rotating blades and Downflow Bubble Contact Aeration) and surface

cover were examined. The experiments in Groups 7-14 were conducted using only two orifice

pore diameters (140 μ and 800 μ) and one diffuser depth (2.9 m).

In addition, two miscellaneous groups were examined. In Misc. 1, the aeration system was

operated in DBCA mode with only the mixing pumps to circulate the water without the airlift

pump. In Misc. 2, the system was run for an extended period of time to determine how the

calculated oxygen saturation (i.e., C^*_s) compared to the measured oxygen saturation (i.e., C^*_m)

on air, and the % saturation achievable on oxygen. This resulted in 14 principal treatment

groups, and two minor treatment groups (Table 3.1).

Table 3.1.   **List of treatment groups for full lift hypolimnetic aeration experiments.**

Group No.	Gas flow (l min^{-1})	Orifice diameter (μ)	Depth (m)	Gas composition	Enhancements
1	10, 20, 30, 40	140	2.9	air/oxygen	n/a
2	10, 20, 30, 40	140	1.5	air/oxygen	n/a
3	10, 20, 30, 40	400	2.9	air/oxygen	n/a
4	10, 20, 30, 40	400	1.5	air/oxygen	n/a
5	10, 20, 30, 40	800	2.9	air/oxygen	n/a
6	10, 20, 30, 40	800	1.5	air/oxygen	n/a
7	10, 20, 30, 40	140	2.9	air/oxygen	DBCA
8	10, 20, 30, 40	800	2.9	air/oxygen	DBCA
9	10, 20, 30, 40	140	2.9	air/oxygen	Bubble screen
10	10, 20, 30, 40	800	2.9	air/oxygen	Bubble screen
11	10, 20, 30, 40	140	2.9	air/oxygen	Surface cover
12	10, 20, 30, 40	800	2.9	air/oxygen	Surface cover
13	10, 20, 30, 40	140	2.9	air/oxygen	Rotating blades
14	10, 20, 30, 40	800	2.9	air/oxygen	Rotating blades
Misc. 1	3	2	n/a	air/oxygen	Pump/DBCA
Misc. 2	10	2/140	2.9	air/oxygen	Extended/DBCA

The experiments were carried out in a randomised complete block design. Gas flow rate and

gas composition could be quickly altered during the experiments hence these two variables were

manipulated in each treatment group, while diffuser orifice diameter and diffuser depth (Groups 1-6) or diffuser orifice diameter, diffuser depth and enhancement (Groups 7-14) remained fixed. This resulted in eight possible combinations of gas flow rate x gas composition for each diffuser depth and orifice diameter. The experimental combinations were as follows (Tables 3.2-3.17):

Table 3.2. **Experimental combinations for Group 1.**

No.	Gas flow (l min^{-1})	Gas composition	Depth (m)	Orifice diameter (μ)
1	10	Air	2.9	140
2	10	PSA	2.9	140
3	20	Air	2.9	140
4	20	PSA	2.9	140
5	30	Air	2.9	140
6	30	PSA	2.9	140
7	40	Air	2.9	140
8	40	PSA	2.9	140

Table 3.3. **Experimental combinations for Group 2.**

No.	Gas flow (l min^{-1})	Gas composition	Depth (m)	Orifice diameter (μ)
1	10	Air	1.5	140
2	10	PSA	1.5	140
3	20	Air	1.5	140
4	20	PSA	1.5	140
5	30	Air	1.5	140
6	30	PSA	1.5	140
7	40	Air	1.5	140
8	40	PSA	1.5	140

Table 3.4. **Experimental combinations for Group 3.**

No.	Gas flow (l min^{-1})	Gas composition	Depth (m)	Orifice diameter (μ)
1	10	Air	2.9	400
2	10	PSA	2.9	400
3	20	Air	2.9	400
4	20	PSA	2.9	400
5	30	Air	2.9	400
6	30	PSA	2.9	400
7	40	Air	2.9	400
8	40	PSA	2.9	400

Table 3.5.   **Experimental combinations for Group 4.**

No.	Gas flow (l min^{-1})	Gas composition	Depth (m)	Orifice diameter (μ)
1	10	Air	1.5	400
2	10	PSA	1.5	400
3	20	Air	1.5	400
4	20	PSA	1.5	400
5	30	Air	1.5	400
6	30	PSA	1.5	400
7	40	Air	1.5	400
8	40	PSA	1.5	400

Table 3.6.   **Experimental combinations for Group 5.**

No.	Gas flow (l min^{-1})	Gas composition	Depth (m)	Orifice diameter (μ)
1	10	Air	2.9	800
2	10	PSA	2.9	800
3	20	Air	2.9	800
4	20	PSA	2.9	800
5	30	Air	2.9	800
6	30	PSA	2.9	800
7	40	Air	2.9	800
8	40	PSA	2.9	800

Table 3.7.   **Experimental combinations for Group 6.**

No.	Gas flow (l min^{-1})	Gas composition	Depth (m)	Orifice diameter (μ)
1	10	Air	1.5	800
2	10	PSA	1.5	800
3	20	Air	1.5	800
4	20	PSA	1.5	800
5	30	Air	1.5	800
6	30	PSA	1.5	800
7	40	Air	1.5	800
8	40	PSA	1.5	800

Table 3.8.   Experimental combinations for Group 7 (Downflow Bubble Contact
              Aeration).*

No.	Gas flow (l min⁻¹)	Gas composition	Depth (m)	DBCA	Orifice diameter (μ)
1	10 (7/3)	Air	2.9	Yes	2/140
2	10 (7/3)	PSA	2.9	Yes	2/140
3	20 (17/3)	Air	2.9	Yes	2/140
4	20 (17/3)	PSA	2.9	Yes	2/140
5	30 (27/3)	Air	2.9	Yes	2/140
6	30 (27/3)	PSA	2.9	Yes	2/140
7	40 (37/3)	Air	2.9	Yes	2/140
8	40 (37/3)	PSA	2.9	Yes	2/140

Table 3.9.   Experimental combinations for Group 8 (Downflow Bubble Contact
              Aeration).

No.	Gas flow (l min⁻¹)	Gas composition	Depth (m)	DBCA	Orifice diameter (μ)
1	10 (7/3)	Air	2.9	Yes	2/800
2	10 (7/3)	PSA	2.9	Yes	2/800
3	20 (17/3)	Air	2.9	Yes	2/800
4	20 (17/3)	PSA	2.9	Yes	2/800
5	30 (27/3)	Air	2.9	Yes	2/800
6	30 (27/3)	PSA	2.9	Yes	2/800
7	40 (37/3)	Air	2.9	Yes	2/800
8	40 (37/3)	PSA	2.9	Yes	2/800

Table 3.10.   Experimental combinations for Group 9 (Bubble screen).

No.	Gas flow (l min⁻¹)	Gas composition	Depth (m)	Screen	Orifice diameter (μ)
1	10	Air	2.9	Yes	140
2	10	PSA	2.9	Yes	140
3	20	Air	2.9	Yes	140
4	20	PSA	2.9	Yes	140
5	30	Air	2.9	Yes	140
6	30	PSA	2.9	Yes	140
7	40	Air	2.9	Yes	140
8	40	PSA	2.9	Yes	140

*7/3 refers to gas flow (l min⁻¹) to the diffuser in the inlet tube, and the 2 μ diffuser in the
separator box.

Table 3.11.   Experimental combinations for Group 10 (Bubble screen).

No.	Gas flow (l min^{-1})	Gas composition	Depth (m)	Screen	Orifice diameter (μ)
1	10	Air	2.9	Yes	800
2	10	PSA	2.9	Yes	800
3	20	Air	2.9	Yes	800
4	20	PSA	2.9	Yes	800
5	30	Air	2.9	Yes	800
6	30	PSA	2.9	Yes	800
7	40	Air	2.9	Yes	800
8	40	PSA	2.9	Yes	800

Table 3.12.   Experimental combinations for Group 11 (Surface cover).

No.	Gas flow (l min^{-1})	Gas composition	Depth (m)	SC	Orifice diameter (μ)
1	10	Air	2.9	Yes	140
2	10	PSA	2.9	Yes	140
3	20	Air	2.9	Yes	140
4	20	PSA	2.9	Yes	140
5	30	Air	2.9	Yes	140
6	30	PSA	2.9	Yes	140
7	40	Air	2.9	Yes	140
8	40	PSA	2.9	Yes	140

Table 3.13.   Experimental combinations for Group 12 (Surface cover).

No.	Gas flow (l min^{-1})	Gas composition	Depth (m)	SC	Orifice diameter (μ)
1	10	Air	2.9	Yes	800
2	10	PSA	2.9	Yes	800
3	20	Air	2.9	Yes	800
4	20	PSA	2.9	Yes	800
5	30	Air	2.9	Yes	800
6	30	PSA	2.9	Yes	800
7	40	Air	2.9	Yes	800
8	40	PSA	2.9	Yes	800

Table 3.14.   Experimental combinations for Group 13 (Counter-rotating blades).

No.	Gas flow (l min⁻¹)	Gas composition	Depth (m)	CRB	Orifice diameter (μ)
1	10	Air	2.9	Yes	140
2	10	PSA	2.9	Yes	140
3	20	Air	2.9	Yes	140
4	20	PSA	2.9	Yes	140
5	30	Air	2.9	Yes	140
6	30	PSA	2.9	Yes	140
7	40	Air	2.9	Yes	140
8	40	PSA	2.9	Yes	140

Table 3.15.   Experimental combinations for Group 14 (Counter-rotating blades).

No.	Gas flow (l min⁻¹)	Gas composition	Depth (m)	CRB	Orifice diameter (μ)
1	10	Air	2.9	Yes	800
2	10	PSA	2.9	Yes	800
3	20	Air	2.9	Yes	800
4	20	PSA	2.9	Yes	800
5	30	Air	2.9	Yes	800
6	30	PSA	2.9	Yes	800
7	40	Air	2.9	Yes	800
8	40	PSA	2.9	Yes	800

Table 3.16.   Experimental combinations for Group Misc. 1 (Pump only/DBCA).

No.	Gas flow (l min⁻¹)	Gas composition	Depth (m)	Pump/ DBCA	Orifice diameter (μ)
1	3	Air	n/a	Yes	2
2	3	PSA	n/a	Yes	2

Table 3.17.   Experimental combinations for Group Misc. 2 (Extended run/DBCA).

No.	Gas flow (l min⁻¹)	Gas composition	Depth (m)	ER/ DBCA	Orifice diameter (μ)
1	10 (7/3)	Air	2.9	Yes	2/140
2	10 (7/3)	PSA	2.9	Yes	2/140

Each of the combinations, within a principal treatment group (i.e., Groups 1-14), was randomly

assigned a number from 1 to 8. Each set of 8 combinations was completed, then repeated with a

different set of random numbers (Rohlf and Sokal, 1969). The purpose of this design was to

remove random error that may occur during any given treatment day. Each principle treatment was replicated 3 times, the minimum number of replicates recommended for non-steady state reaeration tests (ASCE, 1992). A total of 374 individual reaeration tests were completed for the full lift experiments (Table 3.18):

Table 3.18. **List of treatment combinations for the full lift hypolimnetic aeration experiments.**

Group No.	No. of combinations	Replicates	Total number of tests
1	8	3	24
2	8	3	24
3	8	3	24
4	8	3	24
5	8	3	24
6	8	3	24
7	8	3	24
8	8	3	24
9	8	3	24
10	8	3	24
11	8	3	24
12	8	3	24
13	8	3	24
13a (repeated)	8	3	24
14	8	3	24
		Sub-total	**360**
Misc. 1	1	7 O_2/3 air	10
Misc. 2	1	2 O_2/2 air	4
		Sub-total	**14**
		Total	**374**

3.4.1   Termination of Experiments

Each experimental test was terminated when the % saturation recorded at Probe 1 (i.e., the intake to the inlet tube, see Figure 3.3) reached 60% saturation. This represented the % oxygen saturation of the bulk water in the test tank at the end of the test run. The % saturation reading of the remaining probes within the full lift aerator were typically greater than 60% saturation, as

they were subject to the experimental combination being tested, which raised the % saturation above the ambient % saturation in the bulk tank water.

3.5   Downflow Bubble Contact Aerator (Speece Cone) Hypolimnetic Aerator

3.5.1   Aerator Dimensions

The Downflow Bubble Contact Aerator (DBCA) or "Speece Cone" was based on blueprint drawings of the first full sized DBCA which was installed in Newman Lake, WA in 1992 (Doke et al., 1995) (Figure 2.3). The unit was constructed by Burrard Mechanical Ltd. (North Vancouver, B.C.) and consisted of a submersible pump and intake port, a DBCA cone and an outlet port (Figure 3.6). The intake port was connected to the submersible pump by a length (40 cm) of clear 5.08 cm dia. vinyl hose. The aluminum housing portion of the intake port tapered from 5.08 cm dia. (entrance) to 6.35 cm dia. (exit) and turned 180° to connect to the top of the cone through a 6.35 cm dia. flange. The cone was 75 cm (H) x 34 cm (base dia.) with a clear acrylic viewing panel (12 cm x 30 cm) in the middle of the tapered portion of the cone. The lower section of the cone was 15 cm high, and the tapered upper section was 60 cm in height, terminating at the 6.35 cm diameter connection to the intake port. The outlet port was 25 cm in horizontal length, and 6.35 cm in diameter, with a 90° upward facing elbow at the distal end of the outlet port. The unit was constructed of aluminum, and was attached to a 80 cm x 34 cm base plate. The entire unit was lowered to the bottom of the tank by a pulley system, hence the depth of the intake port (Probe 5) and outlet port (Probe 6) was 239 cm and 295 cm respectively, and the operating depth of the cone ranged from 310.5 cm (cone bottom) to 235.5 cm (cone top).
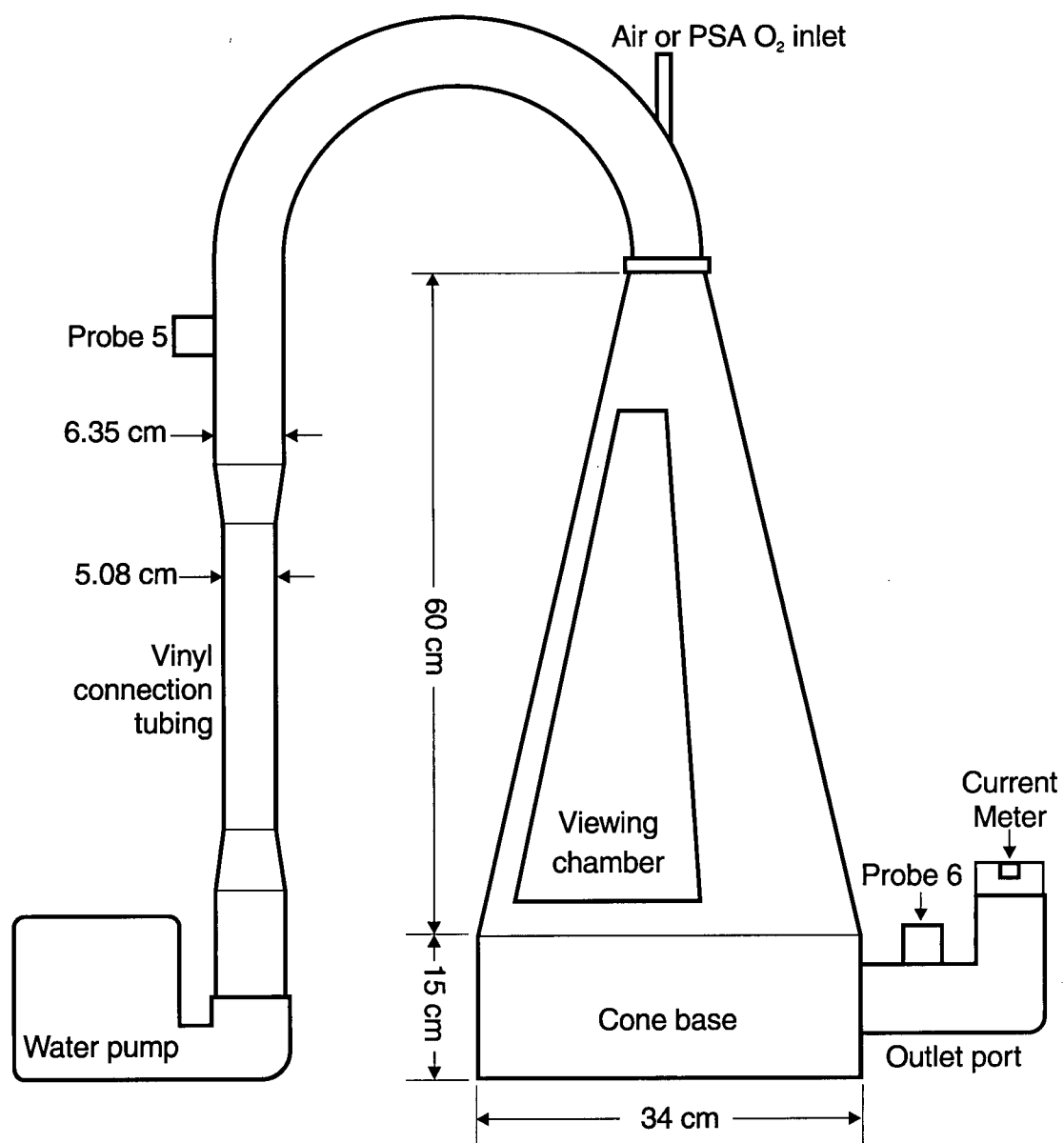
Figure 3.6. **Schematic of Speece Cone aerator with probe locations**

3.5.2   Tank Mixing and Configuration of Submersible Pumps

The same divider used in the full lift experiments (clear 6 mm acrylic, 200 cm H x 38 cm W) was inserted into the tank, to prevent short circuiting of water discharged from the cone outlet port. The separator was positioned on the upper surface of the outlet port between the cone and the 90° elbow of the outlet port, effectively separating the outlet and intake ports over a vertical distance of 200 cm (leaving 110.5 cm for water exchange over the top of the divider). Dye tests indicated the diverter plate was an effective barrier to short circuiting, as dye could be seen discharging from the outlet port, moving upwards on the outlet side of the divider plate, then over the top of the plate and down to the main submersible pump.

Initial dye tests indicated the bulk water in the tank was not mixing as quickly as with the full lift hypolimnetic aeration system, as the airlift pump was not operating. Therefore, the location of the two 4,500 l hr^{-1} submersible pumps was changed so that both pumps were positioned on the tank floor, on the outlet side of the divider, discharging vertically at depths of 1.22 m and 2.02 m. In addition, a third 4,500 l hr^{-1} submersible pump was added near the surface on the inlet side, and oriented so that it discharged vertically downwards at a depth of 0.85 m. The main circulating pump for the Speece Cone was a 10,400 l hr^{-1} submersible pump (Little Giant 6-CIM-R) connected to a Variac voltage control unit that allowed pump voltage to be varied from 0 to 110% of rated power. Dye tests and the oxygen probes confirmed the tank (1,194 l) was adequately mixed with all four pumps operating (maximum pumping rate = 23,900 l hr^{-1}), since the oxygen saturation throughout the tank was reduced to < 1% within an average of 3 minutes, following the addition of a sodium sulfite solution.

3.5.3   Probe Locations

The velocity sensor for the Speece Cone was positioned in the centre of the discharge flow, 10

cm from the end of the outlet port. The oxygen probes were arranged in the tank to ensure the

tank was completed mixed, as incomplete tank mixing tank invalidates the non steady-state

reaeration test (ASCE, 1992). The probes were numbered according to their position in the tank

and the Speece Cone (Figure 3.6):

Probe 1 – suspended in the tank at 1.5 m;

Probe 2 - suspended in the tank at 0.5 m;

Probe 3 - suspended in the tank at 1.0 m;

Probe 4 - suspended in the tank at 2.0 m;

Probe 5 - inlet to the Speece Cone, operating depth – 2.39 m

Probe 6 - outlet to the Speece Cone, operating depth – 2.95 m.

The remaining two probes were identical to the full lift experiments, i.e., Probe 7 was the %

vol/vol probe, located in a probe cup on the manifold board and Probe 8 was the temperature

probe located at a depth of 3.0 m (see Figure 3.2).

3.5.4   Diffuser Description

There was no diffuser fitted to the Speece Cone. Oxygen entered the cone at an operating depth

of 2.3 m, immediately downstream of the 180° elbow in the inlet port, through a 6.4 mm brass

fitting and hose nipple connected to the PSA unit (Figure 3.6).

3.6   Experimental Design

The treatments examined in the Speece Cone experiments were as follows:

1.   the effect of oxygen flow rate (1, 2 and 3) $l\ min^{-1}$;

2.   the effect of cone discharge velocity (20, 30, 40, 50, 60 and 70 cm sec^{-1}). This was equivalent to pumping rates of 38, 57, 76, 95, 114, and 133 $l\ min^{-1}$.

The treatments were arranged into 6 experimental groups, in which the depth of the Speece Cone (i.e., max. tank depth) and gas mixture (i.e., PSA generated oxygen) remained constant while gas flow rate and discharge velocity were varied. In addition, one miscellaneous group was examined where the Speece Cone was operated on compressed air at 3 $l\ min^{-1}$ at a discharge velocity of 50 cm sec^{-1}. This resulted in 6 principal treatment groups, and one minor treatment group (Table 3.19):

Table 3.19.   **List of treatment groups for Speece Cone experiments.**

Group No.	Discharge velocity (cm sec^{-1})	PSA O_2 flow rate ($l\ min^{-1}$)
15	20	1, 2, 3
16	30	1, 2, 3
17	40	1, 2, 3
18	50	1, 2, 3
19	60	1, 2, 3
20	70	1, 2, 3
Misc. 1	50	3 (air)

The experiments were carried out in a randomized complete block design. This resulted in three combinations of gas flow rate x discharge velocity. Each set of 3 combinations was completed, then repeated with a different set of random numbers. The purpose of this design was to remove random error that may occur during any given treatment day. Each treatment was replicated 4

times, 3 being the minimum replicate recommended for non-steadystate reaeration tests (ASCE, 1992). A total of 76 individual reaeration tests were completed (Table 3.20).

Table 3.20. **List of treatment combinations for Speece Cone experiments.**

Group No.	No. of combinations	Replicates	Total number of tests
15	3	4	12
16	3	4	12
17	3	4	12
18	3	4	12
19	3	4	12
20	3	4	12
		Sub-total	72
Misc. 1	1	4	4
		Sub-total	4
		Total	76

3.6.1   Termination of Experiments

Each experimental test was terminated when the % saturation recorded at Probe 5 (see Figure 3.6) reached 65% saturation. This represented the lowest % oxygen saturation of the bulk water in the test tank at the termination of the test run. The % saturation reading of the remaining probes within the tank and Speece Cone were typically greater than 65% saturation, since they were subject to the experimental combination being tested and influence of the tank divider (which raised the % saturation above the average % saturation in the bulk water on the inlet side). The % saturation recorded at Probe 5, following 2 minutes of pump circulation with zero oxygen flow, was then used to represent the terminal % oxygen saturation for the experiment. This value was always > 65% saturation due to the averaging effect of oxygenated water displaced from the Speece Cone and oxygenated water from the outlet side of the tank.

3.7 Bubble Size Measurement

Bubble size was determined by photographing rising bubbles in the tank with a 35 mm camera and flash attachment, synchronized at 1/100 second. A meter ruler graduated in 1 mm increments was suspended in the tank and bubbles were photographed against the ruler for scale. The 35 mm slides were then examined with a Wild dissecting microscope at 25x using an ocular micrometer to determine bubble size.

A minimum of 30 bubbles was counted for each orifice size and gas flow rate setting. Only bubbles that were located between the cylinder wall and the ruler, and were either on or touching the ruler were used for measurement. A spreadsheet program was written to calculate the volume of the bubbles. Since many bubbles were oblate spheriod in shape, the following formula was used to calculate volume:

(3.3) $$V = 4/3\ \pi a^2 b$$

Where:

V = volume in mm^3;

a = ½ long axis of the bubble (mm);

b = ½ short axis of the bubble (mm);

The equivalent diameter of the bubbles was calculated according to:

(3.4) $$d = \sqrt{\frac{6v}{\pi}}$$

where:

d = equivalent diameter (mm);

V = volume in mm^3.

The mean bubble size, standard deviation and coefficient of variation was also calculated for each orifice size and gas flow rate.

3.8 Electrical measurements and power calculations

The electrical current and line voltage for the PSA unit and Speece Cone main pump was measured with a Data Hold digital clamp meter (Model DM 266) and Fluke digital multi-meter. PSA current draw was measured during oxygen production and nitrogen venting cycles, and the average measured amperage (i.e., 0.15 amp) was multiplied by the line voltage (i.e., 110 volts) to determine the energy requirement of the PSA unit (i.e., 16.5 watts). The Speece Cone main pump power requirements were calculated by taking the average of two amperage readings and three voltage readings at each 0.5 increment on the Variac voltage control unit (0-100 scale) from 65 to 85. During the Speece Cone tests, the Variac voltage control unit setting at the end of each test was recorded, and the mean setting determined for each measured water discharge velocity x gas flow combination (i.e, 4 readings). A linear regression of control unit setting and measured energy consumption was then calculated, and the resulting equation used to predict the energy consumption for each of the mean water discharge velocity settings used in the Speece Cone tests (Figure 3.7). The regression equation is as follows:

(3.5) $y = 0.0153x - 0.3386$; $r^2 = 0.99$

where: y = kW energy consumption of the Speece Cone main pump;

x = Variac voltage control unit setting

Speece Cone Power Consumption $y = 0.0153x - 0.3386$
                                      $R^2 = 0.9857$
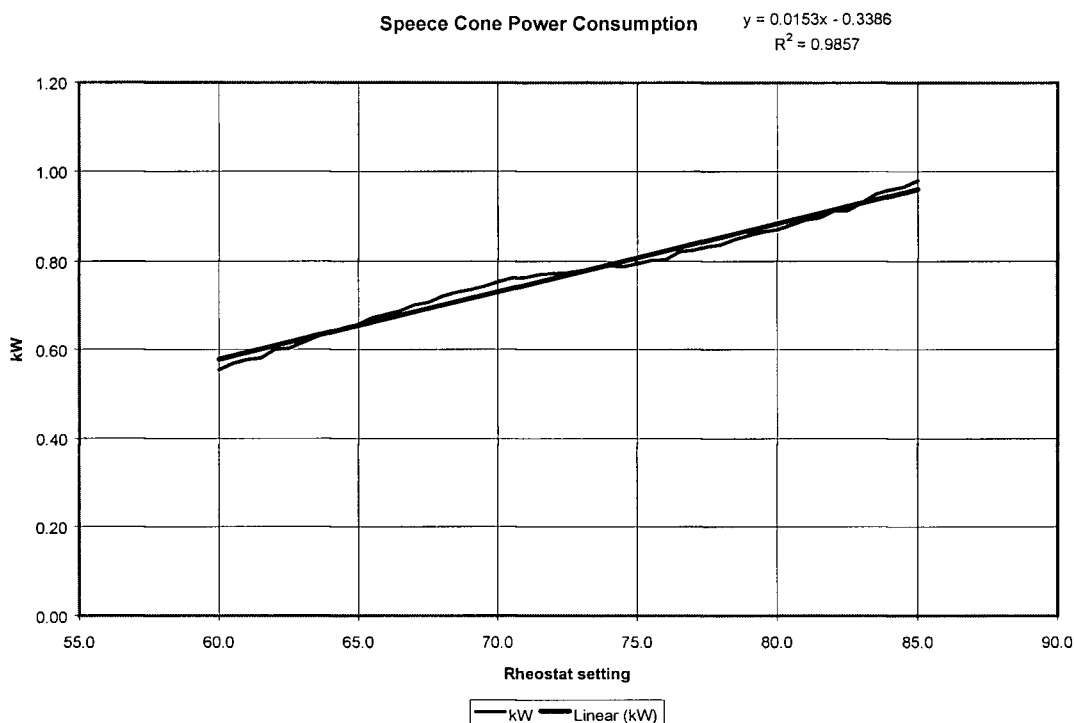
Figure 3.7.   Speece Cone main water pump power consumption vs. rheostat setting

3.9   Parameter Estimation Procedure

The log deficit method of parameter estimation was used to determine K_La as the experimental

tests were terminated at 60-65% saturation, due to the time impracticality of running all tests to

98% of saturation, as is mandatory for the nonlinear regression method of parameter estimation

(ASCE, 1992). The nonlinear regression method is the recommended ASCE method of pa-

rameter estimation for the measurement of oxygen transfer in clean water; "however, if the

engineer/owner so specifies, the log deficit method described in Annex E shall be permitted in

lieu of the nonlinear regression method." (ASCE, 1992).

Prior to adopting the log deficit method, a comparative analysis of K_La and SOTR was conducted for one group of the full lift experiments (i.e., Group 5) on air and PSA generated oxygen using three methods of parameter estimation: the nonlinear regression method, the log deficit method and a "mass balance" method. The mass balance method used the weighted oxygen values of all six oxygen probes and calculated the mass of oxygen in the test tank at each time stamp of the data logger. The SOTR derived from the log deficit method and nonlinear regression method were compared with the SOTR derived from the actual mass balance method. The results indicated the log deficit method was more accurately associated with the mass balance method than the nonlinear regression method. In addition, a number of other problems were found with the nonlinear regression method:

1. the nonlinear regression method was very sensitive to low end truncation, and required up to 18-20% low end truncation in order to get convergence and minimize the sum of squares. Since the tests were terminated at 60-65% saturation, this deleted too much of the experimental data set;

2. unique estimates of K_La could be obtained simply by selecting different low end truncation points;

3. the nonlinear estimation method did not give realistic results for some probes when calculating K_La for all 6 probes;

4. the nonlinear estimation method did not give realistic results when calculating K_La for the experiments using PSA generated oxygen.

In comparison, the log deficit method exhibited minimal sensitivity to low end truncation, worked for all six probes and derived realistic estimates from the experiments using PSA oxygen. The log deficit method is the recommended technique for parameter estimation within the aquacultural and aquatic sciences community (Boyd, 1986; Boyd and Watten, 1989) and was listed as a tentative standard in the 15th Edition of Standard Methods (APHA, 1980).

Therefore, the log deficit method of parameter estimation was selected to determine K_La for these experiments.

K_La_T was calculated according to:

$$(3.6) \qquad K_La_T = \frac{\ln [(C_s^*-C_1)/C_s^*-C_2)]}{t_2-t_1}$$

where:

K_La_T = oxygen transfer coefficient at the temperature of the test water (hr^{-1});

$\ln$ = natural logarithm;

C_s^* = the dissolved oxygen air-solubility value ($mg\ l^{-1}$) for the ambient barometric pressure, temperature and vapor pressure of water;

C_1 = dissolved oxygen concentration at time t_1 ($mg\ l^{-1}$);

C_2 = dissolved oxygen concentration at time t_2 ($mg\ l^{-1}$);

t_1 = time at point 1 on the semi-logarithmic plot (hr);

t_2 = time at point 2 on the semi-logarithmic plot (hr);

T_1 and t_2 are usually chosen as the times at which the measured oxygen concentration is 20% (t_1) and 80% (t_2) of the saturation value for the test water, corrected for temperature, barometric pressure and vapor pressure of water. This study used approx. 10% (t_1) and 60% (t_2) (full lift experiments) and 65% (t_2) (Speece Cone experiments) saturation values for t_1 and t_2 since a sufficient number of data points (i.e., 11) was collected and it was not practical, from a time perspective, to run each test to 80% saturation.

K_La_T was corrected to K_La_{20} according to (ASCE, 1992):

(3.7) $$K_La_{20} = K_La_T\theta^{(20-T)}$$

where:

T = test water temperature in ^oC;

$\theta = 1.024$.

SOTR was calculated as:

(3.8) $$SOTR = K_La_{20}\ C_{s20}\ V$$

where:

SOTR = standard oxygen transfer rate (g O_2 hr^{-1});

K_La_{20} = oxygen transfer coefficient at 20 ^oC (hr^{-1});

C_{s20} = dissolved oxygen concentration (mg l^{-1}) at saturation for 20 ^oC and standard pressure (760 mm Hg);

V = volume of water in the tank (m^3);

Standard Aeration Efficiency (SAE) was calculated as:

(3.9) $$SAE = SOTR/power\ input$$

where:

SAE = standard aeration efficiency (g O_2 $kWhr^{-1}$);

SOTR = standard oxygen transfer rate (g O_2 hr^{-1});

Power input (kW) = total delivered power (kW).

The calculation of power input for the various experimental treatments is described in the next section.

3.9.1   Full Lift Experiments

For the full lift hypolimnetic aeration experiments, Groups 1-14, on air, the power input was

separated into two components. The first component, E_1, is the *delivered blower power* which

is the "theoretical power required at a blower discharge to deliver a given mass flow of gas at a

given discharge pressure, calculated based upon adiabatic compression" (ASCE, 1992). On air,

this pressure was taken as the absolute delivery pressure from the manifold board regulator (i.e.,

4.2 kg cm^{-2}). The second component, E_2, is the same adiabatic compression formula adjusted to

the absolute ambient hydrostatic pressure of gas release (i.e., 1.5 or 2.9 m), rather than the

absolute delivery pressure at the manifold board. The sum of E_1 and E_2 equals the *total deliv-

ered power* (ASCE, 1992) (Table 3.21).

**Table 3.21.   Summary of energy calculations for full lift hypolimnetic aerator
experiments.**

Treatment	E_1	E_2	E_3	E_4
Full lift – air	Adiabatic compression @ 4.2 kg cm^{-2}	Adiabatic compression @ 1.5 or 2.9 m depth		.
Full lift – PSA	Adiabatic compression @ 7.36 kg cm^{-2}	Adiabatic compression @ 1.5 or 2.9 m depth	Average PSA measured *wire power*	
Full lift, pump only – air	Adiabatic compression @ 4.2 kg cm^{-2}	Adiabatic compression = 0	Average measured wire power of the two 4,500 l hr^{-1} submersible mixing pumps	
Full lift, pump only – PSA	Adiabatic compression @ 7.36 kg cm^{-2}	Adiabatic compression = 0	Average PSA measured *wire power*	Average measured wire power of the two 4,500 l hr^{-1} submersible mixing pumps
Full lift – extended aeration – air	Adiabatic compression @ 4.2 kg cm^{-2}	70% of adiabatic compression @ 2.9 m depth		
Full lift – extended aeration – PSA	Adiabatic compression @ 7.36 kg cm^{-2}	70% of adiabatic compression @ 2.9 m depth	Average PSA measured *wire power*	

The delivered blower power was calculated according to the adiabatic compression formula (ASCE, 1992):

$$(3.10) \qquad P_w = wRT_1/29.7ne[(p_2/p_1)^{0.283}-1]$$

where:

P_w = power input (kW);

w = weight of air flow ($kg\ s^{-1}$) (i.e., $1.2927\ g\ l^{-1}$);

R = engineering gas constant for air = 8.314 kJ/k mol ^{o}K;

T_1 = absolute inlet temperature before compression (^{o}K);

p_1 = absolute inlet pressure before compression = $1.03\ kg\ cm^{-2}$;

p_2 = absolute inlet pressure after compression = $4.2\ kg\ cm^{-2}$;

n = (k-1)/k = 0.283 for air (and oxygen);

k = 1.395 for air (and oxygen);

29.7 = constant for SI conversion;

e = compressor efficiency = 0.80.

For the full lift hypolimnetic aeration experiments, Groups 1-14, on PSA generated oxygen, the power input was separated into three components plus an expansion factor for the weight of air flow (i.e., w; $kg\ s^{-1}$) based on the published air input/oxygen output ratio of the AirSep AS-20 unit (i.e., 15.9:1). The first component, E_1, is the delivered blower power required to deliver the mass flow of gas at the absolute minimum pressure requirement of the PSA unit ($7.36\ kg\ cm^{-2}$). The second component, E_2, is the same adiabatic compression formula adjusted to the absolute ambient hydrostatic pressure of gas release (i.e., 1.5 or 2.9 m), rather than the absolute minimum

pressure requirement of the PSA unit. The third component, E_3, is the average measured *wire power* of the AirSep AS-20 PSA unit (i.e., 0.0165 kW). The sum of E_1, E_2 and E_3 equals the total delivered power (Table 3.21).

For the full lift hypolimnetic aeration experiments, Pump Only, on air, the power input was separated into three components. The first component, E_1, is the delivered blower power based upon adiabatic compression, from the manifold. The second component, E_2, is the same adiabatic compression formula adjusted to the absolute ambient hydrostatic pressure of gas release at the surface (i.e., 11 cm) via the 2 μ diffuser, hence this energy component is reduced to zero. The third component is the average measured wire power of the two 4,500 l hr^{-1} submersible mixing pumps (i.e., 0.76 kW). The sum of E_1, E_2 and E_3 equals the total delivered power (Table 3.21).

For the full lift hypolimnetic aeration experiments, Pump Only, on PSA generated oxygen, the power input was separated into four components plus an expansion factor for the weight of air flow (w; kg s^{-1}) based on the published air input/oxygen output ratio of the AirSep AS-20 PSA unit (i.e., 15.9:1). The first component, E_1, is the delivered blower power required to deliver the mass flow of gas at the absolute minimum pressure requirement of the PSA unit (7.36 kg cm^{-2}). The second component, E_2, is the same adiabatic compression formula adjusted to the absolute ambient hydrostatic pressure of gas release at the surface (i.e., 11 cm) via the 2 μ diffuser, hence this energy component is reduced to zero. The third component is the averaged measured wire power of the two 4,500 l hr^{-1} submersible mixing pumps (i.e., 0.76 kW). The fourth component, E_4, is the average measured wire power of the AirSep PSA unit (i.e., 0.0165 kW). The sum of E_1, E_2, E_3 and E_4 equals the total delivered power (Table 3.21).

For the full lift hypolimnetic aeration experiments, Extended Aeration, on air, the power input was separated into two components. The first component, E_1, is the delivered blower power based upon adiabatic compression, from the manifold. The second component, E_2, is the same adiabatic compression formula adjusted to different absolute ambient hydrostatic pressures according to the depth of gas release (i.e., 0.08 m and 2.9 m), and the compression energy proportioned to the two gas flow rates (i.e., 70% to 2.9 m and 30% to 0.08 m). Since the absolute ambient hydrostatic pressure of gas release at the surface (i.e., 11 cm) via the 2 μ diffuser was so small, 30% of the E_2 energy component was reduced to zero. The sum of E_1 and E_2 equals the total delivered power (Table 21).

For the full lift hypolimnetic aeration experiments, Extended Aeration, on PSA generated oxygen, the power input was separated into three components plus a correction factor for the weight of air flow (i.e., w; kg s^{-1}) based on the published air input/oxygen output ratio of the AirSep AS-20 unit (i.e., 15.9:1). The first component, E_1, is the delivered blower power required to deliver the mass flow of gas at the absolute minimum pressure requirement of the compressor (7.36 kg cm^{-2}). The second component, E_2, is the same adiabatic compression formula adjusted to different absolute ambient hydrostatic pressures according to where the gas was released (i.e., 0.08 m and 2.9 m), and the compression energy proportioned between the two gas flow rates (i.e., 70% to 2.9 m and 30% to 0.08 m). Since the absolute ambient hydrostatic pressure of gas release at the surface (i.e., 11 cm) via the 2 μ diffuser was so small, 30% of the E_2 energy component was reduced to zero. The third component, E_3, is the average measured wire power of the AirSep PSA unit (i.e., 0.0165 kW). The sum of E_1, E_2 and E_3 equals the total delivered power (Table 3.21).

3.9.2   Speece Cone Experiments

For the Speece Cone experiments, Groups 15-20, on PSA generated oxygen, the power input

was separated into four components plus an expansion factor for the weight of air flow (i.e., w;

kg s^{-1}) based on the published air input/oxygen output ratio of the AirSep AS-20 PSA unit (i.e.,

15.9:1). The first component, E_1, is the delivered blower power required to deliver the mass

flow of gas at the absolute minimum pressure requirement of the PSA unit (7.36 kg cm^{-2}). The

second component, E_2, is the same adiabatic compression formula adjusted to the absolute

ambient hydrostatic pressure of gas release (i.e., 2.9 m) rather than the absolute minimum

pressure requirement of the PSA unit. The third component, E_3, is the average measured wire

power of the main Speece Cone pump, as derived from the linear regression equation between

control unit setting and measured energy consumption (i.e., Eqn. 3.5; see Figure 3.7). The

fourth component, E_4, is the average measured wire power of the AirSep As-20 PSA unit (i.e.,

0.0165 kW). The sum of E_1, E_2, E_3 and E_4 equals the total delivered power (Table 3.22).

Table 3.22. Summary of energy calculations for Speece Cone experiments

Treatment	E_1	E_2	E_3	E_4
Speece Cone – PSA	Adiabatic compression @ 7.36 kg cm^{-2}	Adiabatic compression @ 2.9 m depth	Average measured wire power of main circulation pump	Average PSA measured *wire power*
Speece Cone – air	Adiabatic compression @ 4.2 kg cm^{-2}	Adiabatic compression @ 2.9 m depth	Average measured wire power of main circulation pump	

For the Speece Cone experiments, Group 21, on air, the power input was separated into three

components. The first component, E_1, is the delivered blower power based upon adiabatic

compression, from the manifold board regulator (i.e., 4.2 kg cm^{-2}). The second component, E_2,

is the same adiabatic compression formula adjusted to the absolute ambient hydrostatic pressure

of gas release (i.e., 2.9 m). The third component, E_3, is the average measured wire power of the

main Speece Cone pump derived from the linear regression equation between control unit

setting and measured energy consumption (i.e., Eqn. 3.5, see Figure 3.7). The sum of E_1, E_2 and

E_3 equals the total delivered power (Table 3.22).

SOTE was calculated as:

(3.11) $$SOTE = SOTR/W_{O2}$$

where:

SOTE = standard oxygen transfer efficiency (%);

SOTR = standard oxygen transfer rate (g O_2 hr^{-1});

W_{O2} = mass flow rate of oxygen in the gas flow stream (g O_2 hr^{-1}).

The calculation of W_{O2} for the various experimental treatments was as follows:

For the Full lift and Speece Cone treatments on air, W_{O2} was calculated as the measured gas

flow (l min^{-1}) (corrected for pressure and density) multiplied by the weight of oxygen in air (0.3

g l^{-1}) and converted to g O_2 hr^{-1} (see Eqn. 3.12):

(3.12) $$W_{O2\ air}\,(g\ O_2\ hr^{-1}) = gas\ flow\ (l\ min^{-1}) \times 0.3\ g\ l^{-1} \times 60\ min\ hr^{-1}$$

For the Full lift and Speece Cone treatments on PSA generated oxygen, W_{O2} was calculated as

the sum of (1) the measured gas flow (l min^{-1}) (corrected for pressure and density) multiplied by

the % of oxygen in the PSA gas (approx. 95 %) as determined by the average reading from

Probe 7 for each individual test times the weight of pure oxygen (1.4286 g l^{-1}) and converted to

g O_2 hr^{-1} and (2) the measured gas flow (l min^{-1}) (corrected for pressure and density) multiplied

by the % of air in the PSA gas (approx. 5%) times weight of oxygen in air (0.3 g l^{-1}) and converted to g O_2 hr^{-1} (see Eqn. 3.13):

(3.13) $W_{O2\ PSA}$ (g O_2 hr^{-1}) = [gas flow (l min^{-1}) x % O_2 x 1.4286 g l^{-1} x 60 min hr^{-1}] + [gas flow (l min^{-1}) x % air x 0.3 g l^{-1} x 60 min hr^{-1}]

3.9.3   Statistical Analysis

The statistical model used to analyze the experimental data was the General Linear Model (i.e., GLM) in the SYSTAT™ 10 statistical package. This model can estimate any univariate or multivariate general linear model, including analysis of variance or covariance (Wilkinson and Coward, 2000). The level of significance was set at $\alpha = 0.01$ for each statistical test. The first step in the analysis was to plot a frequency distribution of K_La_{20}, SOTR, SAE and SOTE to determine if the values were normally distributed. An initial box and whisker plot of the covariate and treatments (e.g., gas flow rate, diffuser depth, gas composition and orifice diameter) was then plotted against K_La_{20}, SOTR, SAE and TE to examine for outliers. A total of four extreme outliers were detected in the 336 trials conducted in the Group 1-14 tests and no outliers were detected in the 72 trials conducted in the Group 15-20 tests. These outliers were a result of equipment malfunction during the tests and were deleted from the data set, resulting in a rejection rate of 0.98%.

The approach used in the statistical analysis was to analyze individual groups of experiments which were designed to test for a particular treatment effect (e.g., effect of depth of gas release; effect of oxygen partial pressure; effect of orifice diameter) as a function of gas flow rate. This resulted in a basic analysis of covariance with first order interactions (e.g., depth by gas flow rate). An alternate approach would have been to develop one large model to analyze all of the data; however, this would have resulted in a 4 (gas flow rates) x 3 (orifice sizes) x 2 (depths) x 2

(% oxygen) matrix design, which would contain first, second and third order interaction effects. Since the experiments were designed as series of discrete tests to be of relevance to the practicing engineer, the basic model approach was used.

An initial analysis of covariance model was then used to determine if there was any significant interaction between the covariate (i.e., gas flow rate for the full lift system, and velocity of water discharge for the Speece Cone) and the experimental treatments. The assumption of parallelism, or homogeneity of slopes, is an important underlying assumption of the analysis of covariance model. The analysis generally indicated a significant interaction effect for K_La_{20} and SOTR, and occasionally for SAE and SOTE. The residuals were then plotted to determine the heterogeneity of the error variance. The residual plots indicated a linear model was appropriate for the data; however, in the majority of cases, the plotted residuals assumed a "right megaphone" shape of distribution. This type of error distribution occurs where an intrinsically positive response varies over a wide range, as the smaller responses have less "room" to vary than larger responses (Weisberg, 1980). As a result of the observed heterogeneity of variance, a variance stabilization transformation was applied to K_La_{20}, SOTR, SAE and SOTE. The logarithm is the most commonly used variance stabilizing transformation, and is appropriate when the error standard deviation is a percentage or proportion of the response (Weisberg, 1980). The analysis of covariance model was then re-run with the log-transformed data to examine for homogeneity of slopes in the form:

(3.14)   model y = constant + treatment + x + treatment*x

If the probability (i.e., p) value of the treatment by covariate interaction was >0.01, the assumption of homogeneity of slopes was accepted, and the model was re-run without the interaction term in the form:

(3.15)   model y = constant + treatment + x

An additional benefit of log transforming the data is that it allows interaction effects, which are multiplicative when observed in the untransformed data, to be converted into an additive effect (which is a prerequisite for quantification with the general linear model). This is obtained by calculating the difference between the adjusted least square mean estimates for the treatment effect, and converting the exponent value back to the untransformed value. In the situations where only two treatment effects were being analysed (i.e., gas composition and depth of air release), the statistical analysis was complete at this stage.

In situations where there were no significant interaction effects, the null hypothesis was rejected and there was more than one treatment effect being analyzed (i.e., orifice size or the effect of full lift modifications), then Scheffe's test was used as the comparison among means test. Scheffe's test is designed to allow all possible linear combinations of group means to be tested. The result is that Scheffe's test is more conservative than other tests, and a larger difference is required to obtain a significant result (Wilkinson and Coward, 2000). Scheffe's test is the most rigorous *a posteriori* test, and is recommended by statistical purists for comparison among means tests (Larkin, 1975).

In situations where significant interaction effects remained after log transformation, the analysis was re-run by removing the particular treatment which exhibited the interaction, and the remaining data analyzed with Scheffe's test. The treatment responsible for the significant interaction effect, and the nature of the interaction was then described and no further statistical analysis conducted.

The protocol adopted for presenting the results is to use the untransformed data to describe the observed value of the adjusted least squares mean for a particular treatment effect. However, when a significant treatment or interaction effect was detected, the transformed data was used to determine the level of significance in the covariance analysis, in Scheffe's comparison among means test, and to quantify the nature of the interaction effect, if appropriate.

CHAPTER 4: RESULTS

4.1 Full Lift Hypolimnetic Aeration – Oxygen Transfer

4.1.1 Depth Effect

This component of the experiment examined the effect of gas flow variation (10 to 40 l min^{-1}) at

two diffuser depths (1.5 m and 2.9 m) in the full lift inlet tube, using air and PSA oxygen at

three different orifice diameters (140 μ, 400 μ and 800 μ). Within each subset of experiments,

the orifice diameter and diffuser depth were held constant, while the gas flow rate and oxygen

content (i.e., air or PSA oxygen) were varied.

4.1.1.1   140 μ diffuser x air   (Note: compares the 140 μ diffuser on air at 1.5 and 2.9 m.

The results for the analysis of covariance for the 140 μ diffuser operating on compressed air are

shown in Table 4.1. Significant results (α ≤ 0.01) were obtained for the depth treatment and

flow rate covariate effect for K_La_{20}, SOTR, SAE and SOTE (Figure 4.1 a-d) with all parameters

increasing in value with depth of gas release. A significant depth x flow rate interaction effect

was observed for K_La_{20} and SOTR (Table 4.1).

Table 4.1.   **Adjusted least squares means (± SE), treatment and interaction effects for the 140 μ diffuser on air at 1.5 m or 2.9 m depth.**

Treatment	K_La_{20} (hr^{-1})	SOTR (g O_2 hr^{-1})	SAE (g O_2 kWhr^{-1})	SOTE (%)	n
1.5 m	2.1 (0.09)	23.2 (0.95)	227.2 (7.39)	5.2 (0.18)	12
2.9 m	3.3 (0.09)	35.7 (0.95)	323.8 (7.39)	7.9 (0.18)	12
Interaction	Yes, 1.52	Yes, 1.52	No	No	
Depth	sig, p = 0.000	sig, p = 0.000	sig, p = 0.000	sig, p = 0.000	
Flow rate	sig, p = 0.000	sig, p = 0.000	sig, p = 0.000	sig, p = 0.000	

The significant depth x flow rate interaction effect indicates that K_La_{20} and SOTR increased 1.5

fold at the 2.9 m diffuser depth, with increasing gas flow rate, as compared to the 1.5 m diffuser
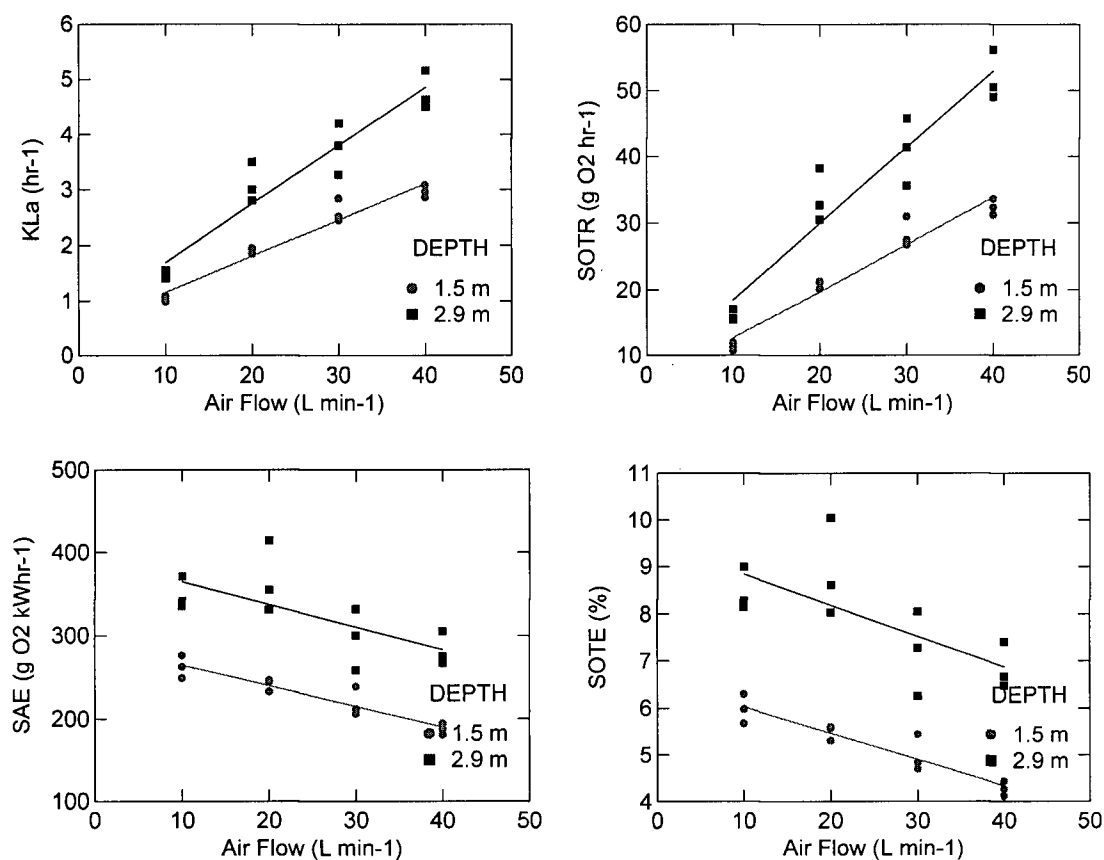
Figure 4.1a-d   KLa20 (a), SOTR (b), SAE (c) and SOTE (d) for 140 μ diffuser on air at 1.5 and 2.9 m depth.

depth (Figure 4.1 a-b). SAE and SOTE were not influenced by the depth x the flow rate interaction effect, and declined with increasing gas flow rate. The mean SAE and SOTE at 2.9 m was 323.8 g O_2 kWhr^{-1} and 7.9%, a 43 % and 52 % increase over the mean SAE of 227.2 g O_2 kWhr^{-1} and SOTE of 5.2 % recorded at 1.5 m (Figure 4.1 c-d and Table 4.1).

4.1.1.2   400 μ diffuser x air   (Note: compares the 400 μ diffuser on air at 1.5 and 2.9 m).

The results for the analysis of covariance for the 400 μ diffuser operating on compressed air are shown in Table 4.2. Significant results ($\alpha \leq 0.01$) were obtained for the depth treatment and

flow rate covariate effect for K_La_{20}, SOTR, SAE and SOTE (Figure 4.2 a-d), with all parameters

increasing in value with depth of gas release. A significant depth x flow rate interaction effect

was observed for K_La_{20} and SOTR (Table 3.2).

Table 4.2. **Adjusted least squares means (± SE), treatment and interaction effects for the 400 μ diffuser on air at 1.5 m or 2.9 m depth.**

Treatment	K_La_{20} (hr⁻¹)	SOTR (g O₂ hr⁻¹)	SAE (g O₂ kWhr⁻¹)	SOTE (%)	n
1.5 m	1.7 (0.04)	18.1 (0.44)	179.6 (5.9)	4.1 (0.14)	12
2.9 m	2.3 (0.04)	25.5 (0.44)	237.8 (5.9)	5.8 (0.14)	12
Interaction	Yes, 1.40	Yes, 1.40	No	No	
Depth	sig, p = 0.000	sig, p = 0.000	sig, p = 0.000	sig, p = 0.000	
Flow rate	sig, p = 0.000	sig, p = 0.000	sig, p = 0.000	sig, p = 0.000	

The significant depth x flow rate interaction effect indicates that K_La_{20} and SOTR increased 1.4

fold at the 2.9 m diffuser depth with increasing gas flow rate, as compared to the 1.5 m diffuser

depth (Figure 4.2 a-b). SAE and SOTE were not influenced by the depth x the flow rate interac-

tion effect, and declined with increasing gas flow rate. The mean SAE and SOTE at 2.9 m was

237.8 g O₂ kWhr⁻¹ and 5.8%, a 32 % and 41 % increase over the mean SAE of 179.6 g O₂ kWhr⁻

¹ and SOTE of 4.1 % recorded at 1.5 m (Figure 4.2 c-d and Table 4.2).

4.1.1.3   800 μ diffuser x air (Note: compares the 800 μ diffuser on air at 1.5 and 2.9 m).

The results for the analysis of covariance for the 800 μ diffuser operating on compressed air are

shown in Table 4.3. Significant results ($\alpha \leq 0.01$) were obtained for the depth treatment and

flow rate covariate effect for K_La_{20}, SOTR, SAE and TE (Figure 4.3 a-d) with all parameters

increasing in value with depth of gas release. A significant depth x flow rate interaction effect

was observed for K_La_{20} and SOTR (Table 4.3).
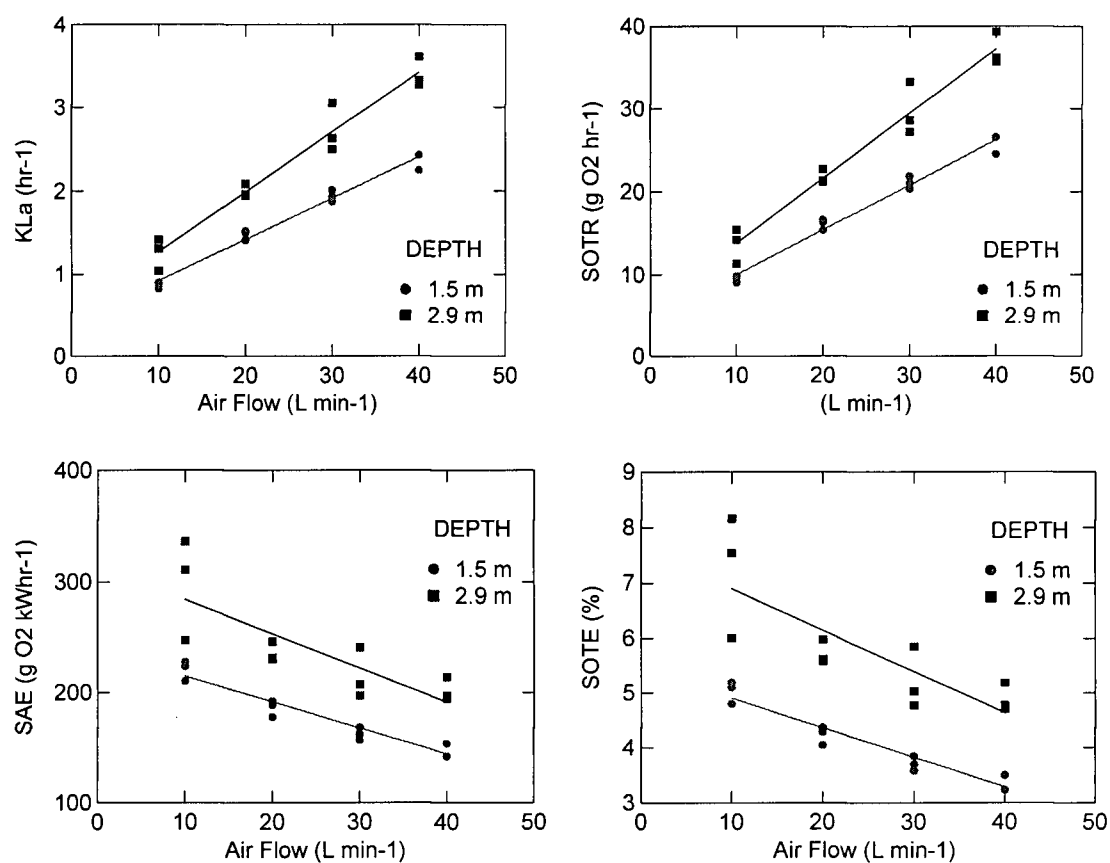
Figure 4.2a-d K_La_{20} (a), SOTR (b), SAE (c) and SOTE (d) for 400 μ diffuser on air at 1.5 and 2.9 m depth.

Table 4.3. Adjusted least squares means ($\pm$ SE), treatment and interaction effects for the 800 μ diffuser on air at 1.5 m or 2.9 m depth.

Treatment	K_La_{20} (hr^{-1})	SOTR (g O_2 hr^{-1})	SAE (g O_2 kWhr^{-1})	SOTE (%)	n
1.5 m	1.3 (0.02)	14.5 (0.21)	139.9 (2.86)	3.2 (0.07)	12
2.9 m	2.0 (0.02)	22.1 (0.21)	197.1 (2.86)	4.8 (0.07)	12
Interaction	Yes, 1.50	Yes, 1.50	No	No	
Depth	sig, p = 0.000	sig, p = 0.000	sig, p = 0.000	sig, p = 0.000	
Flow rate	sig, p = 0.000	sig, p = 0.000	sig, p = 0.000	sig, p = 0.000	

The significant depth x flow rate interaction effect indicates that K_La_{20} and SOTR increased 1.5 fold at the 2.9 m diffuser depth with increasing gas flow rate, as compared to the 1.5 m diffuser depth (Figure 4.3 a-b). SAE and SOTE were not influenced by the depth x the flow rate interaction effect, and declined with increasing gas flow rate. The mean SAE and SOTE at 2.9 m was 197.1 g O_2 kWhr^{-1} and 4.8%, a 41 % and 50 % increase over the mean SAE of 139.9 g O_2 kWhr^{-1} and SOTE of 3.2 % recorded at 1.5 m (Figure 4.3 c-d and Table 4.3).

4.1.1.4   *140 μ diffuser x PSA oxygen (Note: compares the 140 μ diffuser on PSA O_2 at 1.5 and 2.9 m).*

The results for the analysis of covariance for the 140 μ diffuser operating on PSA oxygen are shown in Table 4.4. Significant results ($\alpha \leq 0.01$) were obtained for the depth treatment and flow rate covariate effect for K_La_{20}, SOTR, SAE and SOTE (Figure 4.4 a-d) with all parameters increasing in value with depth of gas release.

Table 4.4. Adjusted least squares means (± SE), treatment and interaction effects for the 140 μ diffuser on PSA oxygen at 1.5 m or 2.9 m depth.

Treatment	K_La_{20} (hr^{-1})	SOTR (g O_2 hr^{-1})	SAE (g O_2 kWhr^{-1})	SOTE (%)	n
1.5 m	13.6 (0.62)	147.6 (6.71)	63.1 (2.03)	8.0 (0.25)	12
2.9 m	17.5 (0.64)	190.9 (7.01)	78.8 (2.12)	10.5 (0.26)	11
Interaction	No	No	No	No	
Depth	sig, p = 0.000	sig, p = 0.000	sig, p = 0.000	sig, p = 0.000	
Flow rate	sig, p = 0.000	sig, p = 0.000	sig, p = 0.000	sig, p = 0.000	

K_La_{20}, SOTR, SAE and TE were not influenced by a depth x flow rate interaction effect. K_La_{20} and SOTR increased with increasing gas flow rate. The mean K_La_{20} and SOTR at 2.9 m was 17.5 hr^{-1} and 190.9 g O_2 hr^{-1}, a 29% increase over the mean K_La_{20} of 13.6 hr^{-1} and SOTR of 147.6 O_2 hr^{-1} recorded at 1.5 m. SAE and SOTE declined with increasing gas flow rate (Figure 4.4 c-d).

The mean SAE and SOTE at 2.9 m was 78.8 g O_2 kWhr^{-1} and 10.5%, a 25 % and 32 % increase

over the mean SAE of 63.1 g O_2 kWhr^{-1} and SOTE of 8.0 % recorded at 1.5 m (Table 4.4).
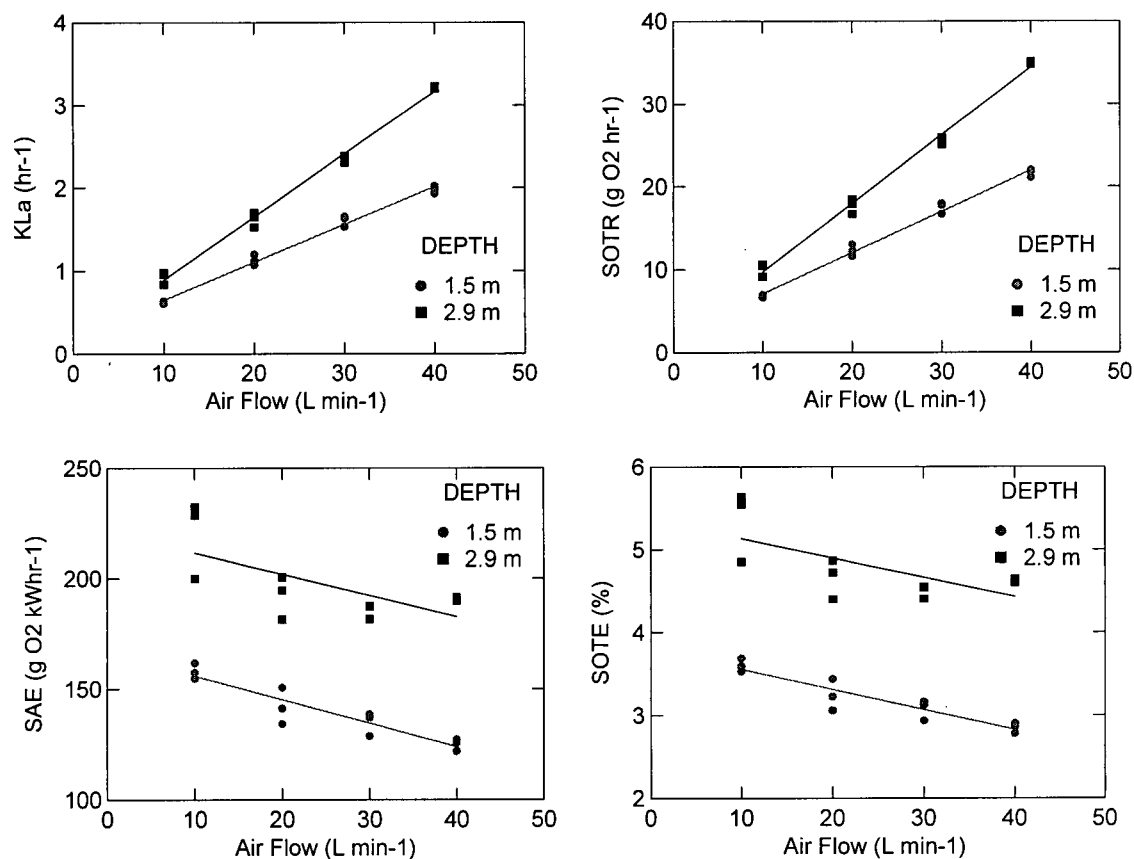
Figure 4.3a-d K_La_{20} (a), SOTR (b), SAE (c) and SOTE (d) for 800 μ diffuser on air at 1.5 and 2.9 m depth.
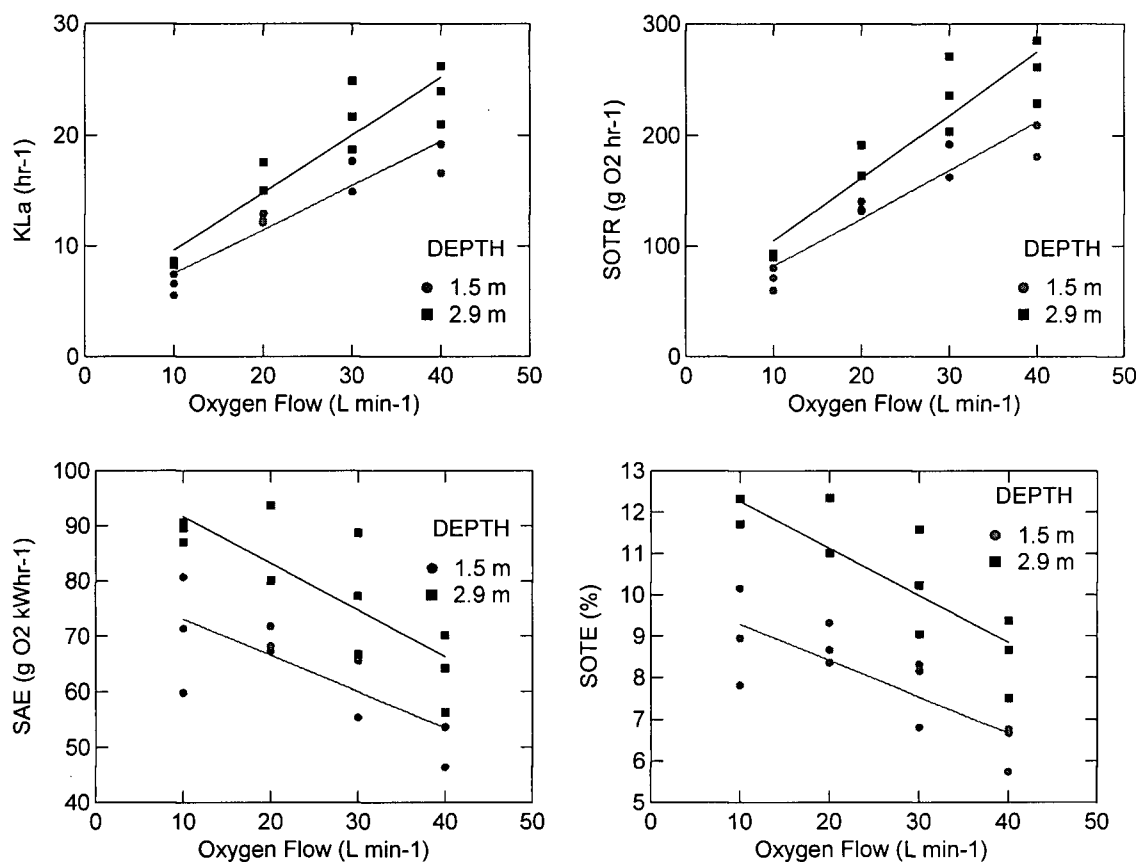
Figure 4.4a-d K_La_{20} (a), SOTR (b), SAE (c) and SOTE (d) for 140 μ diffuser on PSA O_2 at 1.5 and 2.9 m depth.

4.1.1.5 400 μ diffuser x PSA oxygen (Note: compares the 400 μ diffuser on PSA O_2 at 1.5 and 2.9 m).

The results for the analysis of covariance for the 400 μ diffuser operating on PSA oxygen are shown in Table 4.5. Significant results ($\alpha \leq 0.01$) were obtained for the depth treatment and flow rate covariate effect for K_La_{20}, SOTR, SAE and SOTE (Figure 4.5 a-d), with all parameters increasing in value with depth of gas release. A significant depth x flow rate interaction effect was observed for K_La_{20} and SOTR (Table 4.5).

Table 4.5.   Adjusted least squares means (± SE), treatment and interaction effects for the 400 μ diffuser on PSA oxygen at 1.5 m or 2.9 m depth.

Treatment	K_La_{20} (hr^{-1})	SOTR (g O$_2$ hr^{-1})	SAE (g O$_2$ kWhr^{-1})	SOTE (%)	n
1.5 m	10.1 (0.32)	110.2 (3.43)	49.2 (1.31)	5.9 (0.18)	12
2.9 m	13.9 (0.32)	151.0 (3.43)	62.8 (1.31)	8.0 (0.18)	12
Interaction	Yes, 1.34	Yes, 1.34	No	No	
Depth	sig, p = 0.000	sig, p = 0.000	sig, p = 0.000	sig, p = 0.000	
Flow rate	sig, p = 0.000	sig, p = 0.000	sig, p = 0.000	sig, p = 0.000	

The significant depth x flow rate interaction effect indicates that K_La_{20} and SOTR increased 1.3 fold at the 2.9 m diffuser depth with increasing gas flow rate, as compared to the 1.5 m diffuser depth (Figure 4.5 a-b). SAE and SOTE were not influenced by the depth x the flow rate interaction effect, and declined with increasing gas flow rate (Figure 4.5 c-d). The mean SAE and SOTE at 2.9 m was 62.8 g O$_2$ kWhr^{-1} and 8.0%, a 28 % and 35 % increase over the mean SAE of 49.1 g O$_2$ kWhr^{-1} and SOTE of 5.9 % recorded at 1.5 m (Table 4.5).

4.1.1.6   800 μ diffuser x PSA oxygen (Note: compares the 800 μ diffuser on PSA O$_2$ at 1.5 and 2.9 m).

The results for the analysis of covariance for the 800 μ diffuser operating on PSA oxygen are shown in Table 4.6. Significant results (α ≤ 0.01) were obtained for the depth treatment and flow rate covariate effect for K_La_{20}, SOTR, SAE and SOTE (Figure 4.6 a-d), with all parameters increasing in value with depth of gas release. A significant depth x flow rate interaction effect was observed for K_La_{20} and SOTR (Table 4.6).

The significant depth x flow rate interaction effect indicates that K_La_{20} and SOTR increased 1.5 fold at the 2.9 m diffuser depth with increasing gas flow rate as compared to the 1.5 m diffuser depth (Figure 4.6 a-b). SAE and SOTE were not influenced by the depth x the flow rate interaction effect, and declined with increasing gas flow rate (Figure 4.6 c-d). The mean SAE and

SOTE at 2.9 m was 50.4 g O_2 kWhr^{-1} and 6.4%, a 40 % and 45 % increase over the mean SAE

of 35.9 g O_2 kWhr^{-1}and SOTE of 4.4 % recorded at 1.5 m (Table 4.6). A summary of the

adjusted least squares means depth treatment effects showing the percentage increase/decrease

is shown in Table 4.7.
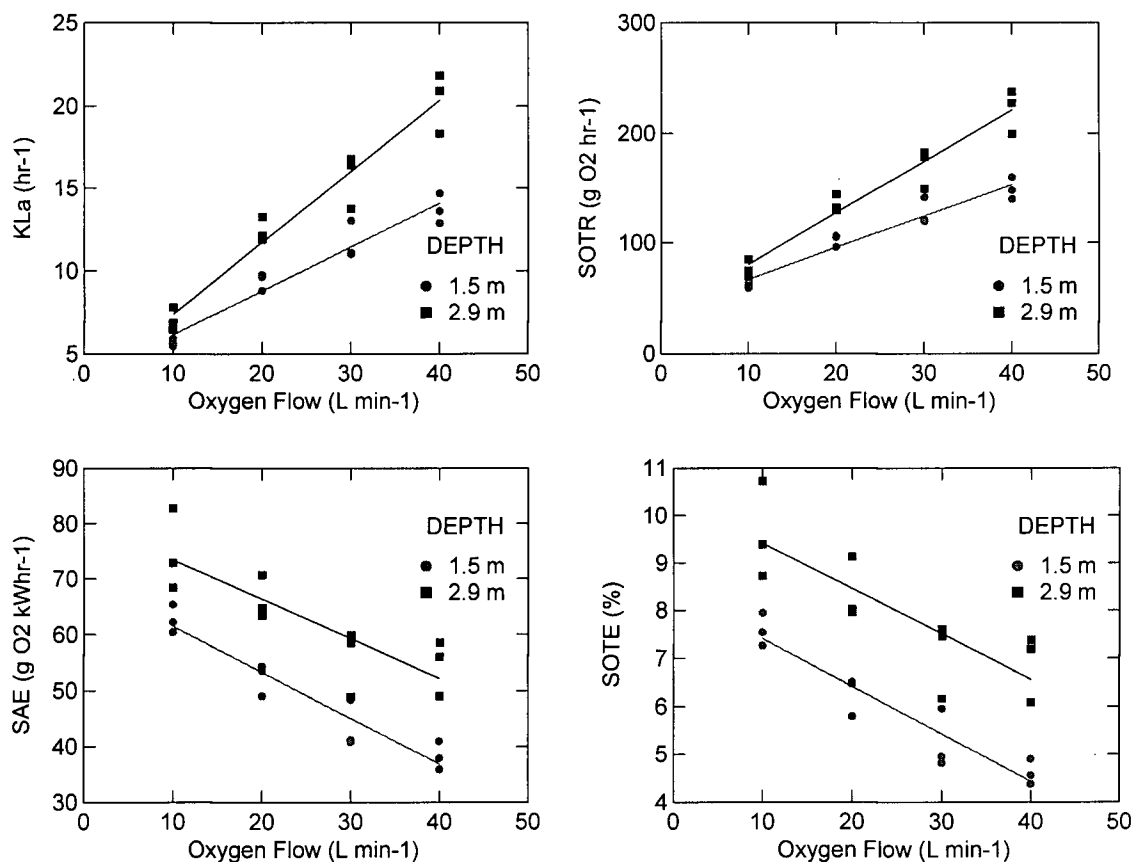
Figure 4.5a-d K_La_{20} **(a), SOTR (b), SAE (c) and SOTE (d) for 400 μ diffuser on PSA**
         O_2 at 1.5 and 2.9 m depth.

Table 4.6. Adjusted least squares means (± SE), treatment and interaction effects for the 800 μ diffuser on PSA oxygen at 1.5 m or 2.9 m depth.

Treatment	K_La_{20} (hr^{-1})	SOTR (g O_2 hr^{-1})	SAE (g O_2 kWhr^{-1})	SOTE (%)	n
1.5 m	7.6 (0.19)	83.1 (2.05)	35.9 (0.79)	4.8 (0.09)	12
2.9 m	11.5 (0.19)	124.8 (2.05)	50.4 (0.79)	6.4 (0.09)	12
Interaction	Yes, 1.47	Yes, 1.47	No	No	
Depth	sig, p = 0.000	sig, p = 0.000	sig, p = 0.000	sig, p = 0.000	
Flow rate	sig, p = 0.000	sig, p = 0.000	sig, p = 0.000	sig, p = 0.000	
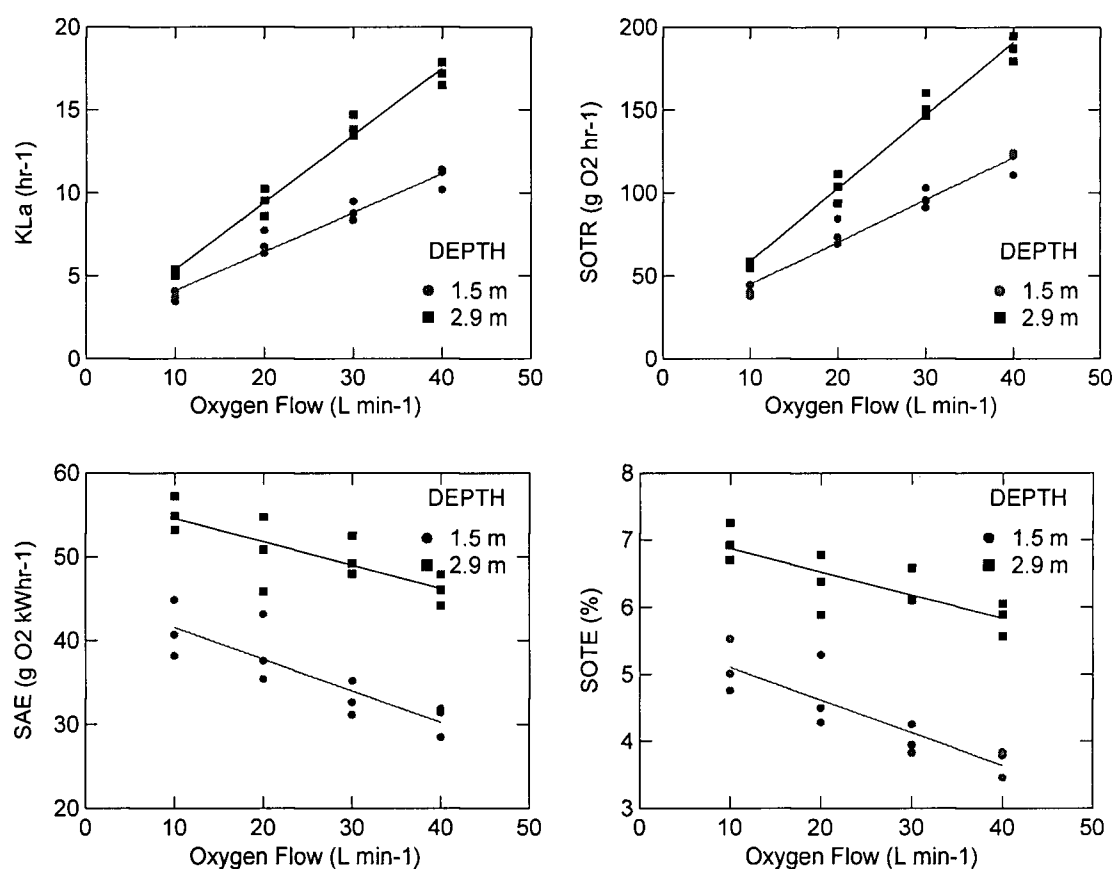
Figure 4.6a-d K_La_{20} (a), SOTR (b), SAE (c) and SOTE (d) for 800 μ diffuser on PSA O_2 at 1.5 and 2.9 m depth.

Table 4.7. Summary of the adjusted least squares means depth treatment effects showing percentage increase/decrease.

Treatment	K_La_{20} (hr^{-1})	SOTR (g O_2 hr^{-1})	SAE (g O_2 kWhr^{-1})	SOTE (%)
1.5 m x Air x 140 μ	2.1	23.2	227.2	5.2
2.9 m x Air x 140 μ	3.3 (+57%)	35.9 (+55%)	323.4 (+42%)	7.8 (+50%)
1.5 m x Air x 400 μ	1.7	18.1	179.6	4.1
2.9 m x Air x 400 μ	2.4 (+41%)	25.5 (+41%)	237.8 (+32%)	5.8 (+41%)
1.5 m x Air x 800 μ	1.3	14.5	139.9	3.2
2.9 m x Air x 800 μ	2.0 (54%)	22.1 (+52%)	197.2 (+41%)	4.8 (+50%)
1.5 m x O_2 x 140 μ	13.5	146.6	63.3	8.0
2.9 m x O_2 x 140 μ	17.5 (+30%)	190.9 (+30%)	79.0 (+25%)	10.5 (+31%)
1.5 m x O_2 x 400 μ	10.1	110.2	49.2	5.9
2.9 m x O_2 x 400 μ	13.9 (+38%)	151.0 (+37%)	62.8 (+28%)	8.0 (+36%)
1.5 m x O_2 x 800 μ	7.6	83.1	35.9	4.4
2.9 m x O_2 x 800 μ	11.5 (+51%)	124.8 (+50%)	50.4 (+40%)	6.4 (+45%)

4.1.2   Oxygen Partial Pressure Effect

This component of the experiment examined the effect of gas flow variation (10 to 40 l min^{-1}) using air and PSA oxygen, at two diffuser depths (1.5 m and 2.9 m) in the full lift inlet tube at three different orifice diameters (140 μ, 400 μ and 800 μ). Within each subset of experiments, the orifice diameter and diffuser depth were held constant, while the gas flow rate and oxygen content (i.e., air or PSA oxygen) were varied.

4.1.2.1   140 μ diffuser x 1.5 m depth (Note: compares the 140 μ diffuser on air and PSA O_2 at 1.5 m).

The results for the analysis of covariance for the 140 μ diffuser at 1.5 m depth are shown in Table 4.8. Significant results ($\alpha \leq 0.01$) were obtained for the gas treatment and flow rate covariate effect for K_La_{20}, SOTR, SAE and TE (Figure 4.7 a-d), with K_La_{20}, SOTR and SOTE increasing in value and SAE decreasing with PSA oxygen. A significant gas x flow rate interaction effect was observed for K_La_{20}, SOTR and SAE (Table 4.8).
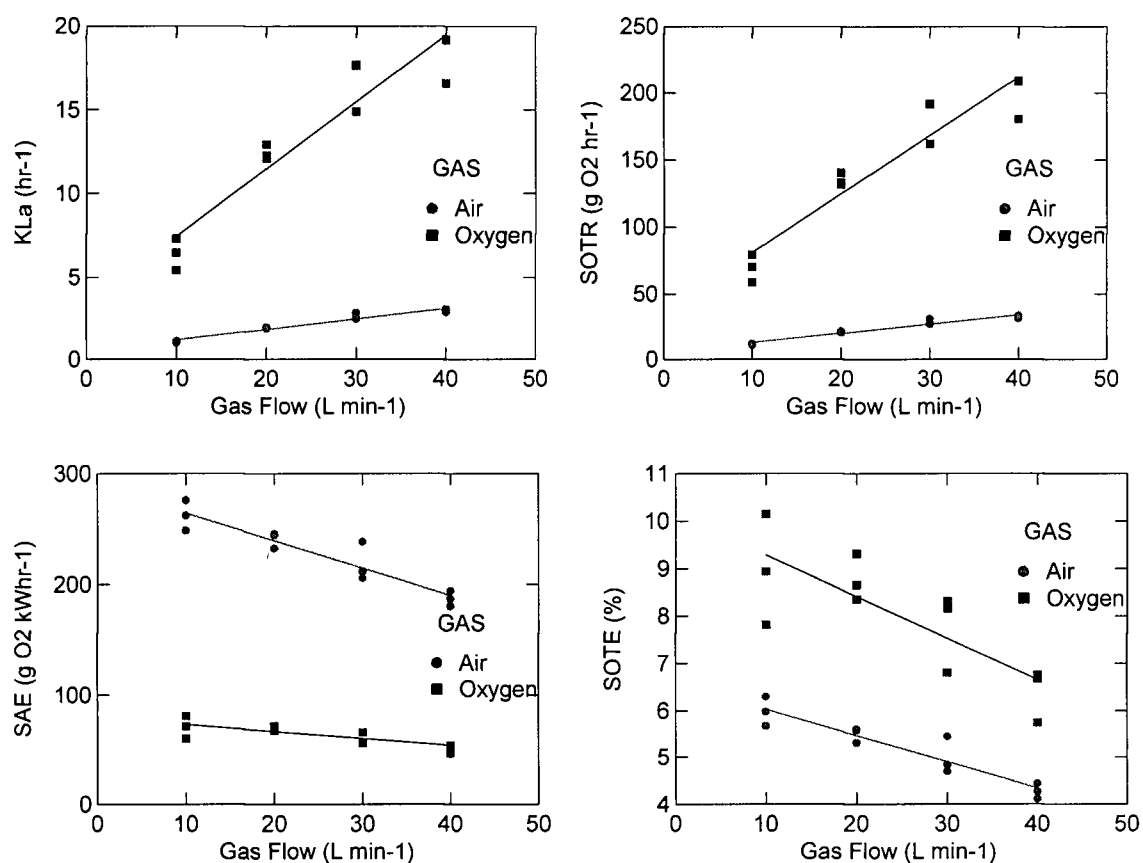
Figure 4.7a-d K_La_{20} (a), SOTR (b), SAE (c) and SOTE (d) for 140 μ diffuser at 1.5 m on air or PSA O_2.

Table 4.8. Adjusted least squares means (± SE), treatment and interaction effects for the 140 μ diffuser at 1.5 m depth on air or PSA oxygen.

Treatment	K_La_{20} (hr^{-1})	SOTR (g O_2 hr^{-1})	SAE (g O_2 kWhr^{-1})	SOTE (%)	n
Air	2.1 (0.33)	23.2 (3.64)	227.2 (2.64)	5.9 (0.18)	12
PSA oxygen	13.5 (0.33)	146.6 (3.64)	63.3 (2.64)	8.0 (0.18)	12
Interaction	Yes, 6.30	Yes, 6.30	Yes, 3.61	No	
Gas	sig, p = 0.000	sig, p = 0.000	sig, p = 0.000	sig, p = 0.000	
Flow rate	sig, p = 0.000	sig, p = 0.000	sig, p = 0.000	sig, p = 0.000	

The significant gas x flow rate interaction effect indicates that K_La_{20} and SOTR increased 6.3

fold on PSA oxygen, with increasing gas flow rate as compared to air, whereas SAE decreased

3.6 fold on PSA oxygen, with increasing gas flow rate as compared to air (Figure 4.7 c). SOTE

was not influenced by the gas x flow rate interaction effect, and declined with increasing gas

flow rate (Figure 4.7 d). The mean SOTE for PSA oxygen was ~ 8%, a 54% increase over the

mean SOTE of 5.9% for air (Table 4.8).

4.1.2.2   400 μ diffuser x 1.5 m depth (Note: compares the 400 μ diffuser on air and PSA O₂ at 1.5 m).

The results for the analysis of covariance for the 400 μ diffuser at 1.5 m depth are shown in

Table 4.9. Significant results ($\alpha \leq 0.01$) were obtained for the gas treatment and flow rate

covariate effect for K_La_{20}, SOTR, SAE and SOTE (Figure 4.8 a-d), with K_La_{20}, SOTR and

SOTE increasing in value and SAE decreasing with PSA oxygen. A significant gas x flow rate

interaction effect was observed for K_La_{20}, SOTR, SAE and SOTE (Table 4.9).

Table 4.9.   Adjusted least squares means (± SE), treatment and interaction effects for the 400 μ diffuser at 1.5 m depth on air or PSA oxygen.

Treatment	K_La_{20} (hr⁻¹)	SOTR (g O₂ hr⁻¹)	SAE (g O₂ kWhr⁻¹)	SOTE (%)	n
Air	1.7 (0.18)	18.1 (1.91)	179.6 (1.9)	4.1 (0.10)	12
PSA oxygen	10.1 (0.18)	110.2 (1.9)	49.2 (1.9)	5.9 (0.10)	12
Interaction	Yes, 6.15	Yes, 6.15	Yes, 3.68	Yes, 1.44	
Gas	sig, p = 0.000	sig, p = 0.000	sig, p = 0.000	sig, p = 0.000	
Flow rate	sig, p = 0.000	sig, p = 0.000	sig, p = 0.000	sig, p = 0.000	
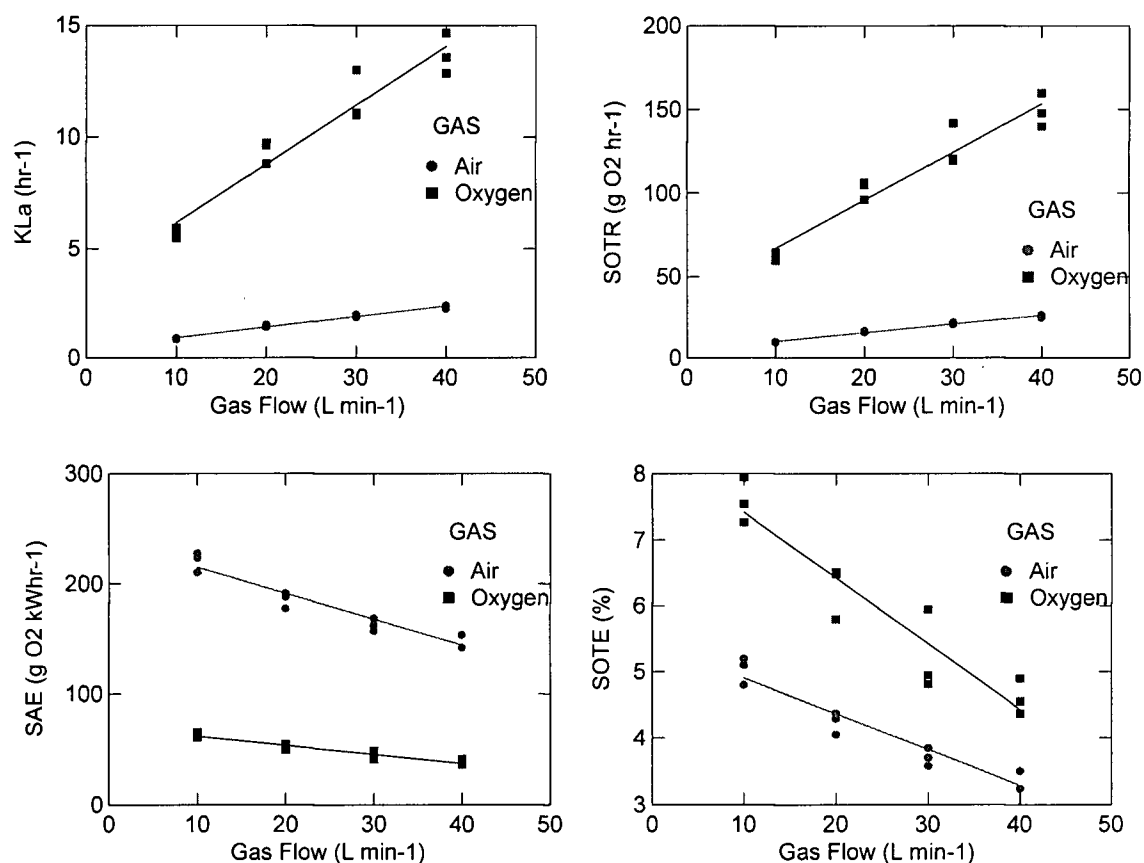
Figure 4.8a-d K_La_{20} (a), SOTR (b), SAE (c) and SOTE (d) for 400 μ diffuser at 1.5 m on air or PSA O_2.

The significant gas x flow rate interaction effect indicates that K_La_{20} and SOTR increased 6.2 fold on PSA oxygen with increasing gas flow rate, as compared to air (Figure 4.8 a-b). SAE decreased 3.7 fold on PSA oxygen with increasing gas flow rate, as compared to air, while SOTE decreased 1.4 fold on PSA oxygen with increasing gas flow rate as compared to air (Figure 4.8 c-d).

4.1.2.3   800 μ diffuser x 1.5 m depth (Note: compares the 800 μ diffuser on air and PSA O₂ at 1.5 m).

The results for the analysis of covariance for the 800 μ diffuser at 1.5 m depth are shown in

Table 4.10. Significant results ($\alpha \leq 0.01$) were obtained for the gas treatment and flow rate

covariate effect for K_La_{20}, SOTR, SAE and TE (Figure 4.9 a-d), with K_La_{20}, SOTR and SOTE

increasing in value and SAE decreasing with PSA oxygen. A significant gas x flow rate interac-

tion effect was observed for K_La_{20}, SOTR and SAE (Table 4.10).

The significant gas x flow rate interaction effect indicates that K_La_{20} and SOTR increased 5.8

fold on PSA oxygen with increasing gas flow rate, as compared to air, whereas SAE decreased

3.9 fold on PSA oxygen with increasing gas flow rate, as compared to air (Figure 4.9 a-c).

SOTE was not influenced by the gas x flow rate interaction effect, and declined with increasing

gas flow rate (Figure 4.9 d). The mean SOTE for PSA oxygen was ~ 4.4%, a 38% increase over

the mean TE of 3.2% for air (Table 4.10).

Table 4.10.   **Adjusted least squares means (± SE), treatment and interaction effects for the 800 μ diffuser at 1.5 m depth on air or PSA oxygen.**

Treatment	K_La_{20} (hr⁻¹)	SOTR (g O₂ hr⁻¹)	SAE (g O₂ kWhr⁻¹)	SOTE (%)	n
Air	1.3 (0.13)	14.5 (1.42)	139.9 (1.22)	3.19 (0.08)	12
PSA oxygen	7.6 (0.13)	83.1 (1.42)	35.9 (1.22)	4.37 (0.08)	12
Interaction	Yes, 5.79	Yes, 5.78	Yes, 3.92	No	
Gas	sig, p = 0.000	sig, p = 0.000	sig, p = 0.000	sig, p = 0.000	
Flow rate	sig, p = 0.000	sig, p = 0.000	sig, p = 0.000	sig, p = 0.000	
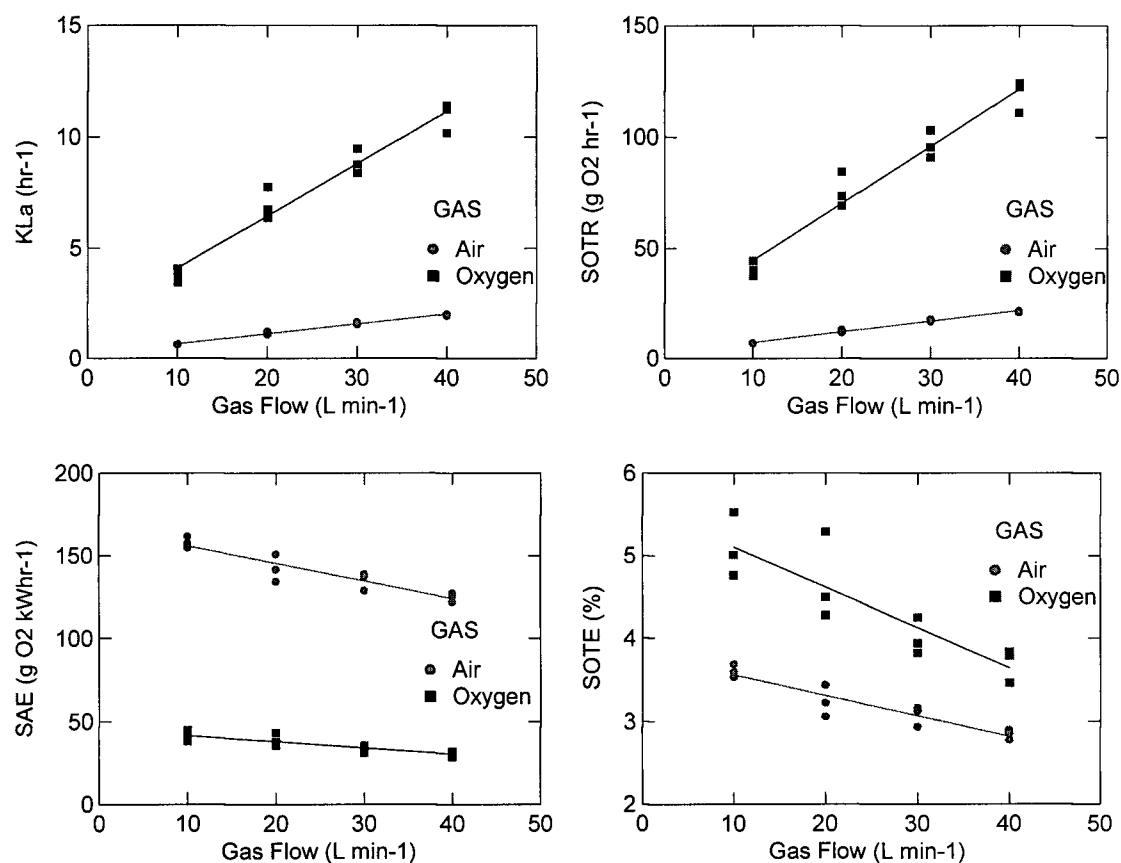
Figure 4.9a-d K_La_{20} (a), SOTR (b), SAE (c) and SOTE (d) for 800 μ diffuser at 1.5 m on air or PSA O_2.

4.1.2.4   140 μ diffuser x 2.9 m depth (Note: compares the 140 μ diffuser on air and PSA O_2 at 2.9 m).

The results for the analysis of covariance for the 140 μ diffuser at 2.9 m depth are shown in

Table 4.11. Significant results ($\alpha \leq 0.01$) were obtained for the gas treatment and flow rate

covariate effect for K_La_{20}, SOTR, SAE and TE (Figure 4.10 a-d), with K_La_{20}, SOTR and TE

increasing in value and SAE decreasing with PSA oxygen. A significant gas x flow rate interaction effect was observed for K_La_{20} and SOTR (Table 4.11).
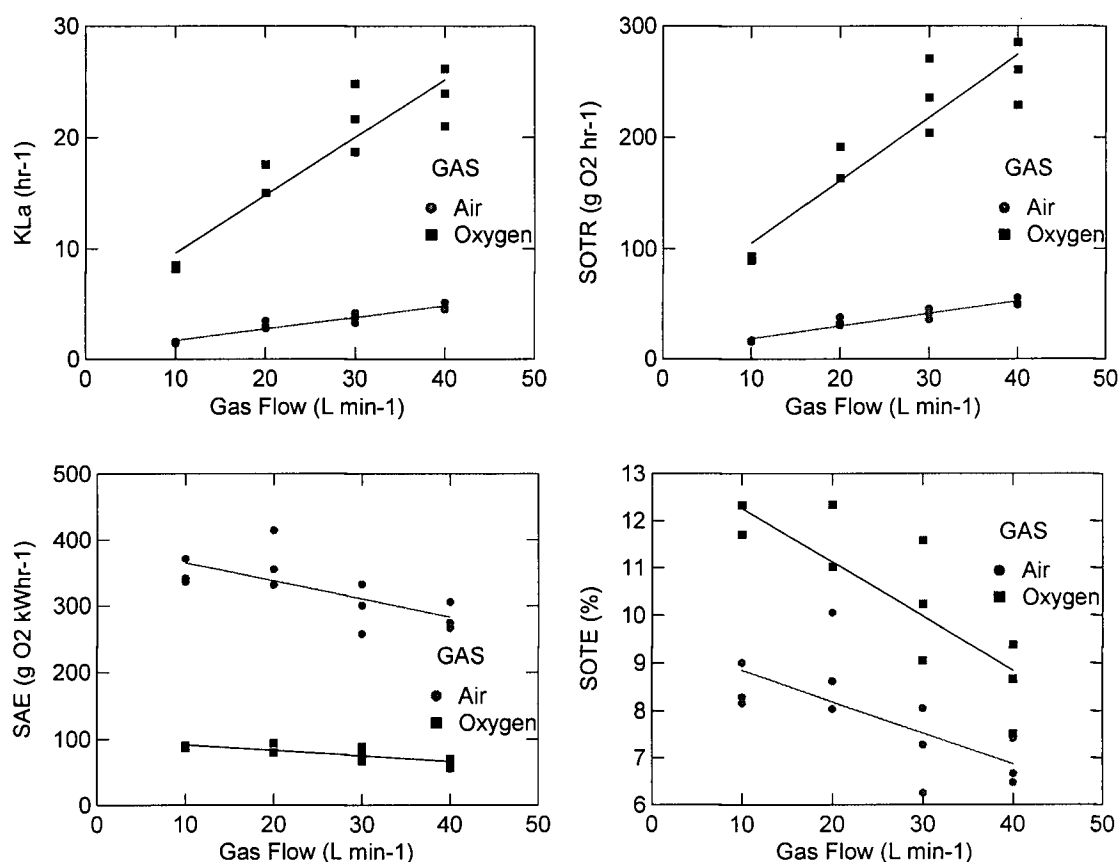
Figure 4.10a-d K_La_{20} (a), SOTR (b), SAE (c) and SOTE (d) for 140 μ diffuser at 2.9 m on air or PSA O_2.

Table 4.11. Adjusted least squares means (± SE), treatment and interaction effects for the 140 μ diffuser at 2.9 m depth on air or PSA oxygen.

Treatment	K_La_{20} (hr^{-1})	SOTR (g O_2 hr^{-1})	SAE (g O_2 kWhr^{-1})	SOTE (%)	n
Air	3.3 (0.52)	35.9 (5.66)	323.4 (7.89)	7.8 (0.26)	12
PSA oxygen	17.5 (0.54)	190.9 (5.91)	79.0 (8.24)	10.5 (0.27)	11
Interaction	Yes, 5.33	Yes, 5.33	No	No	
Gas	sig, p = 0.000	sig, p = 0.000	sig, p = 0.000	sig, p = 0.000	
Flow rate	sig, p = 0.000	sig, p = 0.000	sig, p = 0.000	sig, p = 0.000	

The significant gas x flow rate interaction effect indicates that K_La_{20} and SOTR increased 5.3

fold on PSA oxygen with increasing gas flow rate, as compared to air (Figure 4.10 a-b). SAE

and SOTE were not influenced by the gas x flow rate interaction effect, and declined with increasing gas flow rate (Figure 4.10 c-d). The mean SOTE for PSA oxygen was 10.5%, a 34% increase over the mean SOTE of 7.8% for air (Table 4.11).

4.1.2.5   400 μ diffuser x 2.9 m depth (Note: compares the 400 μ diffuser on air and PSA O$_2$ at 2.9 m).

The results for the analysis of covariance for the 400 μ diffuser at 2.9 m depth are shown in Table 4.12. Significant results ($\alpha \leq 0.01$) were obtained for the gas treatment and flow rate covariate effect for K_La_{20}, SOTR, SAE and SOTE (Figure 4.11 a-d), with K_La_{20}, SOTR and SOTE increasing in value and SAE decreasing with PSA oxygen. A significant gas x flow rate interaction effect was observed for K_La_{20}, SOTR and SAE (Table 4.12).

The significant gas x flow rate interaction effect indicates that K_La_{20} and SOTR increased 5.9 fold on PSA oxygen with increasing gas flow rate, as compared to air, whereas SAE decreased 3.8 fold on PSA oxygen with increasing gas flow rate, as compared to air (Figure 4.11 a-b). SOTE was not influenced by the gas x flow rate interaction effect, and declined with increasing gas flow rate (Figure 4.11 d). The mean TE for PSA oxygen was 8.0%, a 38% increase over the mean TE of 5.8% for air (Table 4.12).

Table 4.12. Adjusted least squares means (± SE), treatment and interaction effects for the 400 μ diffuser at 2.9 m depth on air or PSA oxygen.

Treatment	K_La_{20} (hr^{-1})	SOTR (g O$_2$ hr^{-1})	SAE (g O$_2$ kWhr^{-1})	SOTE (%)	n
Air	2.4 (0.27)	25.5 (2.9)	237.9 (5.75)	5.8 (0.21)	12
PSA oxygen	13.9 (0.27)	151.0 (2.9)	62.8 (5.75)	8.0 (0.21)	12
Interaction	Yes, 5.88	Yes, 5.88	Yes, 3.78	No	
Gas	sig, p = 0.000	sig, p = 0.000	sig, p = 0.000	sig, p = 0.000	
Flow rate	sig, p = 0.000	sig, p = 0.000	sig, p = 0.000	sig, p = 0.000	
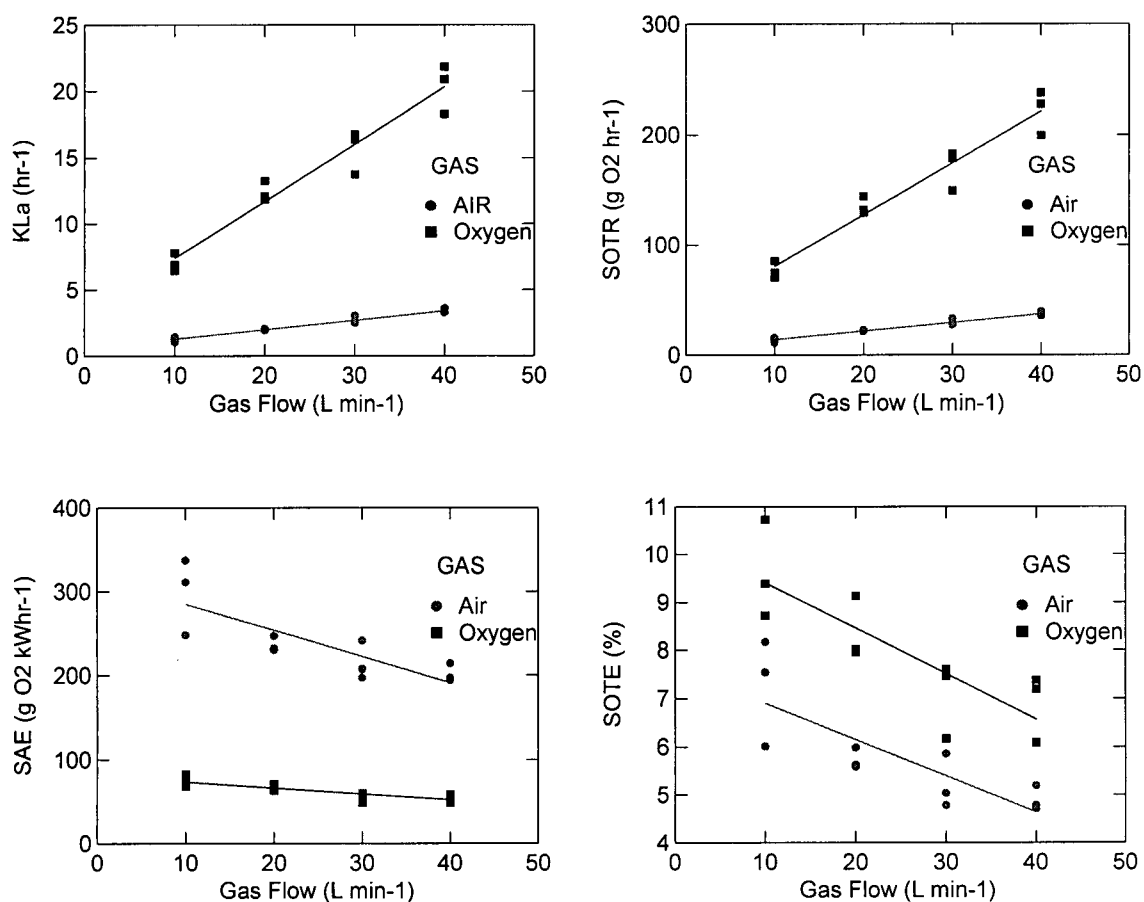
Figure 4.11a-d K_La_{20} (a), SOTR (b), SAE (c) and SOTE (d) for 400 μ diffuser at 2.9 m on air or PSA O$_2$.

4.1.2.6   800 μ diffuser x 2.9 m depth (Note: compares the 800 μ diffuser on air and PSA O₂ at 2.9 m).

The results for the analysis of covariance for the 800 μ diffuser at 2.9 m depth are shown in

Table 4.13. Significant results ($\alpha \leq 0.01$) were obtained for the gas treatment and flow rate

covariate effect for $K_L a_{20}$, SOTR, SAE and SOTE (Figure 4.12 a-d), with $K_L a_{20}$, SOTR and

SOTE increasing in value and SAE decreasing with PSA oxygen. A significant gas x flow rate

interaction effect was observed for $K_L a_{20}$ and SOTR (Table 4.13).

Table 4.13.   Adjusted least squares means (± SE), treatment and interaction effects for the 800 μ diffuser at 2.9 m depth on air or PSA oxygen.

Treatment	$K_L a_{20}$ (hr⁻¹)	SOTR (g O₂ hr⁻¹)	SAE (g O₂ kWhr⁻¹)	SOTE (%)	n
Air	2.0 (0.14)	22.1 (1.50)	197.1 (2.90)	4.8 (0.09)	12
PSA oxygen	11.5 (0.14)	124.8 (1.50)	50.4 (2.90)	6.4 (0.09)	12
Interaction	Yes, 5.68	Yes, 5.68	No	No	
Gas	sig, p = 0.000	sig, p = 0.000	sig, p = 0.000	sig, p = 0.000	
Flow	sig, p = 0.000	sig, p = 0.000	sig, p = 0.000	sig, p = 0.000	

The significant gas x flow rate interaction effect indicates that $K_L a_{20}$ and SOTR increased 5.7

fold on PSA oxygen with increasing gas flow rate, as compared to air (Figure 4.12 a-b). SAE

and SOTE were not influenced by the gas x flow rate interaction effect, and declined with

increasing gas flow rate (Figure 4.12 c-d). The mean SOTE for PSA oxygen was 6.4%, a 33%

increase over the mean SOTE of 4.8% for air (Table 4.13). A summary of the adjusted least

squares means oxygen partial pressure treatment effects showing the percentage in-

crease/decrease are shown in Table 4.14.
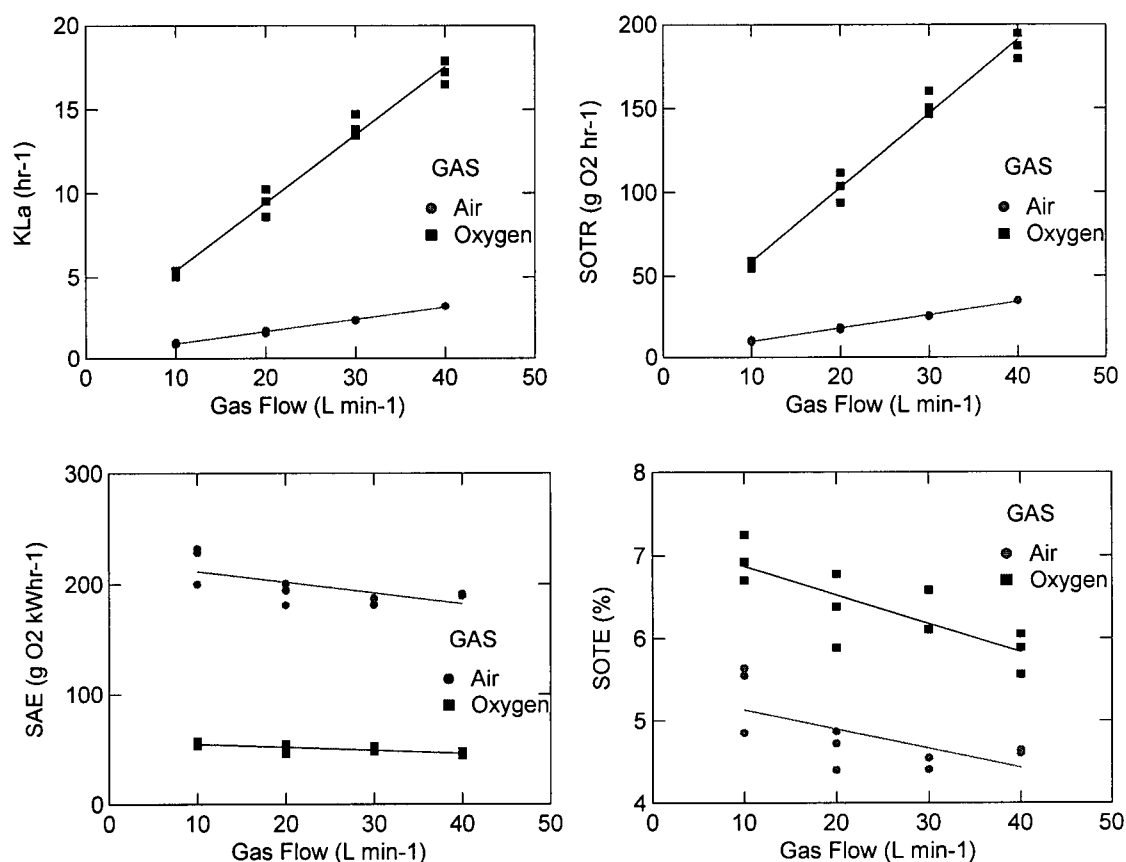
Figure 4.12a-d K_La_{20} (a), SOTR (b), SAE (c) and SOTE (d) for 800 μ diffuser at 2.9 m on air or PSA $O_{2.p}$

Table 4.14. Summary of oxygen partial pressure treatment effects showing percentage increase/decrease.

Treatment	K_La_{20} (hr^{-1})	SOTR ($g\ O_2\ hr^{-1}$)	SAE ($g\ O_2\ kWhr^{-1}$)	SOTE (%)
Air x 140 μ x 1.5 m	2.1	23.2	227.2	5.2
O_2 x 140 μ x 1.5 m	13.5 (+542)	146.6 (+532)	63.3 (-72)	8.0 (+54)
Air x 400 μ x 1.5 m	1.7	18.1	179.6	4.1
O_2 x 400 μ x 1.5 m	10.1 (+494)	110.2 (+509)	49.2 (-73)	5.9 (+44)
Air x 800 μ x 1.5 m	1.3	14.5	139.9	3.2
O_2 x 800 μ x 1.5 m	7.6 (+485)	83.1 (+473)	35.9 (-74)	4.4 (+38)
Air x 140 μ x 2.9 m	3.3	35.9	323.4	7.8
O_2 x 140 μ x 2.9 m	17.5 (+430)	190.9 (+432)	79.0 (-76)	10.5 (+35)
Air x 400 μ x 2.9 m	2.4	25.5	237.8	5.8
O_2 x 400 μ x 2.9 m	13.9 (+479)	151.0 (+492)	62.8 (-74)	8.0 (+38)
Air x 800 μ x 2.9 m	2.0	22.1	197.2	4.8
O_2 x 800 μ x 2.9 m	11.5 (+475)	124.8 (+465)	50.4 (-)74	6.4 (+33)

4.1.3   Orifice Diameter Effect

This component of the experiment examined the effect of gas flow variation (10 to 40 l min^{-1}) at

three different orifice diameters (140 μ, 400 μ and 800 μ), using air and PSA oxygen, at two

diffuser depths (1.5 m and 2.9 m) in the full lift inlet tube. Within each subset of experiments,

the orifice diameter and diffuser depth were held constant, while the gas flow rate and oxygen

content (i.e., air or PSA oxygen) were varied.

*4.1.3.1   Air x 1.5 m depth (Note: compares the 140 μ, 400 μ and 800 μ diffusers on air at 1.5
m).*

The results for the analysis of covariance for the 140 μ, 400 μ and 800 μ diffusers at 1.5 m depth

on air are shown in Table 4.15. Significant results (α ≤ 0.01) were obtained for the orifice

treatment and flow rate covariate effect for K_La_{20}, SOTR, SAE and SOTE (Figure 4.13 a-d),

with K_La_{20}, SOTR, SAE and SOTE decreasing in value with increasing orifice diameter.

A significant orifice diameter x flow rate interaction effect was also observed for K_La_{20}, SOTR,

SAE and TE (Table 4.15).

**Table 4.15.   Adjusted least squares means (± SE), treatment and interaction effects for
the 140 μ, 400 μ and 800 μ diffusers at 1.5 m depth on air.**

Treatment	K_La_{20} (hr^{-1})	SOTR (g O_2 hr^{-1})	SAE (g O_2 kWhr^{-1})	SOTE (%)	n
140 μ	2.1 (0.03)	23.2 (0.37)	227.2 (2.55)	5.2 (0.06)	12
400 μ	1.7 (0.03)	18.1 (0.37)	179.6 (2.55)	4.1 (0.06)	12
800 μ	1.3 (0.03)	14.5 (0.37)	139.9 (2.55)	3.2 (0.06)	12
Interaction	Yes, 1.27/1.62	Yes, 1.27/1.62	Yes, 1.62	Yes, 1.62	
Orifice	sig, p = 0.000	sig, p = 0.000	sig, p = 0.000	sig, p = 0.000	
Flow rate	sig, p = 0.000	sig, p = 0.000	sig, p = 0.000	sig, p = 0.000	
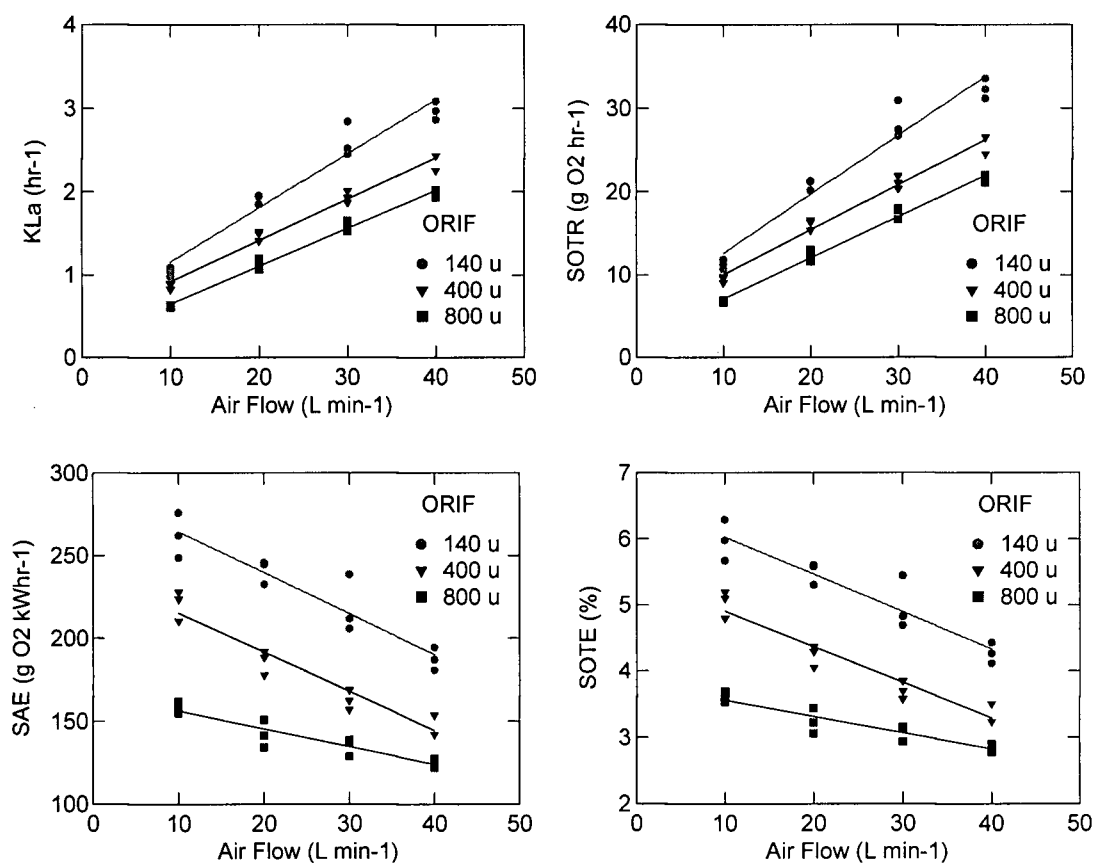
Figure 4.13a-d K_La_{20} (a), SOTR (b), SAE (c) and SOTE (d) for 140, 400 and 800 μ
diffusers on air at 1.5 m.

Scheffe's test indicates that orifice diameter values were significantly different from each other

($\alpha \leq 0.01$) for K_La_{20}, SOTR, SAE and SOTE. The log transformation linearized the orifice

diameter x flow rate interaction effect for K_La_{20} and SOTR, and indicates that, with increasing

gas flow rate, K_La_{20} and SOTR from the 140 μ diffuser increased 1.27 fold as compared to the

400 μ diffuser, and 1.62 fold when compared to the 800 μ diffuser.

The log transformation did not linearize the orifice diameter x flow rate interaction effect for

SAE and SOTE. The analysis was re-run without the 400 μ data, and the results indicate that

SAE and SOTE exhibited parallel slopes for the 140 μ and 800 μ diffuser. The plot of the log transformed data indicated that with increasing gas flow rate, the slope of the 400 μ orifice decreased more rapidly than the 140 μ and 800 μ orifices. An analysis of the 140 and 800 μ treatment pair indicates SAE and SOTE from the 140 μ orifice decreased 1.62 fold, as compared to the 800 μ orifice with increasing gas flow rate. However, the interaction effect could not be separated from the 400 μ and 800 μ treatment pair, and no further statistical analysis was conducted.

4.1.3.2   Air x 2.9 m depth (Note: compares the 140 μ, 400 μ and 800 μ diffusers on air at 2.9 m).

The results for the analysis of covariance for the 140 μ, 400 μ and 800 μ diffusers at 2.9 m depth on air are shown in Table 4.16. Significant results ($\alpha \leq 0.01$) were obtained for the orifice treatment and flow rate covariate effect for $K_La_{20,}$ SOTR, SAE and SOTE (Figure 4.14 a-d), with $K_La_{20,}$ SOTR, SAE and SOTE decreasing in value with increasing orifice diameter. A significant orifice diameter x flow rate interaction effect was observed for K_La_{20} and SOTR (Table 4.16).

Table 4.16.   **Adjusted least squares means (± SE), treatment and interaction effects for the 140 μ, 400 μ and 800 μ diffusers at 2.9 m depth on air.**

Treatment	K_La_{20} (hr^{-1})	SOTR (g O_2 hr^{-1})	SAE (g O_2 kWhr^{-1})	SOTE (%)	n
140 μ	3.3 (0.07)	35.7 (0.79)	323.8 (7.66)	7.85 (0.19)	12
400 μ	2.4 (0.07)	25.5 (0.79)	237.8 (7.66)	5.77 (0.19)	12
800 μ	2.0 (0.07)	22.1 (0.79)	197.1 (7.66)	4.78 (0.19)	12
Interaction	Yes, 1.37/1.63	Yes, 1.37/1.63	No	No	
Orifice	sig, p = 0.000	sig, p = 0.000	sig, p = 0.000	sig, p = 0.000	
Flow rate	sig, p = 0.000	sig, p = 0.000	sig, p = 0.000	sig, p = 0.000	

Scheffe's test indicates that orifice diameter was significantly different from each other ($\alpha \leq$ 0.01) for K_La_{20}, SOTR, SAE and SOTE. The log transformation linearized the orifice diameter x flow rate interaction effect, and indicates that with increasing gas flow rate, K_La_{20} and SOTR from the 140 μ diffuser increased 1.37 fold, as compared to the 400 μ and 1.63 fold, when compared to the 800 μ diffuser.

SAE and SOTE were not influenced by the orifice diameter x flow rate interaction effect, and declined with increasing gas flow rate (Figure 4.14 c-d). The mean SAE and SOTE for the 140 μ diffuser was 323.8 g O_2 kWhr^{-1} and 7.9%, a 36 % increase over the mean SAE of 237.8 g O_2 kWhr^{-1} and SOTE of 5.8 % for the 400 μ diffuser and a 64% increase over the mean SAE of 197.1 g O_2 kWhr^{-1} and SOTE of 4.8 % for the 800 μ diffuser (Table 4.16).

4.1.3.3   PSA oxygen x 1.5 m depth (Note: compares the 140 μ, 400 μ and 800 μ diffusers on PSA O₂ at 1.5 m).

The results for the analysis of covariance for the 140 μ, 400 μ and 800 μ diffusers at 1.5 m depth on PSA oxygen are shown in Table 4.17. Significant results ($\alpha \leq 0.01$) were obtained for the orifice treatment and flow rate covariate effect for K_La_{20}, SOTR, SAE and SOTE (Figure 4.15 a-d), with K_La_{20}, SOTR, SAE and TE decreasing in value with increasing orifice diameter. A significant orifice diameter x flow rate interaction effect was also observed for K_La_{20} and SOTR (Table 4.17).
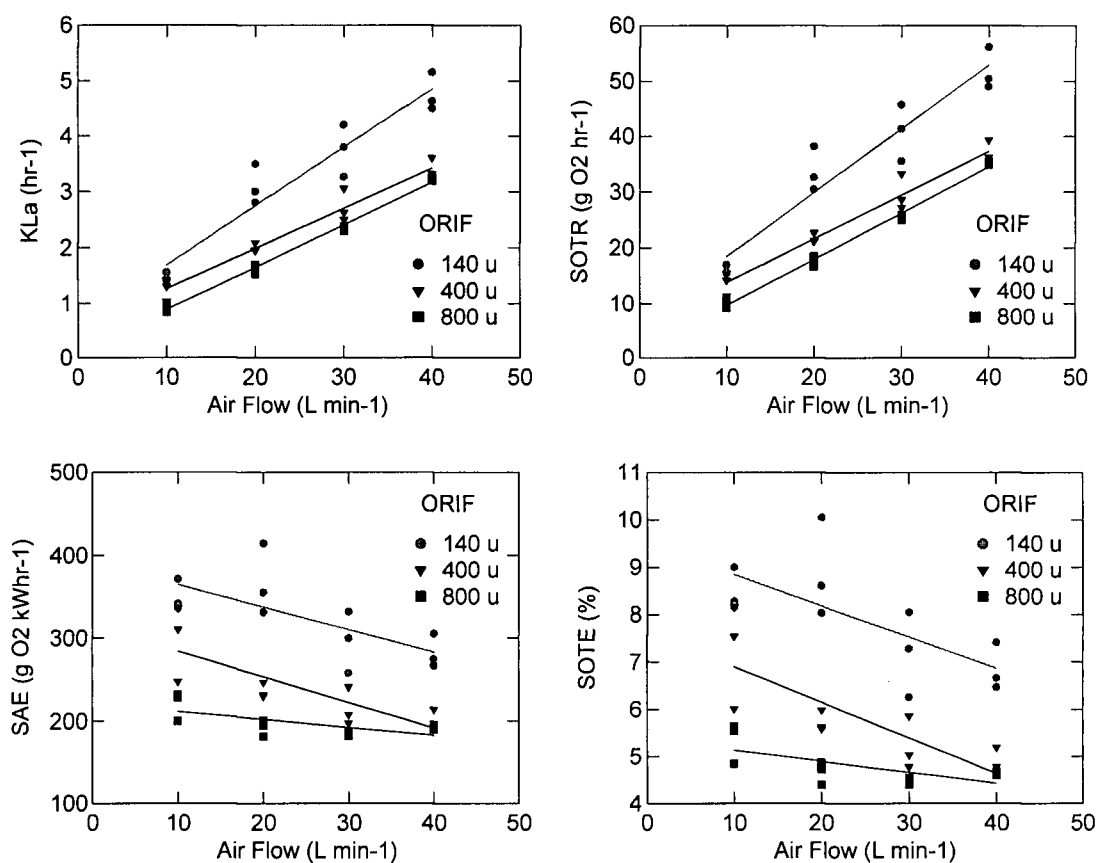
Figure 4.14a-d K_La_{20} (a), SOTR (b), SAE (c) and SOTE (d) for 140, 400 and 800 μ diffusers on air at 2.9 m.

Table 4.17. Adjusted least squares means (± SE), treatment and interaction effects for the 140 μ, 400 μ and 800 μ diffusers at 1.5 m depth on PSA oxygen.

Treatment	K_La_{20} (hr⁻¹)	SOTR (g O₂ hr⁻¹)	SAE (g O₂ kWhr⁻¹)	SOTE (%)	n
140 μ	13.5 (0.32)	146.6 (3.53)	63.3 (1.27)	8.0 (0.16)	12
400 μ	10.1 (0.32)	110.2 (3.53)	49.2 (1.27)	5.9 (0.16)	12
800 μ	7.6 (0.32)	83.1 (3.53)	35.9 (1.27)	4.4 (0.16)	12
Interaction	Yes, 1.30/1.76	Yes, 1.30/1.76	No	No	
Orifice	sig, p = 0.000	sig, p = 0.000	sig, p = 0.000	sig, p = 0.000	
Flow rate	sig, p = 0.000	sig, p = 0.000	sig, p = 0.000	sig, p = 0.000	
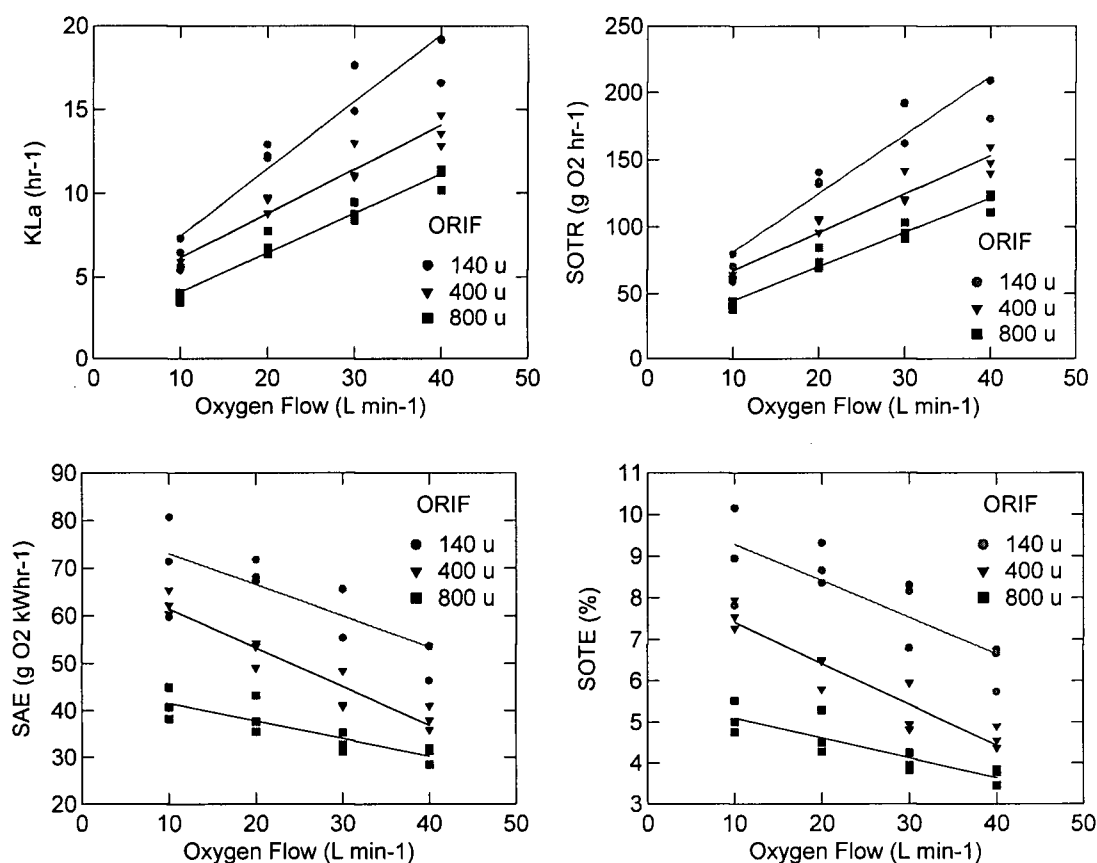
Figure 4.15a-d K_La_{20} (a), SOTR (b), SAE (c) and SOTE (d) for 140, 400 and 800 μ diffusers on PSA O_2 at 1.5 m.

Scheffe's test indicates that orifice diameter was significantly different from each other (α ≤ 0.01) for K_La_{20}, SOTR, SAE and SOTE. The log transformation linearized the orifice diameter x flow rate interaction effect, and indicates that with increasing gas flow rate, K_La_{20} and SOTR from the 140 μ diffuser increased 1.30 fold, as compared to the 400 μ and 1.76 fold, when compared to the 800 μ diffuser.

SAE and SOTE were not influenced by the orifice diameter x flow rate interaction effect, and declined with increasing gas flow rate. The mean SAE and SOTE for the 140 μ diffuser was

63.3 g O_2 kWhr^{-1} and 8.0 %, a 29 % and 35 % increase over the mean SAE of 49.2 g O_2 kWhr^{-1}

and SOTE of 5.9 % for the 400 μ diffuser, and a 76 % and 82 % increase over the mean SAE of

35.9 g O_2 kWhr^{-1} and SOTE of 4.4 % for the 800 μ diffuser (Figure 4.15 c-d and Table 4.17).

4.1.3.4   PSA oxygen x 2.9 m depth (Note: compares the 140 μ, 400 μ and 800 μ diffusers on PSA O_2 at 2.9 m).

The results for the analysis of covariance for the 140 μ, 400 μ and 800 μ diffusers at 2.9 m depth

on PSA oxygen are shown in Table 4.18. Significant results ($\alpha \leq 0.01$) were obtained for the

orifice treatment and flow rate covariate effect for K_La_{20}, SOTR, SAE and SOTE (Figure 4.16

a-d), with K_La_{20}, SOTR, SAE and SOTE decreasing in value with increasing orifice diameter.

No significant orifice diameter x flow rate interaction effect was observed for K_La_{20}, SOTR,

SAE and SOTE (Table 4.18).

Table 4.18.   Adjusted least squares means ($\pm$ SE), treatment and interaction effects for the 140 μ, 400 μ and 800 μ diffusers at 2.9 m depth on PSA oxygen.

Treatment	K_La_{20} (hr^{-1})	SOTR (g O_2 hr^{-1})	SAE (g O_2 kWhr^{-1})	SOTE (%)	n
140 μ	17.5 (0.50)	190.5 (5.49)	78.8 (1.70)	10.5 (0.22)	11
400 μ	13.9 (0.48)	151.7 (5.26)	62.7 (1.63)	8.0 (0.21)	12
800 μ	11.5 (0.48)	125.4 (5.26)	50.4 (1.63)	6.4 (0.21)	12
Interaction	No	No	No	No	
Orifice	sig, p = 0.000	sig, p = 0.000	sig, p = 0.000	sig, p = 0.000	
Flow rate	sig, p = 0.000	sig, p = 0.000	sig, p = 0.000	sig, p = 0.000	

Scheffe's test indicates that orifice diameters were significantly different from each other ($\alpha \leq$

0.01) for K_La_{20}, SOTR, SAE and SOTE. The mean K_La_{20}, SOTR, SAE and SOTE for the 140 μ

diffuser was 26, 26, 26 and 32 % greater, respectively, than the 400 μ diffuser, and 52, 52, 57

and 66 % greater, respectively, than the 800 μ diffuser. A summary of the adjusted least squares
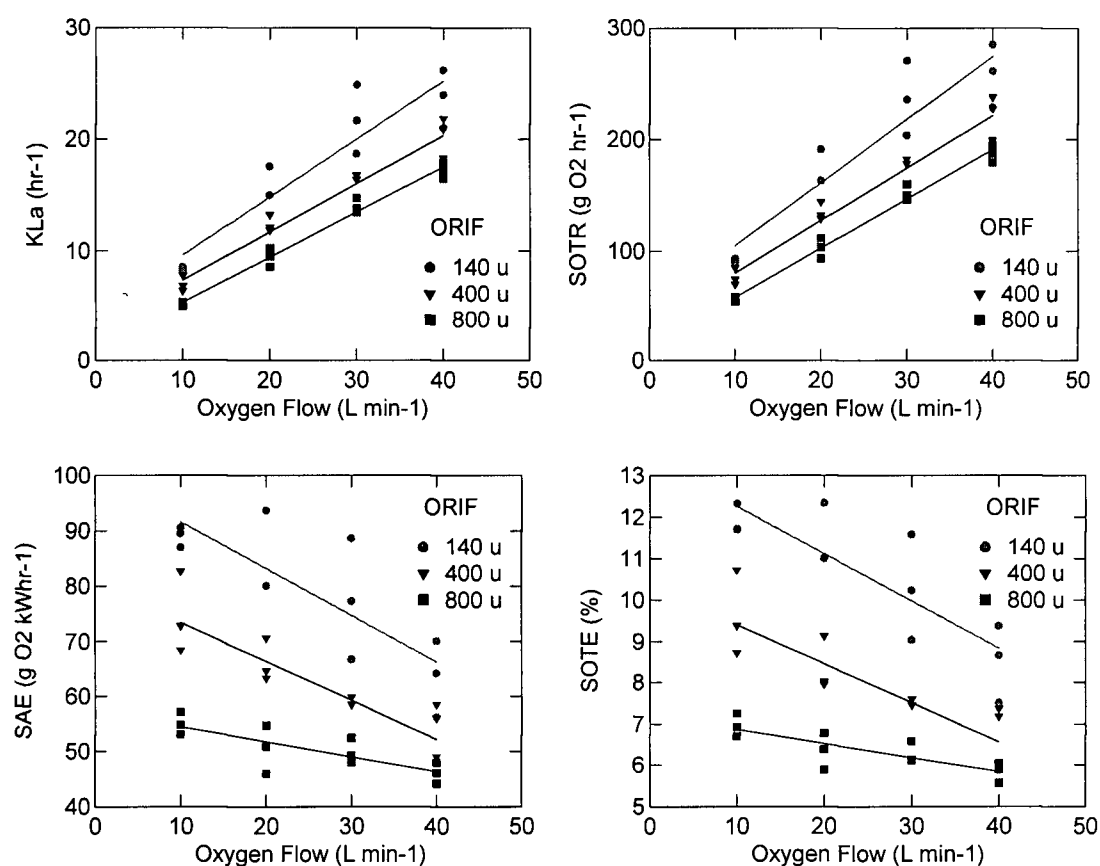
Figure 4.16a-d K_La_{20} (a), SOTR (b), SAE (c) and SOTE (d) for 140, 400 and 800 μ diffusers on PSA O_2 at 2.9 m.

Table 4.19. Summary of diffuser orifice diameter treatment effects showing percentage increase/decrease.

Treatment	K_La_{20} (hr^{-1})	SOTR (g O_2 hr^{-1})	SAE (g O_2 kWhr^{-1})	SOTE (%)
140 μ x Air x 1.5 m	2.1	23.2	227.2	5.2
400 μ x Air x 1.5 m	1.7 (-19)	18.1 (-22)	179.6 (-26)	4.1 (-21)
800 μ x Air x 1.5 m	1.3 (-26)	14.5 (-20)	139.9 (-22)	3.2 (-22)
140 μ x Air x 2.9 m	3.3	35.9	323.4	7.8
400 μ x Air x 2.9 m	2.4 (-27)	25.5 (-29)	237.8 (-26)	5.8 (-29)
800 μ x Air x 2.9 m	2.0 (-17)	22.1 (-13)	197.2 (-17)	4.8 (-17)
140 μ x O_2 x 1.5 m	13.5	146.6	63.3	8.0
400 μ x O_2 x 1.5 m	10.1 (-25)	110.2 (-43)	49.2 (-22)	5.9 (-26)
800 μ x O_2 x 1.5 m	7.6 (-25)	83.1 (-25)	35.9 (-27)	4.4 (-25)
140 μ x O_2 x 2.9 m	17.5	190.9	79.0	10.5
400 μ x O_2 x 2.9 m	13.9 (-21)	151.0 (-21)	62.8 (-21)	8.0 (-24)
800 μ x O_2 x 2.9 m	11.5 (-17)	124.8 (-17)	50.4 (-20)	6.4 (-20)

means diffuser orifice diameter treatment effects showing the percentage increase/decrease are shown in Table 4.19.

4.1.4   Full Lift Modifications Effect

This component of the experiment examined the effect of gas flow variation (10 to 40 l min^{-1}) on four *in situ* modifications (i.e., bubble screen, counter-rotating vanes, surface cover and Downflow Bubble Contact Aeration in the outlet tube), using air and PSA oxygen with two orifice diameters (140 μ and 800 μ) at one diffuser depth (2.9 m) in the full lift inlet tube. Within each subset of experiments, the orifice diameter, diffuser depth and *in situ* modification were held constant, while the gas flow rate and oxygen content (i.e., air or PSA oxygen) were varied.

4.1.4.1   Air x 140 μ diffuser (Note: compares in situ modifications of the full lift hypolimnetic aerator with the 140 μ diffuser on air at 2.9 m).

The results for the analysis of covariance for the various *in situ* modifications of the full lift hypolimnetic aerator with the 140 μ diffuser on air are shown in Table 4.20. All tests were conducted at 2.9 m. Significant results ($\alpha \le 0.01$) were obtained for the *in situ* treatment and flow rate covariate effect for K_La_{20}, SOTR, SAE and SOTE (Figure 4.17 a-d). The no treatment option exhibited the largest mean K_La_{20}, SOTR, SAE and SOTE values, followed in decreasing order by the vanes, DBCA, bubble screen and surface cover treatments. A significant *in situ* treatment x flow rate interaction effect was observed for K_La_{20} and SOTR (Table 4.20).
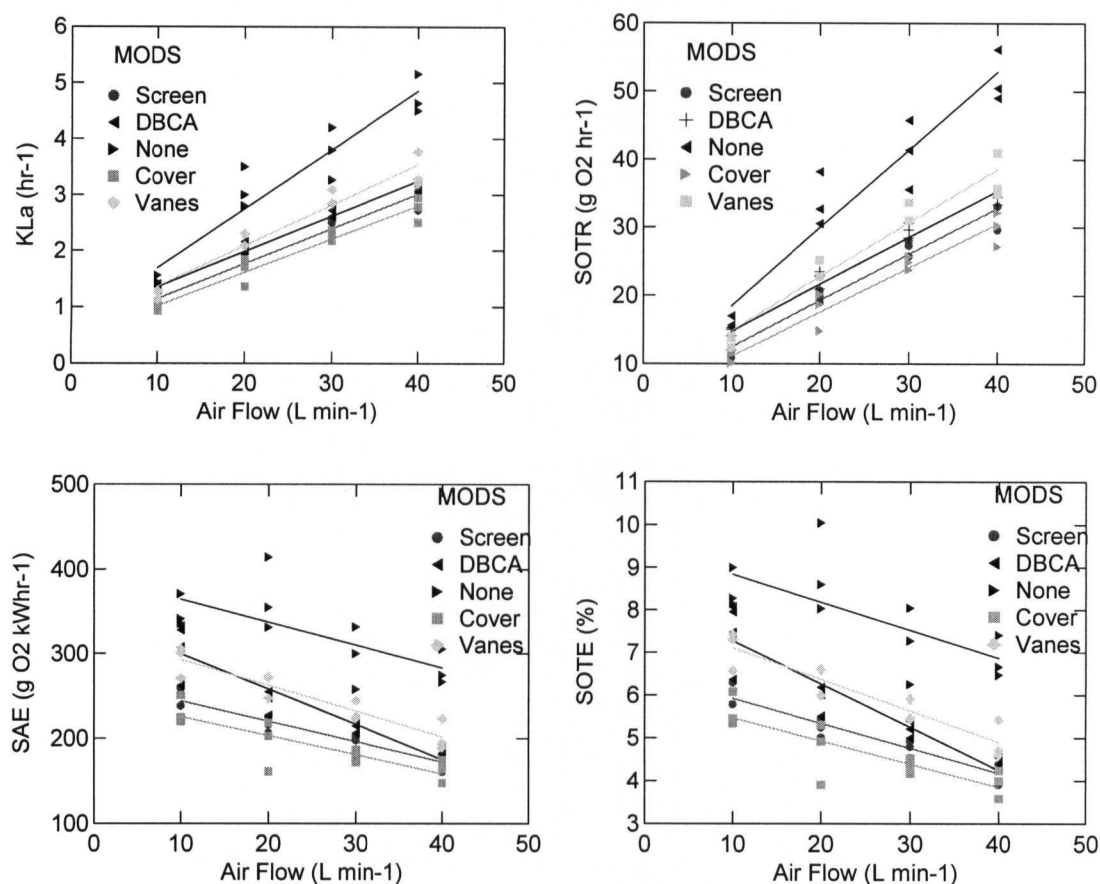
Figure 4.17a-d K_La_{20} (a), SOTR (b), SAE (c) and SOTE (d) for *in situ* modifications on air with 140 µ diffuser at 2.9 m.

Table 4.20. Adjusted least squares means (± SE), treatment and interaction effects for the various *in situ* full lift hypolimnetic aerator treatments on air with the 140 µ diffuser.

Treatment	K_La_{20} (hr^{-1})	SOTR (g O$_2$ hr^{-1})	SAE (g O$_2$ kWhr^{-1})	SOTE (%)	n
Bubble screen	2.1 (0.07)	22.5 (0.77)	209.6 (6.70)	5.1 (0.16)	11
DBCA	2.3 (0.07)	24.9 (0.75)	241.3 (6.43)	5.9 (0.16)	12
None	3.3 (0.07)	35.4 (0.73)	324.5 (6.41)	7.9 (0.16)	12
Surface cover	1.9 (0.07)	20.6 (0.73)	192.7 (6.41)	4.7 (0.16)	12
Vanes	2.4 (0.07)	26.5 (0.73)	248.1 (6.41)	6.0 (0.16)	12
Interaction	Yes	Yes	No	No	
***In situ* effect**	sig, p = 0.000	sig, p = 0.000	sig, p = 0.000	sig, p = 0.000	
Flow effect	sig, p = 0.000	sig, p = 0.000	sig, p = 0.000	sig, p = 0.000	

Scheffe's test indicates that the no modifications treatment was significantly greater than the other *in situ* treatments ($\alpha \leq 0.01$) for $K_L a_{20}$ and SOTR (Tables 4.21 and 4.22). In addition, $K_L a_{20}$ and SOTR values for the vanes and DBCA treatments were significantly greater than the surface cover treatment.

Table 4.21. Matrix of $K_L a_{20}$ pairwise comparison probabilities for Scheffe's test for various *in situ* full lift hypolimnetic aerator treatments on air with the 140 μ diffuser.

Treatments	Bubble screen	DBCA	None	Surface cover	Vanes
Bubble screen	1.000				
DBCA	0.324	1.000			
None	0.000	0.000	1.000		
Surface cover	0.590	0.007	0.000	1.000	
Vanes	0.093	0.971	0.000	0.001	1.000

Table 4.22. Matrix of SOTR pairwise comparison probabilities for Scheffe's test for various *in situ* full lift hypolimnetic aerator treatments on air with the 140 μ diffuser.

Treatments	Bubble screen	DBCA	None	Surface cover	Vanes
Bubble screen	1.000				
DBCA	0.329	1.000			
None	0.000	0.000	1.000		
Surface cover	0.581	0.007	0.000	1.000	
Vanes	0.099	0.974	0.000	0.001	1.000

For SAE and SOTE, Scheffe's test indicates the bubble screen treatment mean was significantly less ($\alpha \leq 0.01$) than the DBCA, no modifications and vanes treatment (Table 4.23). In addition, the no treatment mean was significantly greater than the DBCA, surface cover and vanes, and DBCA was significantly greater than the surface cover treatment (Table 4.23). Finally, the vanes treatment was significantly greater than the surface cover treatment. The log transformation linearized the *in situ* treatment x flow rate interaction effect.

Table 4.23.   Matrix of SAE and SOTE pairwise comparison probabilities for Scheffe's test for various *in situ* full lift hypolimnetic aerator treatments on air with the 140 μ diffuser.

Treatments	Bubble screen	DBCA	None	Surface cover	Vanes
Bubble screen	1.000				
DBCA	**0.010**	1.000			
None	**0.000**	**0.000**	1.000		
Surface cover	0.209	**0.000**	**0.000**	1.000	
Vanes	**0.000**	0.873	**0.000**	**0.000**	1.000

Table 4.24 lists the multiplicative effect (positive or negative) of increasing gas flow rate on K_La_{20} and SOTR.

Table 4.24.   Matrix of multiplicative *in situ* treatment x flow rate interaction effects for K_La_{20} and SOTR for various *in situ* full lift hypolimnetic aerator treatments on air with the 140 μ diffuser.

Treatments	Bubble screen	DBCA	None	Surface cover	Vanes
Bubble screen	0.00				
DBCA	1.13	0.00			
None	1.54	1.36	0.00		
Surface cover	0.91	0.81	0.59	0.00	
Vanes	1.18	1.04	0.76	1.29	0.00

SAE and SOTE were not influenced by the *in situ* treatment x flow rate interaction effect, and declined with increasing gas flow rate, particularly the DBCA treatment.

4.1.4.2   Air x 800 μ diffuser (Note: compares in situ modifications of the full lift hypolimnetic aerator with the 800 μ diffuser on air at 2.9 m).

The results for the analysis of covariance for the various *in situ* modifications of the full lift hypolimnetic aerator with the 800 μ diffuser on air are shown in Table 4.25. Significant results ($\alpha \leq 0.01$) were obtained for the *in situ* treatment and flow rate covariate effect for K_La_{20}, SOTR, SAE and SOTE (Figure 4.18 a-d). The no treatment option exhibited the largest mean K_La_{20}
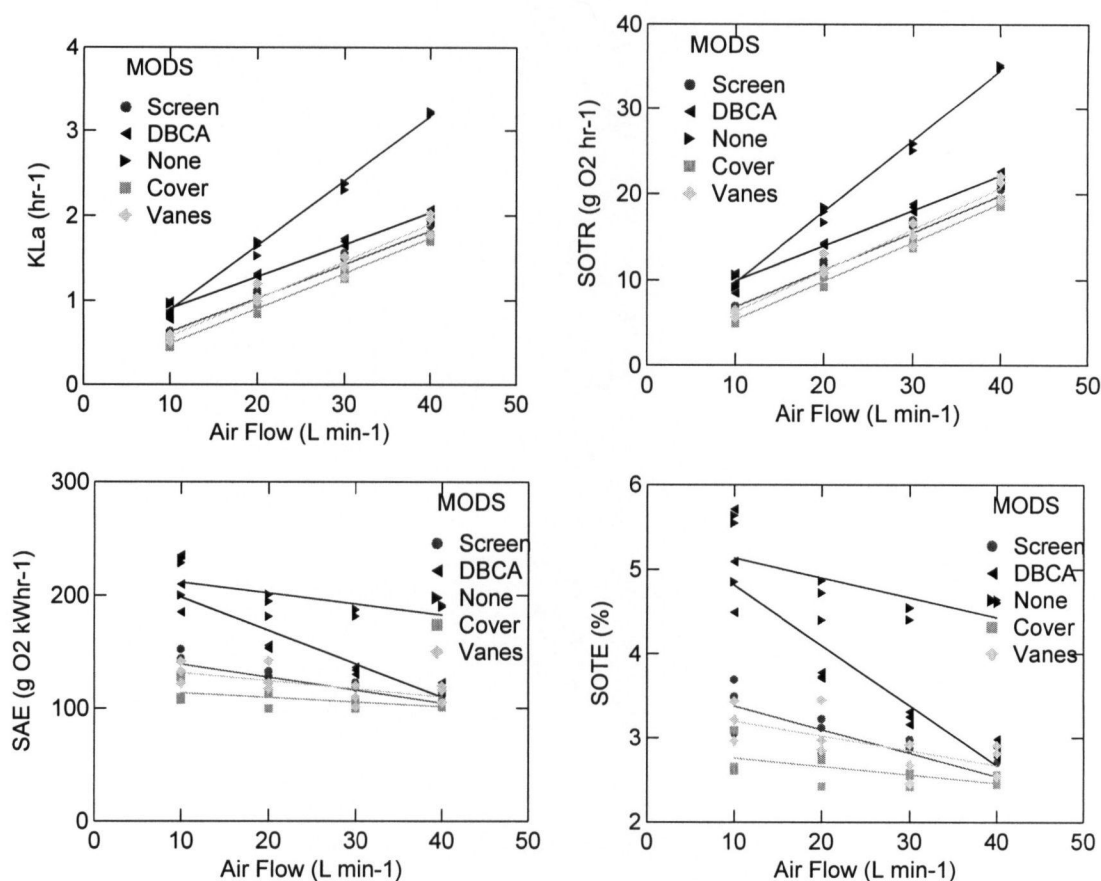
Figure 4.18a-d K_La_{20} (a), SOTR (b), SAE (c) and SOTE (d) for *in situ* modifications on air with 800 µ diffuser at 2.9 m.

and SOTR values, followed in decreasing order by the DBCA, vanes, bubble screen and surface cover treatments. The no treatment option exhibited the largest mean SAE and SOTE values, followed in decreasing order by the DBCA, bubble screen, vanes and surface cover treatments. A significant orifice diameter x flow rate interaction effect was observed for K_La_{20}, SOTR, SAE and SOTE (Table 4.25).

Table 4.25. Adjusted least squares means (± SE), treatment and interaction effects for various *in situ* full lift hypolimnetic aerator treatments on air with the 800 μ diffuser.

Treatment	K_La_{20} (hr^{-1})	SOTR (g O_2 hr^{-1})	SAE (g O_2 kWhr^{-1})	SOTE (%)	n
Bubble screen	1.2 (0.02)	13.4 (0.25)	121.9 (3.32)	3.0 (0.08)	12
DBCA	1.5 (0.02)	16.0 (0.25)	154.2 (3.32)	3.7 (0.08)	12
None	2.2 (0.02)	22.1 (0.25)	197.1 (3.32)	4.8 (0.08)	12
Surface cover	1.1 (0.02)	12.1 (0.25)	107.6 (3.32)	2.6 (0.08)	12
Vanes	1.2 (0.02)	13.5 (0.25)	121.0 (3.32)	2.9 (0.08)	12
Interaction	Yes	Yes	Yes	Yes	
In situ effect	sig, p = 0.000	sig, p = 0.000	sig, p = 0.000	sig, p = 0.000	
Flow effect	sig, p = 0.000	sig, p = 0.000	sig, p = 0.000	sig, p = 0.000	

The log transformation did not linearize the orifice diameter x flow rate interaction effect for K_La_{20}, SOTR, SAE and SOTE, hence the analysis was re-run without the DBCA data, since all of the plots showed that the DBCA values decreased substantially with increasing gas flow. The re-analyzed results indicated K_La_{20}, SOTR, SAE and SOTE exhibited parallel slopes, so the interaction effect was linearized. Scheffe's test indicates the no modifications treatment was significantly greater than the other *in situ* treatments ($\alpha \leq 0.01$) for K_La_{20} and SOTR (Tables 4.26 and 4.27).

Table 4.26. Matrix of K_La_{20} pairwise comparison probabilities for Scheffe's test for various *in situ* full lift hypolimnetic aerator treatments (excluding DBCA) on air with the 800 μ diffuser.

Treatments	Bubble screens	None	Surface Cover	Vanes
Bubble screens	1.000			
None	0.000	1.000		
Surface cover	0.105	0.000	1.000	
Vanes	0.999	0.000	0.136	1.000

Table 4.27. Matrix of SOTR pairwise comparison probabilities for Scheffe's test for various *in situ* full lift hypolimnetic aerator treatments (excluding DBCA) on air with the 800 μ diffuser.

Treatments	Bubble screens	None	Surface cover	Vanes
Bubble screens	1.000			
None	**0.000**	1.000		
Surface cover	0.108	**0.000**	1.000	
Vanes	1.000	**0.000**	0.136	1.000

For SAE and SOTE, Scheffe's test indicates the surface cover treatment was significantly less ($\alpha \leq 0.01$) than the bubble screen, vane and no treatment combinations. The no treatment option was significantly greater than all other treatments (Table 4.28).

Table 4.28. Matrix of SAE and SOTE pairwise comparison probabilities for Scheffe's test for various *in situ* full lift hypolimnetic aerator treatments (excluding DBCA) on air with the 800 μ diffuser.

Treatments	Bubble screen	None	Surface cover	Vanes
Bubble screen	1.000			
None	**0.000**	1.000		
Surface cover	**0.002**	**0.000**	1.000	
Vanes	0.998	**0.000**	**0.004**	1.000

The log transformation linearized the *in situ* treatment x flow rate interaction effect. The multiplicative effects (positive or negative) of increasing gas flow rate on K_La_{20}, SOTR, SAE and SOTE are shown in Tables 4.29 and Table 4.30.

Table 4.29. Matrix of multiplicative *in situ* treatment x flow rate interaction effects for K_La_{20} and SOTR for various *in situ* full lift hypolimnetic aerator treatments (excluding DBCA) on air with the 800 μ diffuser.

Treatments	Bubble screen	None	Surface cover	Vanes
Bubble screen	0.00			
None	1.62	0.00		
Surface cover	0.89	0.55	0.00	
Vanes	0.99	0.61	1.12	0.00

Table 4.30. Matrix of multiplicative *in situ* treatment x flow rate interaction effects for SAE and SOTE for various *in situ* full lift hypolimnetic aerator treatments (excluding DBCA) on air with the 800 μ diffuser.

Treatments	Bubble screen	None	Surface cover	Vanes
Bubble screen	0.00			
None	1.63	0.00		
Surface cover	0.89	0.55	0.00	
Vanes	1.00	0.61	1.12	0.00

A summary of the adjusted least squares means diffuser *in situ* modification treatment effects of the 140 and 800 μ on air showing the percentage increase/decrease relative to No Treatment are shown in Table 4.31.

Table 4.31. Summary of various *in situ* full lift hypolimnetic aerator treatments on air with the 140 μ and 800 μ diffuser showing percentage increase/decrease relative to No Treatment.

Treatment	K_La_{20} (hr^{-1})	SOTR (g O_2 hr^{-1})	SAE (g O_2 kWhr^{-1})	SOTE (%)	n
None x 140 μ	3.3	35.4	324.5	7.9	12
Vanes x 140 μ	2.4 (-27%)	26.5 (-25%)	248.1 (-24%)	6.0 (-24%)	12
DBCA x 140 μ	2.3 (-30%)	24.9 (-30%)	241.3 (-26%)	5.9 (-25%)	12
Screen x 140 μ	2.1 (-36%)	22.5 (-36%)	209.6 (-35%)	5.1 (-35%)	11
Cover x 140 μ	1.9 (-42%)	20.6 (-42%)	192.7 (-41%)	4.7 (-41%)	12
None x 800 μ	2.2	22.1	197.1	4.8	12
DBCA x 800 μ	1.5 (-32%)	16.0 (-28%)	154.2 (-22%)	3.7 (-23%)	12
Vanes x 800 μ	1.2 (-45%)	13.5 (-39%)	121.0 (-39%)	2.9 (-40%)	12
Screen x 800 μ	1.2 (-45%)	13.4 (-39%)	121.9(-38%)	3.0 (-38%)	12
Cover x 800 μ	1.1 (-50%)	12.1 (-45%)	107.6 (-45%)	2.6 (-46%)	12

4.1.4.3 PSA oxygen x 140 μ diffuser (Note: compares in situ modifications of the full lift hypolimnetic aerator with the 140 μ diffuser on PSA O2 at 2.9 m).

The results for the analysis of covariance for the various *in situ* modifications of the full lift hypolimnetic aerator with the 140 μ diffuser on PSA oxygen are shown in Table 4.32. All tests were conducted at 2.9 m. Significant results ($\alpha \leq 0.01$) were obtained for the *in situ* treatment and flow rate covariate effect for K_La_{20}, SOTR, SAE and SOTE (Figure 4.19 a-d). The no
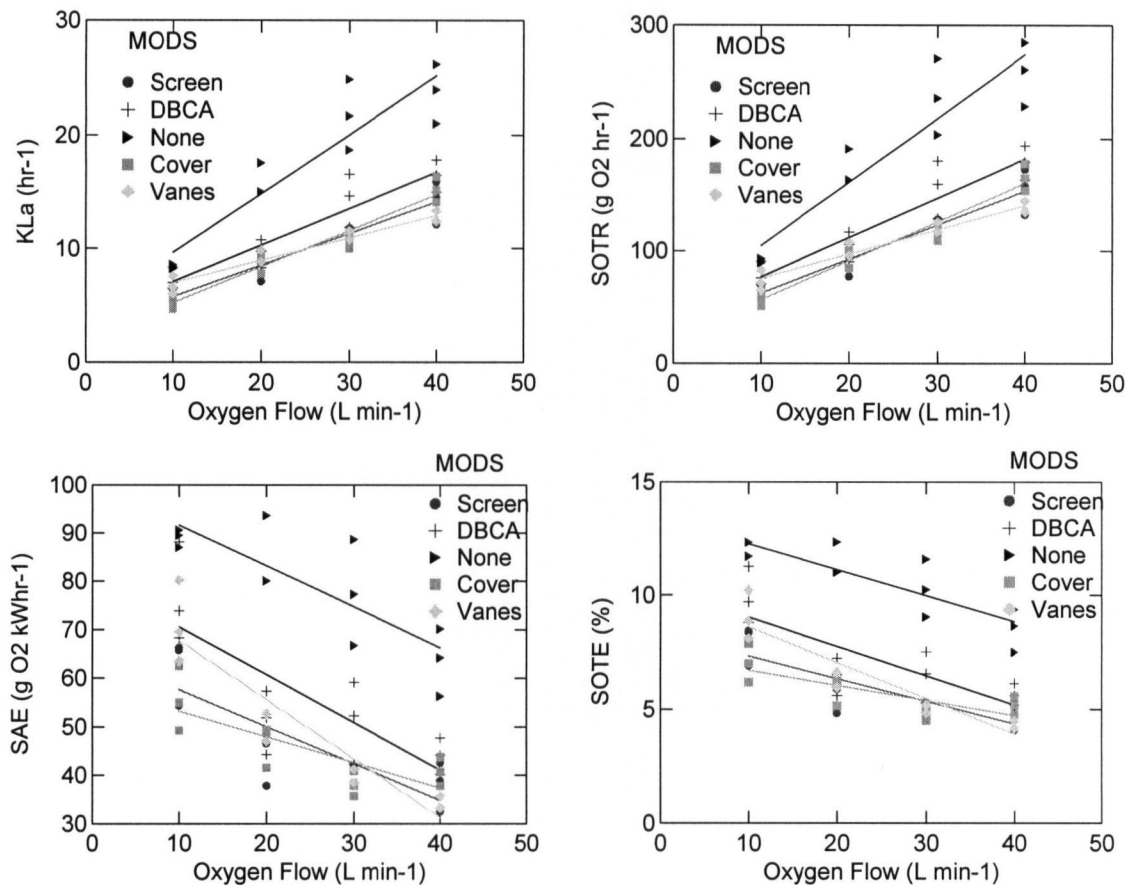
Figure 4.19a-d K_La_{20} (a), SOTR (b), SAE (c) and SOTE (d) for *in situ* modifications on PSA O_2 with 140 μ diffuser at 2.9 m.

treatment option exhibited the largest mean K_La_{20} and SOTR values, followed in decreasing order by the DBCA, surface cover, vanes and bubble screen treatments. The no treatment option exhibited the largest mean SAE and SOTE values, followed in decreasing order by the DBCA, vanes, bubble screen and surface cover treatments. A significant orifice diameter x flow rate interaction effect was observed for K_La_{20} and SOTR (Table 4.32). Scheffe's test indicates the no modifications treatment was significantly greater than the other *in situ* treatments ($\alpha \leq$ 0.01) for K_La_{20} and SOTR (Table 4.33). There were no significant differences among all other pairwise comparisons.

Table 4.32. Adjusted least squares means (± SE), treatment and interaction effects for the various *in situ* full lift hypolimnetic aerator treatments on PSA oxygen with the 140 µ diffuser.

Treatment	K_La_{20} (hr⁻¹)	SOTR (g O_2 hr⁻¹)	SAE (g O_2 kWhr⁻¹)	SOTE (%)	n
Bubble screen	9.9 (0.44)	108.3 (4.75)	46.14 (2.07)	5.8 (0.27)	12
DBCA	11.9 (0.44)	130.0 (4.75)	55.71 (2.07)	7.1 (0.27)	12
None	17.5 (0.47)	190.2 (4.97)	78.9 (2.17)	10.5 (0.28)	12
Surface cover	10.0 (0.44)	108.9 (4.75)	45.2 (2.07)	5.7 (0.27)	12
Vanes	10.0 (0.48)	108.3 (5.21)	49.4 (2.27)	6.3 (0.29)	10
Interaction	Yes	Yes	No	No	
In situ effect	sig, p = 0.000	sig, p = 0.000	sig, p = 0.000	sig, p = 0.000	
Flow effect	sig, p = 0.000	sig, p = 0.000	sig, p = 0.000	sig, p = 0.000	

Table 4.33. Matrix of K_La_{20} and SOTR pairwise comparison probabilities for Scheffe's test for various *in situ* full lift hypolimnetic aerator treatments on PSA oxygen with the 140 µ diffuser.

Treatments	Bubble screen	DBCA	None	Surface cover	Vanes
Bubble screen	1.000				
DBCA	0.038	1.000			
None	**0.000**	**0.000**	1.000		
Surface cover	1.000	0.024	**0.000**	1.000	
Vanes	0.996	0.128	**0.000**	0.985	1.000

For SAE and SOTE, Scheffe's test indicates the no treatment option was significantly ($\alpha \leq 0.01$) greater than the bubble breaker, DBCA, surface cover and vanes treatments (Tables 4.34 and 4.35). There were no significant differences among all other pairwise comparisons.

Table 4.34. Matrix of SAE pairwise comparison probabilities for Scheffe's test for various *in situ* full lift hypolimnetic aerator treatments on PSA oxygen with the 140 µ diffuser.

Treatments	Bubble screen	DBCA	None	Surface cover	Vanes
Bubble screen	1.000				
DBCA	0.026	1.000			
None	**0.000**	**0.000**	1.000		
Surface cover	1.000	0.016	**0.000**	1.000	
Vanes	0.957	0.194	**0.000**	0.911	1.000

Table 4.35. Matrix of SOTE pairwise comparison probabilities for Scheffe's test for various *in situ* full lift hypolimnetic aerator treatments on PSA oxygen with the 140 μ diffuser.

Treatments	Bubble screen	DBCA	None	Surface cover	Vanes
Bubble screen	1.000				
DBCA	0.022	1.000			
None	**0.000**	**0.000**	1.000		
Surface cover	1.000	0.012	**0.000**	1.000	
Vanes	0.961	0.166	**0.000**	0.908	1.000

The log transformation linearized the *in situ* treatment x flow rate interaction effect on K_La_{20} and SOTR. Table 4.36 lists the multiplicative effect (positive or negative) of increasing gas flow rate on K_La_{20} and SOTR for various *in situ* treatments.

Table 4.36. Matrix of multiplicative *in situ* treatment x flow rate interaction effects for K_La_{20} and SOTR for various *in situ* full lift hypolimnetic aerator treatments on PSA oxygen with the 140 μ diffuser.

Treatments	Bubble screen	DBCA	None	Surface cover	Vanes
Bubble screen	0.00				
DBCA	1.20	0.00			
None	1.71	1.43	0.00		
Surface cover	0.99	0.82	0.58	0.00	
Vanes	1.03	0.85	0.60	1.04	0.00

SAE and SOTE were not influenced by the *in situ* treatment x flow rate interaction effect, and declined with increasing gas flow rate, particularly the DBCA treatment.

4.1.4.4   PSA oxygen x 800 μ diffuser (Note: compares in situ modifications of the full lift hypolimnetic aerator with the 800 μ diffuser on PSA O_2 at 2.9 m).

The results for the analysis of covariance for the various *in situ* modifications of the full lift hypolimnetic aerator with the 800 μ diffuser on PSA oxygen are shown in Table 4.37. Significant results ($\alpha \leq 0.01$) were obtained for the *in situ* treatment and flow rate covariate effect for

K_La_{20}, SOTR, SAE and SOTE (Figure 4.20 a-d). The no treatment option exhibited the largest

mean K_La_{20}, SOTR, SAE and SOTE values, followed in decreasing order by the DBCA, bubble

screen, vanes and surface cover treatments. A significant *in situ* treatment x flow rate interac-

tion effect was observed for K_La_{20}, SOTR, SAE and SOTE (Table 4.37).

Table 4.37. Adjusted least squares means (± SE), treatment and interaction effects for various *in situ* full lift hypolimnetic aerator treatments on PSA oxygen with the 800 μ diffuser.

Treatment	K_La_{20} (hr^{-1})	SOTR (g O_2 hr^{-1})	SAE (g O_2 kWhr^{-1})	SOTE (%)	n
Bubble screen	6.8 (0.16)	74.3 (1.69)	30.0 (0.83)	3.8 (0.10)	12
DBCA	8.2 (0.16)	89.7 (1.69)	39.3 (0.83)	5.0 (0.10)	12
None	11.5 (0.16)	124.8 (1.69)	50.4 (0.83)	6.4 (0.10)	12
Surface cover	6.2 (0.16)	67.2 (1.69)	26.4 (0.83)	3.3 (0.10)	12
Vanes	6.7 (0.16)	73.3 (1.69)	29. 0 (0.83)	3.7 (0.10)	12
Interaction	Yes	Yes	Yes	Yes	
In situ effect	sig, p = 0.000	sig, p = 0.000	sig, p = 0.000	sig, p = 0.000	
Flow effect	sig, p = 0.000	sig, p = 0.000	sig, p = 0.000	sig, p = 0.000	

The log transformation did not linearize the orifice diameter x flow rate interaction effect for

K_La_{20}, SOTR, SAE and SOTE, hence the analysis was re-run without the DBCA data, since all

of the plots showed the DBCA values decreasing more rapidly with increasing gas flow than the

other treatments. The re-analyzed results indicated K_La_{20}, SOTR, SAE and SOTE exhibited

parallel slopes, so the interaction effect was linearized. Scheffe's test indicates the no modifica-

tions treatment was significantly greater than the remaining *in situ* treatments ($\alpha \leq 0.01$) for

K_La_{20} and SOTR (Table 4.38).
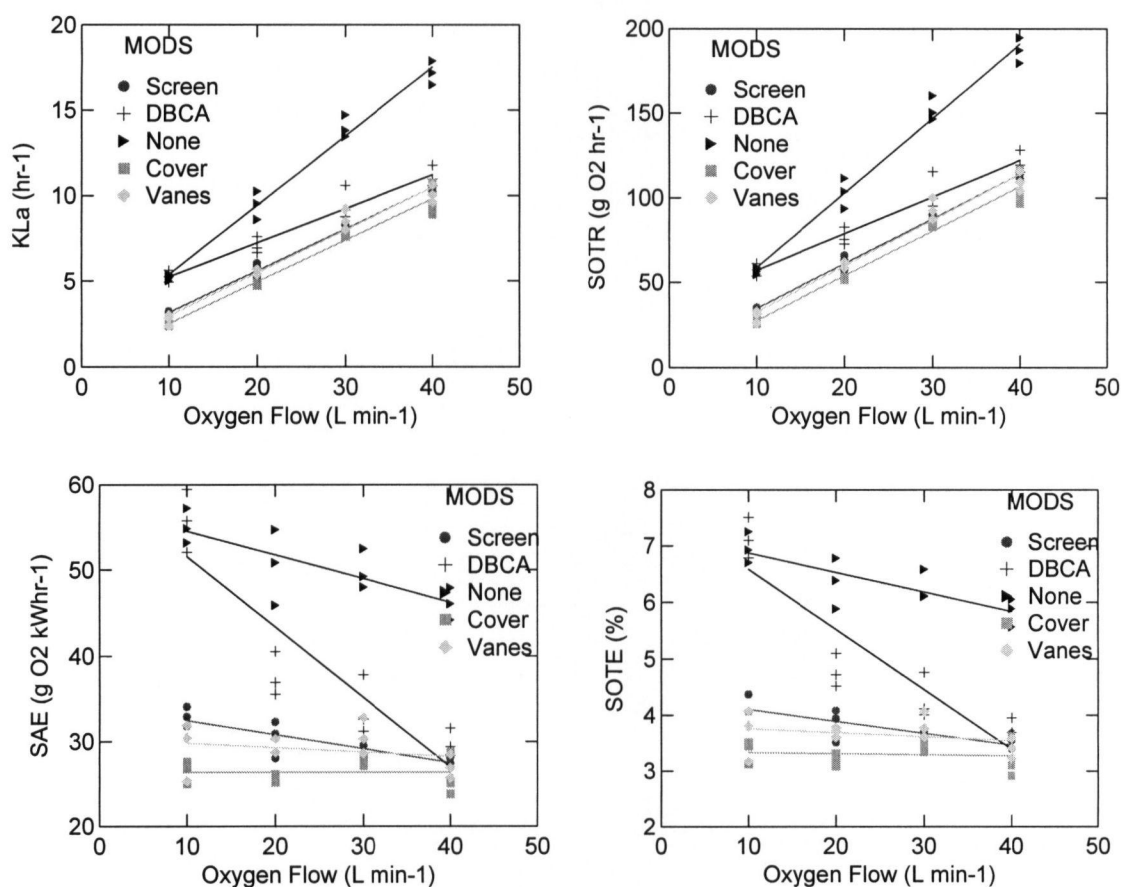
Figure 4.20a-d K_La_{20} (a), SOTR (b), SAE (c) and SOTE (d) for *in situ* modifications on PSA O_2 with 800 μ diffuser at 2.9 m.

Table 4.38. Matrix of K_La_{20} and SOTR pairwise comparison probabilities for Scheffe's test for various *in situ* full lift hypolimnetic aerator treatments (excluding DBCA) on PSA oxygen with the 800 μ diffuser.

Treatments	Bubble screen	None	Surface Cover	Vanes
Bubble screen	1.000			
None	**0.000**	1.000		
Surface cover	0.130	**0.000**	1.000	
Vanes	0.939	**0.000**	0.364	1.000

Scheffe's test indicates that the no treatment SAE and SOTE was significantly greater

($\alpha \leq 0.01$) than the bubble screen, vane and surface cover treatments and that SAE and SOTE

for the bubble screen treatment was significantly greater than the surface cover treatment (Table

4.39).

Table 4.39. **Matrix of SAE pairwise comparison probabilities for Scheffe's test for various *in situ* full lift hypolimnetic aerator treatments (excluding DBCA) on PSA oxygen with the 800 μ diffuser.**

Treatments	Bubble screen	None	Surface cover	Vanes
Bubble screen	1.000			
None	**0.000**	1.000		
Surface cover	**0.000**	**0.000**	1.000	
Vanes	0.673	**0.000**	0.011	1.000

The log transformation linearized the *in situ* treatment x flow rate interaction effect. The

multiplicative effects (positive or negative) of increasing gas flow rate on K_La_{20} and SOTR are

shown in Table 4.40, and for SAE and SOTE in Table 4.41.

Table 4.40. **Matrix of multiplicative *in situ* treatment x flow rate interaction effects for K_La_{20} and SOTR for various *in situ* full lift hypolimnetic aerator treatments (excluding DBCA) on PSA oxygen with the 800 μ diffuser.**

Treatments	Bubble screen	None	Surface cover	Vanes
Bubble screen	0.00			
None	1.68	0.00		
Surface cover	0.88	0.53	0.00	
Vanes	0.97	0.58	1.10	0.00

A summary of the adjusted least squares means diffuser *in situ* modification treatment effects of

the 140 and 800 μ on PSA O_2 showing the percentage increase/decrease relative to No Treat-

ment are shown in Table 4.42.

Table 4.41. Matrix of multiplicative *in situ* treatment x flow rate interaction effects for SAE and SOTE for various *in situ* full lift hypolimnetic aerator treatments (excluding DBCA) on PSA oxygen with the 800 μ diffuser.

Treatments	Bubble screen	None	Surface cover	Vanes
Bubble screen	0.00			
None	1.68	0.00		
Surface cover	0.88	0.53	0.00	
Vanes	0.97	0.58	1.10	0.00

Table 4.42. Summary of various *in situ* full lift hypolimnetic aerator treatments on PSA O_2 with the 140 μ and 800 μ diffuser showing percentage increase/decrease relative to No Treatment.

Treatment	K_La_{20} (hr^{-1})	SOTR (g O_2 hr^{-1})	SAE (g O_2 kWhr^{-1})	SOTE (%)	n
None x 140 μ	17.5	190.2	78.9	10.5	12
DBCA x 140 μ	11.9 (-32%)	130.0 (-32%)	55.7 (-29%)	7.1 (-32%)	12
Vanes x 140 μ	10.0 (-43%)	108.3 (-43%)	49.4 (-37%)	6.3 (-40%)	10
Cover x 140 μ	10.0 (-43%)	108.9 (-43%)	45.2 (-43%)	5.7 (-46%)	12
Screen x 140 μ	9.9 (-43%)	108.3 (-43%)	46.1 (-43%)	5.8 (-45%)	12
None x 800 μ	11.5	124.8	50.4	6.4	12
DBCA x 800 μ	8.2 (-29%)	89.7 (-28%)	39.3 (-22%)	5.0 (-22%)	12
Screen x 800 μ	6.8 (-41%)	74.3 (-40%)	30.0 (-41%)	3.8 (-41%)	12
Vanes x 800 μ	6.7 (-42%)	73.3 (-41%)	29. 0 (-42%)	3.7 (-42%)	12
Cover x 800 μ	6.2 (-46%)	67.2 (-46%)	26.4 (-48%)	3.3 (-48%)	12

4.1.5   Miscellaneous Tests

The results of the Pump Only full lift tests in DBCA mode were considerably different from the regular performance of the full lift hypolimnetic aerator. The mean values for K_La_{20}, SOTR and SAE were among the lowest recorded for any of the full lift tests; however, the mean SOTE values were among the highest recorded (Table 4.43).

The results of the Extended Aeration tests at the lowest gas flow rate in DBCA mode were similar to the values obtained for K_La_{20}, SOTR, SAE and SOTE during the Group 7 (i.e., 140 μ

at 2.9 m) tests at the 7 and 3 l min^{-1} gas flow rates (Table 4.44). The standard error of the

Extended Aeration tests was larger, due to the smaller sample size and increased variance for the

7/3 l min^{-1} – Ext. air tests.

Table 4.43. Mean (± SE) K_La_{20}, SOTR, SAE and SOTE values for full lift hypolimnetic aerator operating in pump only DBCA mode on air or PSA oxygen at 3 l min^{-1}.

Treatment	K_La_{20} (hr^{-1})	SOTR (g O_2 hr^{-1})	SAE (g O_2 kWhr^{-1})	SOTE (%)	n
Pump only – air	0.6 (0.01)	6.2 (0.14)	8.0 (0.18)	11.3 (0.25)	3
Pump only – PSA O_2	2.7 (0.07)	29.6 (0.74)	28.4 (0.71)	12.7 (0.33)	7

Table 4.44. Mean (± SE) K_La_{20}, SOTR, SAE and TE values for the full lift hypolimnetic aerator operating in DBCA mode on air or PSA oxygen at 7 and 3 l min^{-1} at 2.9 m using a 140 μ diffuser. (Note: 7/3 refers to the gas flow, in l min^{-1}, to the diffuser in the inlet tube, and the DBCA diffuser in the separator box).

Treatment	K_La_{20} (hr^{-1})	SOTR (g O_2 hr^{-1})	SAE (g O_2 kWhr^{-1})	SOTE (%)	n
7/3 l min^{-1} – Ext. air	1.5 (0.32)	15.8 (3.48)	359.3 (78.99)	8.4 (1.84)	2
7/3 l min^{-1} – Grp 7 air	1.4 (0.03)	14.8 (0.35)	322.9 (7.57)	7.8 (0.18)	3
7/3 l min^{-1} – Ext. PSA O_2	7.1 (0.16)	77.3 (1.78)	77.1 (1.78)	9.7 (0.23)	2
7/3 l min^{-1} – Grp 7 PSA O_2	7.3 (0.56)	79.0 (6.09)	76.8 (5.92)	9.9 (0.72)	3

The purpose of the extended aeration tests was to determine the oxygen saturation value

achieved after an extended period of operation. The lowest gas flow rate setting was required as

the PSA unit could not generate high purity oxygen for extend periods at flow rates exceeding

10 l min^{-1}. The highest oxygen concentration achieved on air was 11.47 mg l^{-1} after 247 min-

utes of operation, and the % saturation achieved (i.e., 96.4%) exceeded the C^*_s calculated for the

day (i.e., 93.3 %) by 3.1%. The highest oxygen concentration achieved on PSA oxygen was

50.44 mg l^{-1} or 446.4 % saturation after 206 minutes of operation, thus exceeding the C^*_s for the

day for air (i.e., 103.2 %) by a ratio of 4.33 (Table 4.45).

Table 4.45.   Laboratory measurements recorded during extended aeration tests.

Treatment	Date	Time (min)	O_2 mg l^{-1}	% Sat.	C^*_s	Temp (^{o} C)
Ext. Air-1	July 19/00	247	11.47	96.4	93.3	11.8
Ext. Air-2	July 20/00	270	11.37	100.6	103.2	12.4
Ext. O_2-1	July 19/00	183	48.45	407.1	93.3	12.6
Ext. O_2-2	July 20/00	206	50.44	446.4	103.2	11.2

4.2   Full Lift Hypolimnetic Aeration – Water Velocity

4.2.1   Gas Effect

Note: this component of the experiment examined the effect of gas flow variation (10 to 40 l min^{-1}) on water velocity in the outlet tube, using air and PSA oxygen, at three different orifice diameters (140 μ, 400 μ and 800 μ), at two diffuser depths (1.5 m and 2.9 m) in the full lift inlet tube. Within each subset of experiments, the orifice diameter and diffuser depth were held constant, while the gas flow rate and oxygen content (i.e., air or PSA oxygen) were varied.

The results for the analysis of covariance for the 140, 400 and 800 μ diffusers operating on air or PSA oxygen at 1.5 and 2.9 m depth are shown in Table 4.46. As was expected, their were no significant differences in water velocity in the full lift aerator as a function of air or PSA oxygen among all combinations of diffuser orifice diameter and depth of gas release (Figures 4.21 a-c and 4.22 a-b). Water velocity was significantly influenced ($\alpha \leq 0.01$) by gas flow rate in all treatment combinations, increasing in value with increasing gas flow rates. The water velocity measurements for the PSA O_2 x 800 μ @ 2.9 m treatment were not analyzed as they were too erratic, and not believable due to a measurement error. The Air x 800 μ @ 2.9 m treatment data was useable; however, the SE was inflated due to the erratic behavior of the PSA O_2 x 800 μ @ 2.9 m data, which was caused by equipment malfunction.
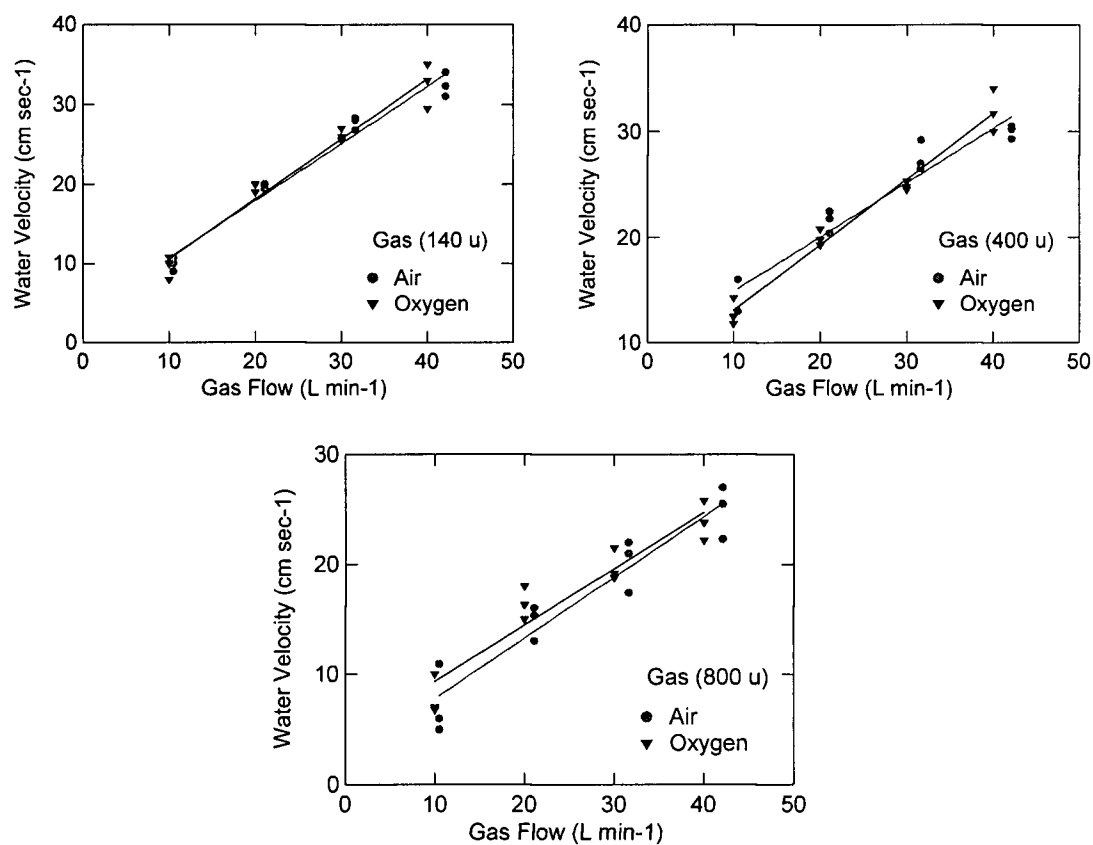
Figure 4.21a-c Water velocity vs. gas flow rate on air or PSA O_2 at 1.5 m using
140 μ (a), 400 μ (b) and 800 μ (c) diffusers.
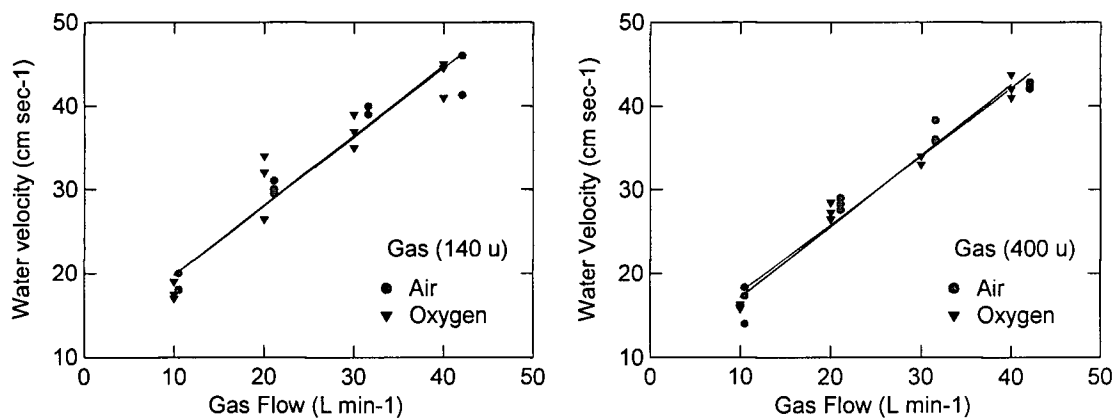
Figure 4.22a-b Water velocity vs. gas flow rate on air or PSA O_2 at 2.9 m using 140 μ
(a) and 400 μ (b) diffusers.

Table 4.46. Mean (± SE) water velocity (cm sec^{-1}) measured near the top of the downflow tube in the full lift hypolimnetic aerator – gas effect.

Treatment	Velocity (cm sec^{-1})	Gas flow sig.	Gas composition sig.	n
Air x 140 μ @ 1.5 m	22.0 (0.48)	Yes	No	12
PSA O$_2$ x 140 μ @ 1.5 m	22.4 (0.48)			12
Air x 400 μ @ 1.5 m	22.9 (0.48)	Yes	No	12
PSA O$_2$ x 400 μ @ 1.5 m	22.8 (0.48)			12
Air x 800 μ @ 1.5 m	16.4 (0.61)	Yes	No	12
PSA O$_2$ x 800 μ @ 1.5 m	17.4 (0.62)			12
Air x 140 μ @ 2.9 m	32.7 (0.75)	Yes	No	12
PSA O$_2$ x 140 μ @ 2.9 m	32.8 (0.75)			12
Air x 400 μ @ 2.9 m	30.4 (0.51)	Yes	No	12
PSA O$_2$ x 400 μ @ 2.9 m	30.4 (0.51)			12
Air x 800 μ @ 2.9 m	32.1 (2.56)	Yes	No	12
PSA O$_2$ x 800 μ @ 2.9 m	N/A			N/A

4.2.2 Depth Effect

Note: this component of the experiment examined the effect of gas flow variation (10 to 40 l min^{-1}) on water velocity in the outlet tube, using air only, at two diffuser depths (1.5 m and 2.9 m) in the full lift inlet tube with three orifice diameters (140 μ, 400 μ and 800 μ). Within each subset of experiments, the orifice diameter and diffuser depth were held constant, while the gas flow rate and oxygen content (i.e., air or PSA oxygen) were varied.

Since there was no significant effect of gas composition on water velocity, the remaining depth effect analyses were conducted on air only, since the erratic PSA O$_2$ x 800 μ @ 2.9 m data set was discarded. The results for the analysis of covariance for the 1.5/2.9 m x 140 μ diffuser treatment are shown in Table 4.47. Significant results ($\alpha \leq 0.01$) were obtained for the depth and gas flow rate covariate effect (Figure 4.23 a-c), with water velocity increasing in value with depth of gas release and gas flow rate. No depth x gas flow rate interaction effect was observed
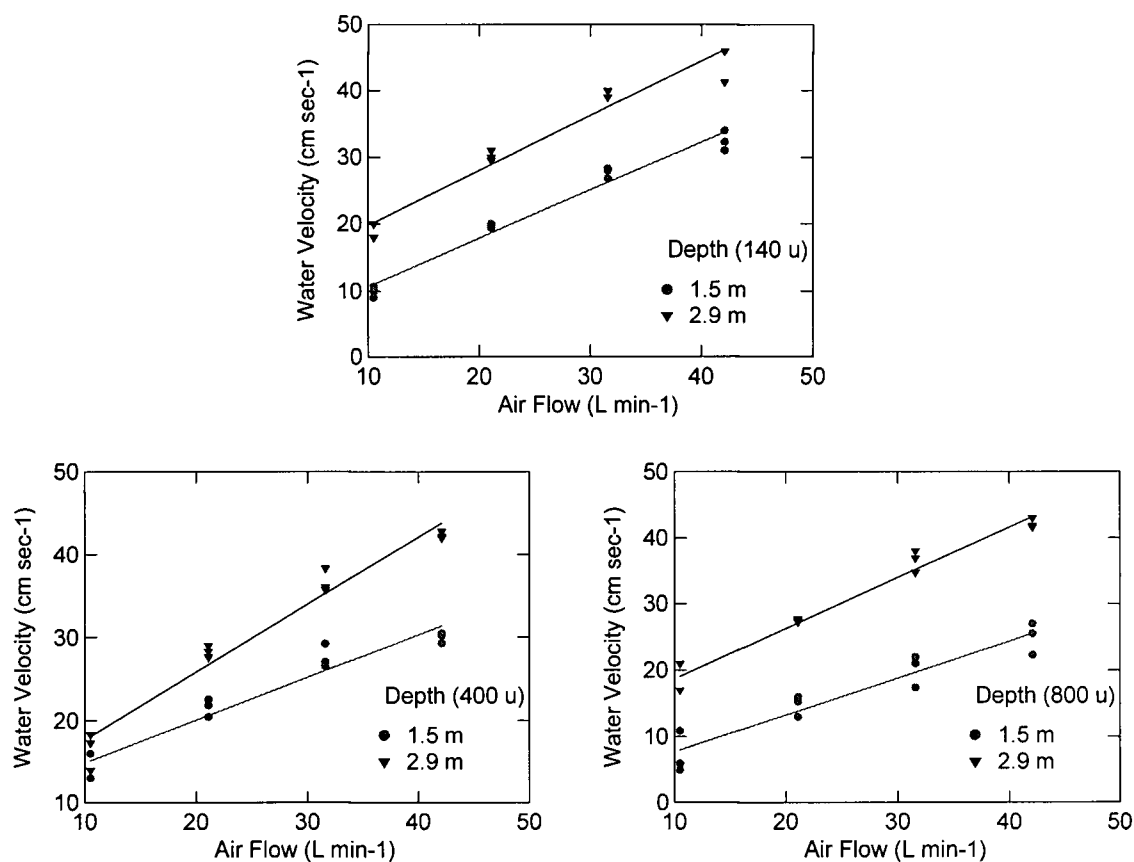
Figure 4.23a-c Water velocity vs. air flow rate at 1.5 or 2.9 m using 140 μ (a), 400 μ (b) and 800 μ (c) diffusers.

Table 4.47. Mean (± SE) water velocity (cm sec⁻¹) measured near the top of the downflow tube in the full lift hypolimnetic aerator – depth effect.

Treatment	Velocity (cm sec⁻¹)	Gas flow sig.	Depth sig.	Interaction	n
1.5 m x 140 μ - Air	22.4 (0.60)	Yes	Yes	No	12
2.9 m x 140 μ - Air	33.2 (0.60)				12
1.5 m x 400 μ - Air	23.3 (0.56)	Yes	Yes	Yes, 1.30	12
2.9 m x 400 μ - Air	31.0 (0.56)				12
1.5 m x 800 μ - Air	16.8 (0.59)	Yes	Yes	Yes, 1.98	12
2.9 m x 800 μ - Air	31.1 (0.59)				12

for the 1.5/2.9 m x 140 μ diffuser treatment (Table 4.46). A significant depth x gas flow rate interaction effect was observed for the 1.5/2.9 m x 400 μ and 1.5/2.9 m x 800 μ diffuser treatments, hence the data was log transformed and re-analyzed. The log transformation linearized the interaction effect, and indicates that velocity is significantly influenced by depth of release and gas flow rate, and that water velocity increases 1.30 fold at 2.9 m depth as compared to the 1.5 m depth of gas release with the 400 μ diffuser, and increases 1.98 fold at 2.9 m depth as compared to the 1.5 m depth of gas release with the 800 μ diffuser (Table 4.47).

4.2.3   Orifice Effect

Note: this component of the experiment examined the effect of gas flow variation (10 to 40 l min^{-1}) on water velocity in the outlet tube, using air only, with three orifice diameters (140 μ, 400 μ and 800 μ) at two diffuser depths (1.5 m and 2.9 m) in the full lift inlet tube. Within each subset of experiments, the orifice diameter and diffuser depth were held constant, while the gas flow rate and oxygen content (i.e., air or PSA oxygen) were varied.

The results for the analysis of covariance for the 140, 400 and 800 μ diffusers operating on air at 1.5 and 2.9 m depth are shown in Table 4.48. At the 1.5 m release depth, water velocity was significantly influenced by orifice diameter and gas flow rate, with velocity increasing with gas flow rate (Figure 4.24 a-b). Scheffe's test indicates the 140 and 400 μ diffusers induced significantly greater velocities than the 800 μ diffuser; however, there was no significant difference between the 140 and 400 μ diffusers. There was no significant interaction effect; however, the graph of the data (Figure 4.24 a) suggests an interaction between gas flow rate and water velocity for the 140 μ diffuser. The significance of the orifice by gas flow rate interaction effect was near the significance level cutoff (i.e., 0.012 vs. 0.01); hence, given the sample size and variance of the response, the test was not able to detect a significant interaction effect.
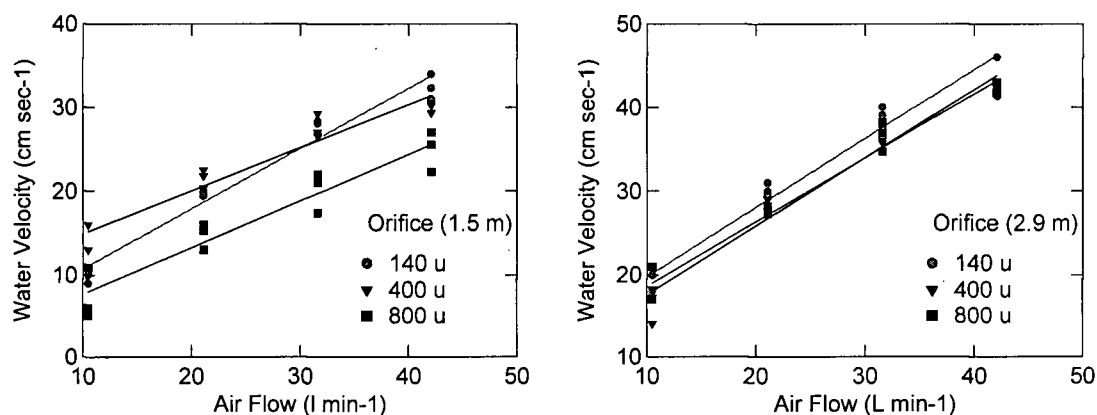
Figure 4.24a-b Water velocity vs. air flow rate for 140, 400 and 800 μ diffusers at 1.5 m (a) and 2.9 m (b).

Table 4.48. Mean (± SE) water velocity (cm sec^{-1}) measured near the top of the downflow tube in the full lift hypolimnetic aerator – orifice effect.

Treatment	Velocity (cm sec^{-1})	Gas flow sig.	Orifice sig.	Interaction	n
140 μ x 1.5 m – Air	22.4 (0.63)	Yes	Yes	No	12
400 μ x 1.5 m – Air	23.3 (0.63)				12
800 μ x 1.5 m – Air	16.8 (0.63)				12
140 μ x 2.9 m – Air	33.2 (0.58)	Yes	No	No	12
400 μ x 2.9 m – Air	31.0 (0.58)				12
800 μ x 2.9 m – Air	31.1 (0.58)				12

There was no statistically significant effect of orifice diameter on water velocity at the 2.9 m release depth, nor any orifice diameter x gas flow rate interaction effect (Table 4.47). There was a significant gas flow rate effect as would be expected, with water velocity increasing with increasing gas flow rate.

4.2.4   Full Lift Modifications Effect

Note: this component of the experiment examined the effect of gas flow variation (10 to 40 1

min^{-1}) on water velocity in the outlet tube, using air only, on four *in situ* modifications, using

two orifice diameters (140 µ and 800 µ) at a single diffuser depth (i.e., 2.9 m) in the full lift inlet

tube. Within each subset of experiments, the orifice diameter and diffuser depth were held

constant, while the gas flow rate and oxygen content (i.e., air or PSA oxygen) were varied.

The results for the analysis of covariance for the various *in situ* modifications of the full lift

hypolimnetic aerator with the 140 and 800 µ diffuser are shown in Table 4.49. All tests were

conducted at 2.9 m. Water velocity was significantly influenced ($\alpha \leq 0.01$) by the *in situ*

treatment and flow rate covariate effect (Figure 4.25 a-b). The no treatment option exhibited the

highest mean velocity, followed in decreasing order by the surface cover, bubble screen, DBCA

and vanes treatments. There were no significant modifications x flow rate interaction effect for

velocity. A similar result was obtained for the 800 µ diffuser (Figure 4.25 b and Table 4.49).

For the 140 µ diffuser, Scheffe's test indicates the no modifications treatment was significantly

greater than the DBCA and vanes treatments ($\alpha \leq 0.01$) for velocity (Table 4.50). In addition,

velocity for the surface cover treatment was significantly greater than the vanes treatment.

For the 800 µ diffuser, Scheffe's test indicates the no modifications treatment velocity was

significantly greater than the other treatments ($\alpha \leq 0.01$) (Table 4.51). In addition, velocity for

the bubble screen and DBCA treatment were significantly greater than the vanes treatment.
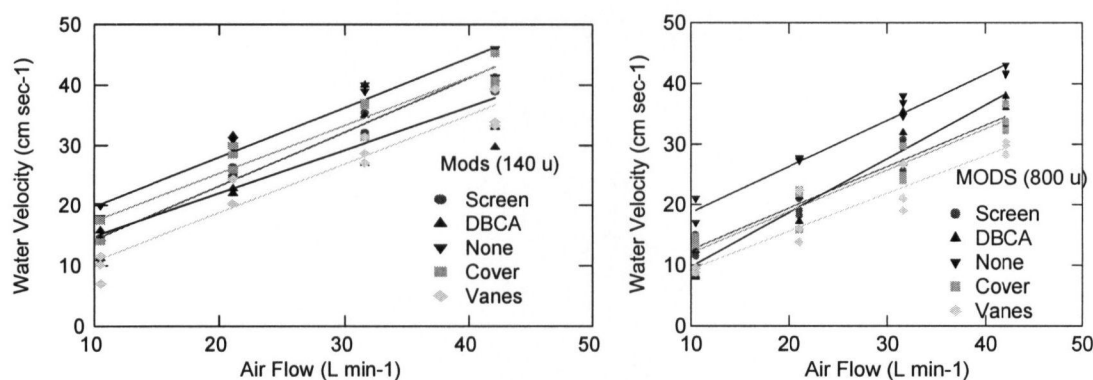
Figure 4.25a-b Water velocity vs. air flow rate at 2.9 m using 140 μ (a) or 800 μ (b) diffusers with *in situ* modifications.

Table 4.49.   Mean (± SE) water velocity (cm sec^{-1}) measured near the top of the downflow tube in the full lift hypolimnetic aerator – full lift *in situ* modifications effect.

Treatment	Velocity (cm sec^{-1})	Gas flow sig.	*In situ* sig.	Interaction	n
Bubble screen x 140 μ	29.0 (1.04)	Yes	Yes	No	11
DBCA x 140 μ	26.7 (0.95)				13
None x 140 μ	33.2 (0.99)				12
Surface cover x 140 μ	30.4 (0.99)				12
Vanes x 140 μ	23.9 (0.09)				12
Bubble screen x 800 μ	23.8 (0.77)	Yes	Yes	No	12
DBCA x 800 μ	24. 5 (0.81)				11
None x 800 μ	31.2 (0.77)				12
Surface cover x 800 μ	23.2 (0.77)				12
Vanes x 800 μ	19.6 (0.77)				12

Table 4.50.   Matrix of water velocity pairwise comparison probabilities for Scheffe's test for various *in situ* full lift hypolimnetic aerator treatments with the 140 μ diffuser.

Treatments	Bubble screen	DBCA	None	Surface cover	Vanes
Bubble screen	1.000				
DBCA	0.600	1.000			
None	0.085	**0.001**	1.000		
Surface cover	0.924	0.139	0.395	1.000	
Vanes	0.021	0.414	**0.000**	**0.001**	1.000

Table 4.51. Matrix of water velocity pairwise comparison probabilities for Scheffe's test for various *in situ* full lift hypolimnetic aerator treatments with the 800 μ diffuser.

Treatments	Bubble screen	DBCA	None	Surface cover	Vanes
Bubble screen	1.000				
DBCA	0.989	1.000			
None	0.000	0.000	1.000		
Surface cover	0.990	0.880	0.000	1.000	
Vanes	0.010	0.003	0.000	0.038	1.000

4.3 Full Lift Hypolimnetic Aeration – Bubble Size

A total of 1,890 bubble measurements were used in the statistical analysis (Table 4.52). A frequency histogram of the mean Equivalent Bubble Diameter (EQD) indicates the majority of bubbles were < 5 mm in equivalent diameter (Figure 4.26 a), with a mean equivalent bubble diameter of 3.7 mm and a range of 13.6 mm from the smallest to the largest bubble size. Due to the left skewed distribution of the equivalent bubble diameters, the data was transformed using a log x 2 transformation (Figure 4.26 b), and the statistical analyses conducted on the transformed data. The bubble photography was conducted during a 1.5 day photography session after the Group 1-14 tests had been completed, in order to minimize the cost of the photographer.

Table 4.52. Summary statistics for bubble measurements.

Number of cases	1,890
Min. EQD dia. (mm)	0.7
Max. EQD dia. (mm)	14.3
Range EQD dia. (mm)	13.6
Mean EQD dia. (mm)	3.7
Standard Dev. (mm)	1.9
CV (%)	52.4
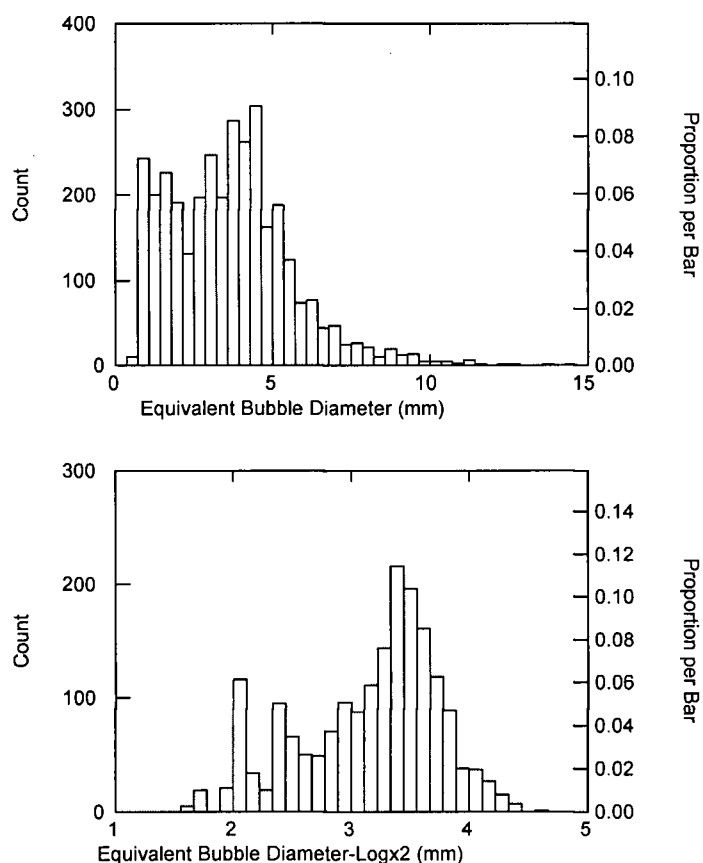
Figure 4.26a-b Frequency histogram, untranformed (a) and log x 2 transformed (b), of Equivalent Bubble Diameters.

The data are presented in two series of tables. The first series of tables (Tables 4.53, 4.54 and 4.55) illustrates the effect of gas flow rate on equivalent bubble diameter for the 140 μ, 400 μ and 800 μ diffusers measured under three different diffuser arrangements: (1) bubbles generated by each diffuser at 2.9 m and measured at 2.7 m; (2) bubbles generated by each diffuser at 2.9 m and measured at 0.5 m and (3) bubbles generated by each diffuser at 1.5 m and measured at 0.5 m. The purpose of this section of the experiments was to determine if bubble diameter changed as a function of depth of gas release (i.e., 2.9 m vs. 1.5 m), and if bubble diameter changed as

they rose through the water column (i.e., 2.7 m vs. 0.5 m), due to changes in hydrostatic pressure and possible coalescence/breakup during ascent through the water column.

Table 4.53. Mean equivalent bubble diameter, standard deviation and coefficient of variation of bubbles produced by the 140 μ diffuser at various depths of gas release and bubble measurement.

Gas flow (l min^{-1})	Orifice dia. (μ)	Diffuser depth (m)	Photo depth (m)	Mean equiv. Bubble dia. (mm)	SD (mm)	CV (%)	n
10	140	2.9	2.7	3.6	0.89	24.9	30
20	140	2.9	2.7	3.4	0.98	28.5	30
30	140	2.9	2.7	3.4	0.93	27.8	30
40	140	2.9	2.7	3.7	0.86	23.3	30
10	140	2.9	0.5	3.6	1.54	42.7	30
20	140	2.9	0.5	3.9	1.25	32.1	30
30	140	2.9	0.5	4.1	1.26	30.7	30
40	140	2.9	0.5	4.6	0.94	20.7	30
10	140	1.5	0.5	4.4	0.89	20.2	30
20	140	1.5	0.5	4.4	0.98	22.5	30
30	140	1.5	0.5	4.2	0.75	18.0	30
40	140	1.5	0.5	4.6	1.26	27.3	30

Table 4.54. Mean equivalent bubble diameter, standard deviation and coefficient of variation of bubbles produced by the 400 μ diffuser at various depths of gas release and bubble measurement.

Gas flow (l min^{-1})	Orifice dia. (μ)	Diffuser depth (m)	Photo depth (m)	Mean equiv. Bubble dia. (mm)	SD (mm)	CV (%)	n
10	400	2.9	2.7	4.3	1.01	23.3	30
20	400	2.9	2.7	4.7	1.22	25.8	30
30	400	2.9	2.7	5.0	1.43	28.5	30
40	400	2.9	2.7	4.3	1.93	45.2	30
10	400	2.9	0.5	4.2	1.52	36.2	30
20	400	2.9	0.5	4.1	1.7	41.2	30
30	400	2.9	0.5	4.0	2.13	54.0	30
40	400	2.9	0.5	4.2	2.31	54.8	30
10	400	1.5	0.5	3.3	1.97	60.2	30
20	400	1.5	0.5	4.3	1.87	43.3	30
30	400	1.5	0.5	3.2	1.95	61.8	30
40	400	1.5	0.5	3.4	2.10	61.3	30

Table 4.55.   Mean equivalent bubble diameter, standard deviation and coefficient of variation of bubbles produced by the 800 μ diffuser at various depths of gas release and bubble measurement.

Gas flow (l min⁻¹)	Orifice dia. (μ)	Diffuser depth (m)	Photo depth (m)	Mean equiv. Bubble dia. (mm)	SD (mm)	CV (%)	n
10	800	2.9	2.7	5.7	2.57	45.4	30
20	800	2.9	2.7	3.5	2.26	64.5	30
30	800	2.9	2.7	5.3	2.38	44.7	30
40	800	2.9	2.7	3.5	2.16	62.4	30
10	800	2.9	0.5	2.8	2.06	73.1	30
20	800	2.9	0.5	3.3	2.40	72.3	30
30	800	2.9	0.5	3.5	2.43	70.4	30
40	800	2.9	0.5	3.6	2.05	56.8	30
10	800	1.5	0.5	2.8	2.91	104.2	30
20	800	1.5	0.5	3.3	2.45	74.0	30
30	800	1.5	0.5	3.1	2.45	79.2	30
40	800	1.5	0.5	3.9	3.11	80.5	30

The second series of tables (Tables 4.56 and 4.57) shows the effect of gas flow rate on equivalent bubble diameter for the 140 μ and 800 μ diffusers with a control case (i.e. None) and three *in situ* modifications: (1) DBCA; (2) bubble screen and (3) vanes. The bubbles were generated at a fixed depth of 2.9 m and measured at 0.5 m. The purpose of this was to determine if bubble diameter changed as a function of the *in situ* modifications.

Table 4.56.   Mean equivalent bubble diameter, standard deviation and coefficient of variation of bubbles produced by the 140 μ diffuser with *in situ* modifications. (Note: 7/3, 17/3, 27/3 and 37/3 refers to the gas flow, in l min⁻¹, to the diffuser in the inlet tube, and the DBCA diffuser in the separator box).

Group	Gas flow (l min⁻¹)	Orifice dia. (μ)	Diffuser depth (m)	Photo depth (m)	Mean equiv. Bubble dia. (mm)	SD (mm)	CV (%)	n
1-Cont.	10	140	2.9	0.5	3.6	1.54	42.7	30
1-Cont.	20	140	2.9	0.5	3.9	1.25	32.1	30
1-Cont.	30	140	2.9	0.5	4.1	1.26	30.7	30
1-Cont.	40	140	2.9	0.5	4.6	0.94	20.7	30
7-DBCA	7/3	140	2.9	0.5	1.7	0.87	50.0	30
7-DBCA	17/3	140	2.9	0.5	1.7	0.96	55.5	30

Group	Gas flow (l min^{-1})	Orifice dia. (μ)	Diffuser depth (m)	Photo depth (m)	Mean equiv. Bubble dia. (mm)	SD (mm)	CV (%)	n
7-DBCA	27/3	140	2.9	0.5	2.0	0.91	45.9	30
7-DBCA	37/3	140	2.9	0.5	1.5	0.83	55.5	30
9-Screen	10	140	2.9	0.5	4.3	0.96	22.3	30
9-Screen	20	140	2.9	0.5	3.7	1.28	35.1	30
9-Screen	30	140	2.9	0.5	3.7	0.90	24.6	30
9-Screen	40	140	2.9	0.5	4.0	1.43	35.6	30
13-Vane	10	140	2.9	0.5	4.5	0.91	20.4	30
13-Vane	20	140	2.9	0.5	4.5	0.79	17.6	30
13-Vane	30	140	2.9	0.5	4.1	0.90	22.1	30
13-Vane	40	140	2.9	0.5	4.4	1.13	25.6	30

Table 4.57. Mean equivalent bubble diameter, standard deviation and coefficient of variation of bubbles produced by the 800 μ diffuser with *in situ* modifications (Note: 7/3, 17/3, 27/3 and 37/3 refers to the gas flow, in l min^{-1}, to the diffuser in the inlet tube, and the DBCA diffuser in the separator box).

Group	Gas flow (l min^{-1})	Orifice dia. (μ)	Diffuser depth (m)	Photo depth (m)	Mean equiv. Bubble dia. (mm)	SD (mm)	CV (%)	n
5-Cont.	10	800	2.9	0.5	2.8	2.06	73.1	30
5-Cont.	20	800	2.9	0.5	3.3	2.40	72.3	30
5-Cont.	30	800	2.9	0.5	3.5	2.43	70.4	30
5-Cont.	40	800	2.9	0.5	3.6	2.05	56.8	30
8-DBCA	7/3	800	2.9	0.5	2.8	1.10	39.4	30
8-DBCA	17/3	800	2.9	0.5	1.8	0.72	41.3	30
8-DBCA	27/3	800	2.9	0.5	1.7	1.02	60.2	30
8-DBCA	37/3	800	2.9	0.5	1.6	0.79	49.6	30
10-Screen	10	800	2.9	0.5	3.7	1.49	40.3	30
10-Screen	20	800	2.9	0.5	3.4	1.53	45.1	30
10-Screen	30	800	2.9	0.5	3.9	1.11	28.2	30
10-Screen	40	800	2.9	0.5	3.9	1.09	28.1	30
14-Vane	10	800	2.9	0.5	5.7	2.61	46.2	30
14-Vane	20	800	2.9	0.5	4.5	2.31	51.0	30
14-Vane	30	800	2.9	0.5	5.0	2.43	48.6	30
14-Vane	40	800	2.9	0.5	3.7	1.21	32.8	30

4.3.1   Depth Effect

This component of the experiment examined the effect of gas flow variation (10 to 40 l min⁻¹)

and three combinations of diffuser/bubble measurement depth (i.e., 1.5/0.5 m, 2.9/0.5 m and

2.9/2.7 m) in the full lift inlet tube, on EQD, on air, with three orifice diameters (140 μ, 400 μ

and 800 μ).

4.3.1.1   140 μ diffuser at 1.5/0.5 m, 2.9/0.5 m and 2.9/2.7 m

The results for the analysis of covariance for the 140 μ diffuser x 1.5/0.5 m, 2.9/0.5 m and

2.9/2.7 m (i.e., bubble release depth/bubble measurement depth) treatments are shown in Table

4.58. Significant results ($\alpha \leq 0.01$) were obtained for the depth effect, and a borderline effect

(i.e., $\alpha = 0.01$) was observed for the gas flow rate covariate effect (Figure 4.27). Bubble size

was largest for the 1.5/0.5 m combination, then decreased in size at the 2.9/0.5 m and 2.9/2.7 m

depth combinations. No depth x gas flow rate interaction effect was observed for any of the

treatments (Table 4.58).

Table 4.58.   **Adjusted least squares means (± SE), treatment and interaction effects for the 140 μ diffuser on air at bubble release depth/bubble measurement depth combinations of 1.5/0.5 m, 2.9/0.5 m and 2.9/2.7 m depths. (* = marginal effect; $\alpha = 0.01$).**

Treatment	EQD dia. (mm)	Gas flow sig.	Depth sig.	Interaction	n
1.5/0.5 m	4.4 (0.10)	Yes*	Yes	No	120
2.9/0.5 m	4.0 (0.10)				120
2.9/2.7 m	3.5 (0.10)				120

Scheffe's test indicates the equivalent bubble diameter (i.e., EQD) for the 2.9/2.7 m treatment

was significantly smaller ($\alpha \leq 0.01$) than the 1.5/0.5 m treatment combination. There were no

significant differences with the other pairwise comparisons.
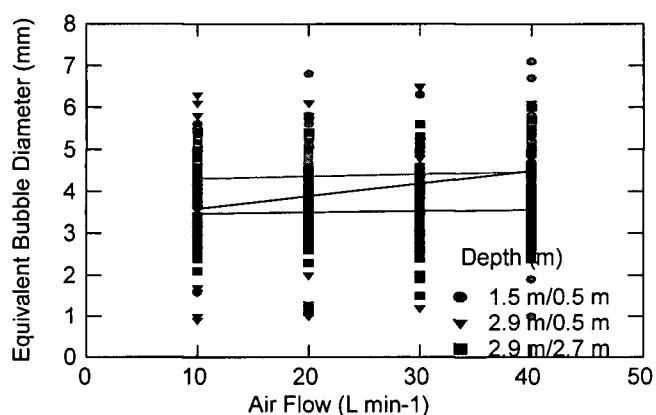
Figure 4.27 Equivalent Bubble Diameter vs. air flow rate with 140 μ diffuser at diffuser submergence depth and measurement depth combinations of 1.5/0.5 m, 2.9/0.5 m and 2.9/2.7 m.

4.3.1.2   400 μ diffuser at 1.5/0.5 m, 2.9/0.5 m and 2.9/2.7 m

The results for the analysis of covariance for the 400 μ diffuser x 1.5/0.5 m, 2.9/0.5 m and

2.9/2.7 m treatments are shown in Table 4.59. A significant result (α ≤ 0.01) was obtained for

the depth effect (Figure 4.28). Bubble size was smallest for the 1.5/0.5 m combination, then

increased in size at the 2.9/0.5 m and 2.9/2.7 m depth combinations. No depth x gas flow rate

interaction effect was observed for any of the treatments (Table 4.59).
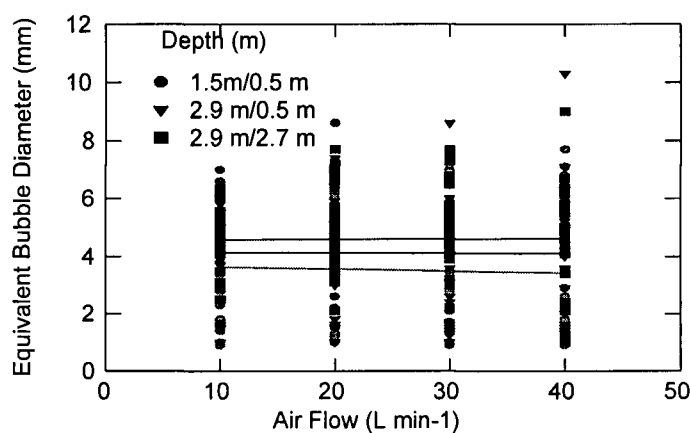
Figure 4.28 Equivalent Bubble Diameter vs. air flow rate with 400 μ diffuser at diffuser submergence depth and measurement depth combinations of 1.5/0.5 m, 2.9/0.5 m and 2.9/2.7 m.

Table 4.59.   Adjusted least squares means (± SE), treatment and interaction effects for the 400 μ diffuser on air at bubble release depth/bubble measurement depth combinations of 1.5/0.5 m, 2.9/0.5 m and 2.9/2.7 m depths.

Treatment	EQD dia. (mm)	Gas flow sig.	Depth sig.	Interaction	n
1.5/0.5 m	3.5 (0.17)	No	Yes	No	120
2.9/0.5 m	4.1 (0.17)				120
2.9/2.7 m	4.6 (0.17)				120

Scheffe's test indicates the 2.9/2.7 m treatment was significantly larger ($\alpha \leq 0.01$) than the 1.5/0.5 m treatment combination for bubble size. There were no significant differences with the other pairwise comparisons.

4.3.1.3   800 μ diffuser at 1.5/0.5 m, 2.9/0.5 m and 2.9/2.7 m

The results for the analysis of covariance for the 800 μ diffuser x 1.5/0.5 m, 2.9/0.5 m and 2.9/2.7 m treatments are shown in Table 4.60. A significant result ($\alpha \leq 0.01$) was obtained for the depth effect (Figure 4.29). The results were similar to the 400 μ treatment combination, i.e., EQD was smallest for the 1.5/0.5 m combination, then increased in size at the 2.9/0.5 m and 2.9/2.7 m depth combinations. A depth x gas flow rate interaction effect was observed for the treatments 2.9/2.7 m depth combinations, with bubble size tending to decrease with increasing gas flow rate (Figure 4.29, Table 4.60).

Table 4.60.   Adjusted least squares means (± SE), treatment and interaction effects for the 800 μ diffuser on air at bubble release depth/bubble measurement depth combinations of 1.5/0.5 m, 2.9/0.5 m and 2.9/2.7 m depths.

Treatment	EQD dia. (mm)	Gas flow sig.	Depth sig.	Interaction	n
1.5/0.5 m	3.3 (0.23)	No	Yes	Yes	120
2.9/0.5 m	3.3 (0.23)				120
2.9/2.7 m	4.5 (0.23)				120
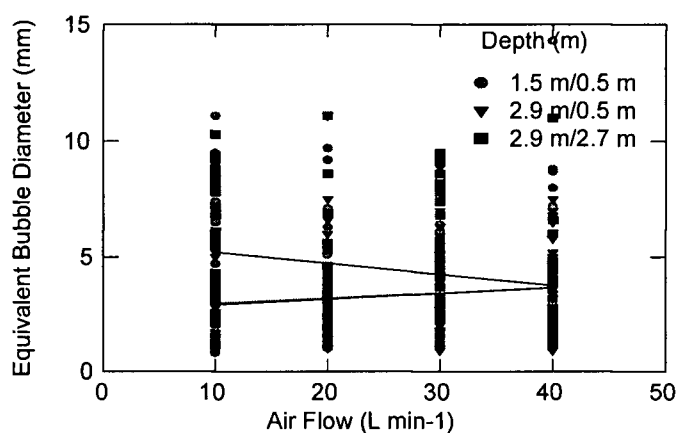
Figure 4.29 Equivalent Bubble Diameter vs. air flow rate with 800 μ diffuser at diffuser submergence depth and measurement depth combinations of 1.5/0.5 m, 2.9/0.5 m and 2.9/2.7 m.

Scheffe's test was not conducted due to the confounding effect of the gas flow rate by depth interaction.

4.3.2 Orifice Diameter Effect

This component of the experiment examined the effect of gas flow variation (10 to 40 l min^{-1}) and orifice diameter (140 μ, 400 μ and 800 μ), on EQD, on air, at three combinations of diffuser/bubble measurement depth (i.e., 1.5/0.5 m, 2.9/0.5 m and 2.9/2.7 m) in the full lift inlet tube.

4.3.2.1 1.5/0.5 m with 140 μ, 400 μ and 800 μ diameter orifice

The results of the analysis of covariance for the 1.5/0.5 m combination with the 140 μ, 400 μ and 800 μ diameter orifice treatments are shown in Table 4.61. A significant result ($\alpha \leq 0.01$) was obtained for the orifice diameter effect (Figure 4.30). EQD was smallest for the 800 μ
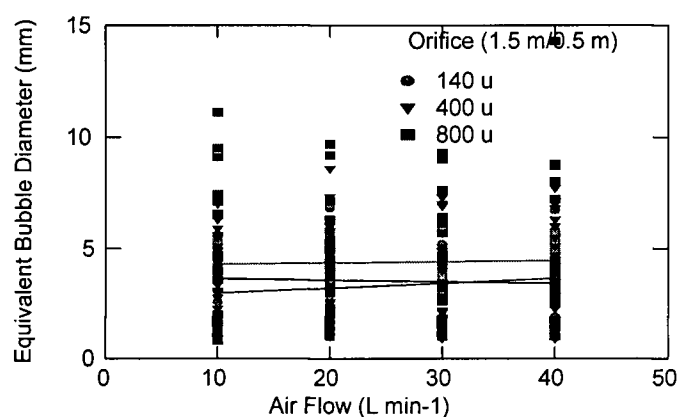
Figure 4.30 Equivalent Bubble Diameter vs. air flow rate at diffuser submergence depth and measurement depth combination of 1.5/0.5 m with 140, 400 and 800 μ diffuser.

diameter diffuser, then increased in size for the 400 μ and 140 μ treatments. No orifice diameter

x gas flow rate interaction effect was observed for any of the treatments (Table 4.61).

Table 4.61. Adjusted least squares means (± SE), treatment and interaction effects for the bubble release depth/bubble measurement depth combination of 1.5/0.5 m with 140 μ, 400 μ and 800 μ diameter diffuser orifices.

Treatment	EQD dia. (mm)	Gas flow sig.	Orifice sig.	Interaction	n
140 μ	4.4 (0.19)	No	Yes	No	120
400 μ	3.5 (0.19)				120
800 μ	3.3 (0.19)				120

Scheffe's test indicates the equivalent bubble diameter for the 400 μ and 800 μ diameter orifice treatments were significantly smaller ($\alpha \leq 0.01$) than the 140 μ diameter orifice treatment; however, they were not significantly different from each other.

4.3.2.2   2.9/0.5 m with 140 μ, 400 μ and 800 μ diameter orifice

The results of the analysis of covariance for the 2.9/0.5 m combination with the 140 μ, 400 μ

and 800 μ diameter orifice treatments are shown in Table 4.62. A significant result ($\alpha \leq 0.01$)

was obtained for the orifice diameter effect (Figure 4.31). Bubble size was smallest for the 800

μ diameter diffuser, then increased in diameter for the 400 μ and 140 μ treatments. No orifice

diameter x gas flow rate interaction effect was observed for any of the treatments (Table 4.62).

Scheffe's test indicates the equivalent bubble diameter for the 800 μ diameter orifice treatment

was significantly smaller ($\alpha \leq 0.01$) than the 140 μ and 400 μ diameter orifice treatments. The

140 μ and 400 μ orifice diameter treatments were not significantly different from each other.
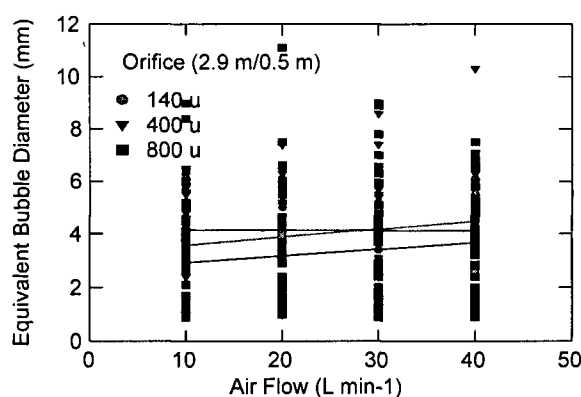
Figure 4.31   **Equivalent Bubble Diameter vs. air flow rate at diffuser submergence depth and measurement depth combination of 2.9/0.5 m with 140, 400 and 800 μ diffuser.**

Table 4.62.   **Adjusted least squares means (± SE), treatment and interaction effects for the bubble release depth/bubble measurement depth combination of 2.9/0.5 m with 140 μ, 400 μ and 800 μ diameter diffuser orifices.**

Treatment	EQD dia. (mm)	Gas flow sig.	Orifice sig.	Interaction	n
140 μ	4.0 (0.17)	No	Yes	No	120
400 μ	4.1 (0.17)				120
800 μ	3.3 (0.17)				120

4.3.2.3 2.9/2.7 m with 140 μ, 400 μ and 800 μ diameter orifice

The results of the analysis of covariance for the 2.9/2.7 m combination with the 140 μ, 400 μ

and 800 μ diameter orifice treatments are shown in Table 4.63. A significant result ($\alpha \leq 0.01$)

was obtained for the orifice diameter effect (Figure 4.32). Bubble size was largest for the 400 μ

and 800 μ diameter diffusers, then decreased in diameter for the140 μ treatment. No orifice

diameter x gas flow rate interaction effect was observed for any of the treatments (Table 4.63).

Scheffe's test indicates the equivalent bubble diameter for the 400 μ diameter orifice treatment

was significantly larger ($\alpha \leq 0.01$) than the 140 μ diameter orifice treatment. There were no

significant differences with the other pairwise comparisons.
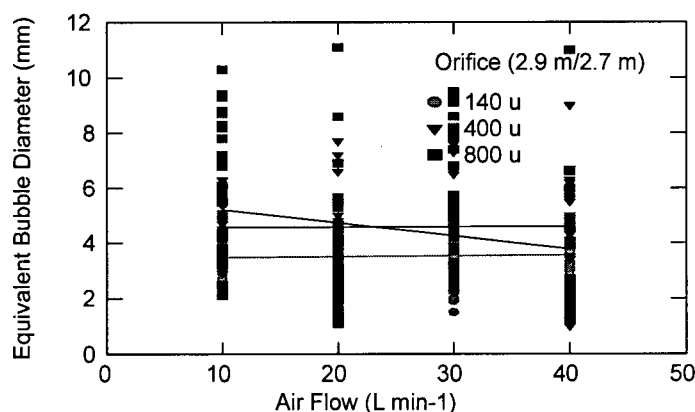
Figure 4.32 **Equivalent Bubble Diameter vs. air flow rate at diffuser submergence depth and measurement depth combinations of 2.9/2.7 m with 140, 400 and 800 μ diffuser.**

Table 4.63. Adjusted least squares means (± SE), treatment and interaction effects for the air release depth/photo measurement depth combination of 2.9 m/2.7 m with 140 μ, 400 μ and 800 μ diameter diffuser orifices.

Treatment	EQD dia. (mm)	Gas flow sig.	Orifice sig.	Interaction	n
140 μ	3.5 (0.16)	No	Yes	No	120
400 μ	4.6 (0.16)				120
800 μ	4.5 (0.16)				120

4.3.3   Full Lift Modifications Effect

This component of the experiment examined the effect of gas flow variation (10 to 40 l min^{-1})

and *in situ* modifications (i.e., DBCA, Vanes and Screen), on EQD, on air, with the 140 μ and

800 μ diffuser in the full lift inlet tube. All tests were conducted at a bubble release depth of 2.9

m, and measurement depth of 0.5 m. The Surface Cover treatment was not included in the tests.

4.3.3.1   140 μ orifice with DBCA, Screen, Vanes and Control

The results of the analysis of covariance for the 140 μ orifice with the *in situ* modification

treatments are shown in Table 4.64. A significant interaction effect was observed (Figure

4.33 a), hence the data was re-analyzed without the Control treatment which caused the interac-

tion effect (Figure 4.33 b). Bubble size was largest for the Vanes treatment, then decreased

slightly in diameter for the bubble breaker treatment, then a large decrease for the DBCA

treatment (Table 4.64). No *in situ* modifications x gas flow rate interaction effect was observed

for any of the treatments once the Control treatment data was removed from the analysis (Table

4.64).

Table 4.64.   Mean (± SE) equivalent bubble diameter (mm) for the air release
depth/bubble measurement depth combination of 2.9 m/0.5 m with 140 μ
for the full lift hypolimnetic aerator – full lift *in situ* modifications effect.

Treatment	EQD dia. (mm)	Gas flow sig.	Mods sig.	Interaction	n
Screen	3.9 (0.09)	No	Yes	No	120
DBCA	1.7 (0.09)				120
Vanes	4.4 (0.09)				120

Scheffe's test indicates the equivalent bubble diameter for the DBCA treatment was signifi-

cantly smaller (α ≤ 0.01) than the Screens or Vanes treatment. There were no significant

differences with the other pairwise comparisons.
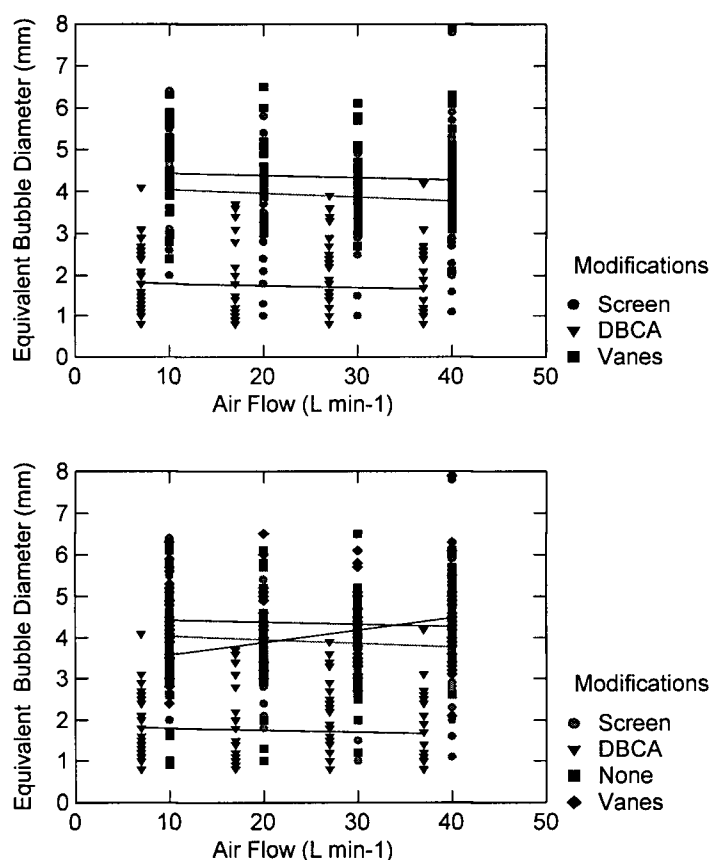
Figure 4.33a-b Equivalent Bubble Diameter vs. air flow rate at diffuser submergence depth and measurement depth combinations of 2.9/0.5 m with 140 μ diffuser with *in situ* modifications (a), and without the Control treatment (b).

4.3.3.2   800 μ orifice with DBCA, Screen, Vanes and Control

The results of the analysis of covariance for the 800 μ orifice with the *in situ* modification

treatments are shown in Table 4.65. A significant interaction effect was observed (Figure 4.34

a), hence the data was re-analyzed in two data sets. The first data set included the DBCA and

Vanes treatments (Figure 4.34 b) without the Screen or Control treatments that caused the
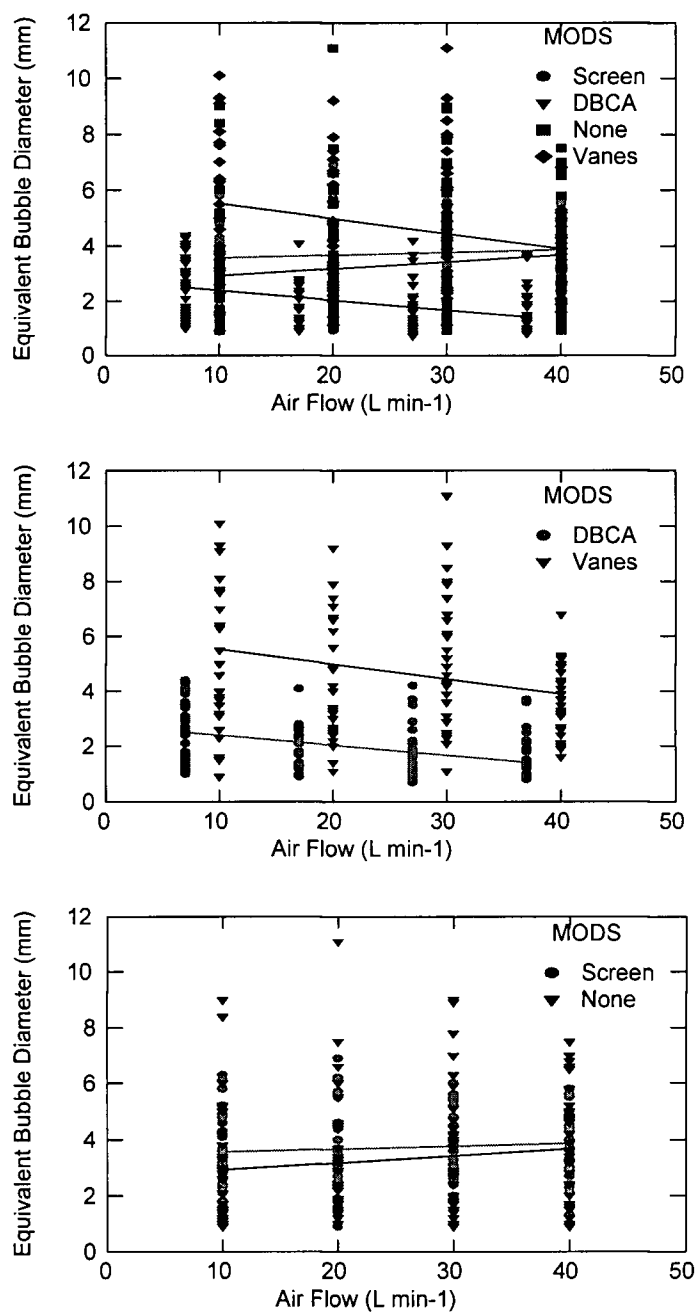
Figure 4.34a-c Equivalent Bubble Diameter on air at diffuser submergence depth and measurement depth combinations of 2.9/0.5 m with 800 μ diffuser and *in situ* modifications (a), with DBCA and Vanes only (b), and with Control and Screen treatments only (c).

interaction effect. The results were similar to the 140 μ analysis, i.e., bubble size was largest for

the Vanes treatment, then a large decrease for the DBCA treatment (Table 4.64). No *in situ*

modifications x gas flow rate interaction effect was observed for the DBCA and Vanes treat-

ment pair, however, the *in situ* modifications effect and gas flow effect were both significant

(Table 4.65).

Table 4.65.   Mean (± SE) equivalent bubble diameter (mm) for the air release
depth/bubble measurement depth combination of 2.9 m/0.5 m with 800 μ
for the full lift hypolimnetic aerator – full lift *in situ* modifications effect:
DBCA and vanes.

Treatment	EQD dia. (mm)	Gas flow sig.	Mods sig.	Interaction	n
DBCA	1.9 (0.16)	Yes	Yes	No	120
Vanes	4.8 (0.16)				120

The second data set included the Screen and Control treatments (Figure 4.34 c) without the

DBCA or Vanes treatments. The results indicate EQD was significantly larger for the Screens

treatment (Table 4.66). No *in situ* modifications x gas flow rate interaction effect was observed

for the Screen and Control treatment pair, however, the *in situ* modifications effect was signifi-

cant (Table 4.66).

Table 4.66.   Mean (± SE) equivalent bubble diameter (mm) for the air release
depth/bubble measurement depth combination of 2.9 m/0.5 m with 800 μ
for the full lift hypolimnetic aerator – full lift *in situ* modifications effect:
Screen and Control.

Treatment	EQD dia. (mm)	Gas flow sig.	Mods sig.	Interaction	n
Screen	3.7 (0.17)	No	Yes	No	120
Control	3.3 (0.17)				120

4.4   Full Lift Hypolimnetic Aeration – Oxygen Transfer Locations

As indicated in the Methods (3.3.2), the six oxygen probe locations for the full lift aerator were

located at the top, middle and bottom of the inlet and outlet tubes. This placement was designed

to identify five zones of oxygen transfer: Zone 1 - between the entrance (Probe 1) and midpoint

of the inlet tube (Probe 2); Zone 2 - between the midpoint (Probe 2) and top of the inlet tube at

the entrance to the separator box (Probe 3); Zone 3 – between the entrance (Probe 3) and exit

(Probe 4) of the separator box; Zone 4 - between the top of the outlet tube at the exit of the

separator box (Probe 4) and midpoint of the outlet tube (Probe 5); and Zone 5 - between the

midpoint (Probe 5) and exit of the outlet tube (Probe 6) (see Figure 3.3). The data for each

aeration zone was obtained by calculating the differential oxygen concentration from the six

probes at each time stamp during the particular test, thus creating a series of graphs showing

five lines of differential oxygen concentrations for the duration of each test. The data is pre-

sented qualitatively, as the net result of the various experimental treatments has already been

quantitatively discussed for K_La_{20}, SOTR, SAE and SOTE. In order to minimize the number of

graphs presented, only one graph per treatment combination is shown, although the trends were

similar for each of the three replicates per treatment. The rationale for presenting this data is to

identify patterns or zones of oxygen transfer within the full lift aerator as a function of specific

treatments, which document the performance of the current system, and provide insight into

future design modifications to potentially improve oxygen transfer.

4.4.1   140 μ x 2.9 m x air

The oxygen differential was greatest in Zone 1, followed by Zones 2 and Zone 3 (Figure 4.35

a-d). The oxygen differential was slightly negative in Zones 4 and 5; indicating oxygen concen-

trations were decreasing in these zones. A slight downward trend was observed over the

Concentration reading differences between two adjacent probes

Concentration reading differences between two adjacent probes
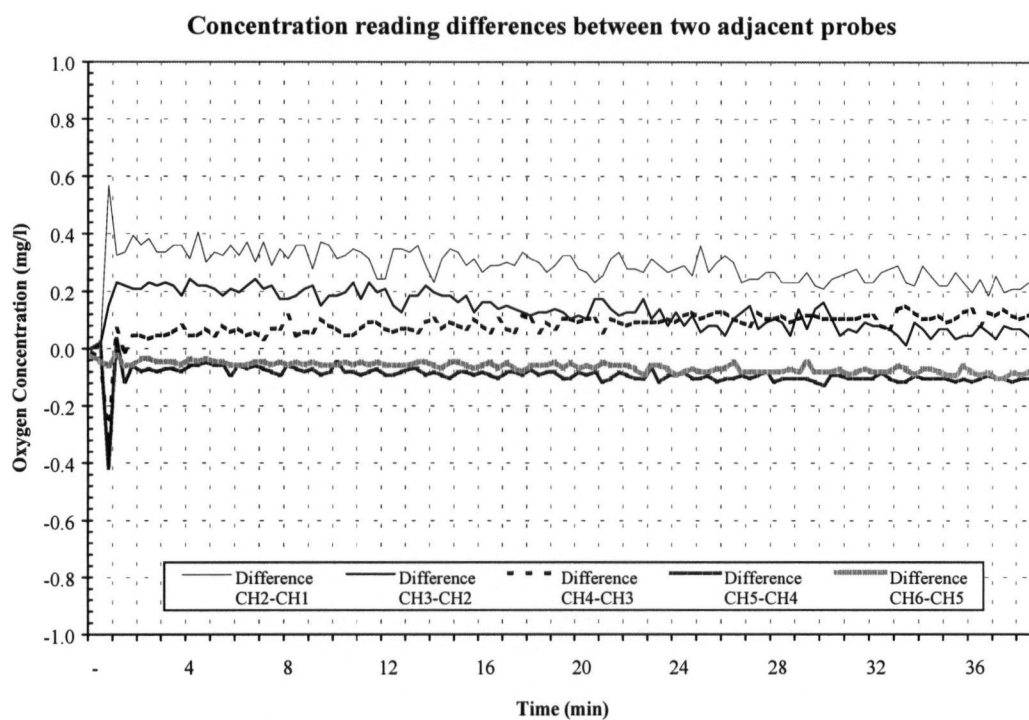
Figure 4.35a-d Oxygen differentials in full lift aerator on air at 2.9 m with 140 μ diffuser at 10 l min^{-1} (a), 20 l min^{-1} (b), 30 l min^{-1} (c), 40 l min^{-1} (d).

Figure 4.35 continued
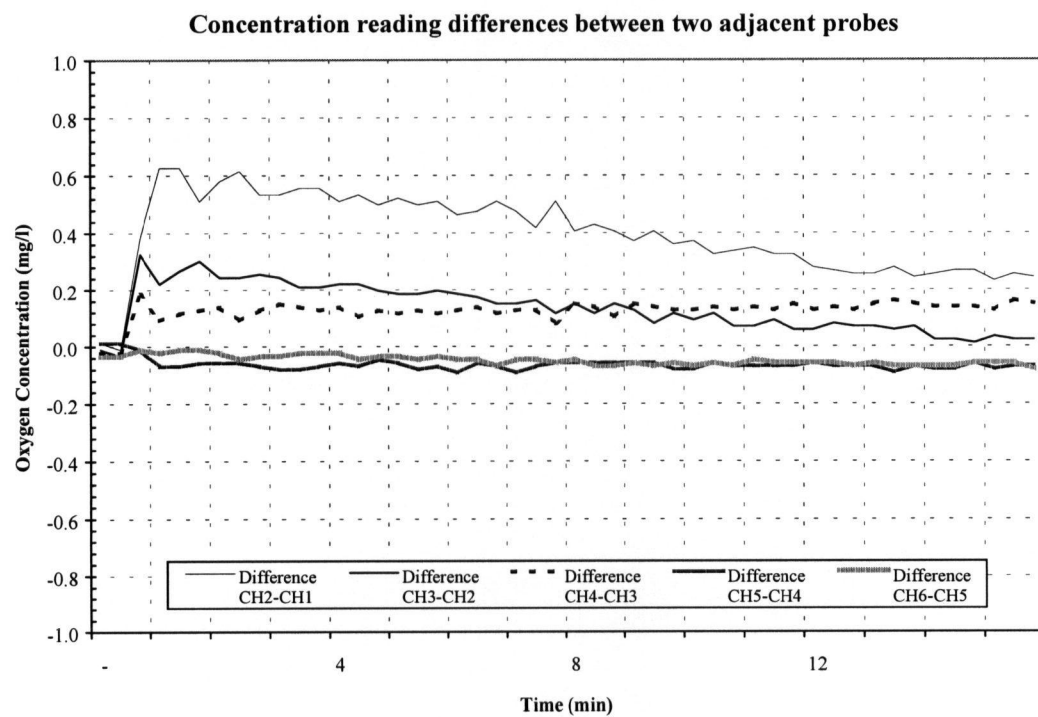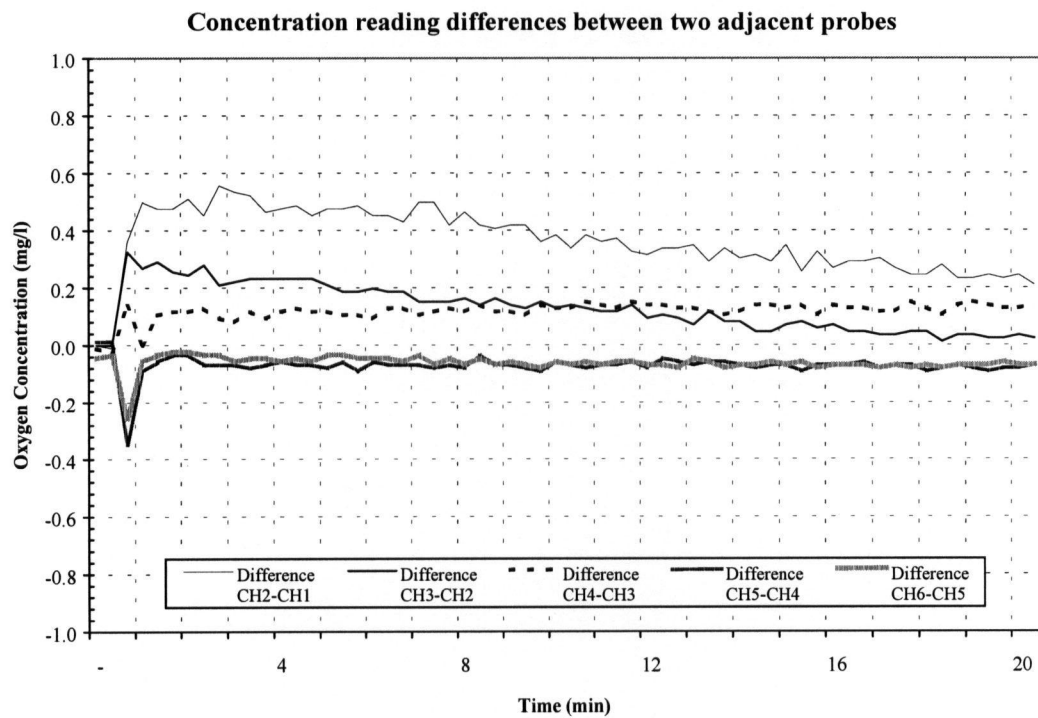
Concentration reading differences between two adjacent probes

Concentration reading differences between two adjacent probes

duration of the test in Zones 1 and 2, whereas Zones 3, 4 and 5 were fairly constant. The general trend with increasing gas flows from 10 to 40 l min^{-1} was an increase in the oxygen differential in Zone 1, and an increase in slope for Zones 2 and 3.

4.4.2   140 μ x 1.5 m x air

The oxygen differential was greatest in Zone 2, followed by Zone 3 (Figure 4.36 a-d). The oxygen differential was near zero in Zone 1, and slightly negative in Zones 4 and 5, indicating oxygen concentrations were decreasing in these zones. A downward trend was observed over the duration of the test in Zones 2, whereas Zones 1, 3, 4 and 5 were fairly constant. The general trend with increasing gas flows was an increase in the oxygen differential and slope in Zone 2, and a greater loss of oxygen in Zone 5.

4.4.3   400 μ x 2.9 m x air

The oxygen differential was greatest in Zone 1, followed by Zones 2 and Zone 3 (Figure 4.37 a-d). The oxygen differential was slightly negative in Zones 4 and 5; indicating oxygen concentrations were decreasing in these zones. No downward trend was observed over the duration of the test in Zones 1-5. The general trend with increasing gas flows was an increase in the oxygen differential and slope in Zones 1 and 2, and an increased loss of oxygen in Zone 5.

4.4.4   400 μ x 1.5 m x air

The oxygen differential was greatest in Zone 2, followed by Zone 3 (Figure 4.38 a-d). The oxygen differential was near zero in Zone 1, and slightly negative in Zones 4 and 5. A downward trend was observed over the duration of the test in Zone 2, whereas Zones 1, 3, 4 and 5

Concentration reading differences between two adjacent probes

Concentration reading differences between two adjacent probes
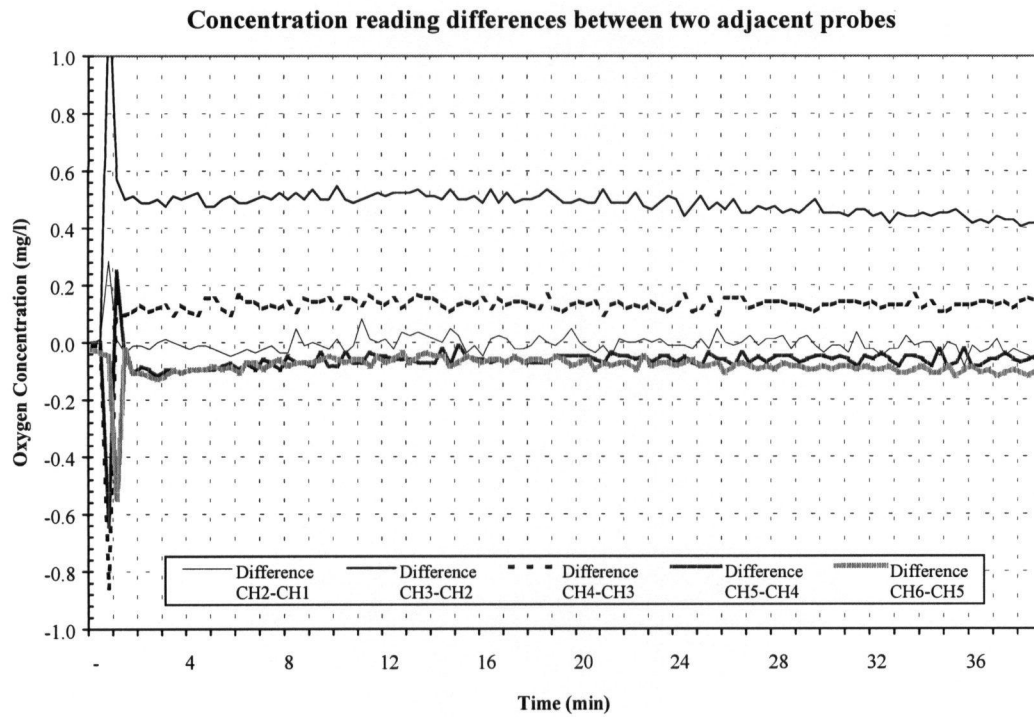
Figure 4.36a-d Oxygen differentials in full lift aerator on air at 1.5 m with 140 μ diffuser at 10 l min^{-1} (a), 20 l min^{-1} (b), 30 l min^{-1} (c), 40 l min^{-1} (d).

Figure 4.36 continued

Concentration reading differences between two adjacent probes

Concentration reading differences between two adjacent probes
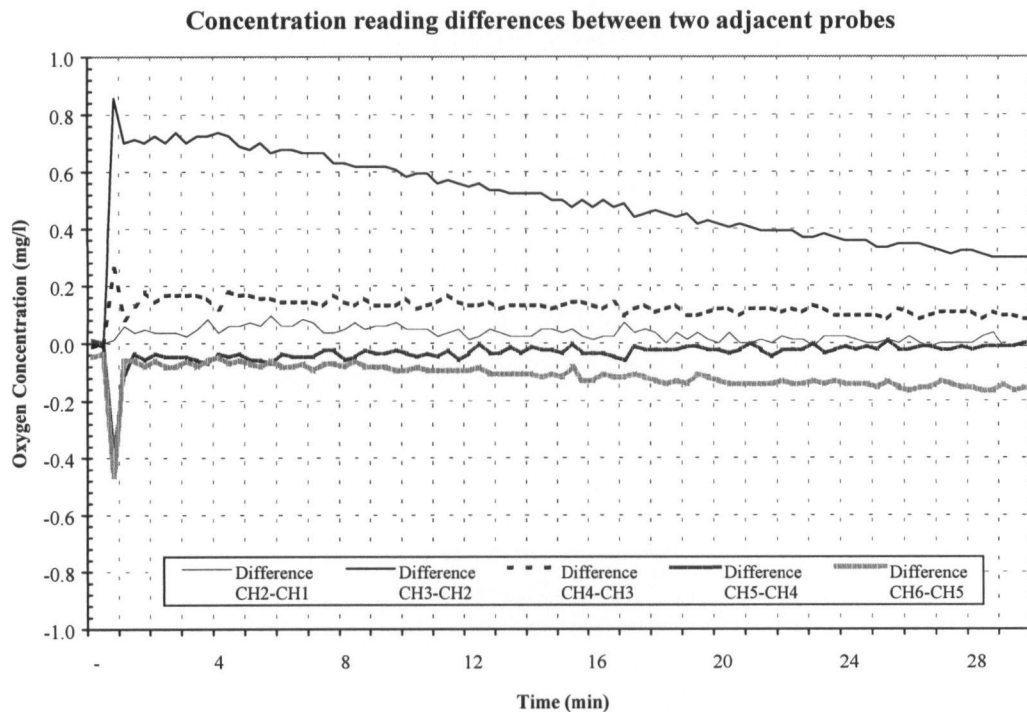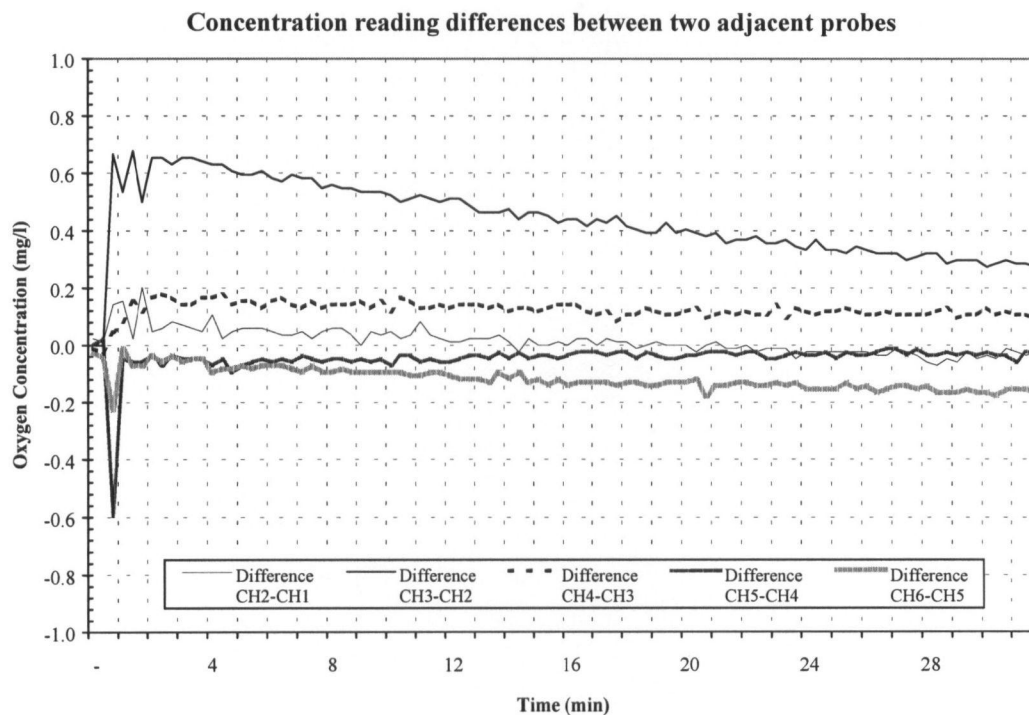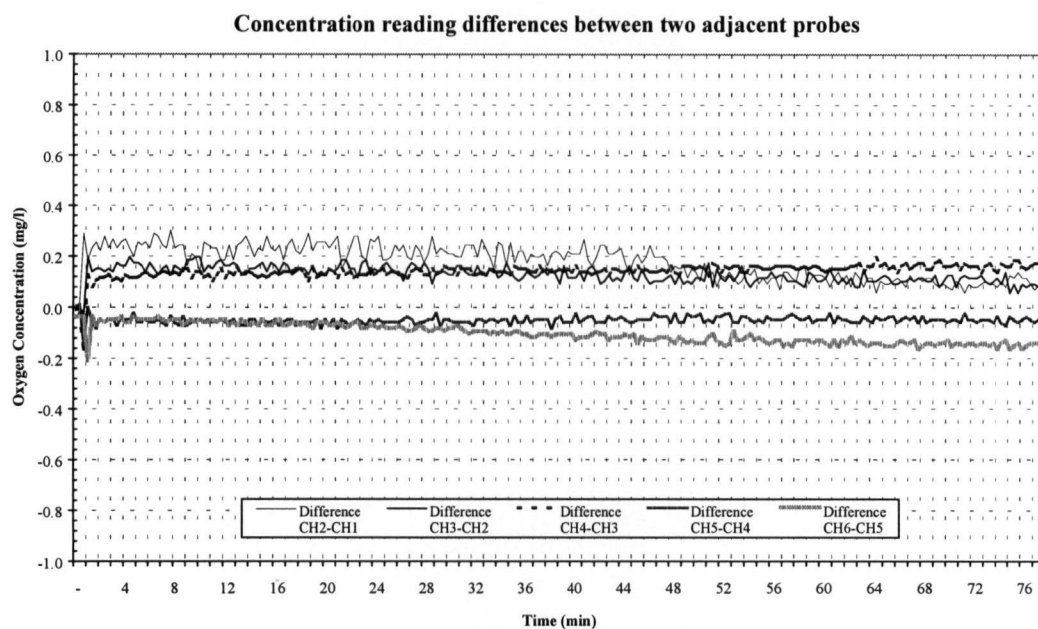
Figure 4.37a-d Oxygen differentials in full lift aerator on air at 2.9 m with 400 µ diffuser at 10 l min^{-1} (a), 20 l min^{-1} (b), 30 l min^{-1} (c), 40 l min^{-1} (d).

Figure 4.37 continued

Concentration reading differences between two adjacent probes

Concentration reading differences between two adjacent probes
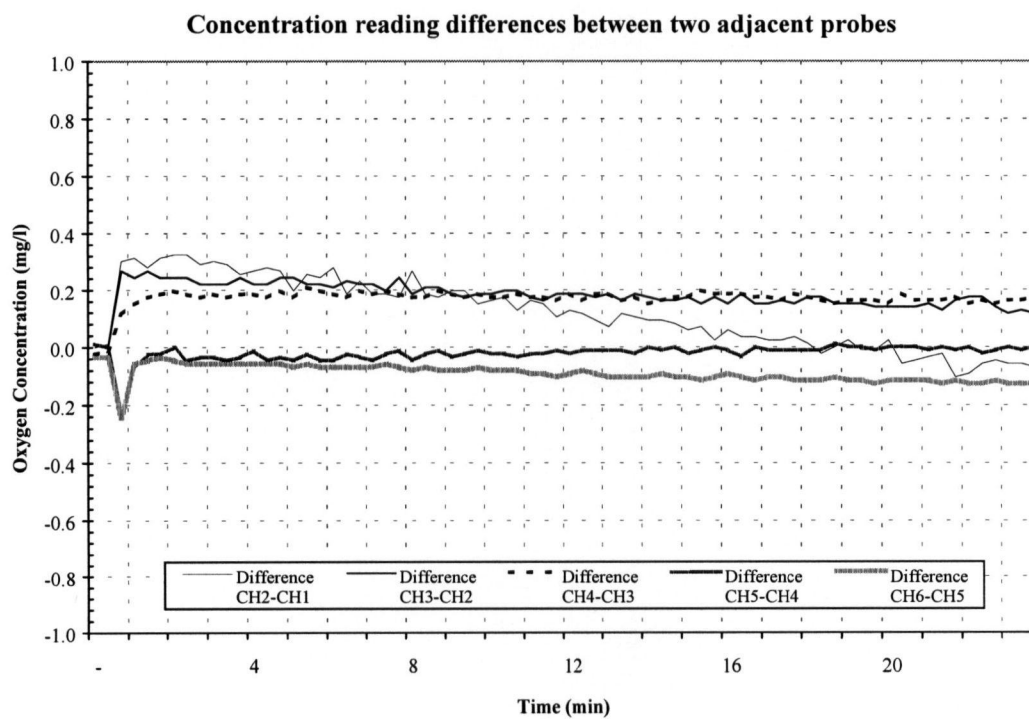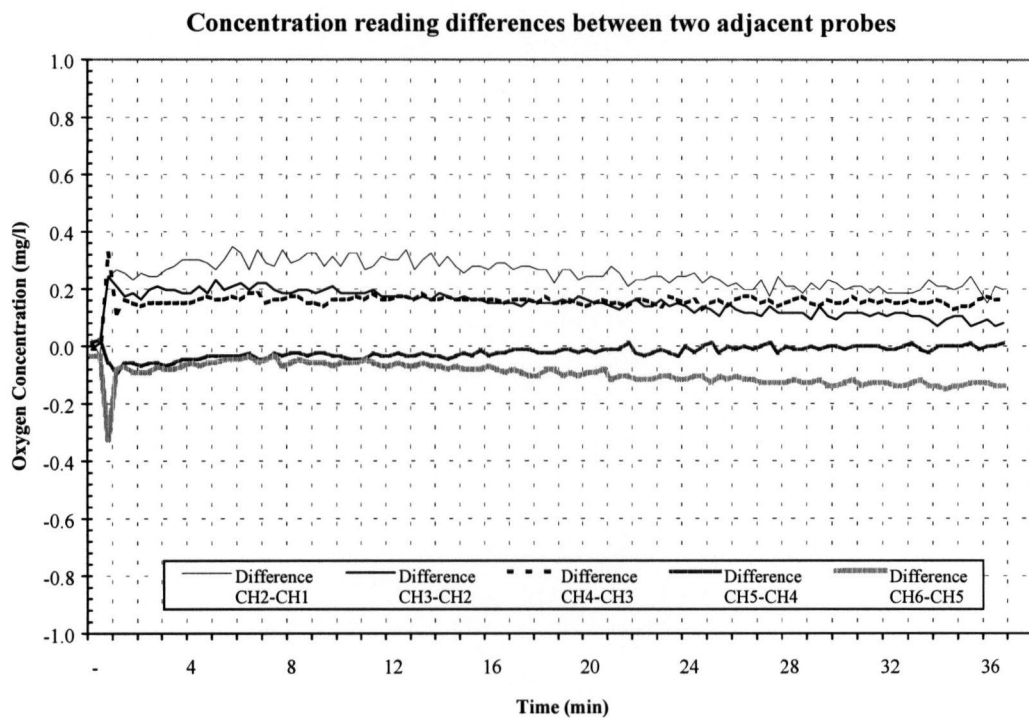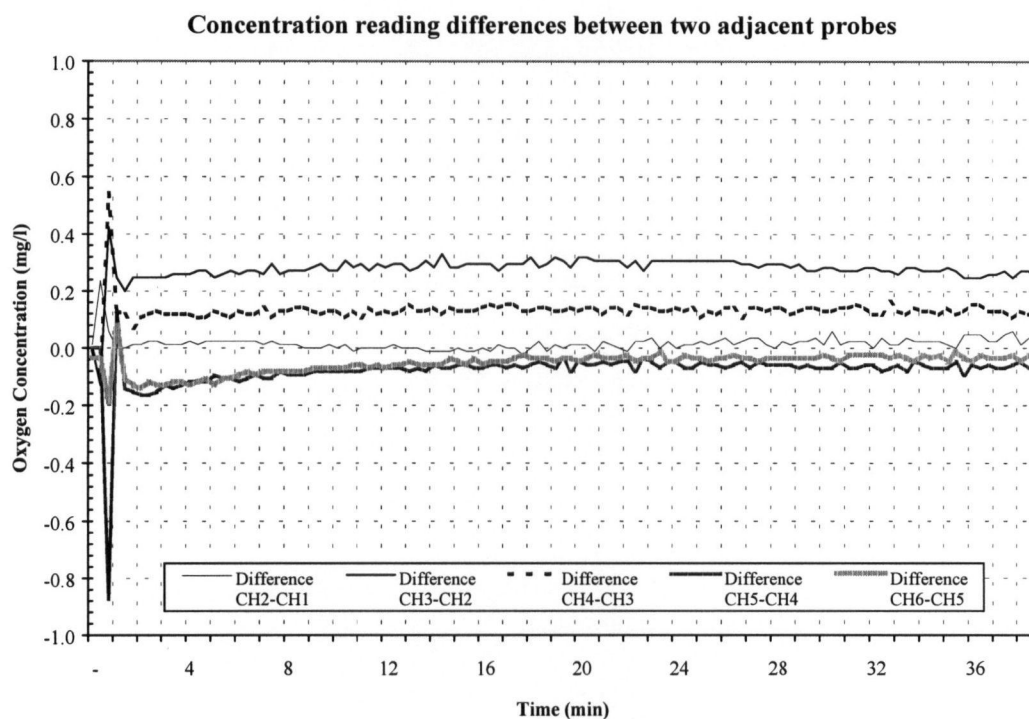
Figure 4.38a-d Oxygen differentials in full lift aerator on air at 1.5 m with 400 μ diffuser at 10 l min⁻¹ (a), 20 l min⁻¹ (b), 30 l min⁻¹ (c), 40 l min⁻¹ (d).

Figure 4.38 continued
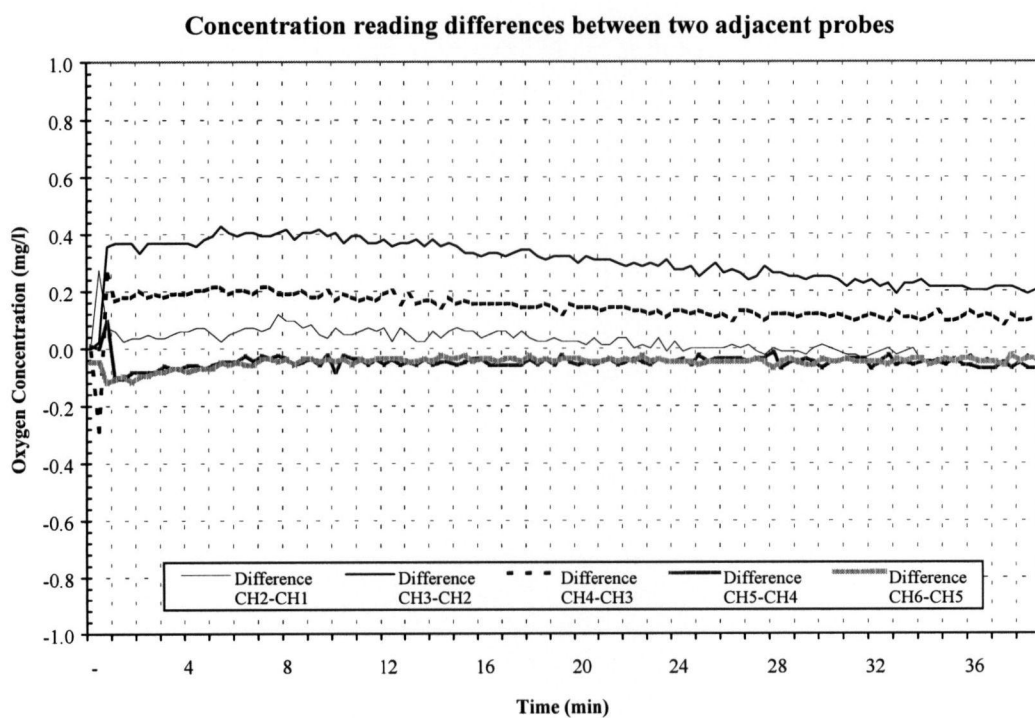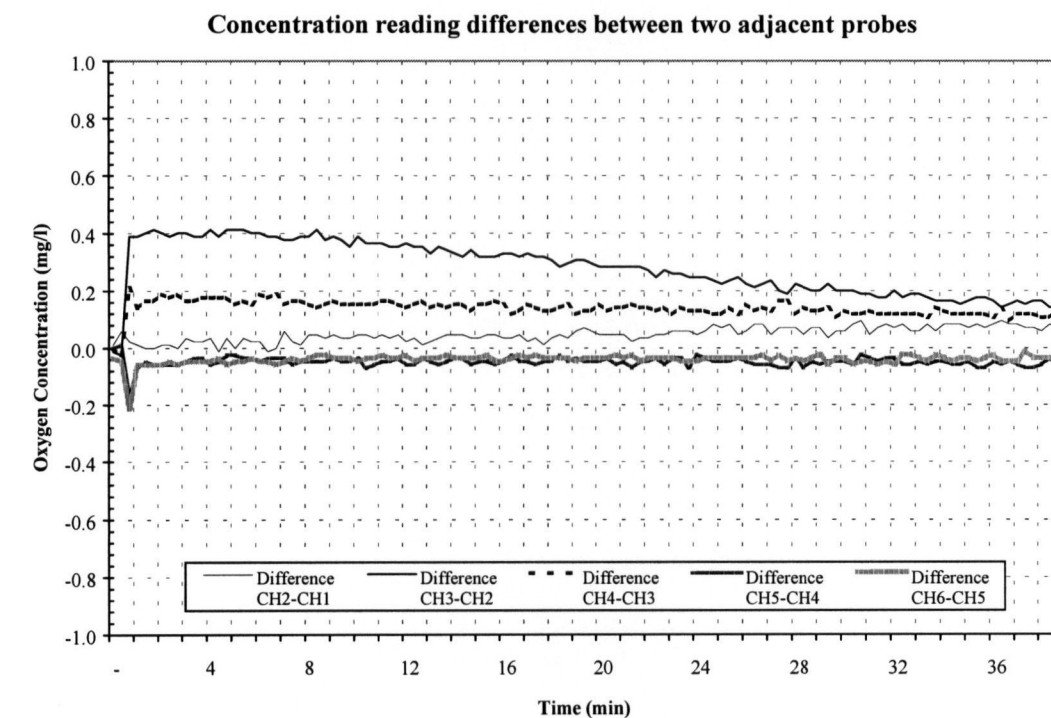
Concentration reading differences between two adjacent probes

Concentration reading differences between two adjacent probes

were fairly constant. The general trend with increasing gas flows was an increase in the oxygen differential and slope in Zone 2.

4.4.5   800 μ x 2.9 m x air

The oxygen differentials were similar in Zones 1, 2 and 3, and similar, but negative, in Zones 4 and 5 (Figure 4.39 a-d). As gas flow increased, the differentials become more distinct, with Zone 1 being the highest, followed by Zones 2 and 3; while the Zone 5 differential became increasingly negative.

4.4.6   800 μ x 1.5 m x air

The oxygen differential was greatest in Zone 2, followed by Zone 3 (Figure 4.40 a-d). The oxygen differential was near zero in Zone 1, and slightly negative in Zones 4 and 5. A slight downward trend was observed over the duration of the test in Zone 2, whereas Zones 1, 3, 4 and 5 were fairly constant. The general trend with increasing gas flows was an increase in the oxygen differential and slope in Zone 2, an increase in the differential in Zone 3, and an increase in the negative differential in Zone 4. A summary of the qualitative observations of the oxygen differentials, on air, are shown in Table 4.67.

4.4.7   140 μ x 2.9 m x O_2

The oxygen differential was greatest in Zone 1, followed by Zones 2 and Zone 3 (Figure 4.41 a-d). The oxygen differential was slightly negative in Zones 4 and 5, indicating oxygen concentrations were decreasing in these zones. A slight downward trend was observed over the duration of the test in Zones 1 and 2, whereas Zones 3, 4 and 5 were fairly constant. The general trend with increasing oxygen flows from 10 to 40 l min^{-1} was an increase in the oxygen differential in Zone 1 with no clear trend in slope.

Concentration reading differences between two adjacent probes

Concentration reading differences between two adjacent probes

**Figure 4.39a-d Oxygen differentials in full lift aerator on air at 2.9 m with 800 μ
diffuser at 10 l min⁻¹ (a), 20 l min⁻¹ (b), 30 l min⁻¹ (c), 40 l min⁻¹ (d).**

Figure 4.39

Concentration reading differences between two adjacent probes

Concentration reading differences between two adjacent probes

Concentration reading differences between two adjacent probes

Concentration reading differences between two adjacent probes
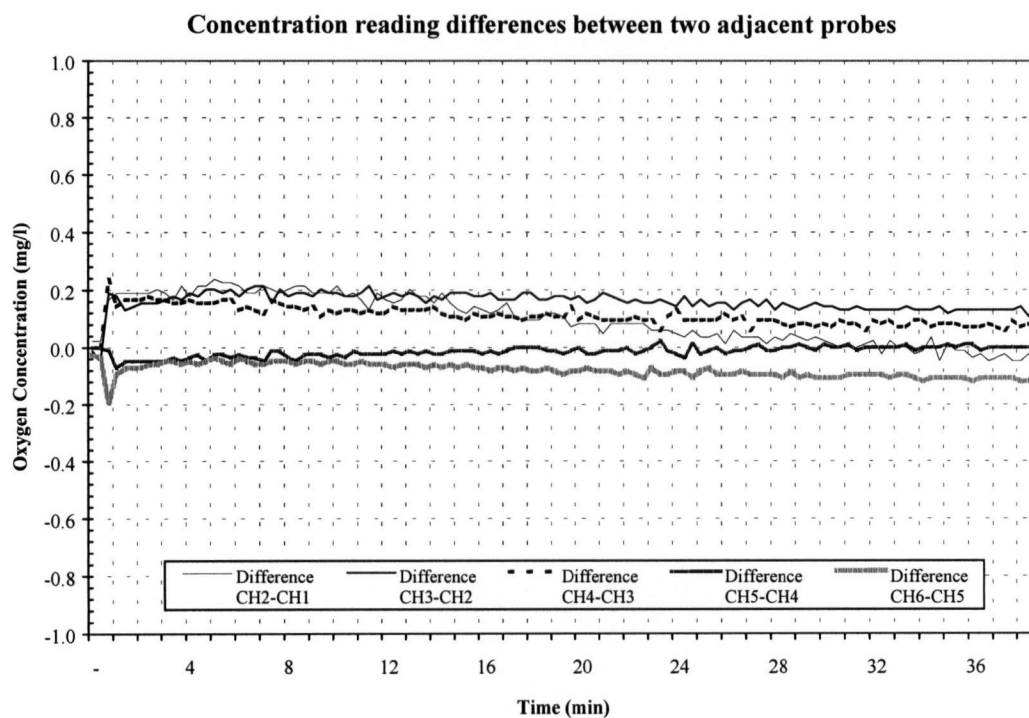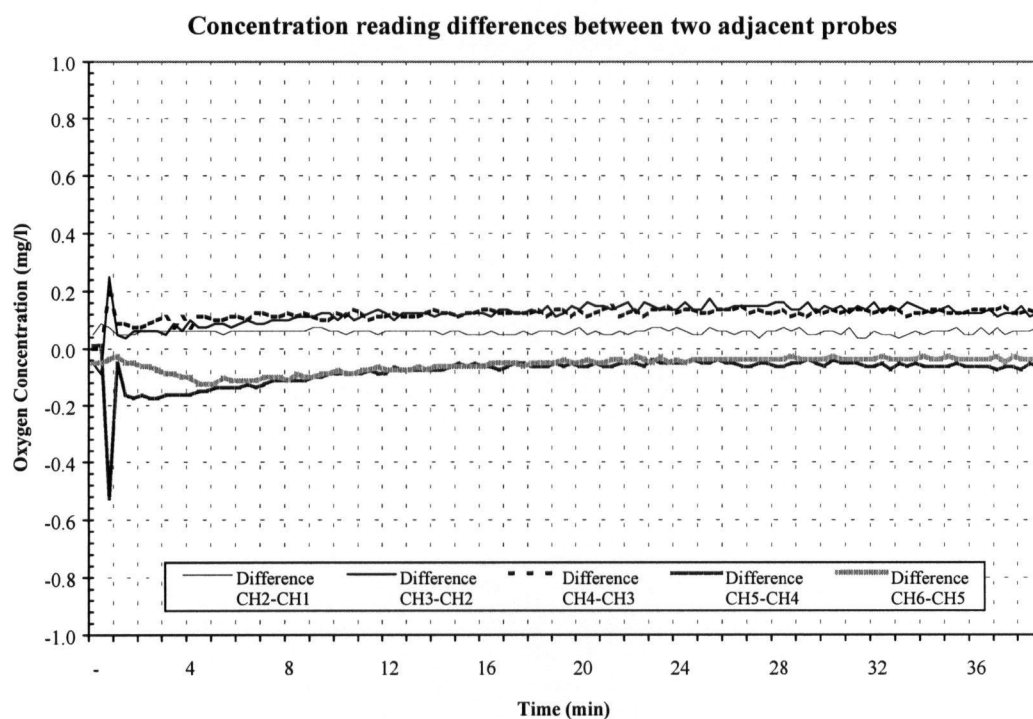
Figure 4.40a-d Oxygen differentials in full lift aerator on air at 1.5 m with 800 μ diffuser at 10 l min^{-1} (a), 20 l min^{-1} (b), 30 l min^{-1} (c), 40 l min^{-1} (d).

Figure 4.40 continued

Concentration reading differences between two adjacent probes

Concentration reading differences between two adjacent probes

Concentration reading differences between two adjacent probes

Concentration reading differences between two adjacent probes
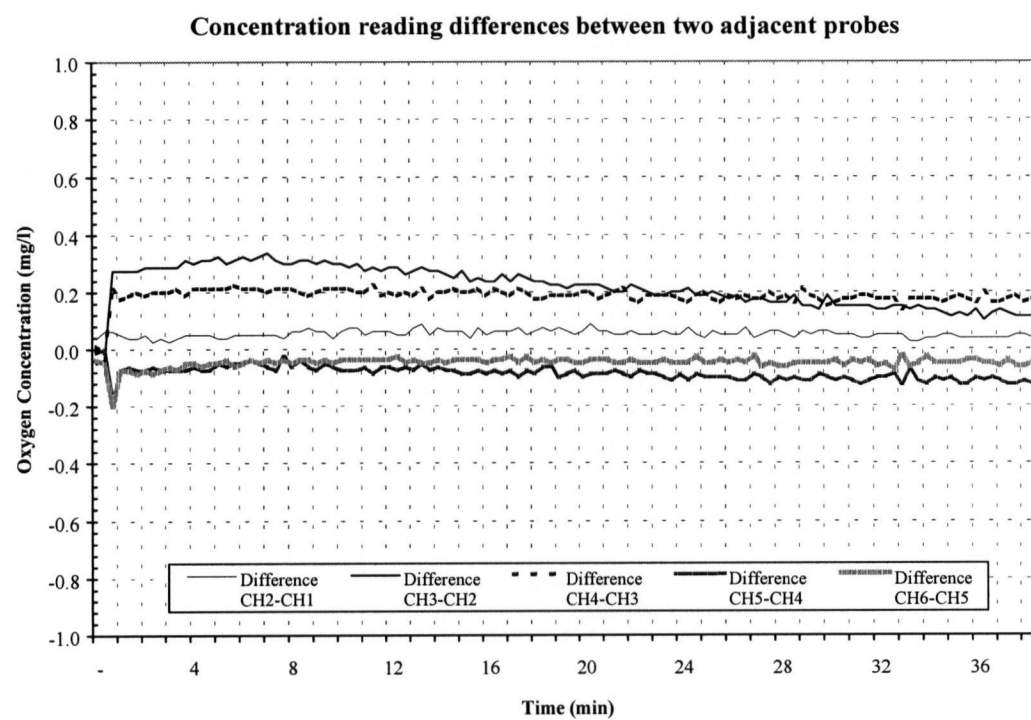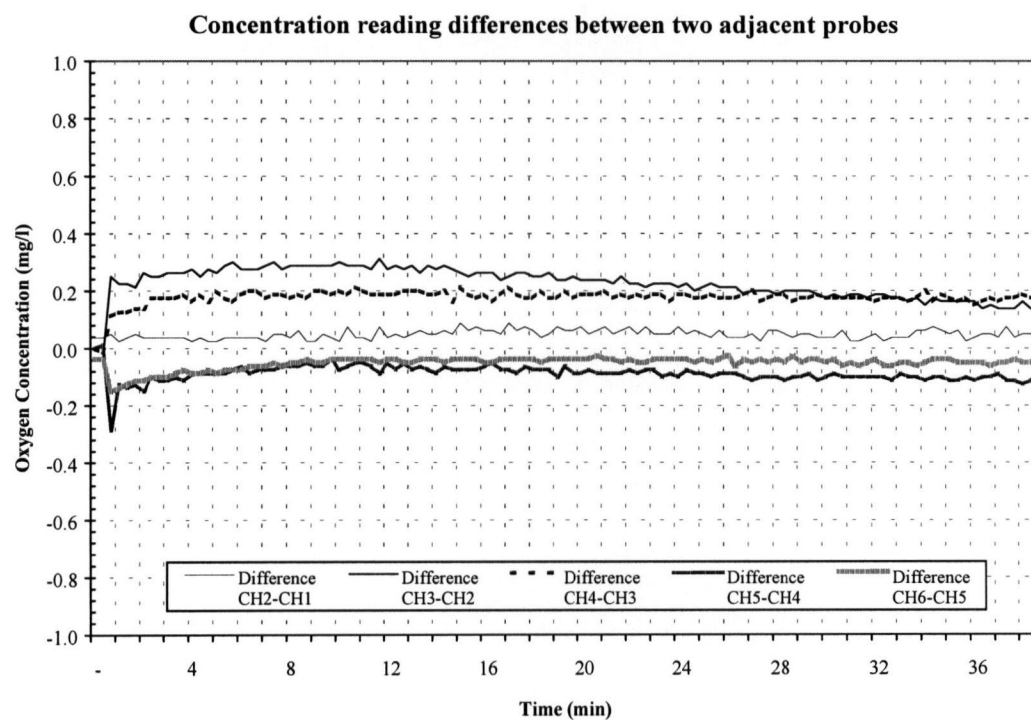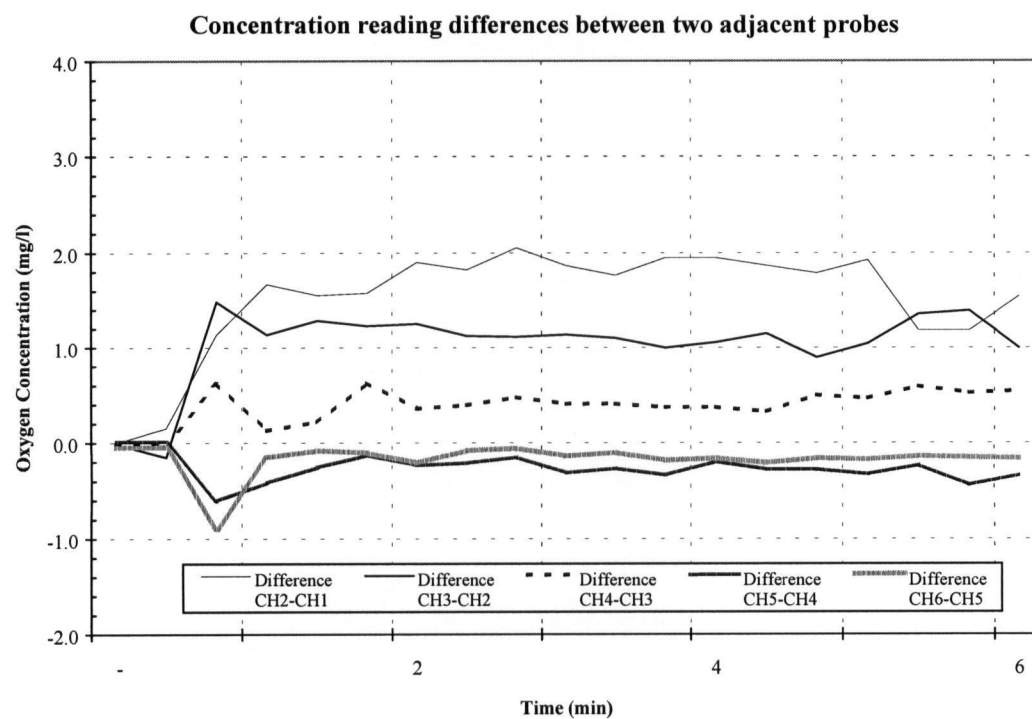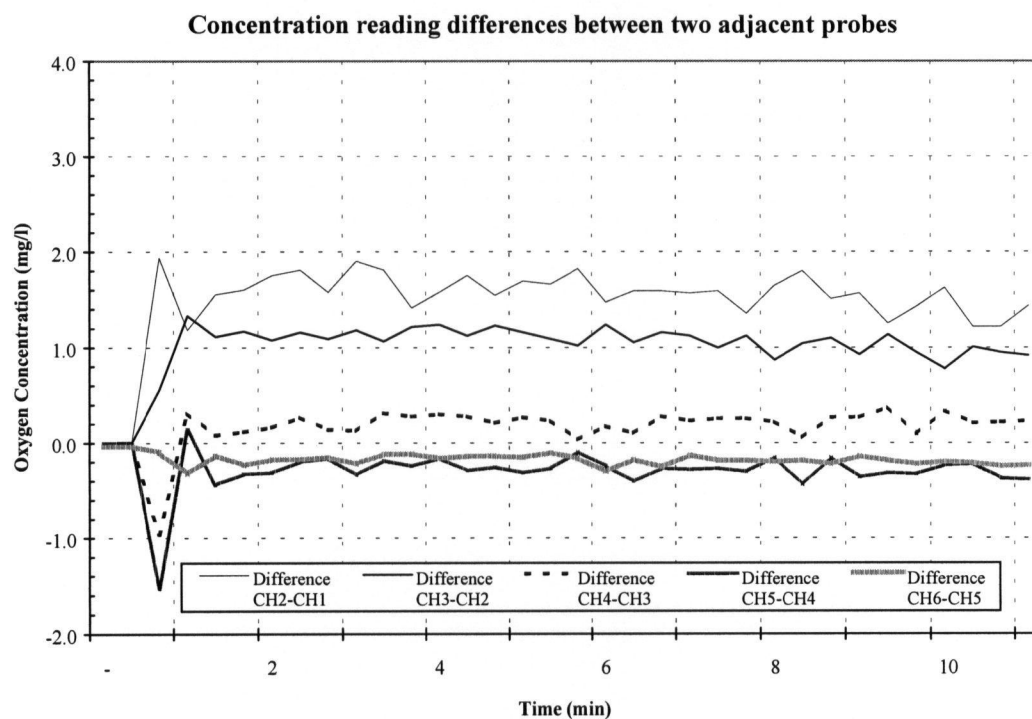
Figure 4.41a-d Oxygen differentials in full lift aerator on PSA O_2 at 2.9 m with 140 μ diffuser at 10 l min^{-1} (a), 20 l min^{-1} (b), 30 l min^{-1} (c), 40 l min^{-1} (d).

Figure 4.41 continued

Concentration reading differences between two adjacent probes

Concentration reading differences between two adjacent probes
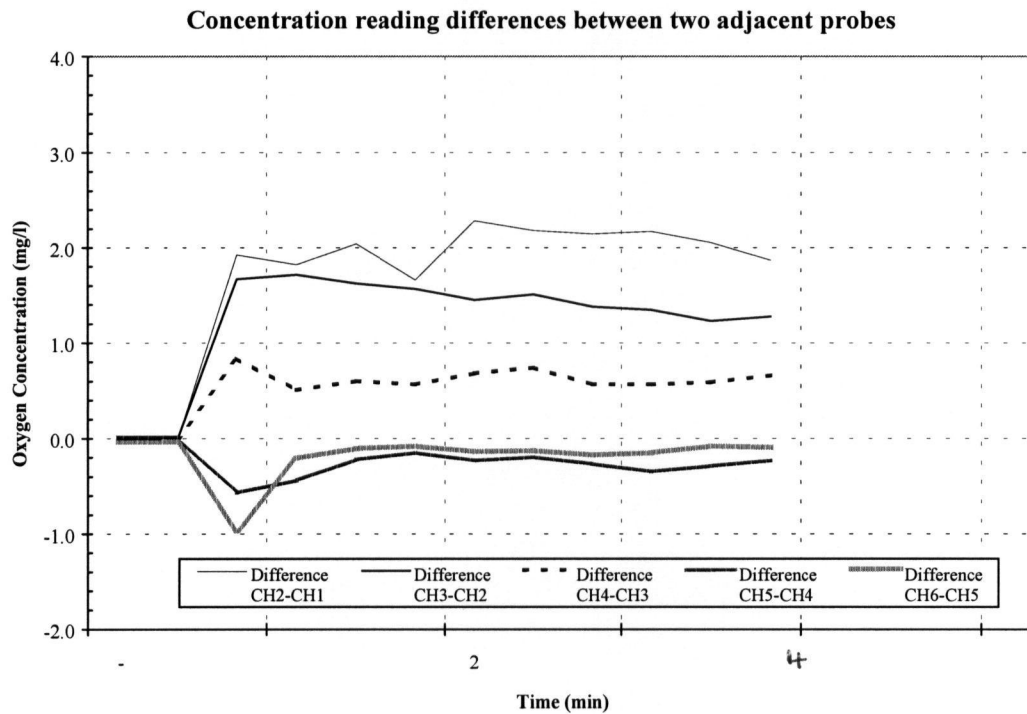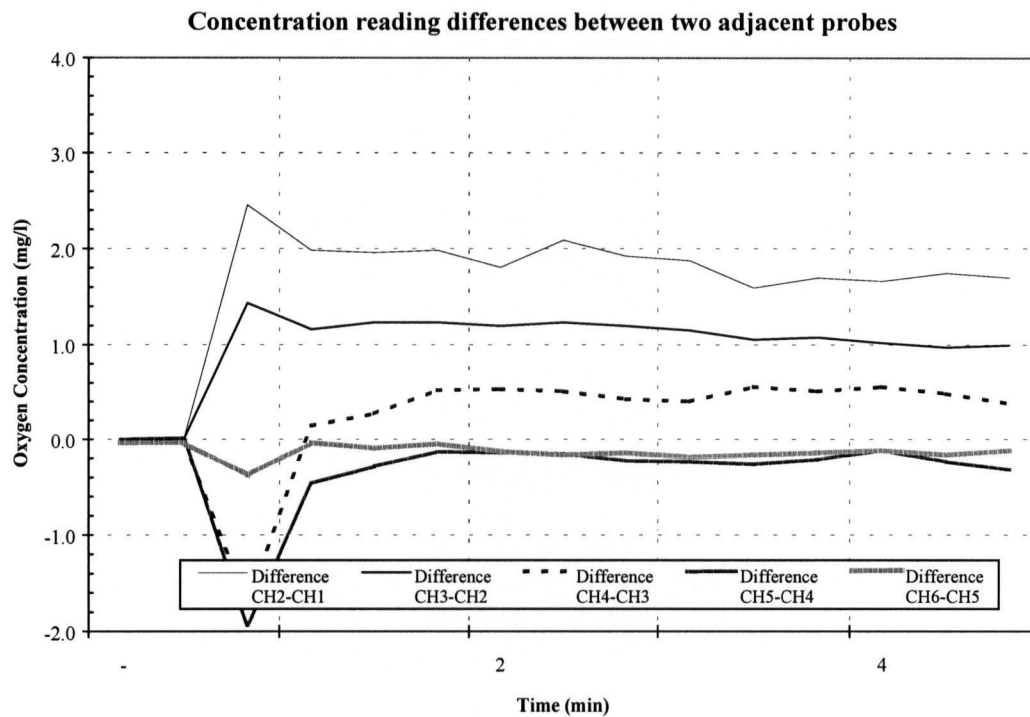
Table 4.67. Summary of qualitative observations of the relative magnitude, slope and response to increasing air flows for oxygen differentials in Zones 1-5.

Treat-ment	Zone 1 Ch. 2-1	Zone 2 Ch. 3-2	Zone 3 Ch. 4-3	Zone 4 Ch. 5-4	Zone 5 Ch. 6-5	$10 \rightarrow 40$ l min^{-1}
140 μ x 2.9 m x air	Highest differential, Negative slope	2nd highest differential, less slope	3rd highest differential, less slope	Negative differential, neutral slope	Negative differential, neutral slope	Increase in Zone 1 differential and slope, increase in slope for Zones 2 and 3
140 μ x 1.5 m x air	Zero differential, neutral slope	Highest differential, Negative slope	2nd highest differential, less slope	Negative differential, neutral slope	Negative differential, neutral slope	Increase in Zone 2 differential and slope, change from neutral to negative slope in Zone 5
400 μ x 2.9 m x air	Highest differential, Negative slope	2nd highest differential, less slope	3rd highest differential, neutral slope	Negative differential, neutral slope	Negative differential, neutral slope	Increase in Zone 1 and 2 differential and slope, change from neutral to negative slope in Zone 5
400 μ x 1.5 m x air	Zero differential, neutral slope	Highest differential, Negative slope	2nd highest differential, less slope	Negative differential, neutral slope	Negative differential, neutral slope	Increase in Zone 2 differential and slope
800 μ x 2.9 m x air	Similar differential, neutral slope	Similar differential, neutral slope	Similar differential, neutral slope	Negative differential, neutral slope	Negative differential, neutral slope	Increase in Zone 1 and 2 differential and slope, change from neutral to negative slope in Zone 5
800 μ x 1.5 m x air	Zero differential, neutral slope	Highest differential, Negative slope	2nd highest differential, less slope	Negative differential, neutral slope	Negative differential, neutral slope	Increase in Zone 2 differential and slope, increase in Zone 3 differential, and change from neutral to negative slope in Zone 4

4.4.8   140 μ x 1.5 m x O$_2$

The oxygen differential was greatest in Zone 2, followed by Zone 3 (Figure 4.42 a-d). The oxygen differential was near zero in Zone 1, and slightly negative in Zones 4 and 5. A minimal slope was observed over the duration of the test in all zones. The general trend with increasing oxygen flows was an increase in the oxygen differential in Zone 2.

4.4.9   400 μ x 2.9 m x O$_2$

The oxygen differential was greatest in Zones 1 and 2, followed by Zone 3 (Figure 4.43 a-d). The oxygen differential was slightly negative in Zones 4 and 5. Minimal change in slope was observed over the duration of the test in all zones. The general trend with increasing oxygen flows was an increase in the oxygen differential in Zones 1, 2, and 3.

4.4.10   400 μ x 1.5 m x O$_2$

The oxygen differential was greatest in Zone 2, followed by Zone 3 (Figure 4.44 a-d). The oxygen differential was near zero in Zone 1, and slightly negative in Zones 4 and 5. A slight downward trend was observed over the duration of the test in Zone 2, whereas Zones 1, 3, 4 and 5 were fairly constant. The general trend with increasing oxygen flows was an increase in the oxygen differential in Zones 2 and 3.

Concentration reading differences between two adjacent probes

Concentration reading differences between two adjacent probes
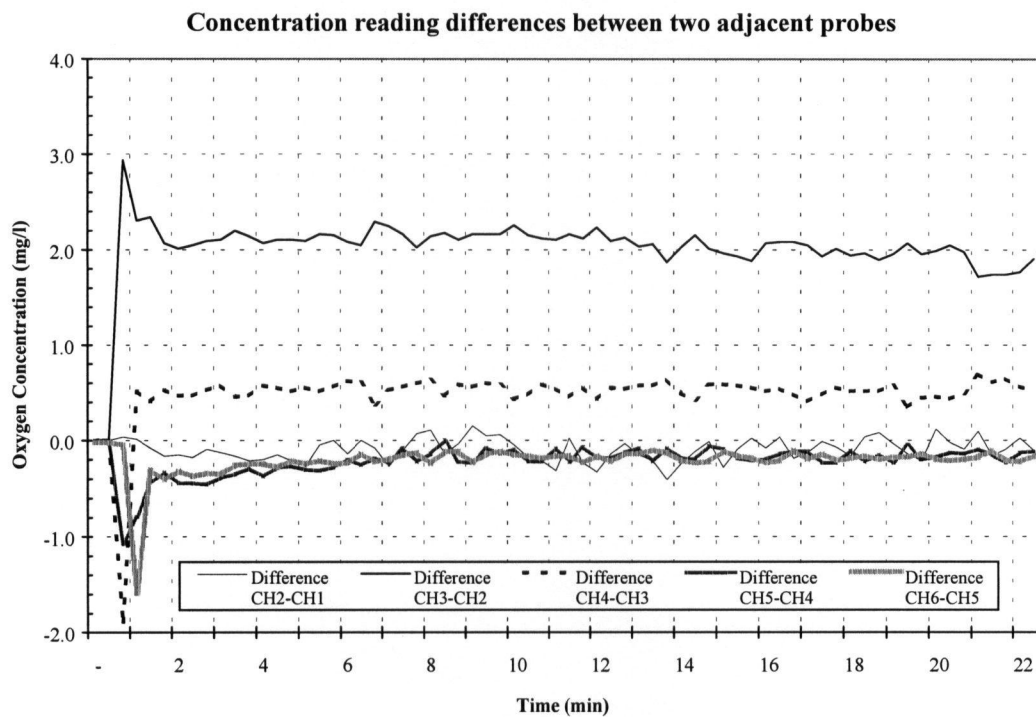
Figure 4.42a-d Oxygen differentials in full lift aerator on PSA O_2 at 1.5 m with 140 µ diffuser at 10 l min^{-1} (a), 20 l min^{-1} (b), 30 l min^{-1} (c), 40 l min^{-1} (d).

Figure 4.42 continued

Concentration reading differences between two adjacent probes

Time (min)

Concentration reading differences between two adjacent probes

Time (min)
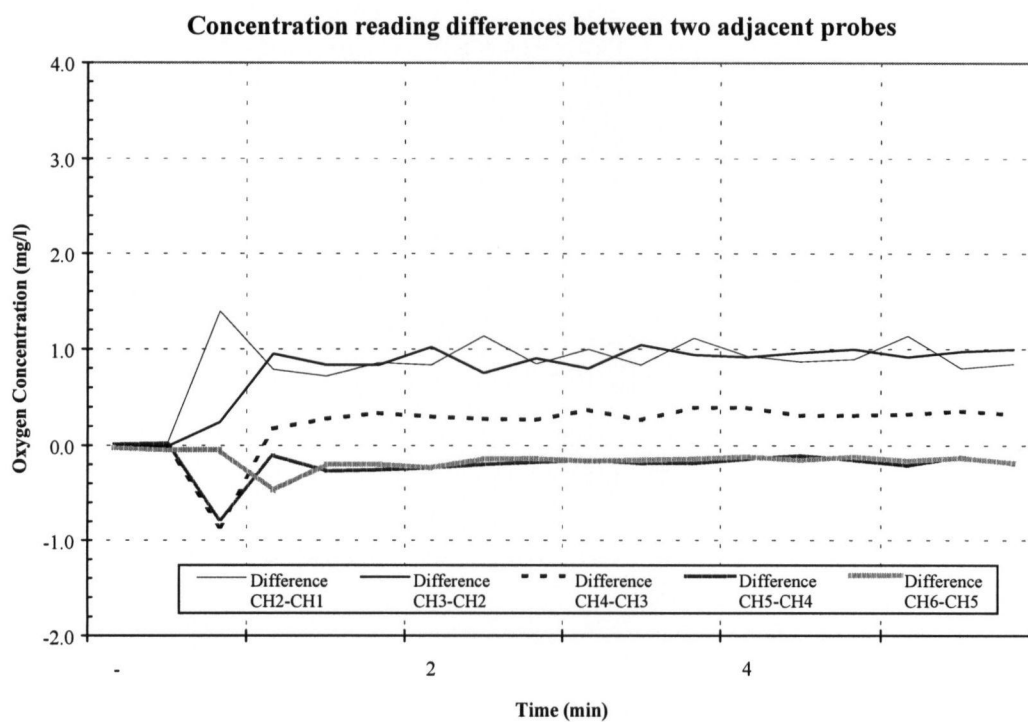
Figure 4.43a-d Oxygen differentials in full lift aerator on PSA O_2 at 2.9 m with 400 μ diffuser at 10 l min^{-1} (a), 20 l min^{-1} (b), 30 l min^{-1} (c), 40 l min^{-1} (d).

Figure 4.43

Concentration reading differences between two adjacent probes

Concentration reading differences between two adjacent probes
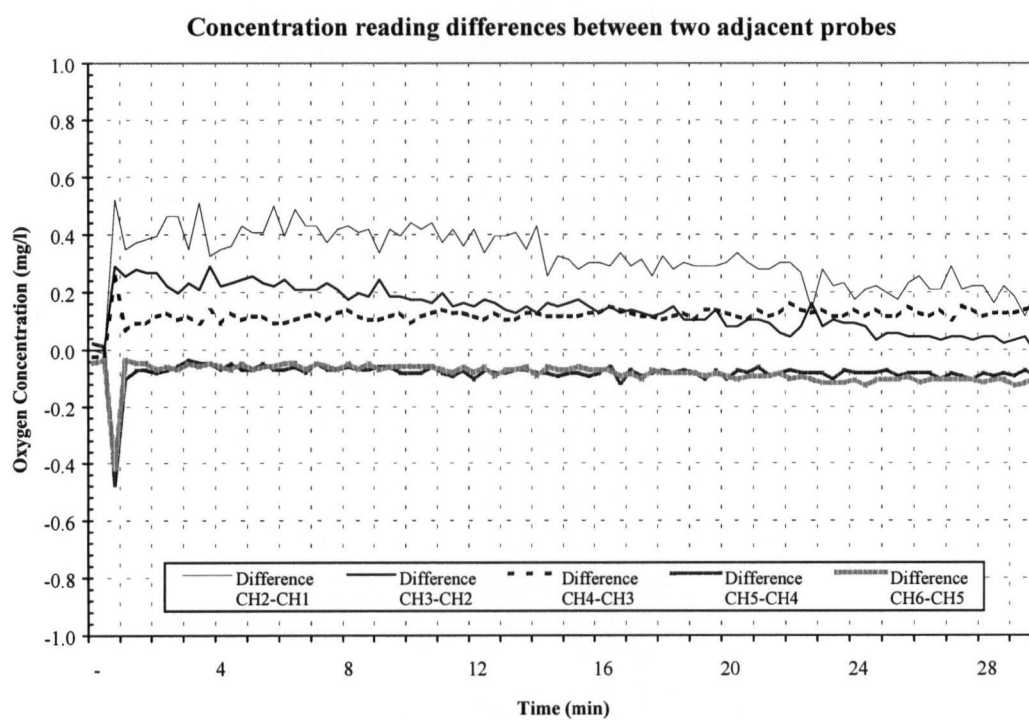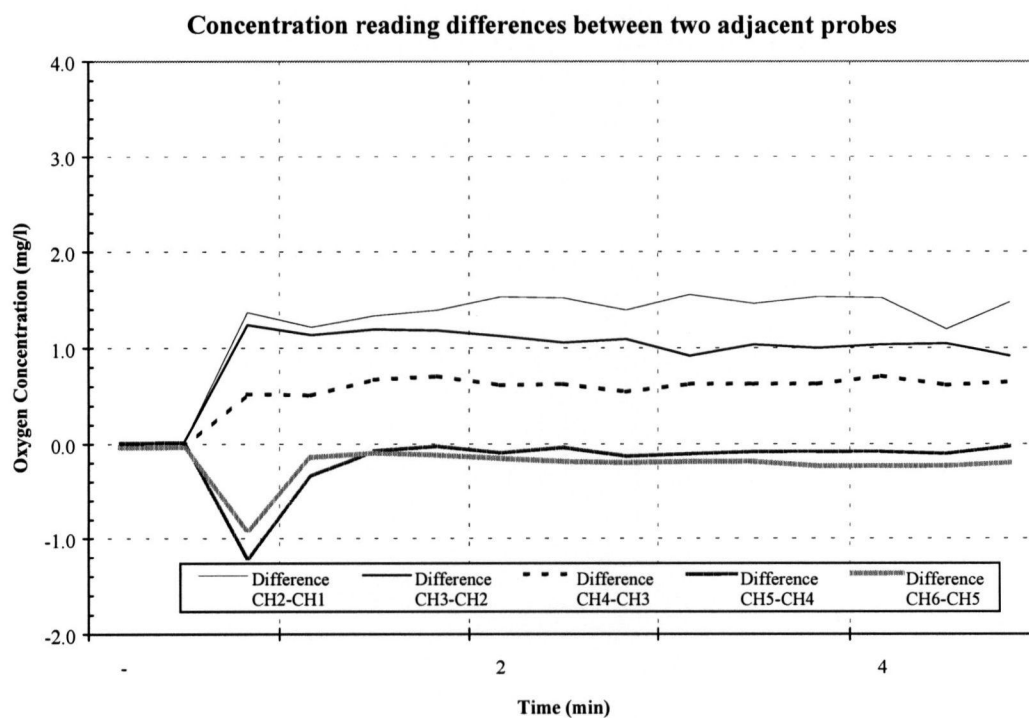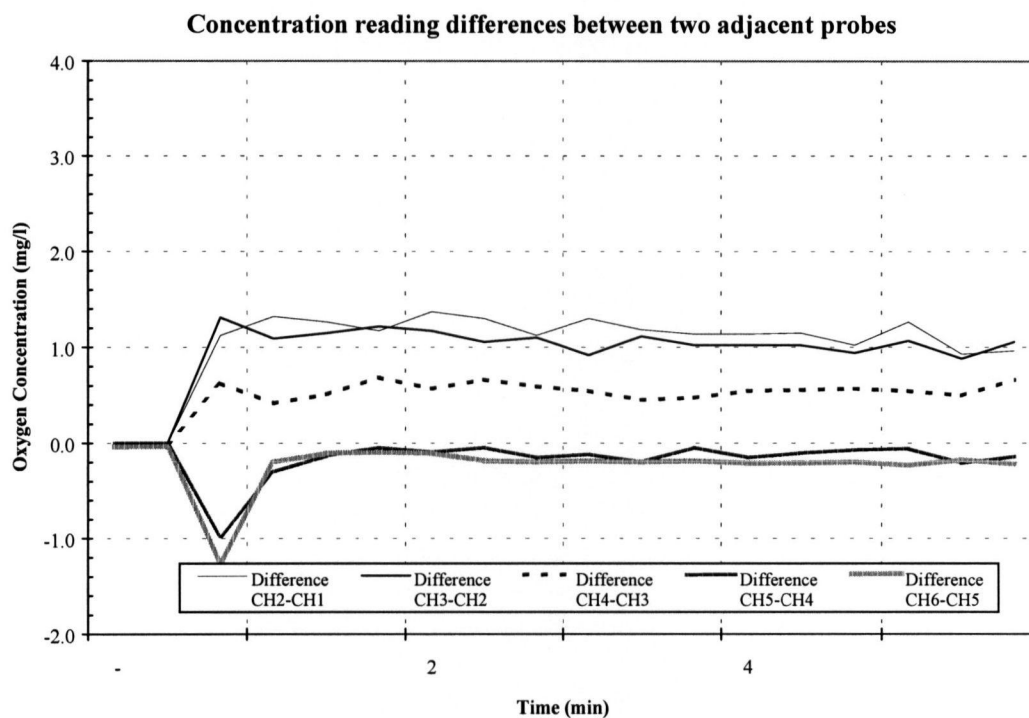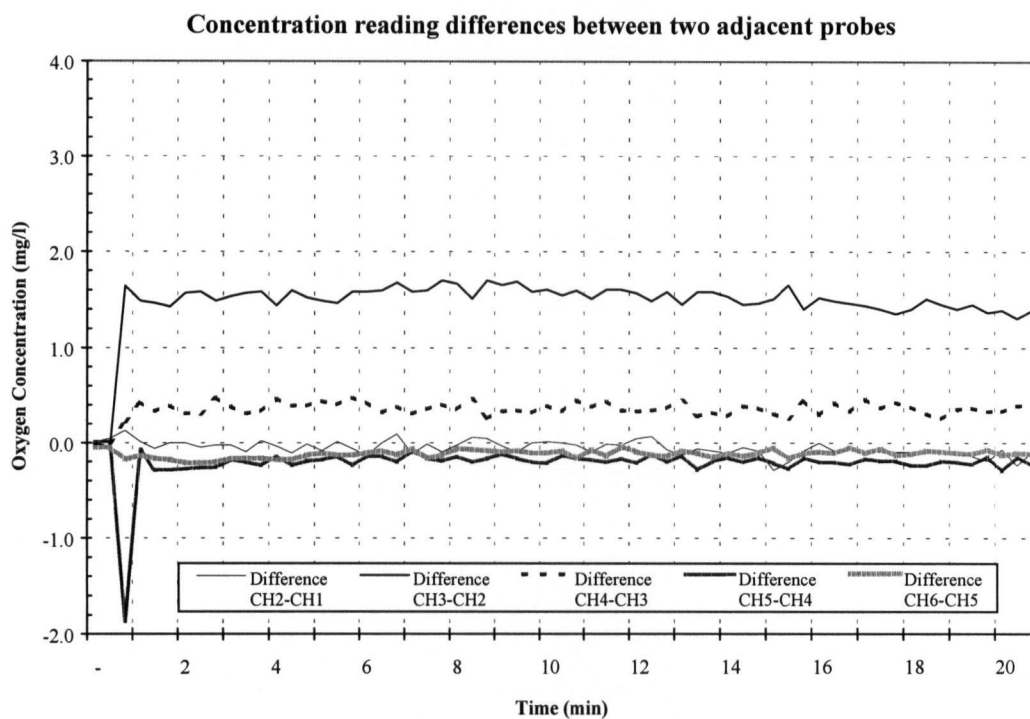
Figure 4.44a-d Oxygen differentials in full lift aerator on PSA O$_2$ at 1.5 m with 400 μ diffuser at 10 l min^{-1} (a), 20 l min^{-1} (b), 30 l min^{-1} (c), 40 l min^{-1} (d) 40 l min^{-1}.

Figure 4.44 continued

Concentration reading differences between two adjacent probes

Concentration reading differences between two adjacent probes
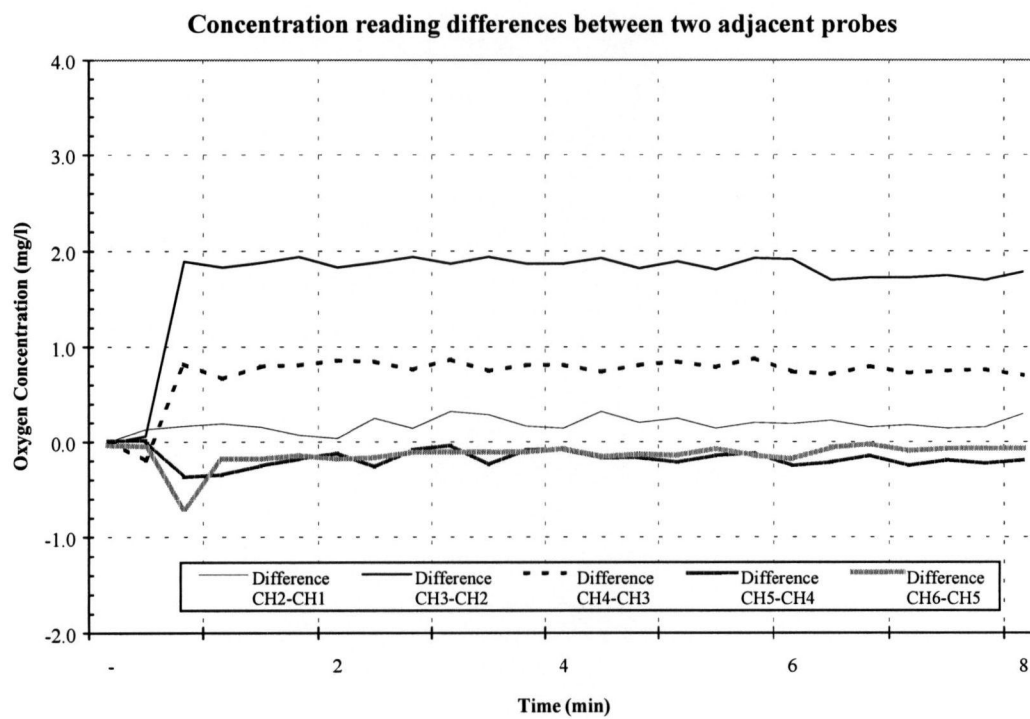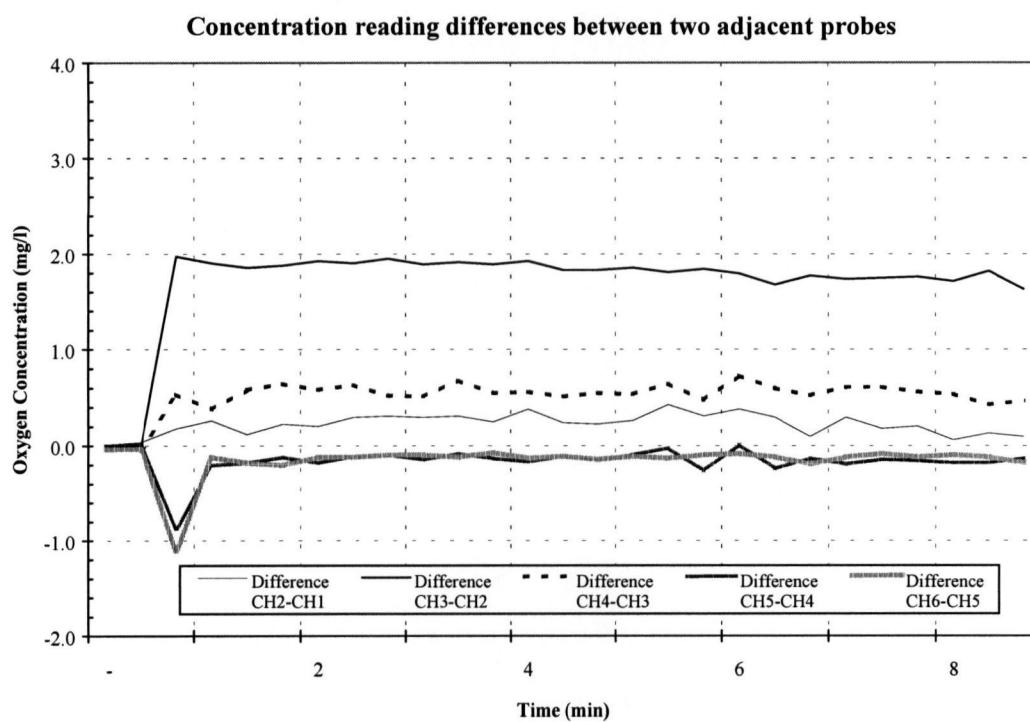
4.4.11   800 μ x 2.9 m x O_2

The oxygen differentials were highest in Zones 1 and 2, and next highest in Zone 3. Zones 4 and 5 were negative through the tests (Figure 4.45 a-d). As gas flow increased, the separation between the zone differentials become more distinct, with Zone 1 being the highest, followed by Zones 2 and 3; while Zone 4 and 5 differentials remained negative with a neutral slope.

4.4.12   800 μ x 1.5 m x O_2

The oxygen differential was greatest in Zone 2, followed by Zone 3 (Figure 4.46 a-d). The oxygen differential was near zero in Zone 1, and slightly negative in Zones 4 and 5. A slight downward trend was observed over the duration of the test in Zone 2, whereas Zones 1, 3, 4 and 5 were fairly constant. The general trend with increasing oxygen flows was an increase in the oxygen differential and slope in Zones 2 and 3, and a minimal change in slope for all zones. A summary of the qualitative observations of the oxygen differentials, on PSA oxygen, are shown in Table 4.68.

4.4.13   DBCA x 140 μ x air

The oxygen differential was greatest in Zone 1, followed by a tight grouping of Zones 2, 3, and slightly negative in Zone 5 (Figure 4.47 a-d). Minimal trend was observed over the duration of the test in all zones. The general trend with increasing oxygen flows was a slight increase in slope in Zones 1, 2 and 3, and an increase in the negative oxygen differential in Zone 4.

Concentration reading differences between two adjacent probes

Concentration reading differences between two adjacent probes
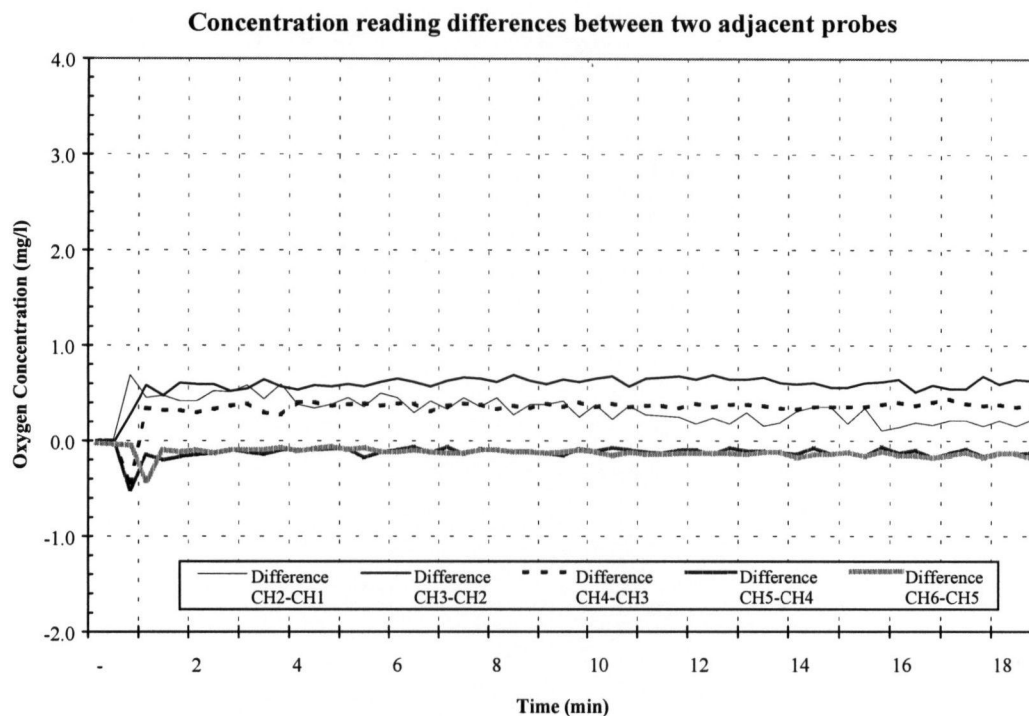
Figure 4.45a-d Oxygen differentials in full lift aerator on PSA O_2 at 2.9 m with 800 μ diffuser at 10 l min^{-1} (a), 10 l min^{-1} (b), 20 l min^{-1} (c), 30 l min^{-1} (d).

Figure 4.45 continued

Concentration reading differences between two adjacent probes

Concentration reading differences between two adjacent probes

Concentration reading differences between two adjacent probes

Concentration reading differences between two adjacent probes
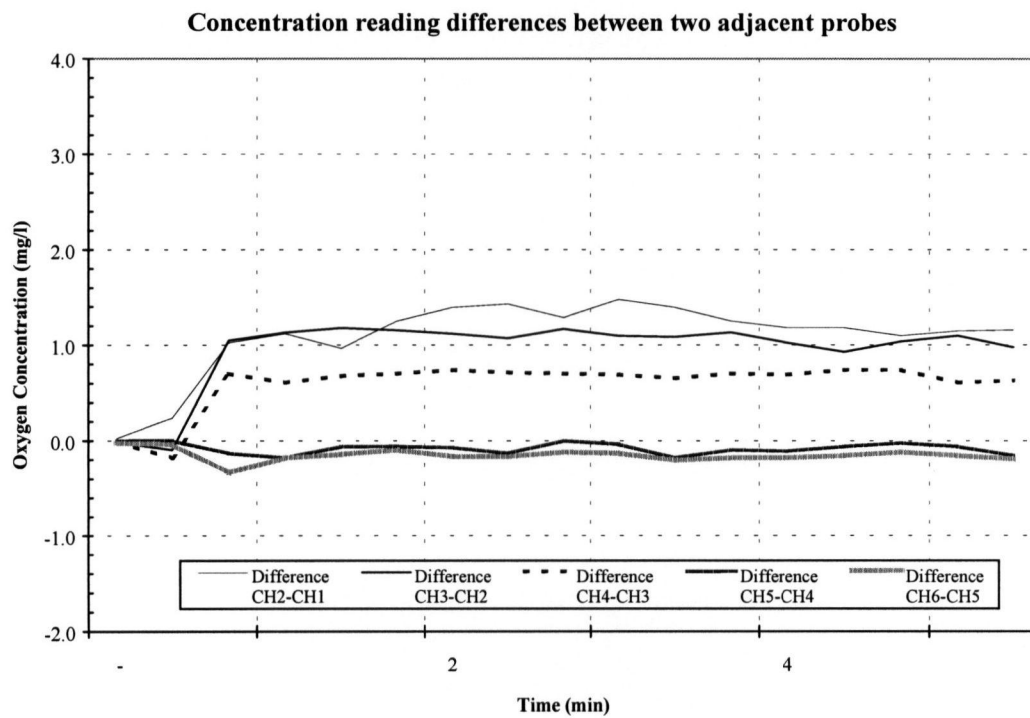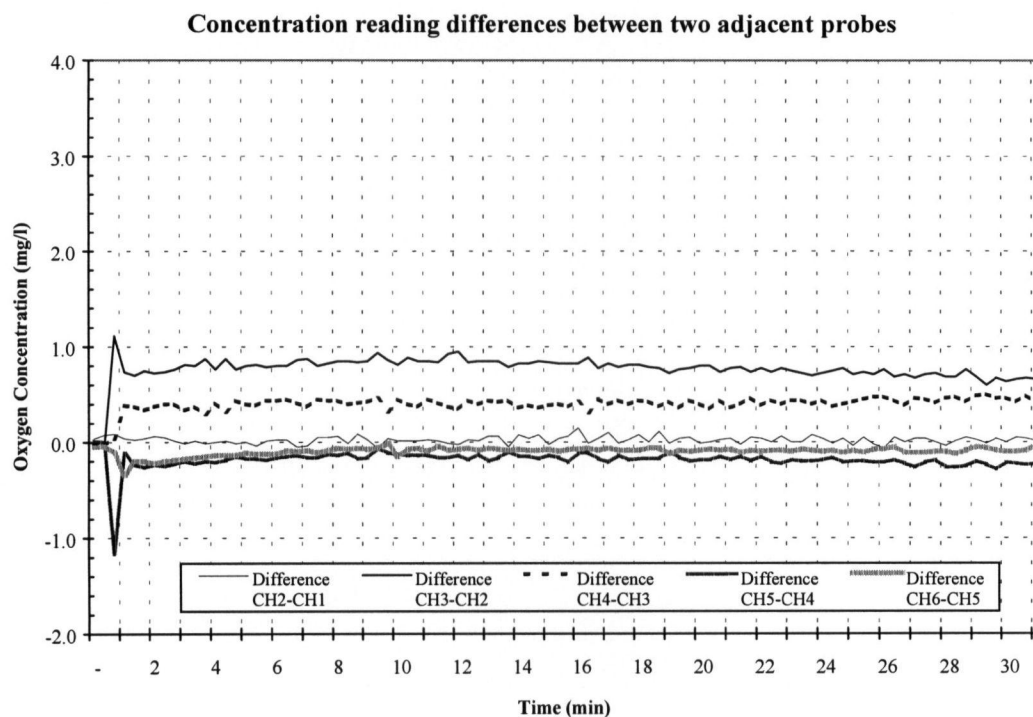
Figure 4.46a-d Oxygen differentials in full lift aerator on PSA O_2 at 1.5 m with 800 µ diffuser at 10 l min^{-1} (a), 20 l min^{-1} (b), 30 l min^{-1} (c), 40 l min^{-1} (d).

Figure 4.46 continued

Concentration reading differences between two adjacent probes

Concentration reading differences between two adjacent probes

Concentration reading differences between two adjacent probes

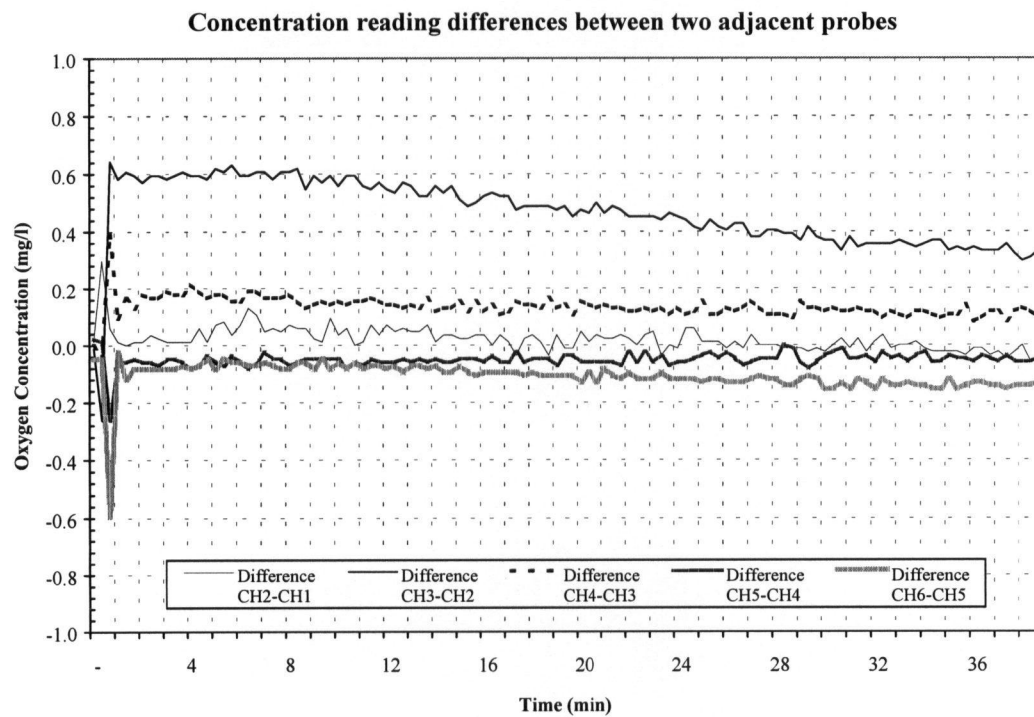**Concentration reading differences between two adjacent probes**
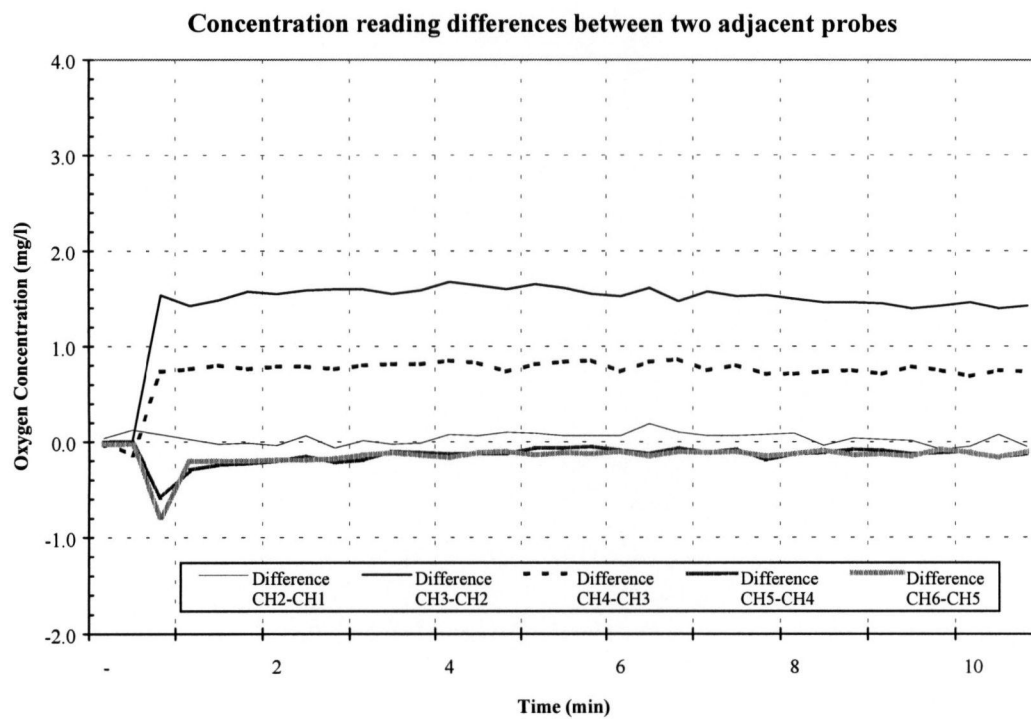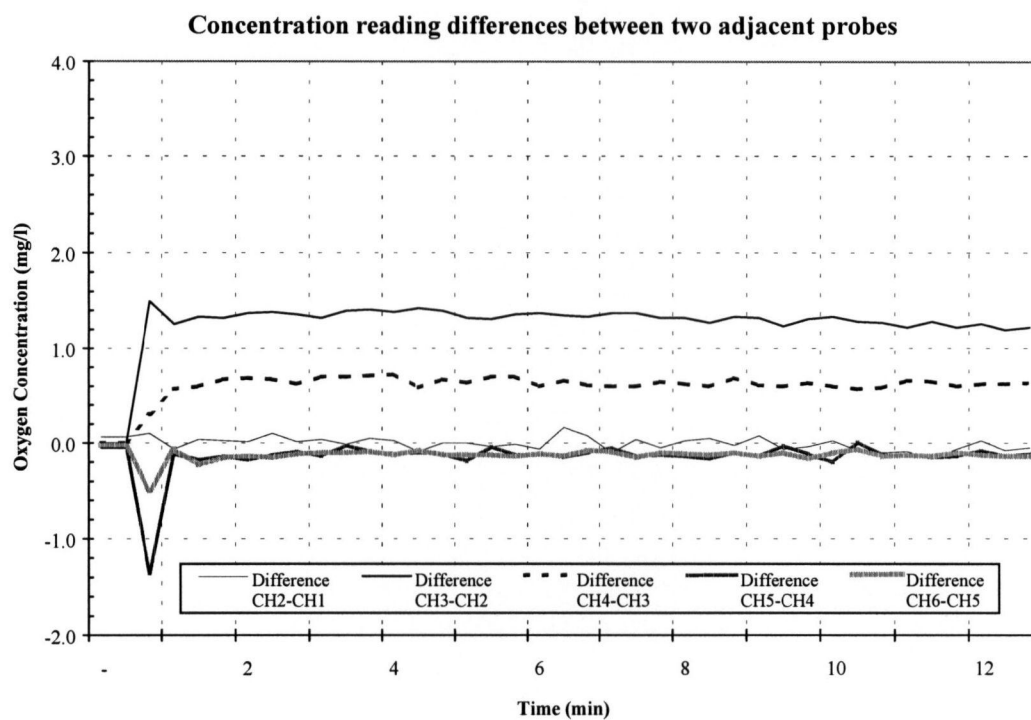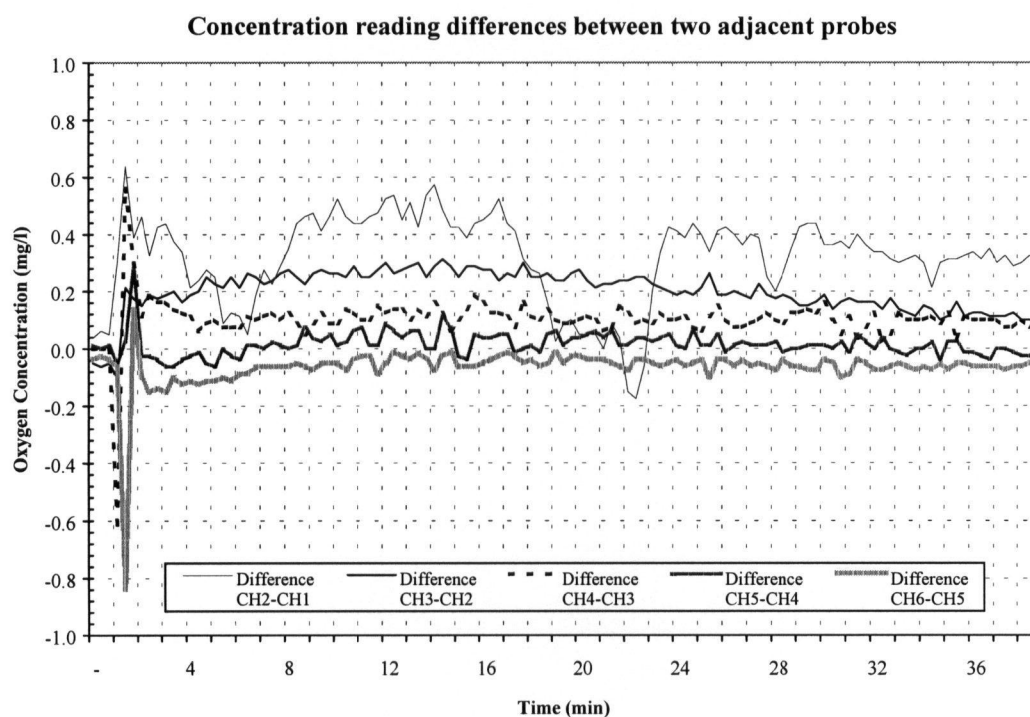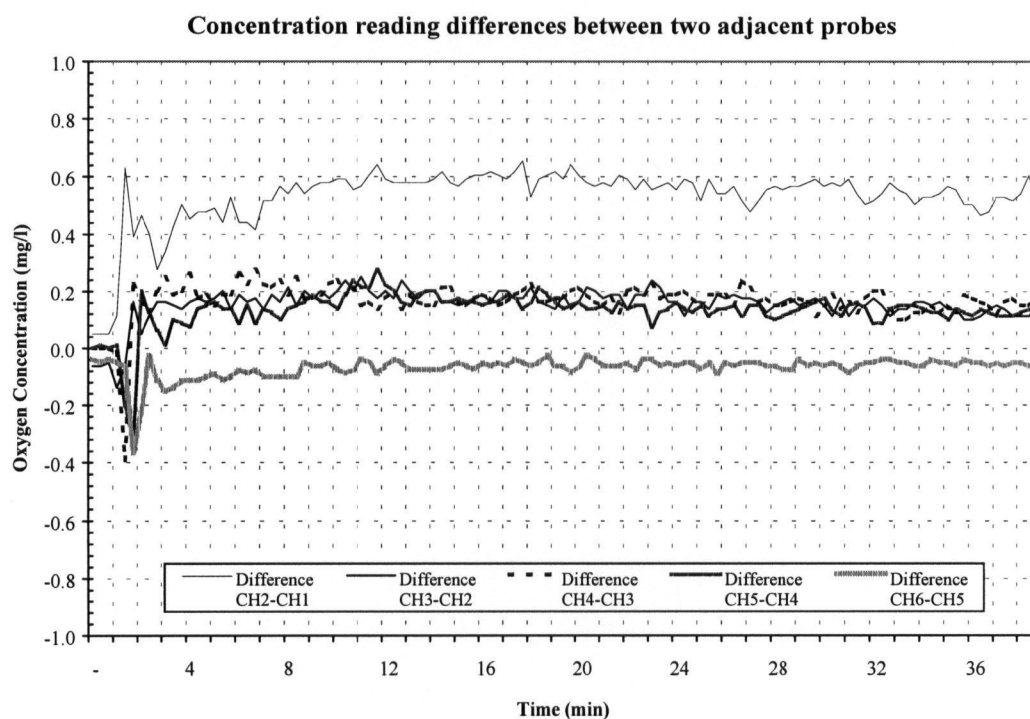
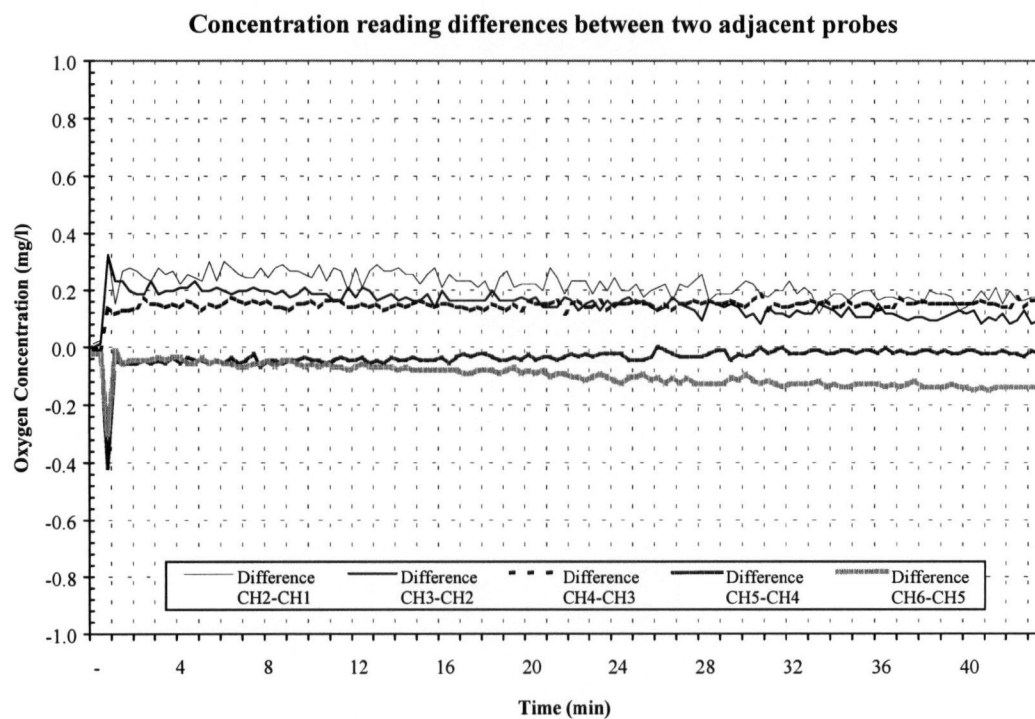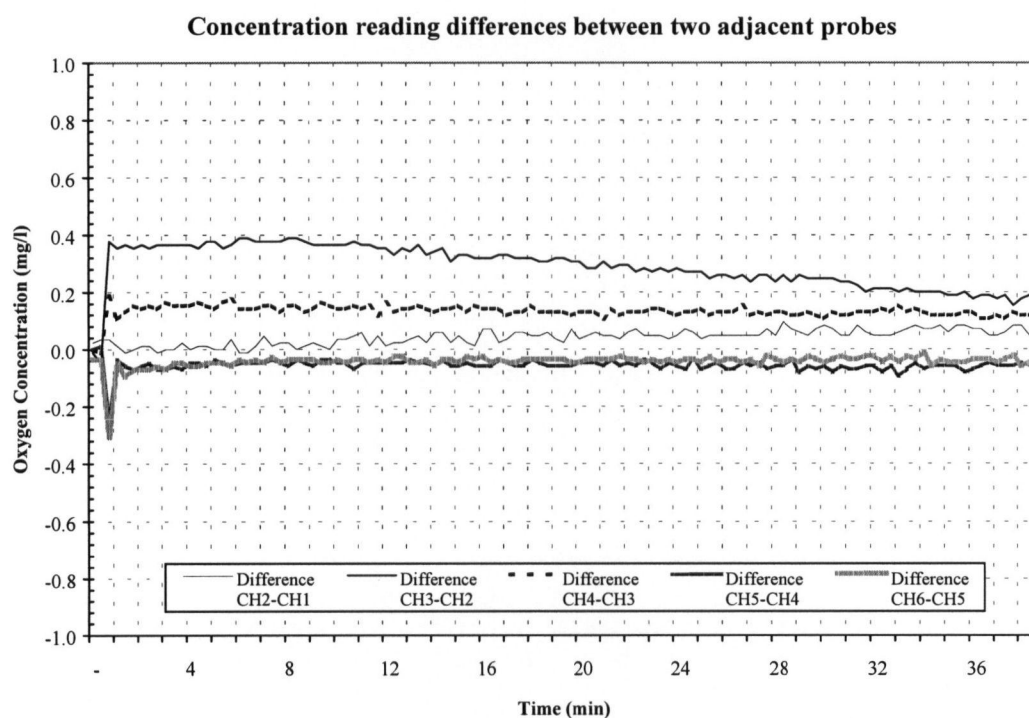**Figure 4.47a-d Oxygen differentials in full lift aerator on air at 2.9 m with 140 μ diffuser and DBCA at 10 l min^{-1} (a), 20 l min^{-1} (b), 30 l min^{-1} (c), 40 l min^{-1} (d).**

Figure 4.47

Concentration reading differences between two adjacent probes

Concentration reading differences between two adjacent probes
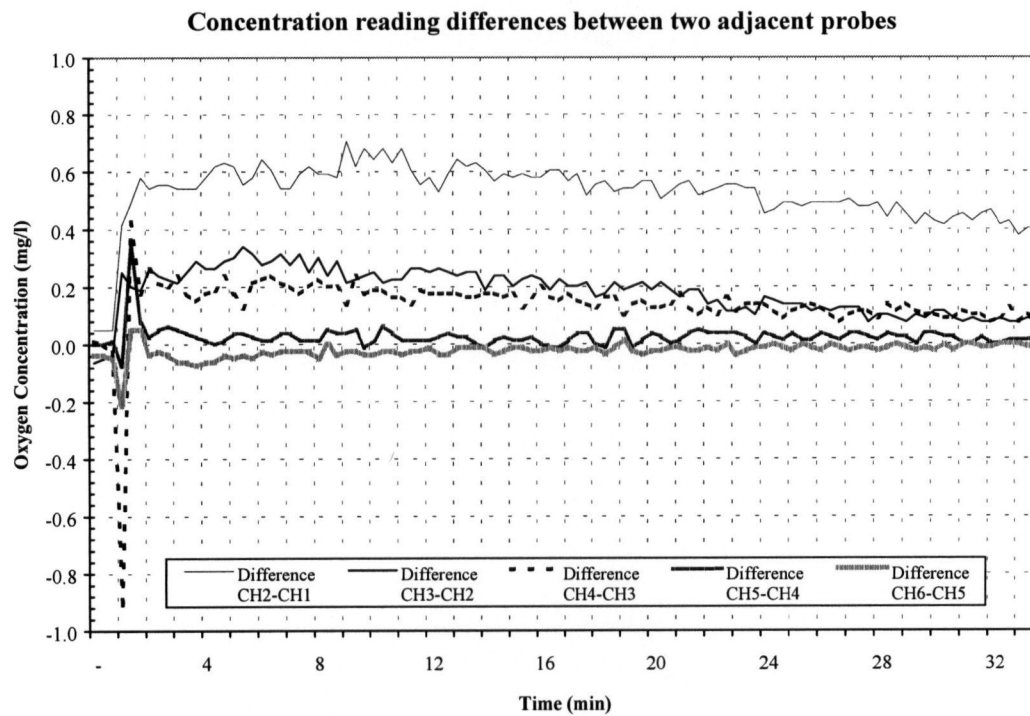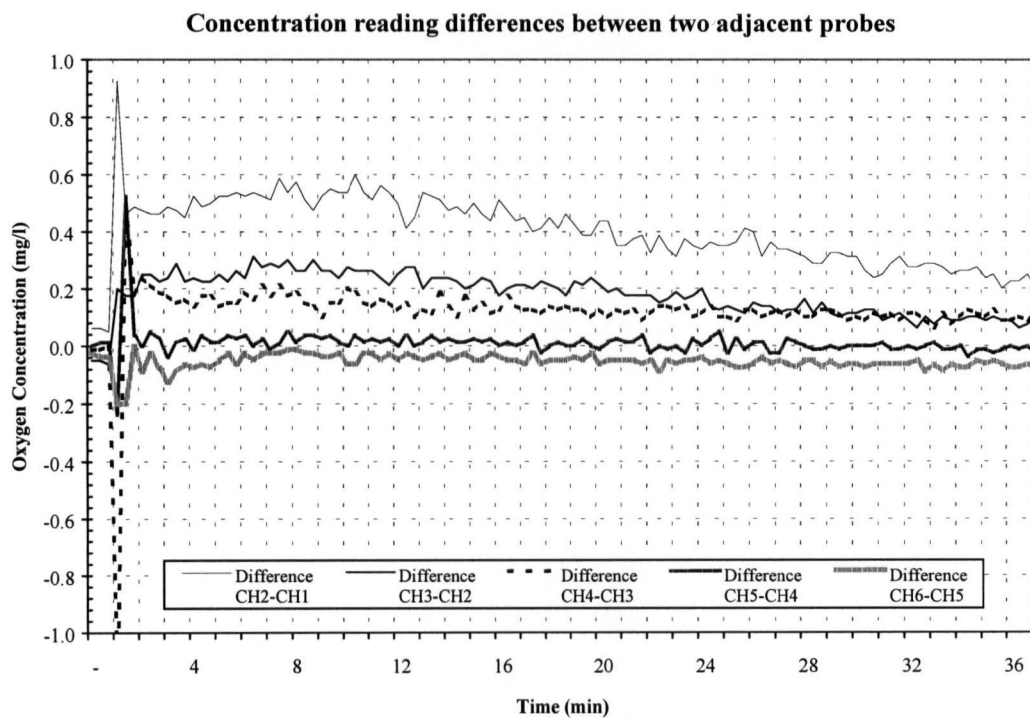
Table 4.68.   Summary of qualitative observations of the relative magnitude, slope and response to increasing PSA oxygen flows for oxygen differentials in Zones 1-5.

Treatment	Zone 1 Ch. 2-1	Zone 2 Ch. 3-2	Zone 3 Ch. 4-3	Zone 4 Ch. 5-4	Zone 5 Ch. 6-5	$10 \rightarrow 40$ l min^{-1}
140 μ x 2.9 m x O_2	Highest differential, Negative slope	2nd highest differential, less slope	3rd highest differential, less slope	Negative differential, neutral slope	Negative differential, neutral slope	Increase in Zone 1 differential and slope, variable slope
140 μ x 1.5 m x O_2	Zero differential, neutral slope	Highest differential, Negative slope	2nd highest differential, neutral slope	Negative differential, neutral slope	Negative differential, neutral slope	Increase in Zone 2 differential and slope
400 μ x 2.9 m x O_2	Highest differential, Neutral slope	Highest differential, neutral slope	2nd highest differential, neutral slope	Negative differential, neutral slope	Negative differential, neutral slope	Increase in Zone 1, 2 and 3 differential
400 μ x 1.5 m x O_2	Zero differential, neutral slope	Highest differential, Minimal slope	2nd highest differential, neutral slope	Negative differential, neutral slope	Negative differential, neutral slope	Increase in Zone 2 and 3 differential
800 μ x 2.9 m x O_2	Highest differential, neutral slope	Similar differential, neutral slope	Lower differential, neutral slope	Negative differential, neutral slope	Negative differential, neutral slope	Increase in Zone 1, 2 and 3 differential
800 μ x 1.5 m x O_2	Zero differential, neutral slope	Highest differential, Neutral slope	2nd highest differential, neutral slope	Negative differential, neutral slope	Negative differential, neutral slope	Increase in Zone 2 and 3 differential

4.4.14   DBCA x 800 μ x air

The oxygen differentials with this treatment combination changed with each increase in gas flow rate. Initially, the oxygen differential was greatest in Zones 3 and 4, followed by Zone 1, Zone 2 and Zone 5, which was positive (Figure 4.48 a-d), with all zones exhibiting a slight positive slope over the duration of the test. At the 17/3 l min^{-1} treatment, Zones 1, 2 and 3 were grouped together in a neutral slope, and Zones 4 and 5 behaved similarly. For the 27/3 min^{-1} treatment, Zones 1, 2 and 3 remained grouped, but the oxygen differential in Zone 5 increased substantially, while Zone 4 became increasingly negative. The pattern of the oxygen differentials were similar at the highest flows of 37/3 min^{-1}.

Concentration reading differences between two adjacent probes

Concentration reading differences between two adjacent probes
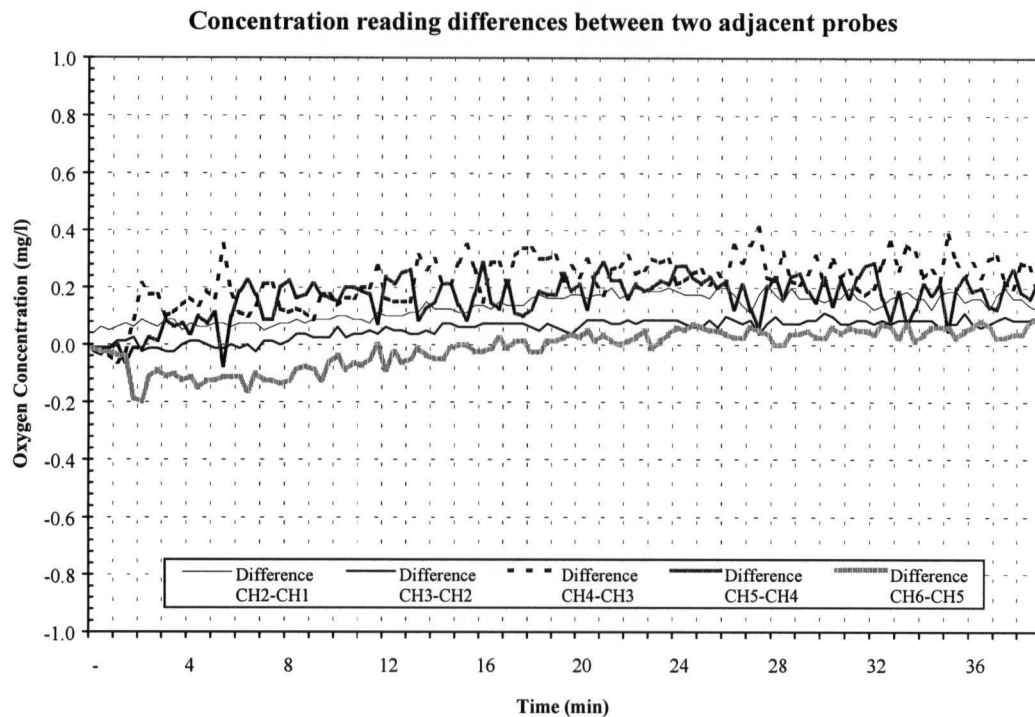
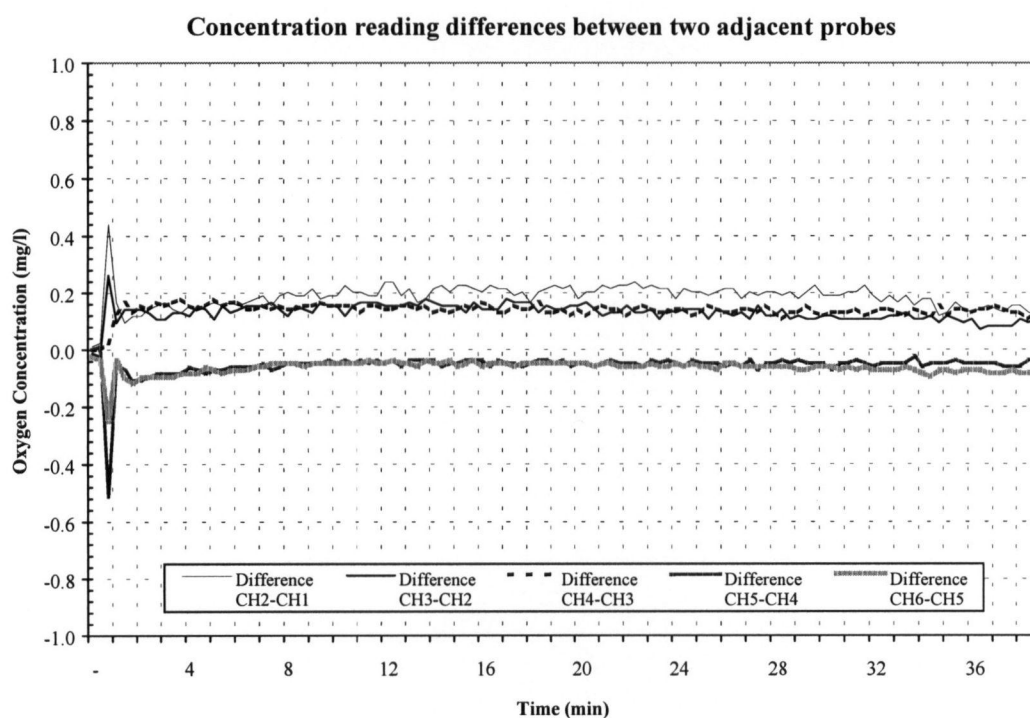**Figure 4.48a-d   Oxygen differentials in full lift aerator on air at 2.9 m with 800 μ diffuser and DBCA at 10 l min^{-1} (a), 20 l min^{-1} (b), 30 l min^{-1} (c), 40 l min^{-1} (d).**

Figure 4.48
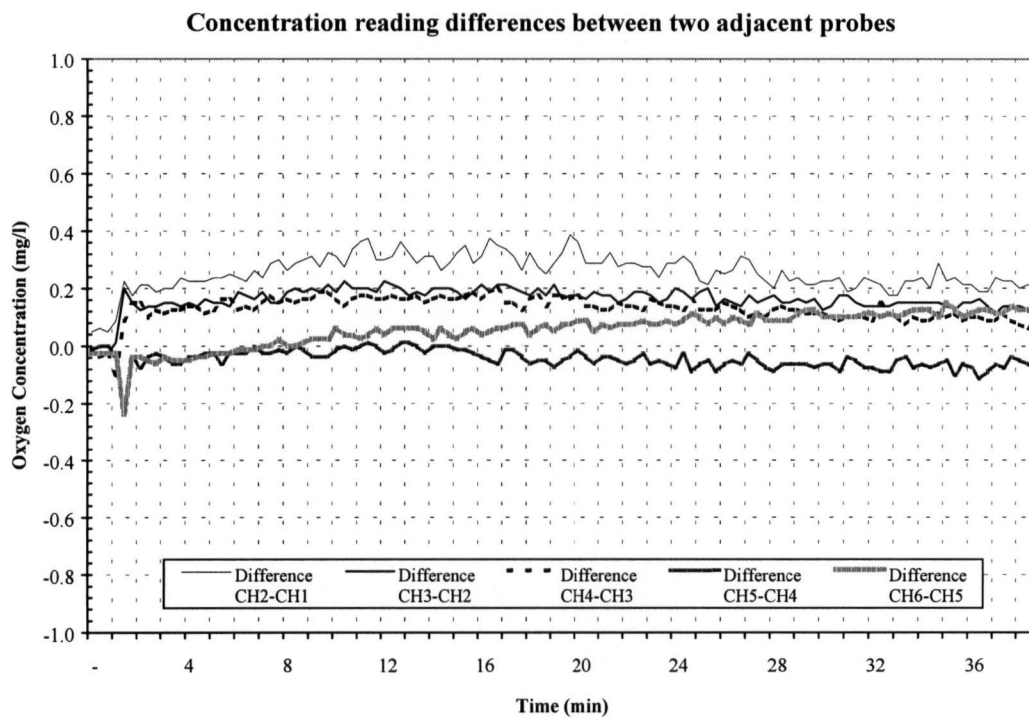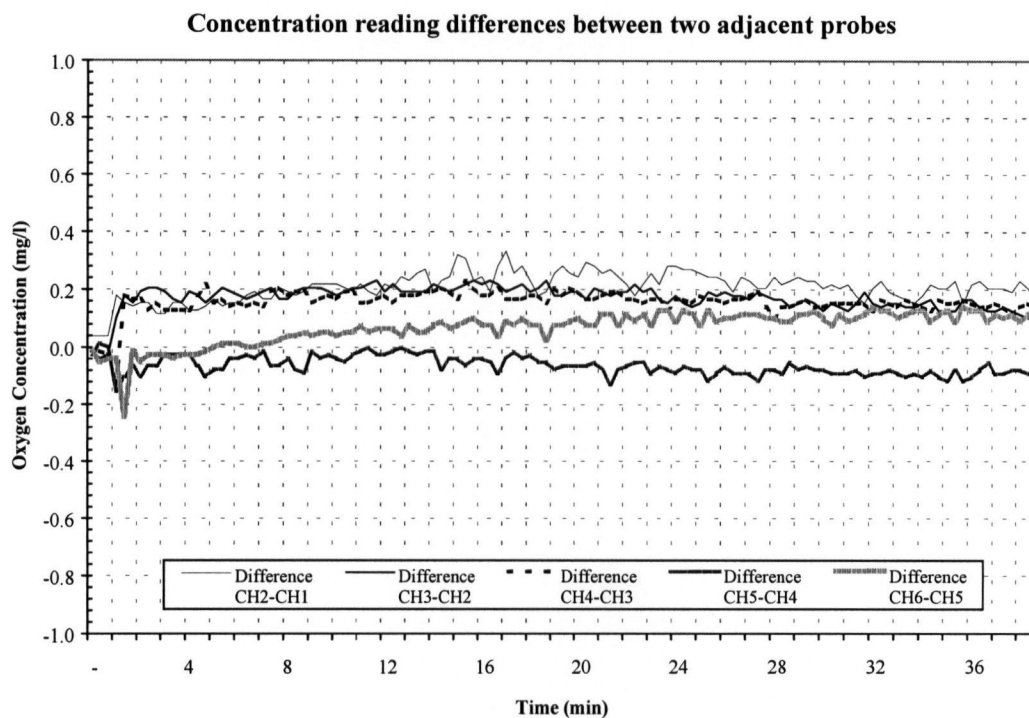
Concentration reading differences between two adjacent probes

Concentration reading differences between two adjacent probes

4.4.15   Screen x 140 μ x air

The oxygen differential was greatest in Zone 1, followed by Zones 2 and 3, and neutral to negative in Zone 5, and negative in Zone 4 (Figure 4.49 a-d). A downward trend was observed over the duration of the test in Zones 1, 2 and 3, whereas Zones 4 and 5 were fairly constant. The general trend with increasing gas flows was an increase in the oxygen differential and slope in Zone 2 and 3, and a decrease in oxygen differential for Zone 5.

4.4.16   Screen x 800 μ x air

The oxygen differential was greatest in Zones 1 and 2, followed by Zones 3, and negative in Zones 4 and 5 (Figure 4.50 a-d). Minimal downward trend was observed over the duration of the test in Zones 1, 2 and 3, except at the highest gas flow rates, whereas Zones 4 and 5 exhibited a negative differential with neutral slope. The general trend with increasing gas flows was an increase in the oxygen differential and slope in Zones 1 and 2.

4.4.17   Surface cover x 140 μ x air

The oxygen differential was greatest in Zone 1, followed by Zones 2 and Zone 3 (Figure 4.51 a-d). The oxygen differential was slightly negative in Zones 4 and 5; indicating oxygen concentrations were decreasing in these zones. A slight downward trend was observed over the duration of the test in Zones 1 and 2, whereas Zones 3, 4 and 5 were fairly constant. The general trend with increasing gas flows from 10 to 40 l min^{-1} was an increase in the oxygen differential in Zone 1, and an increase in slope for Zones 2 and 3.
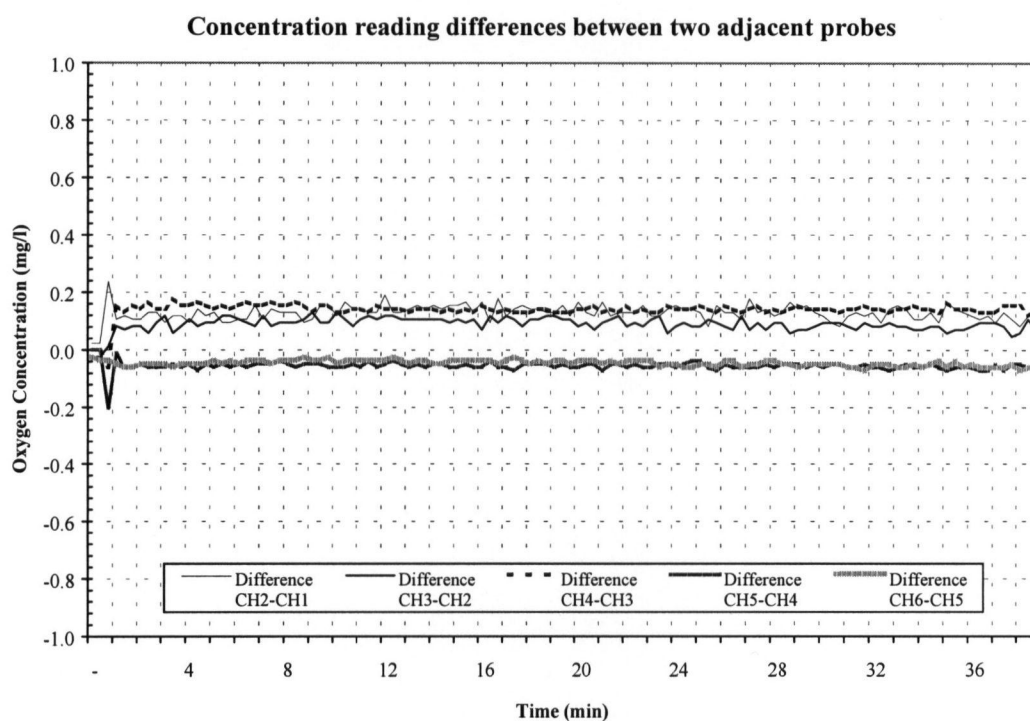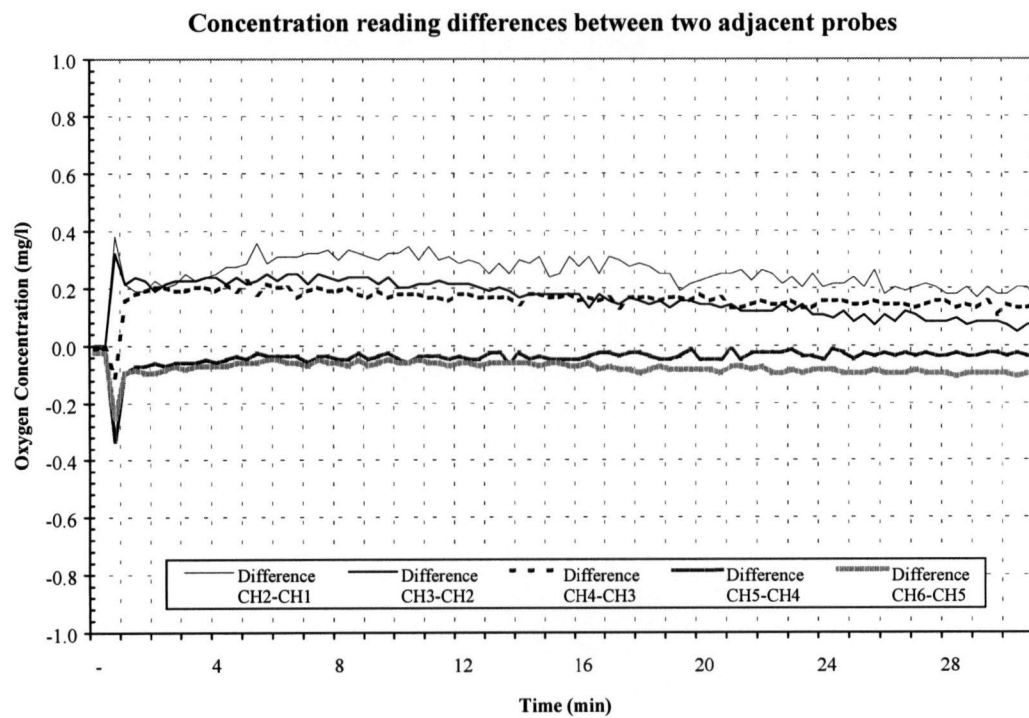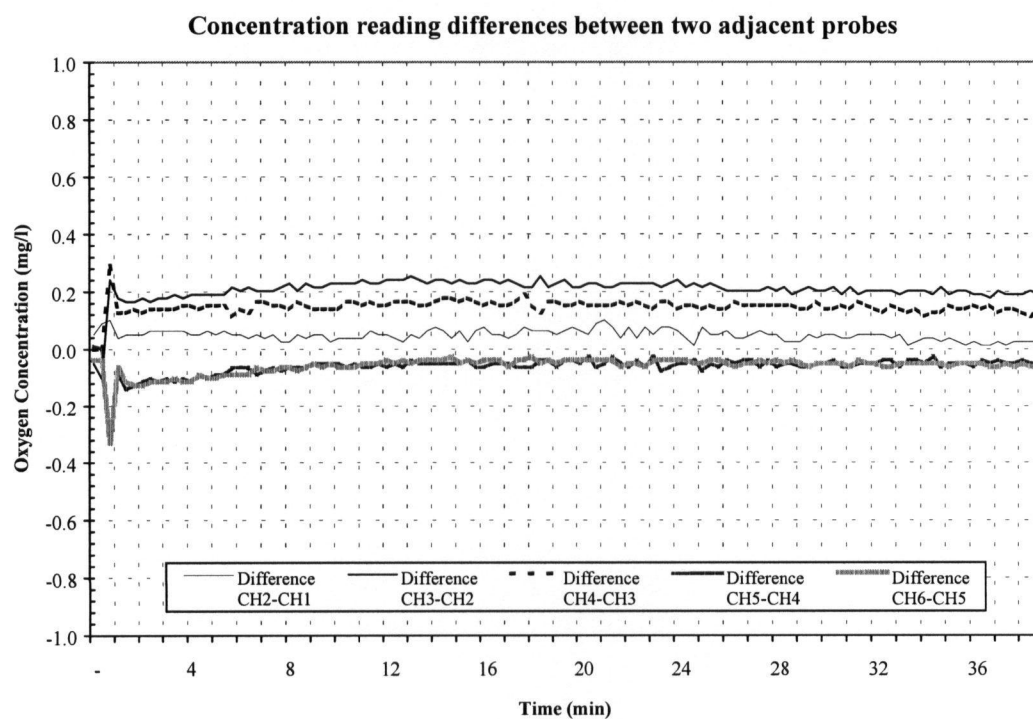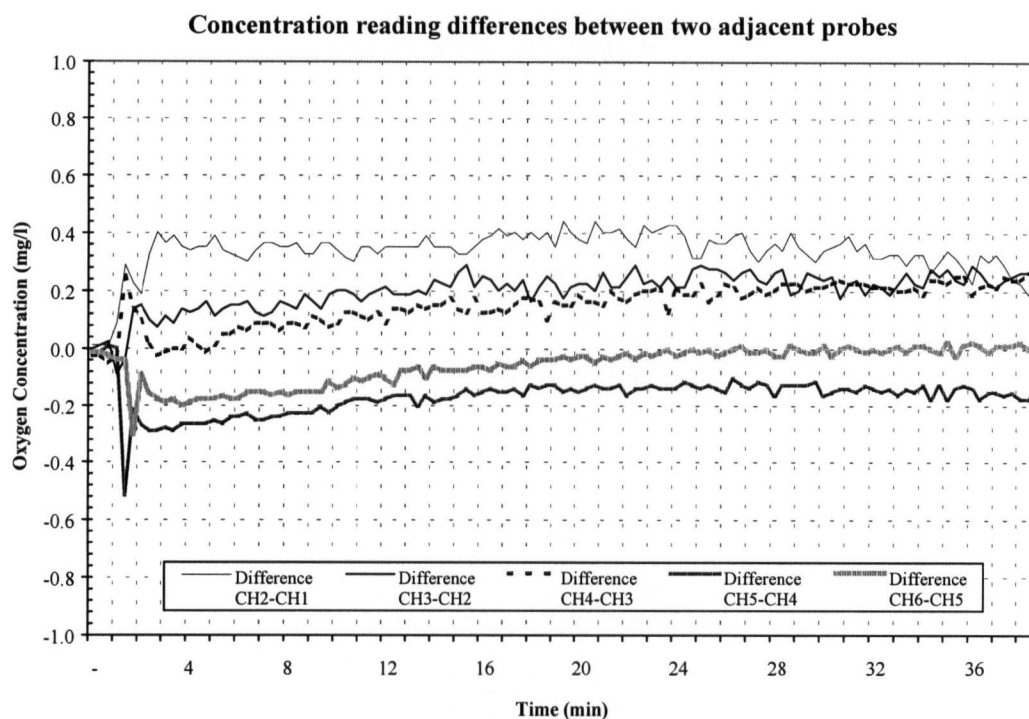
Figure 4.49a-d Oxygen differentials in full lift aerator on air at 2.9 m with 140 µ diffuser and Bubble screen at 10 l min^{-1} (a), 20 l min^{-1} (b), 30 l min^{-1} (c), 40 l min^{-1} (d).

Figure 4.49 continued

Concentration reading differences between two adjacent probes

Concentration reading differences between two adjacent probes

Concentration reading differences between two adjacent probes

Concentration reading differences between two adjacent probes
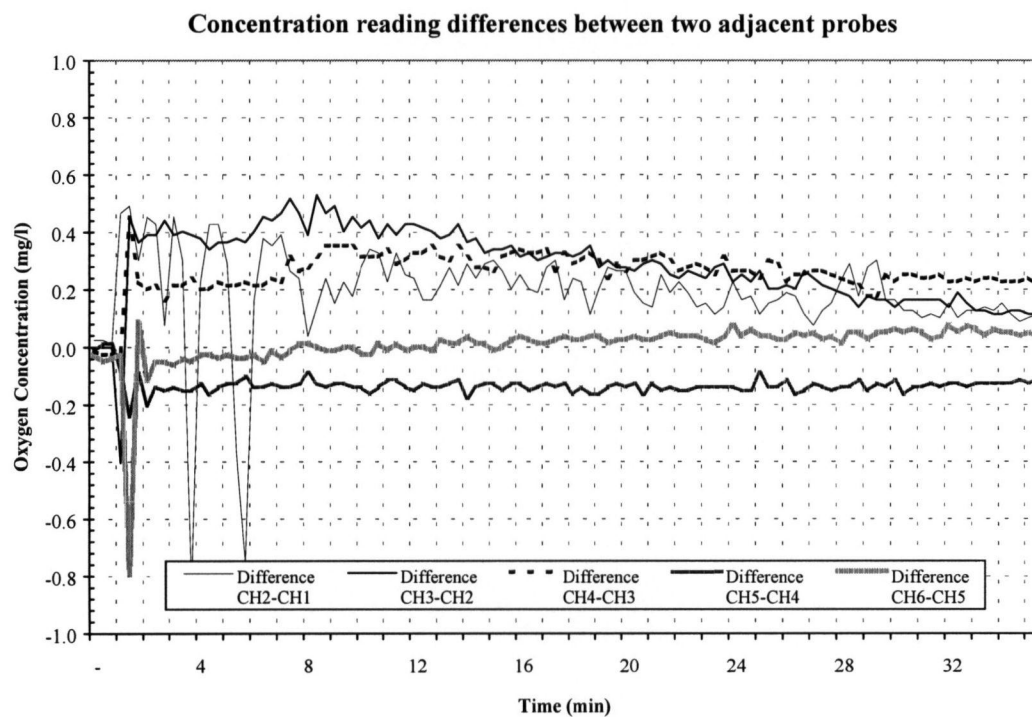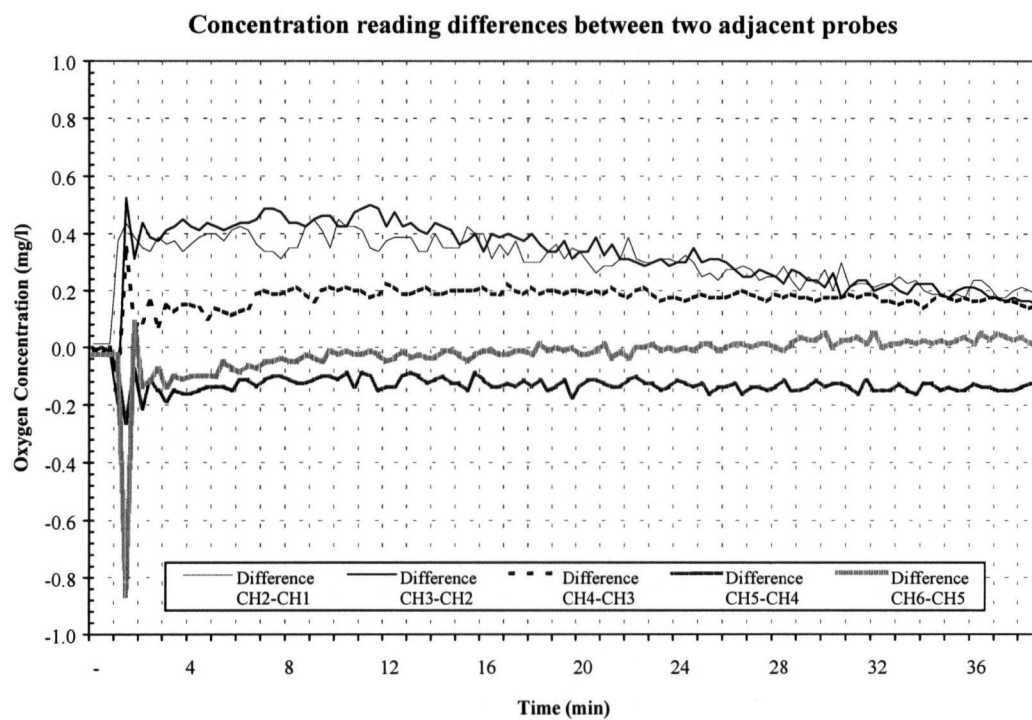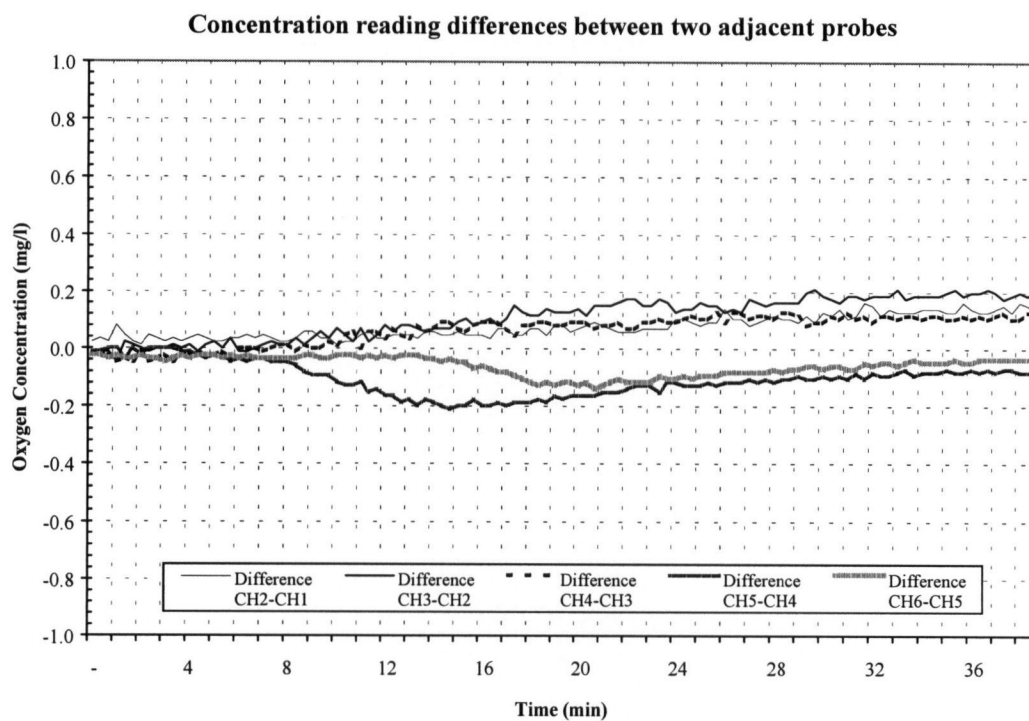
Figure 4.50a-d Oxygen differentials in full lift aerator on air at 2.9 m with 800 μ diffuser and Bubble screen at 10 l min^{-1} (a), 20 l min^{-1} (b), 30 l min^{-1} (c), 40 l min^{-1} (d).

Figure 4.50 continued

Concentration reading differences between two adjacent probes

Concentration reading differences between two adjacent probes

Concentration reading differences between two adjacent probes

Concentration reading differences between two adjacent probes
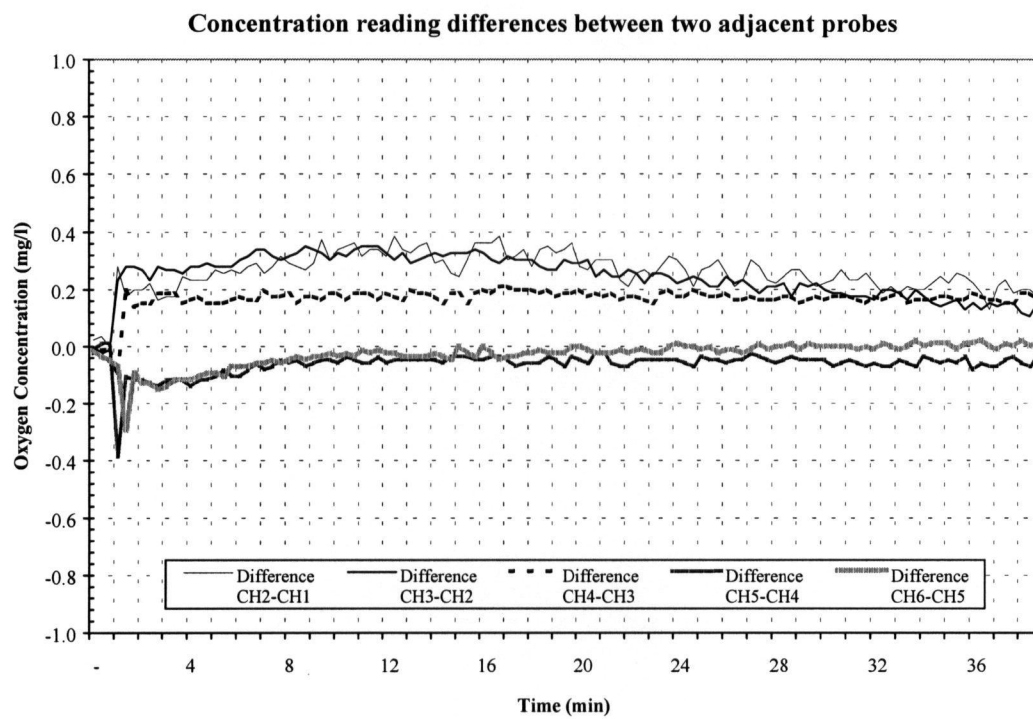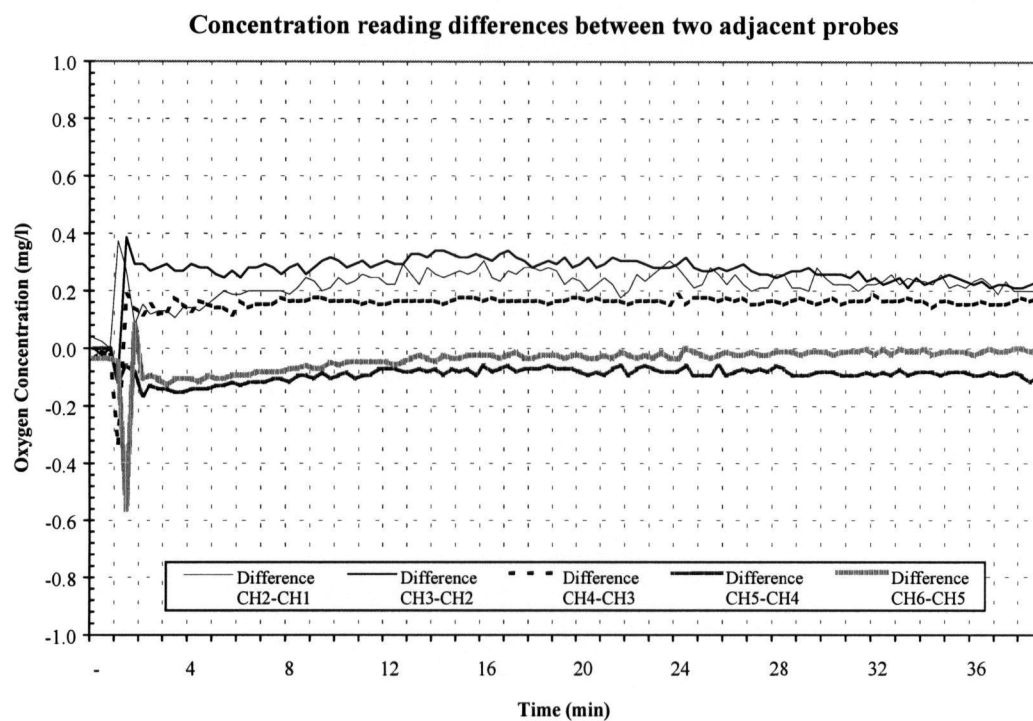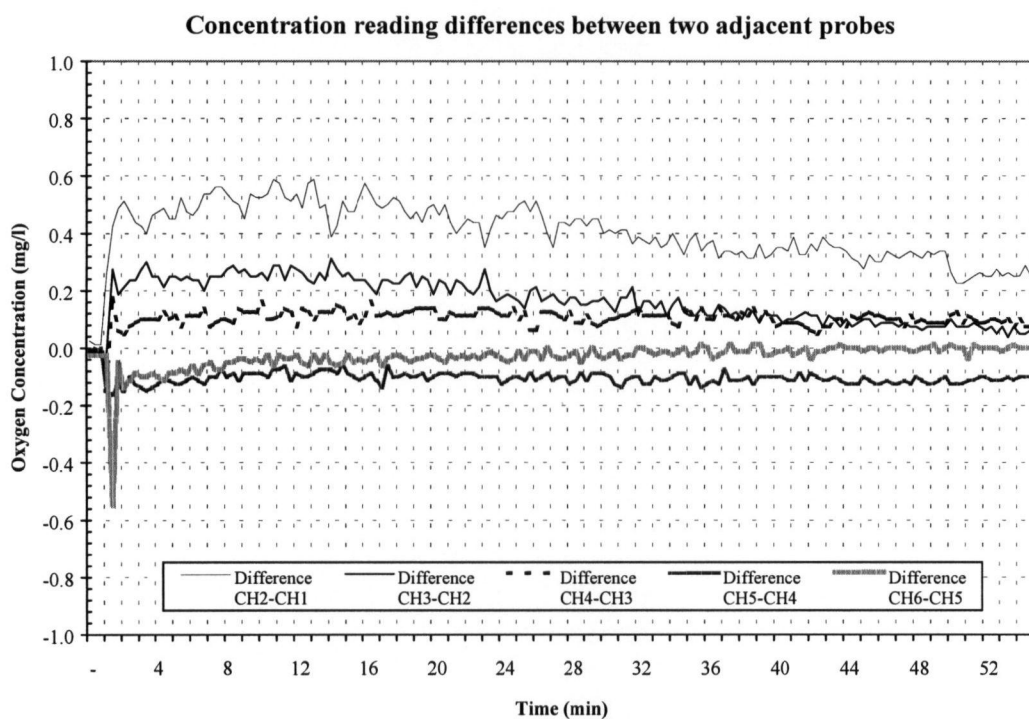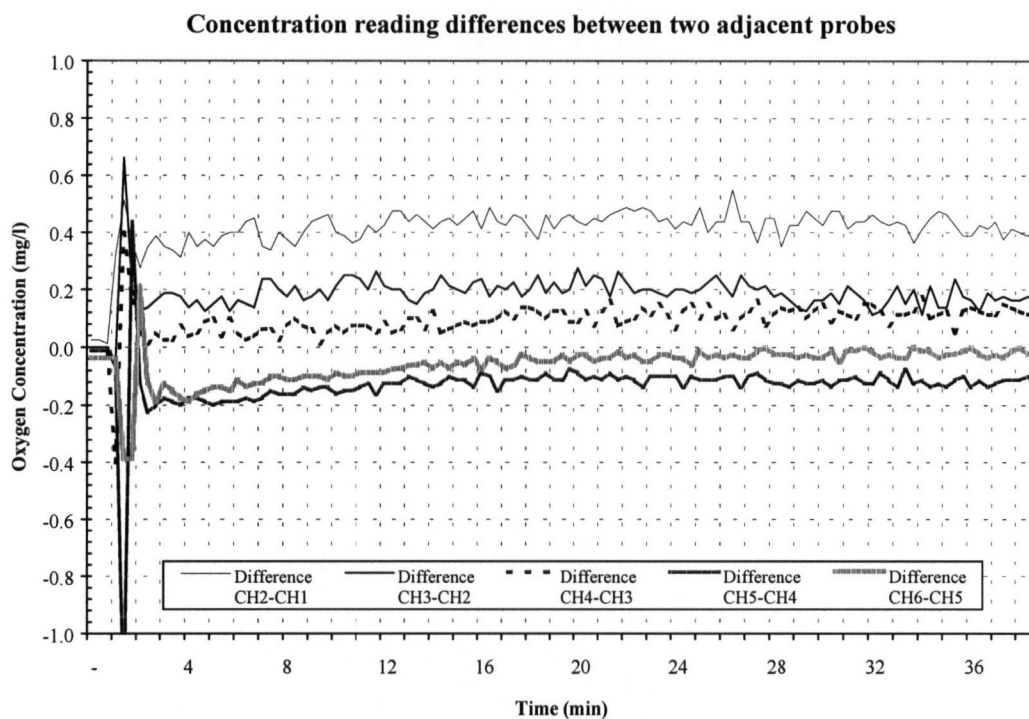
Figure 4.51a-d Oxygen differentials in full lift aerator on air at 2.9 m with 140 μ diffuser and Surface cover at 10 l min^{-1} (a), 20 l min^{-1} (b), 30 l min^{-1} (c), 40 l min^{-1} (d).

Figure 4.51 continued

Concentration reading differences between two adjacent probes

Concentration reading differences between two adjacent probes
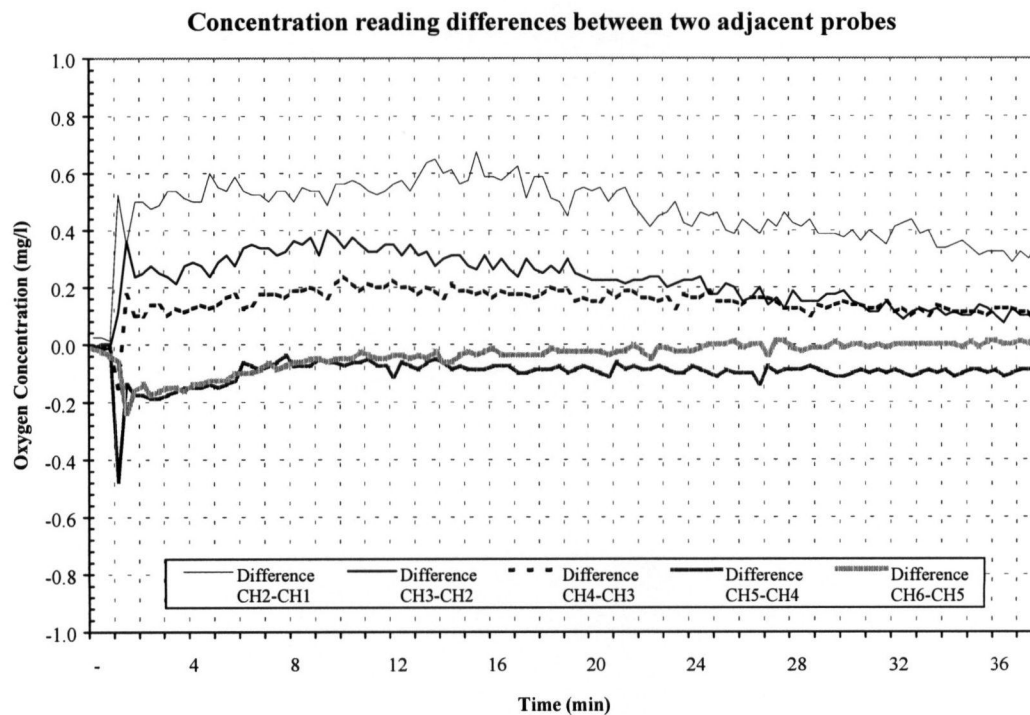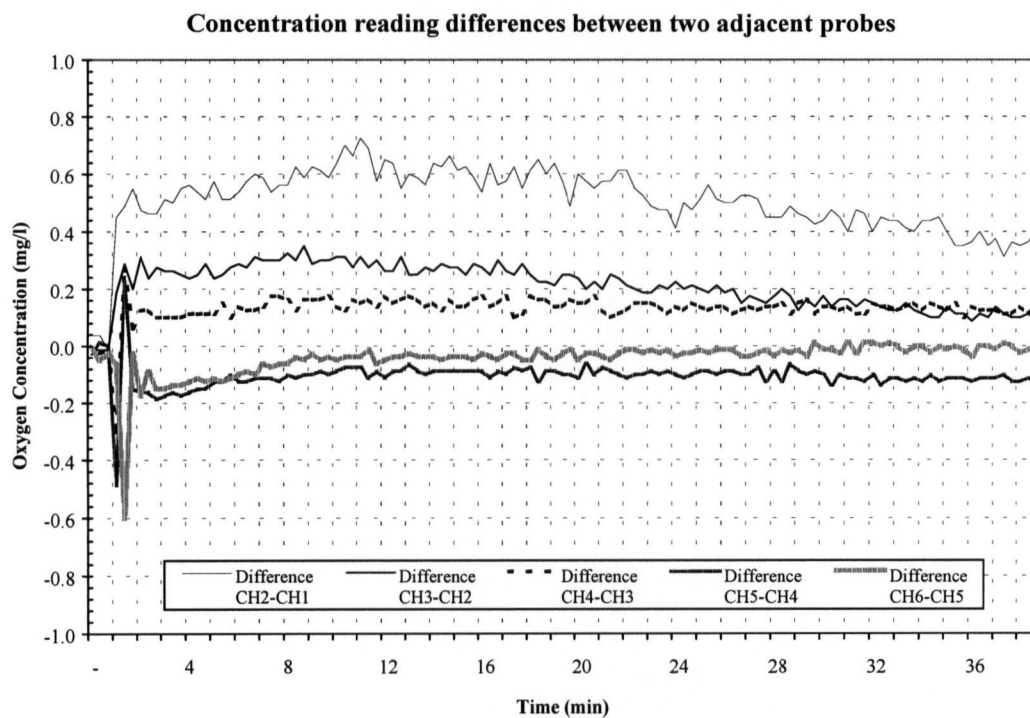
4.4.18   Surface cover x 800 μ x air

The oxygen differentials were similar in Zones 1, 2 and 3, and similar, but negative, in Zones 4 and 5 (Figure 4.52 a-d). As gas flow increased, the differentials in Zones 1, 2 and 3 increased but remained tightly grouped; while the Zone 5 differential became less negative.

4.4.19   Vanes x 140 μ x air

The oxygen differential was greatest in Zone 1, followed by Zones 2 and Zone 3, and slightly negative in Zones 4 and 5 (Figure 4.53 a-d). A slight downward trend was observed over the duration of the test in Zones 1 and 2, whereas Zones 3, 4 and 5 were fairly constant. No trends were apparent with increasing gas flows.

4.4.20   Vanes x 800 μ x air

The oxygen differentials were similar in Zones 1, 2 with Zone 3 being lower, and similar, but negative, in Zones 4 and 5 (Figure 4.54 a-d). As gas flow increased, the differentials and negative slope in Zones 1 and 2 increased but remained tightly grouped; while Zones 4 and 5 remained negative with minimal change in slope. A summary of the qualitative observations of the *in situ* modifications oxygen differentials, on air, are shown in Table 4.69.

4.4.21   DBCA x 140 μ x O_2

The oxygen differential was greatest in Zone 1, followed by Zone 2 and a tight grouping of Zones 3, and 4, and slightly negative in Zone 5 (Figure 4.55 a-d). Minimal trend was observed over the duration of the test in all zones. There was minimal change with increasing oxygen flows in Zones 1,2, 3 and 5, while the Zone 4 oxygen differential decreased.

Concentration reading differences between two adjacent probes

Concentration reading differences between two adjacent probes
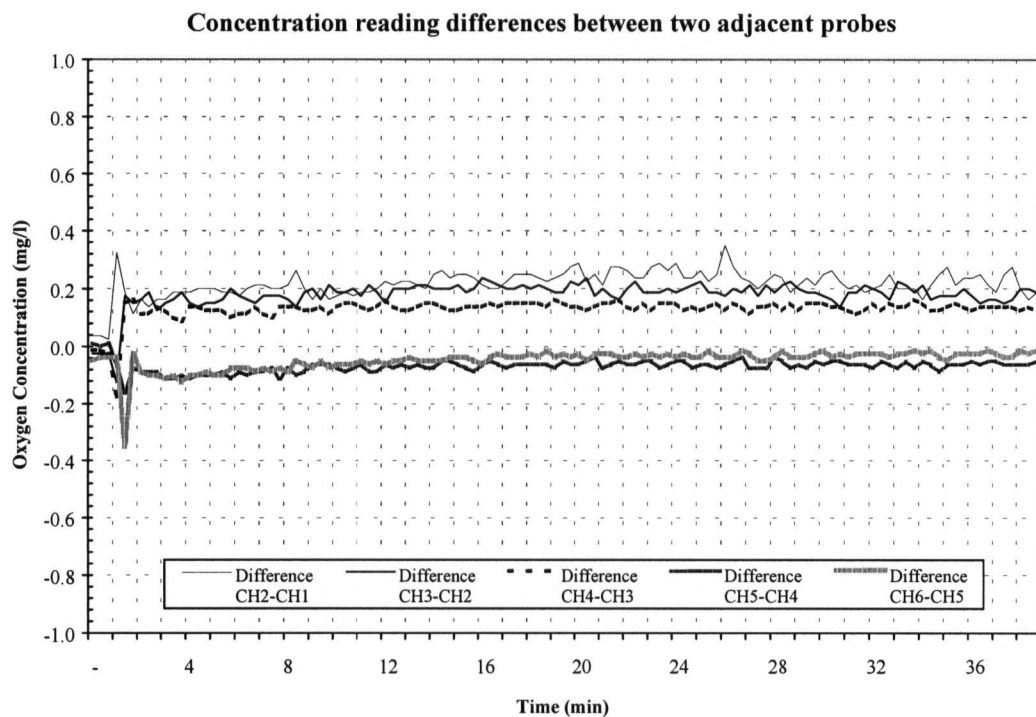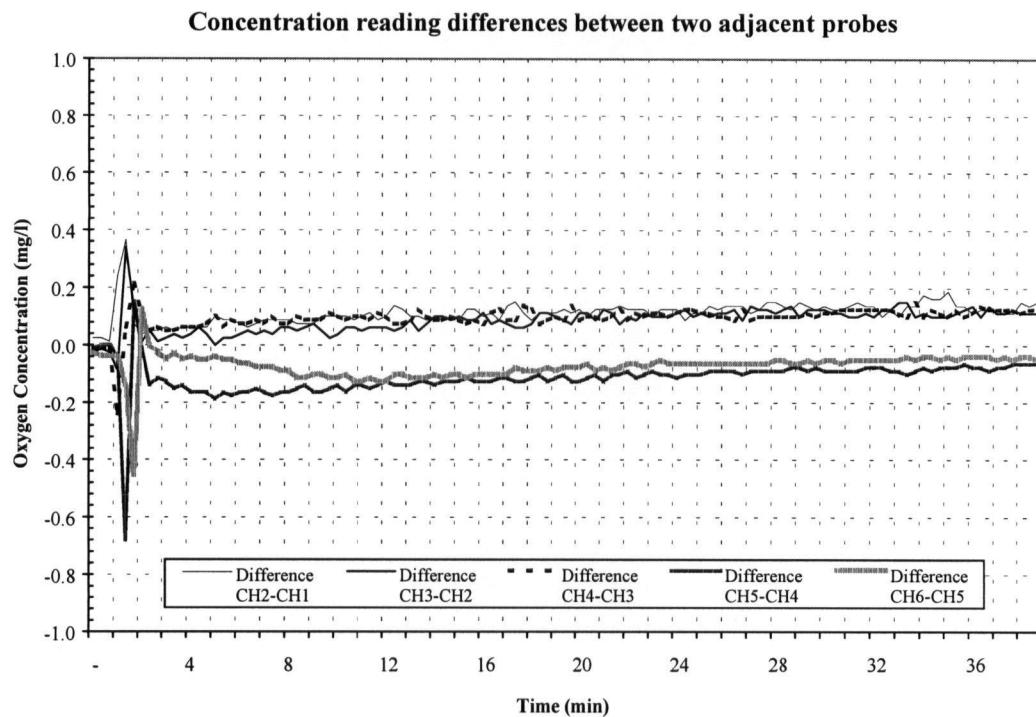
Figure 4.52a-d Oxygen differentials in full lift aerator on air at 2.9 m with 800 μ diffuser and Surface cover at 10 l min^{-1} (a), 20 l min^{-1} (b), 30 l min^{-1} (c), 40 l min^{-1} (d).

Figure 4.52 continued

Concentration reading differences between two adjacent probes

Concentration reading differences between two adjacent probes

Concentration reading differences between two adjacent probes

Concentration reading differences between two adjacent probes
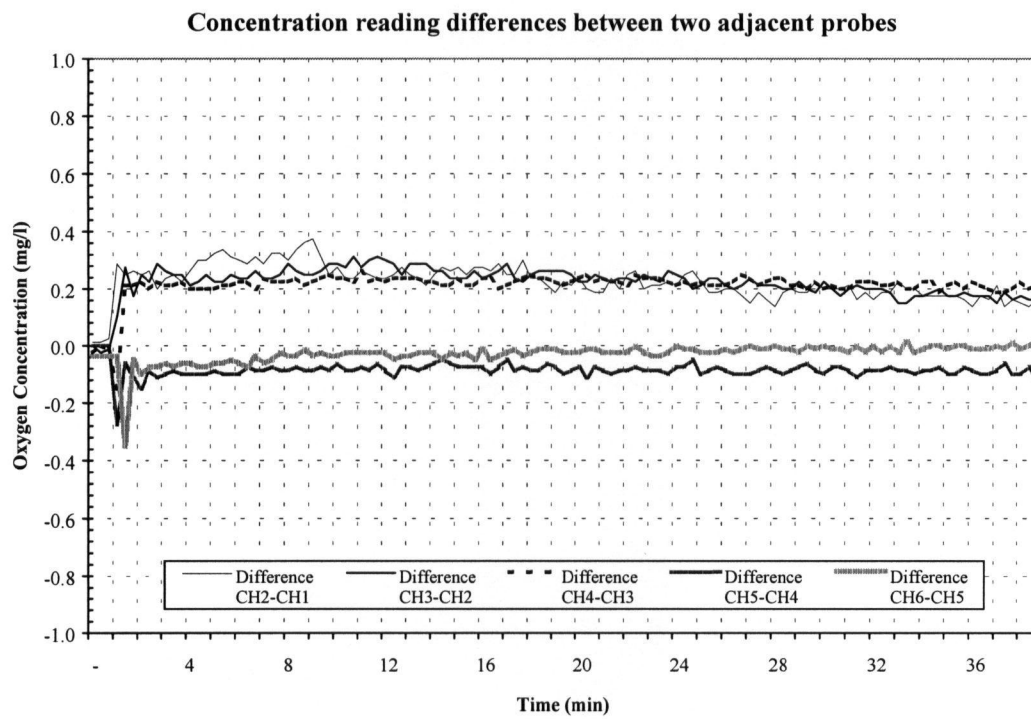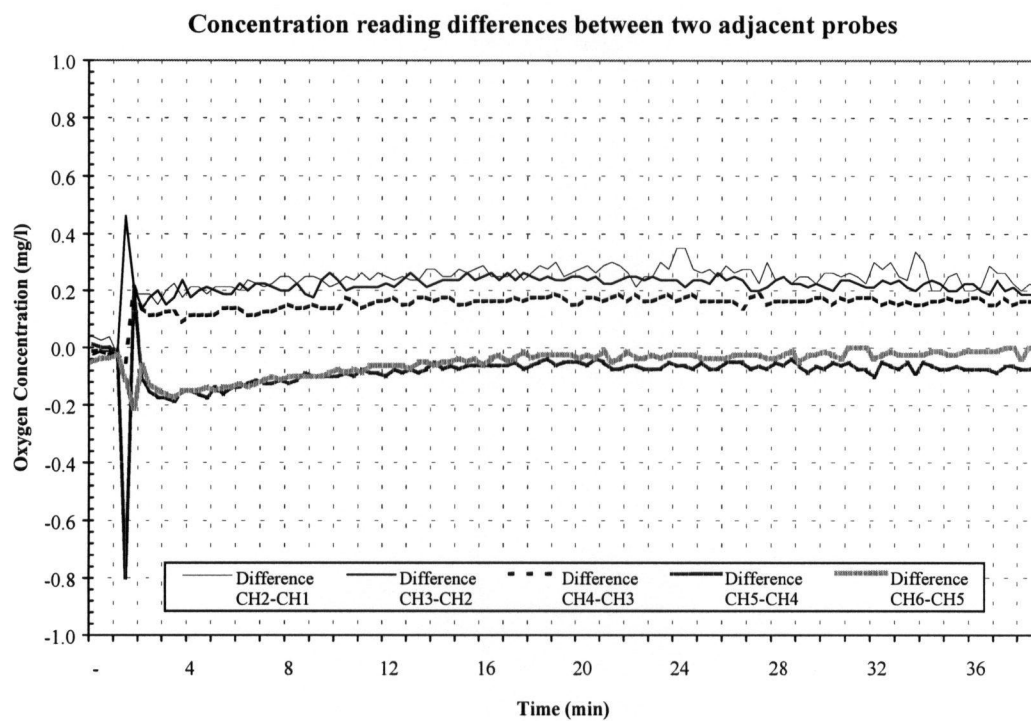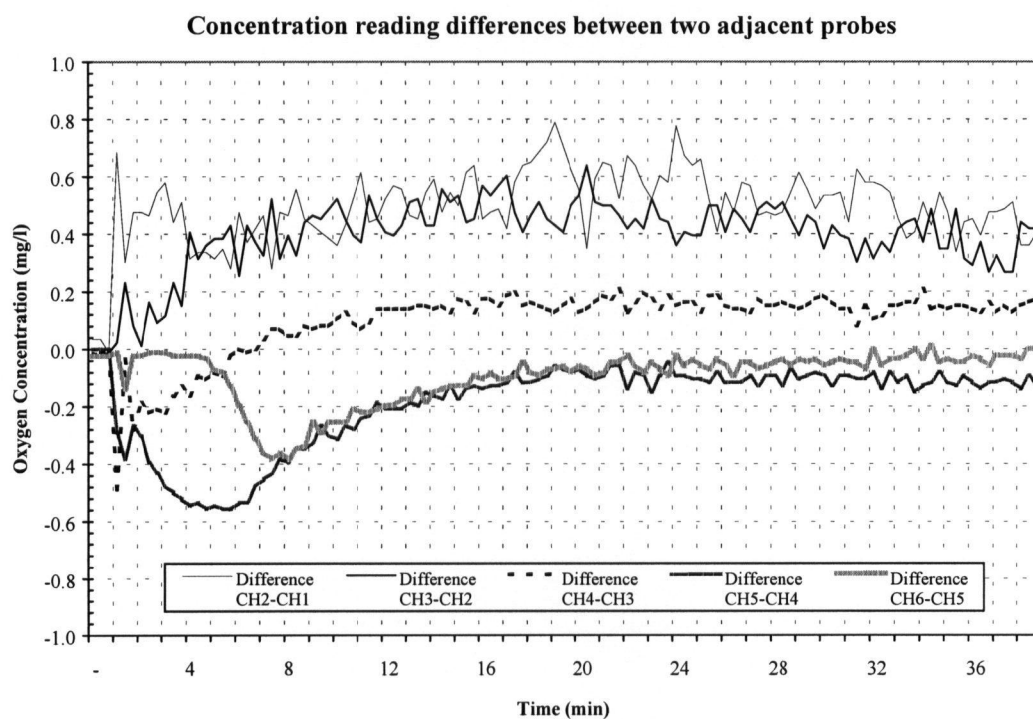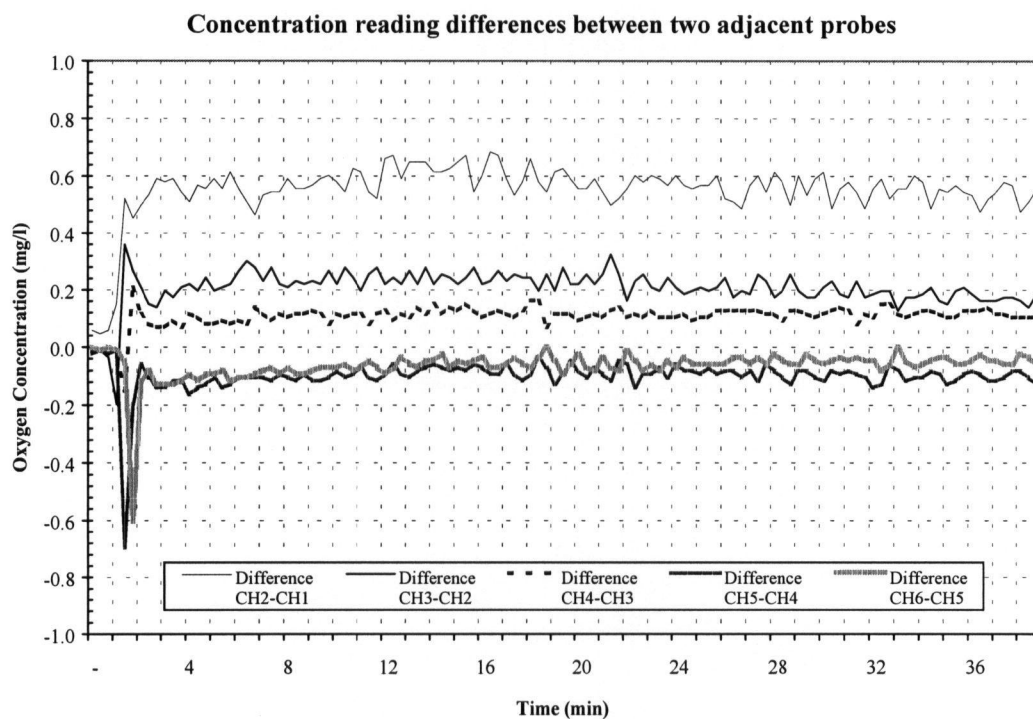
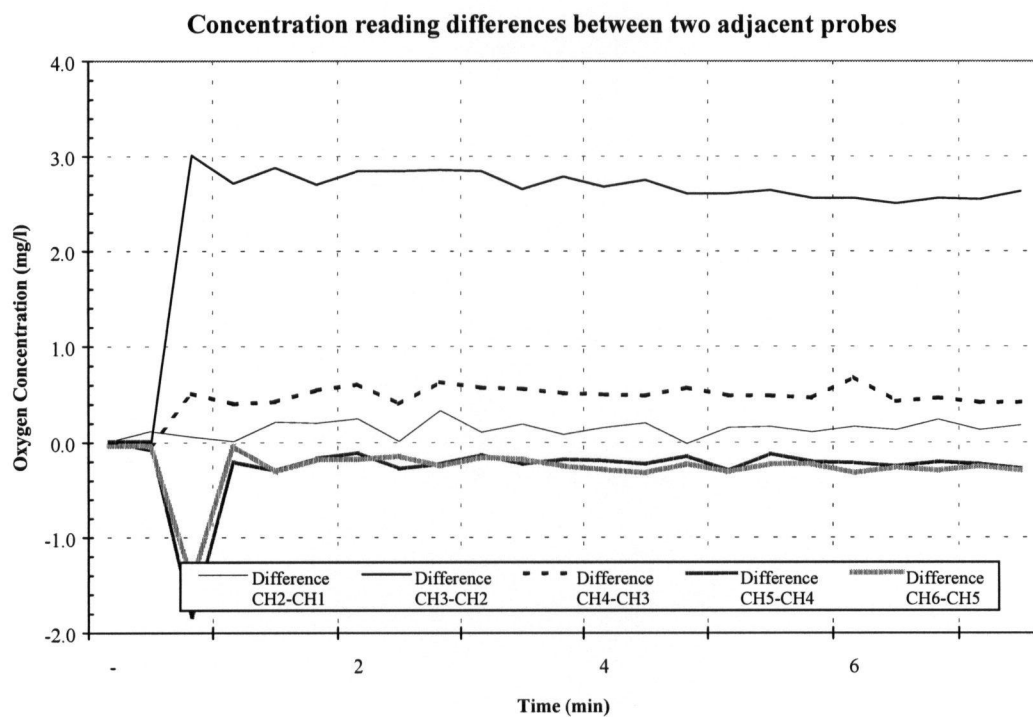**Figure 4.53a-d Oxygen differentials in full lift aerator on air at 2.9 m with 140 μ diffuser and Counter-rotating blades at 10 l min^{-1} (a), 20 l min^{-1} (b), 30 l min^{-1} (c), 40 l min^{-1} (d).**

Figure 4.53 continued

Concentration reading differences between two adjacent probes

Concentration reading differences between two adjacent probes

Concentration reading differences between two adjacent probes

Concentration reading differences between two adjacent probes
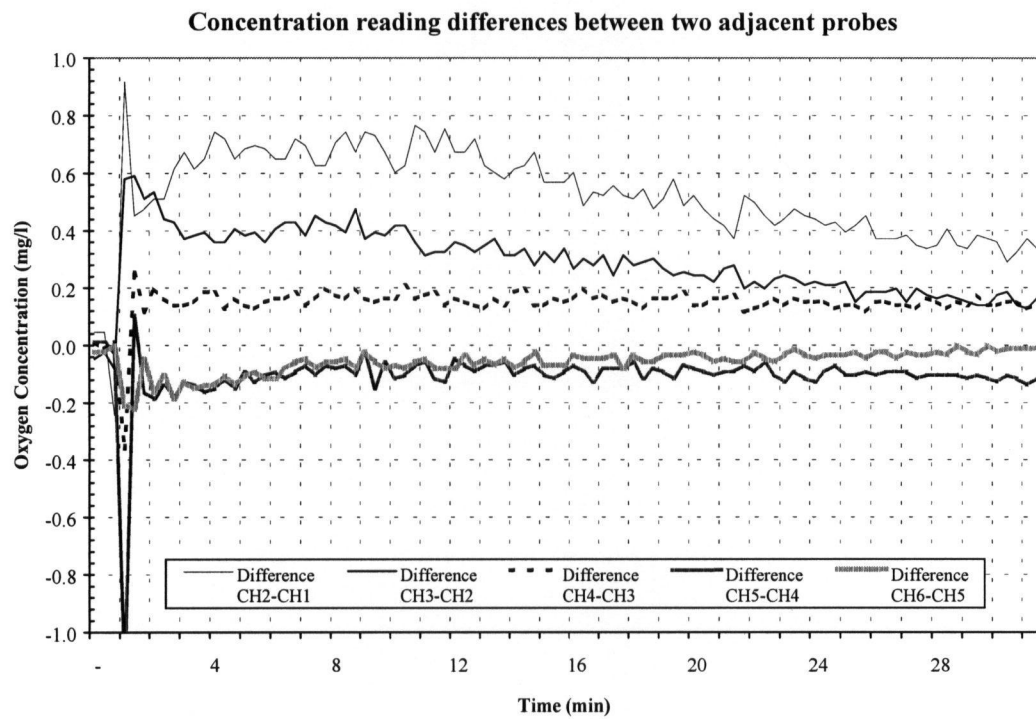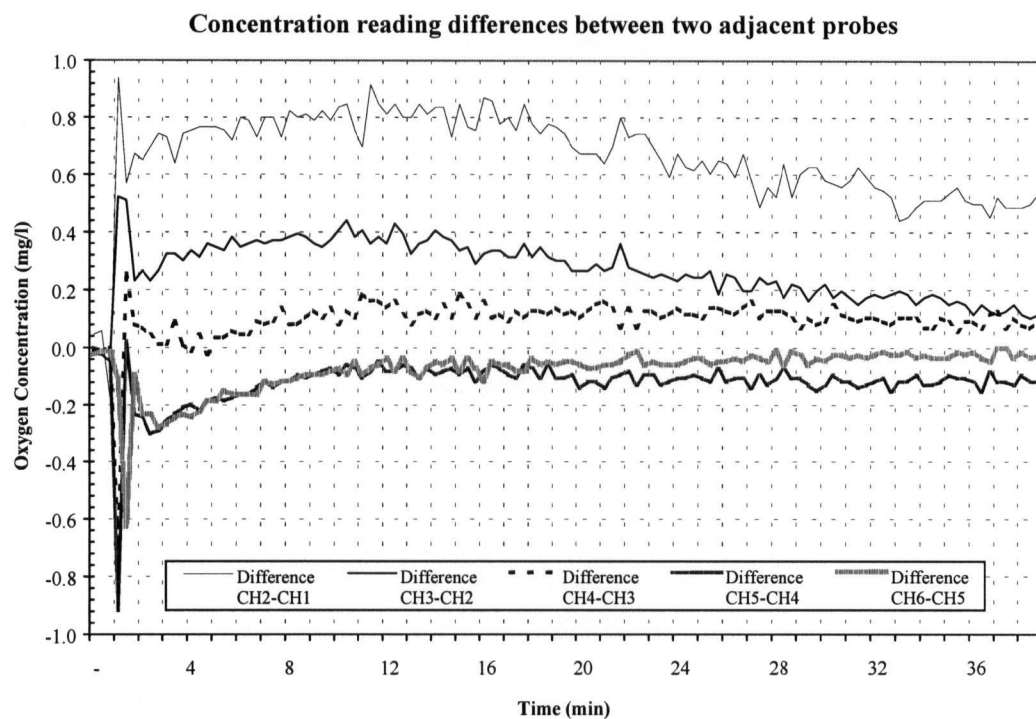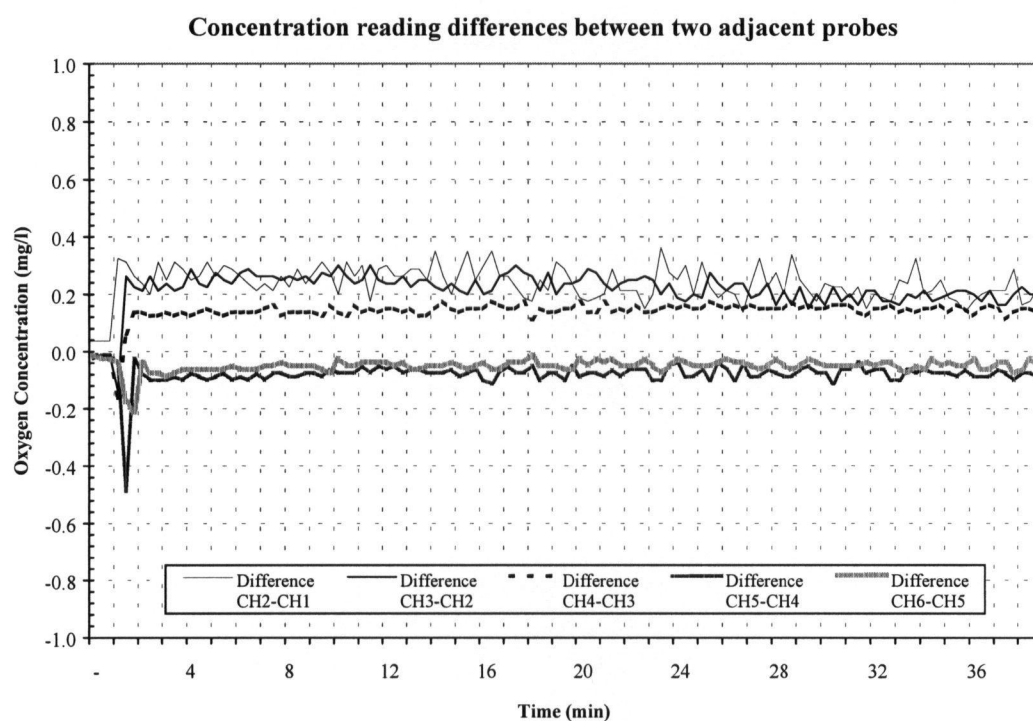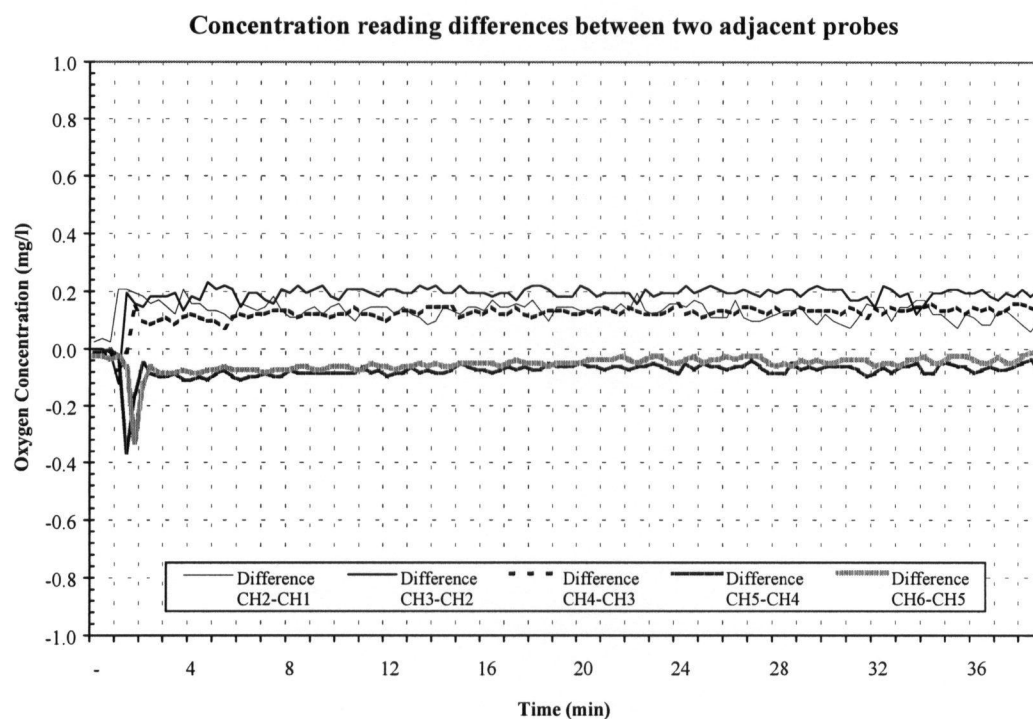
Figure 4.54a-d Oxygen differentials in full lift aerator on air at 2.9 m with 800 μ diffuser and Counter-rotating blades at 10 l min^{-1} (a), 20 l min^{-1} (b), 30 l min^{-1} (c), 40 l min^{-1} (d).

Figure 4.54 continued

Concentration reading differences between two adjacent probes

Concentration reading differences between two adjacent probes

Concentration reading differences between two adjacent probes

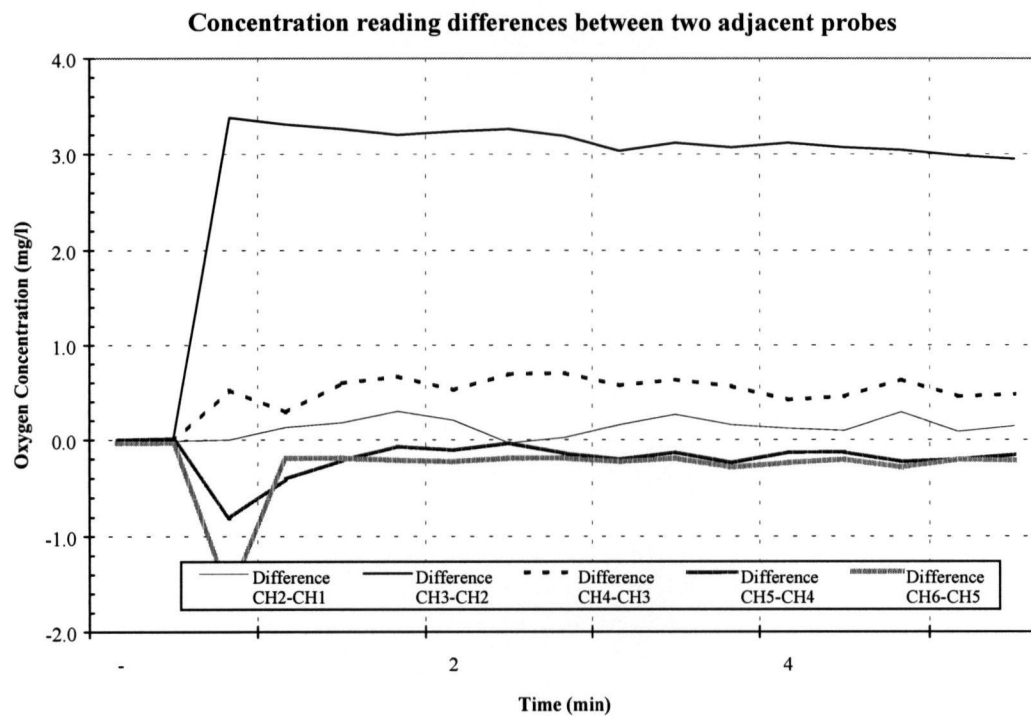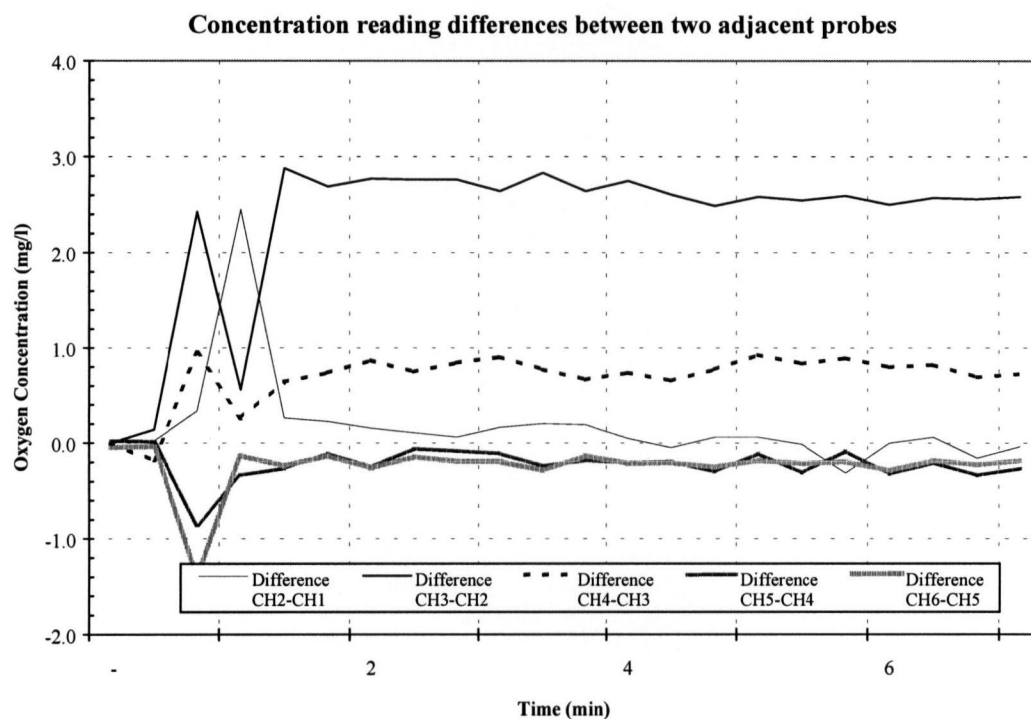**Concentration reading differences between two adjacent probes**
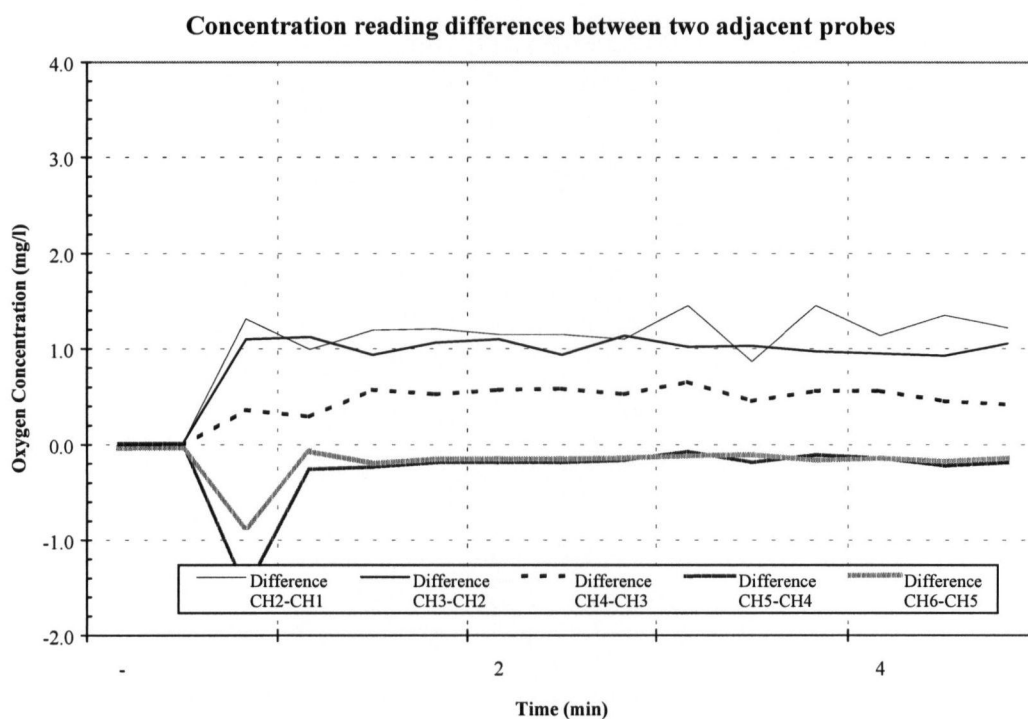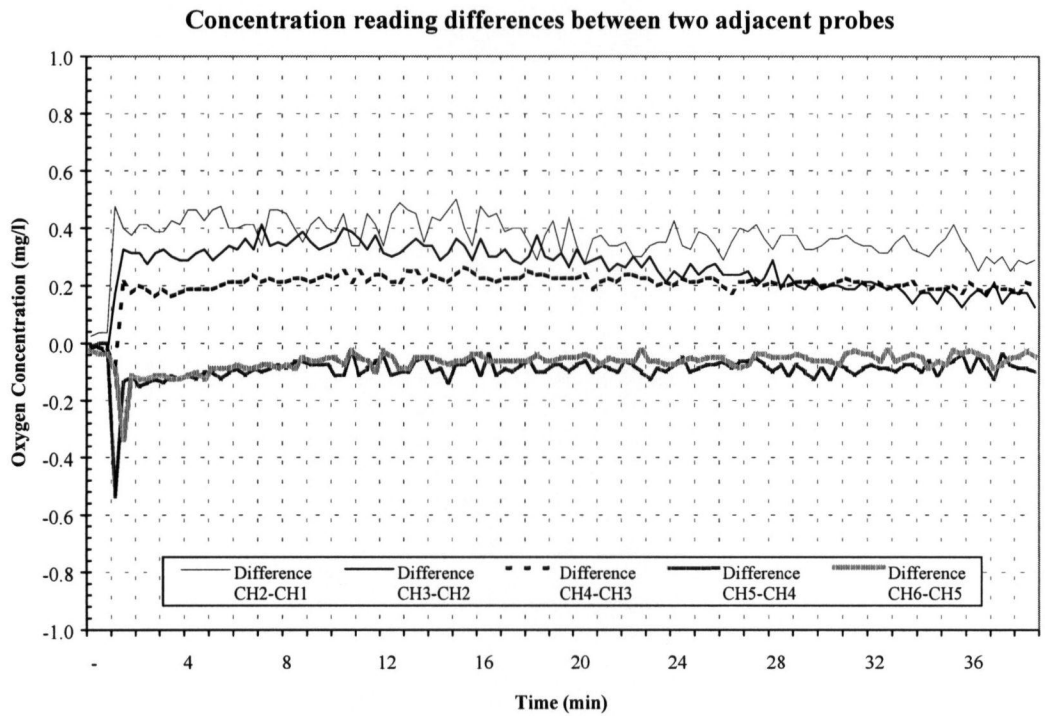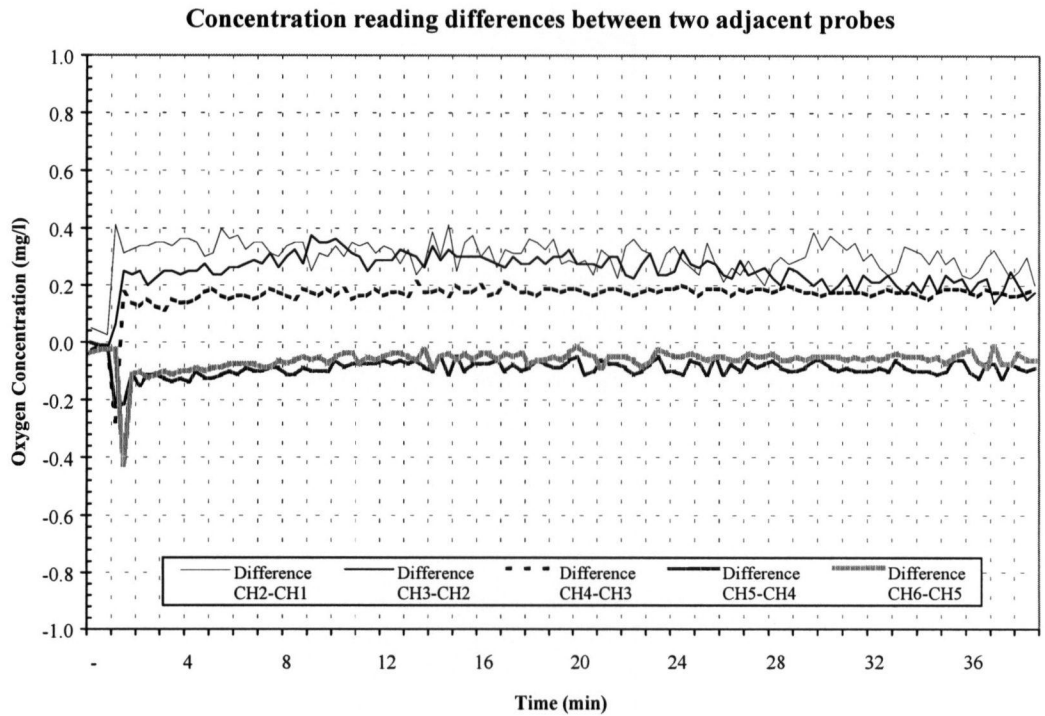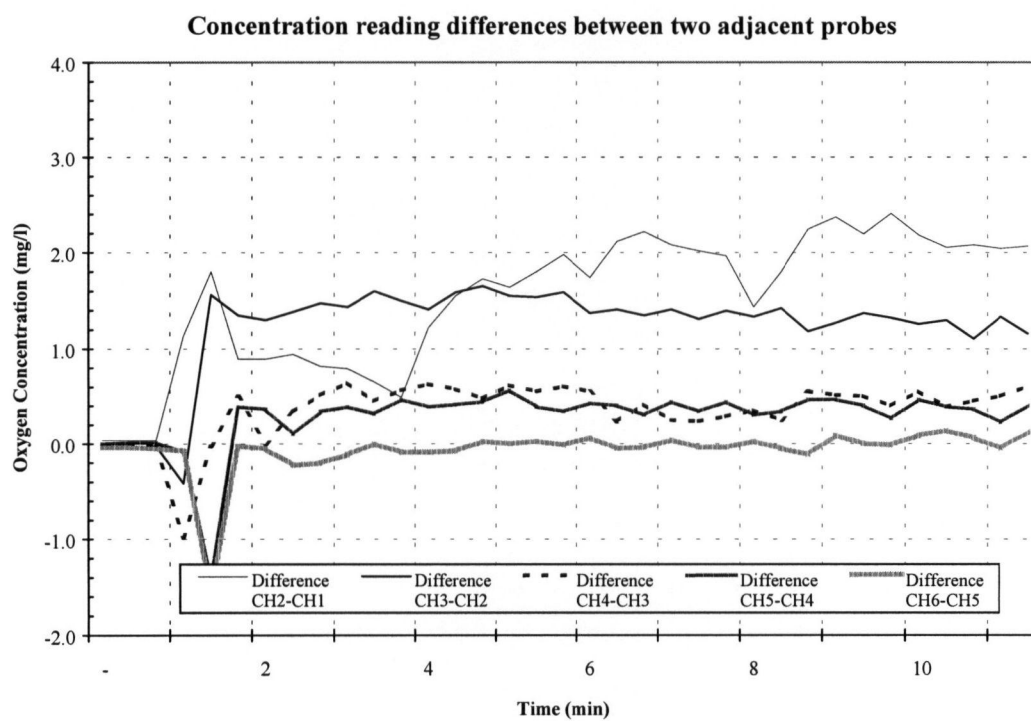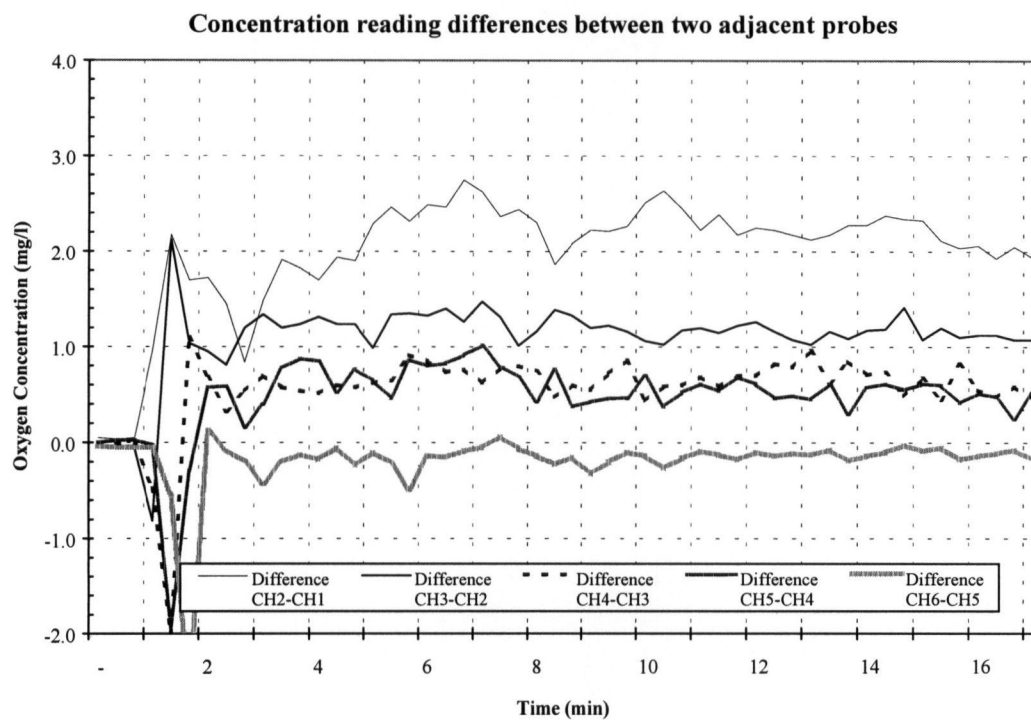

Figure 4.55a-d   Oxygen differentials in full lift aerator on PSA O_2 at 2.9 m with 140 μ diffuser and DBCA at 10 l min^{-1} (a), 20 l min^{-1} (b), 30 l min^{-1} (c), 40 l min^{-1} (d).

Figure 4.55 continued

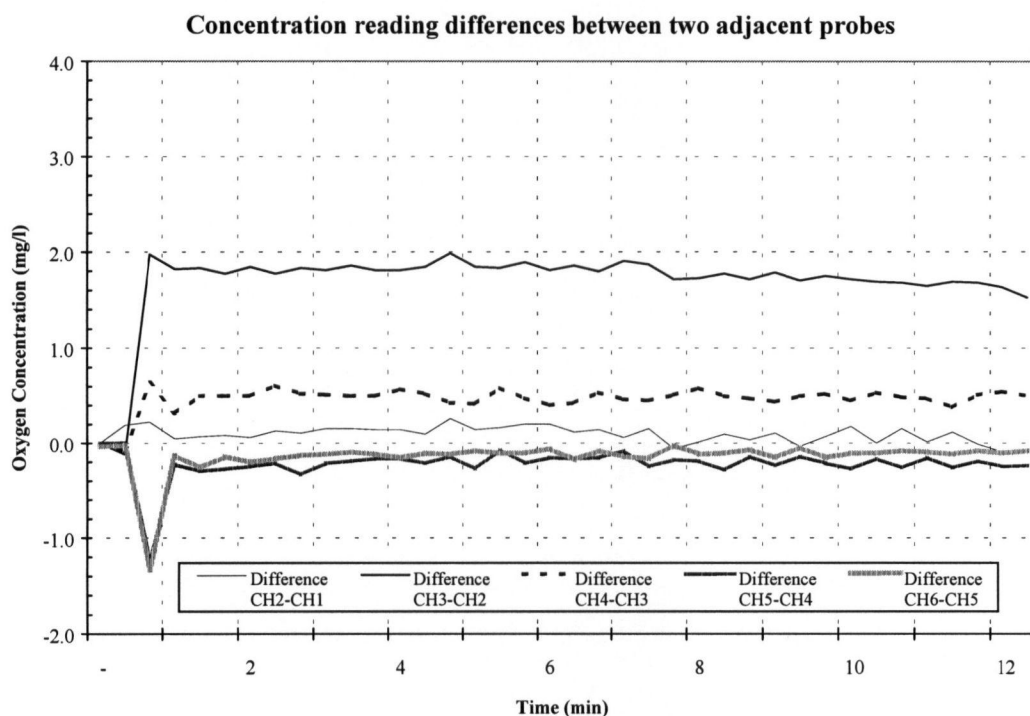**Concentration reading differences between two adjacent probes**

Concentration reading differences between two adjacent probes
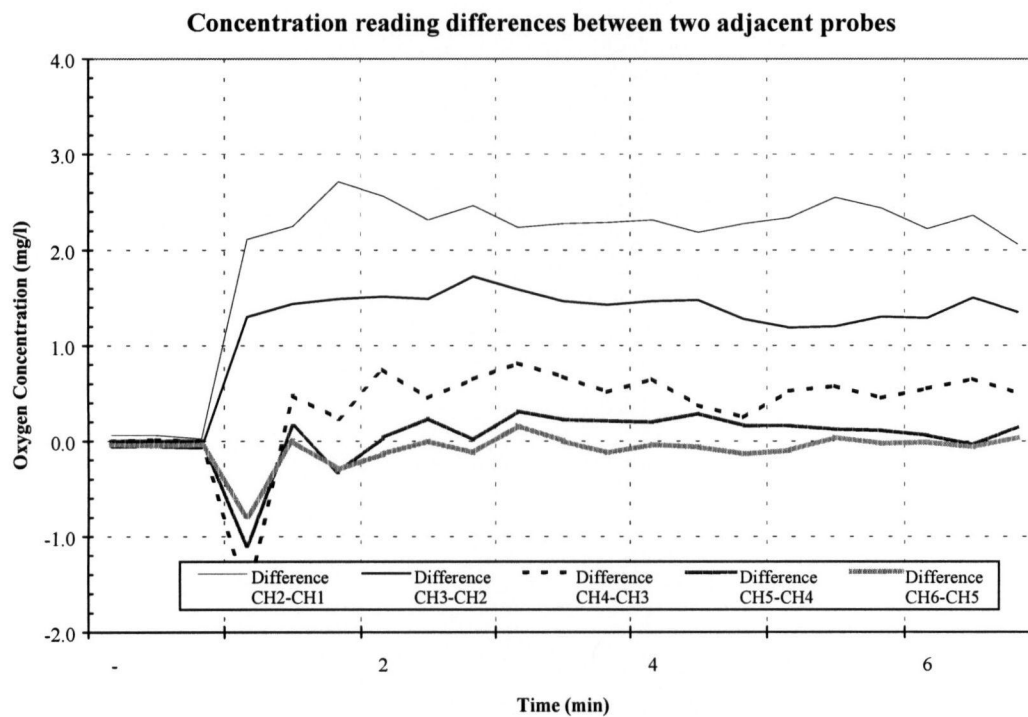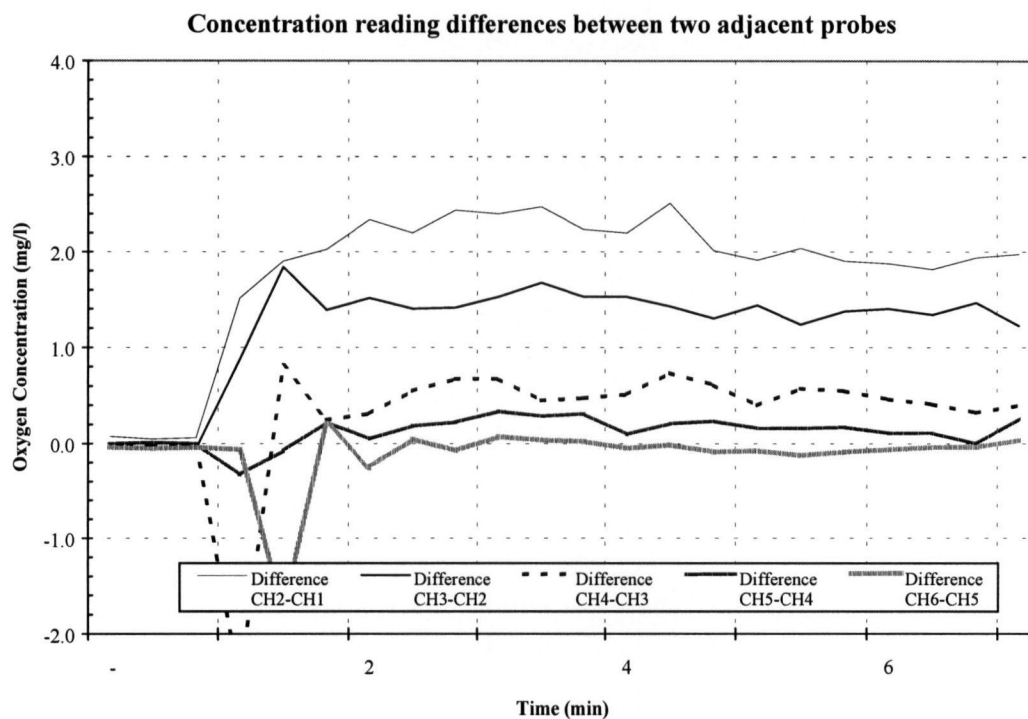
Table 4.69. Summary of qualitative observations of the relative magnitude, slope and response to increasing air flows for oxygen differentials in Zones 1-5 for *in situ* modifications.

Treatment	Zone 1 Ch. 2-1	Zone 2 Ch. 3-2	Zone 3 Ch. 4-3	Zone 4 Ch. 5-4	Zone 5 Ch. 6-5	$10 \rightarrow 40 \text{ l min}^{-1}$
DBCA x 140 μ x air	Highest differential, Neutral slope	2nd highest differential, neutral slope	2nd highest differential, neutral slope	2nd highest differential, neutral slope	Negative differential, neutral slope	Increase in slope for Zones 1, 2 and 3, increase in negative differential in Zone 4
DBCA x 800 μ x air	Highest differential, Neutral slope	Highest differential, neutral slope	Highest differential, neutral slope	Variable differential and slope	Variable differential and slope	Increase in differential for Zones 1 and 5, increase in negative differential in Zone 4
Screen x 140 μ x air	Highest differential, Negative slope	2nd highest differential, negative slope	3rd highest differential, negative slope	Negative differential, neutral slope	Neutral differential and slope	Increase in differential and slope for Zones 2 and 3, decrease in differential in Zone 5
Screen x 800 μ x air	Highest differential, Neutral slope	Highest differential, neutral slope	2nd highest differential, neutral slope	Negative differential, neutral slope	Negative differential, neutral slope	Increase in oxygen differential and slope for Zones 1 and 2
Surface cover x 140 μ x air	Highest differential, Negative slope	2nd highest differential, less slope	3rd highest differential, less slope	Negative differential, neutral slope	Negative differential, neutral slope	Increase in Zone 1 differential and slope, increase in slope for Zones 2 and 3
Surface cover x 800 μ x air	Similar differential, neutral slope	Similar differential, neutral slope	Similar differential, neutral slope	Negative differential, neutral slope	Negative differential, neutral slope	Increase in Zone 1, 2 and 3 differential slope, Zone 5 differential becomes neutral
Vanes x 140 μ x air	Highest differential, Minimal slope	2nd highest differential, less slope	3rd highest differential, neutral slope	Negative differential, neutral slope	Negative differential, neutral slope	Minimal change
Vanes x 800 μ x air	Highest differential, Minimal slope	Highest differential, less slope	2nd highest differential, neutral slope	Negative differential, neutral slope	Negative differential, neutral slope	Increase in differential and negative slope in Zones 1 and 2.

4.4.22 DBCA x 800 μ x O₂

The oxygen differentials with this treatment combination changed with each increase in gas

flow rate. Initially, the oxygen differential was greatest in Zone 3, followed by Zones 4, 1, 2

and 5, all of which were positive (Figure 4.56 a-d), with all zones exhibiting minimal slope over

the duration of the test. At the 17/3 l min⁻¹ treatment, Zones 1, 2 and 3 were grouped

Concentration reading differences between two adjacent probes

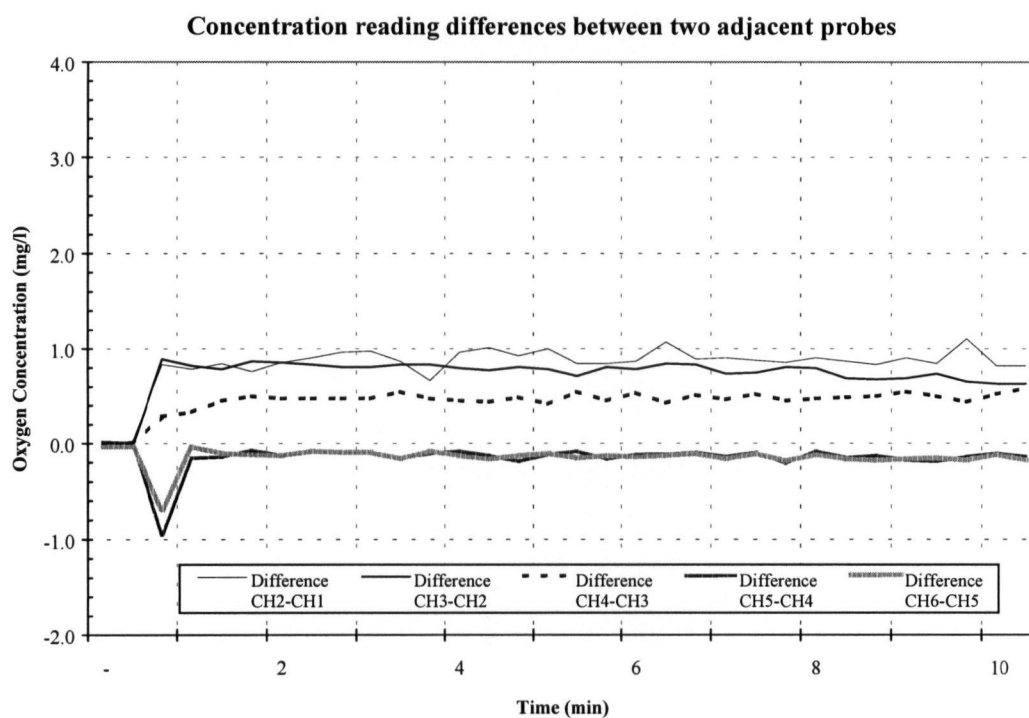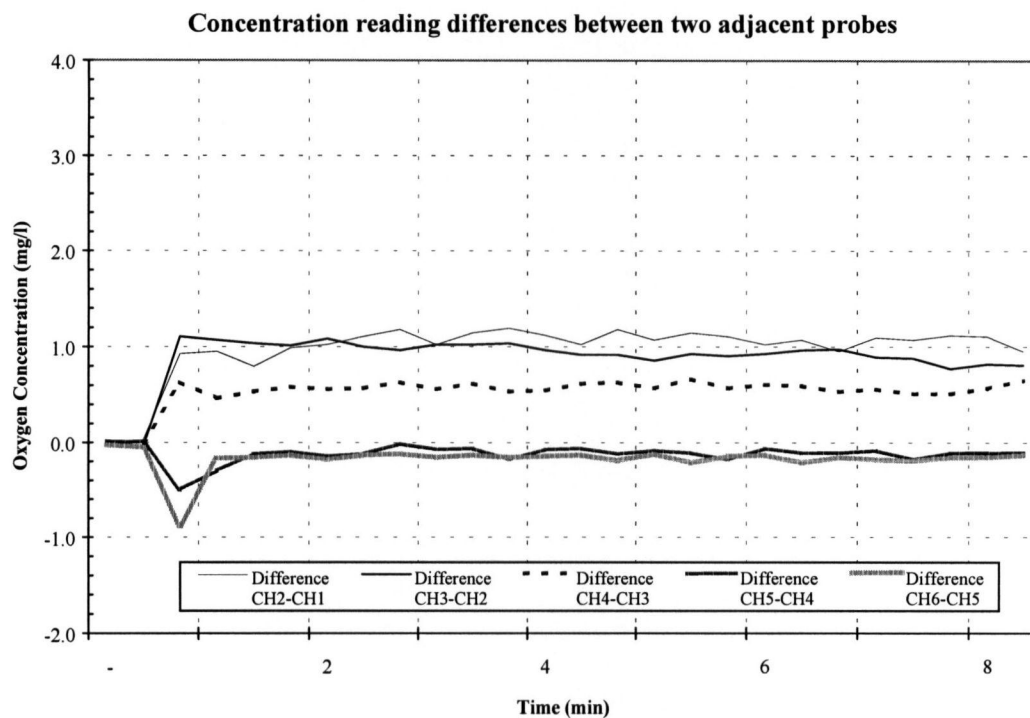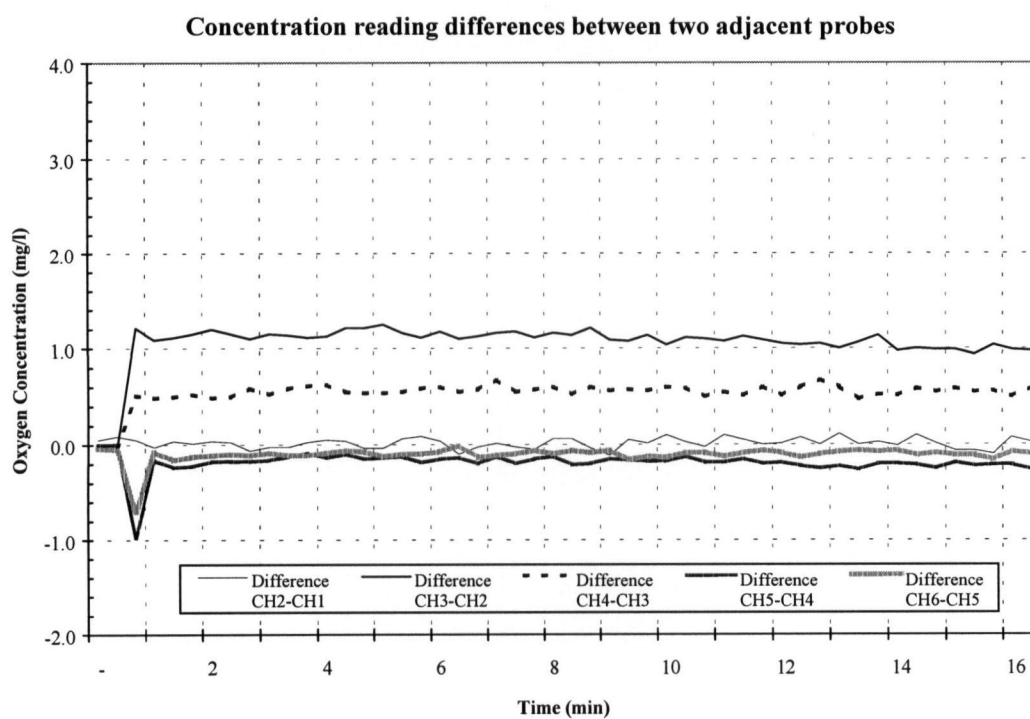**Concentration reading differences between two adjacent probes**
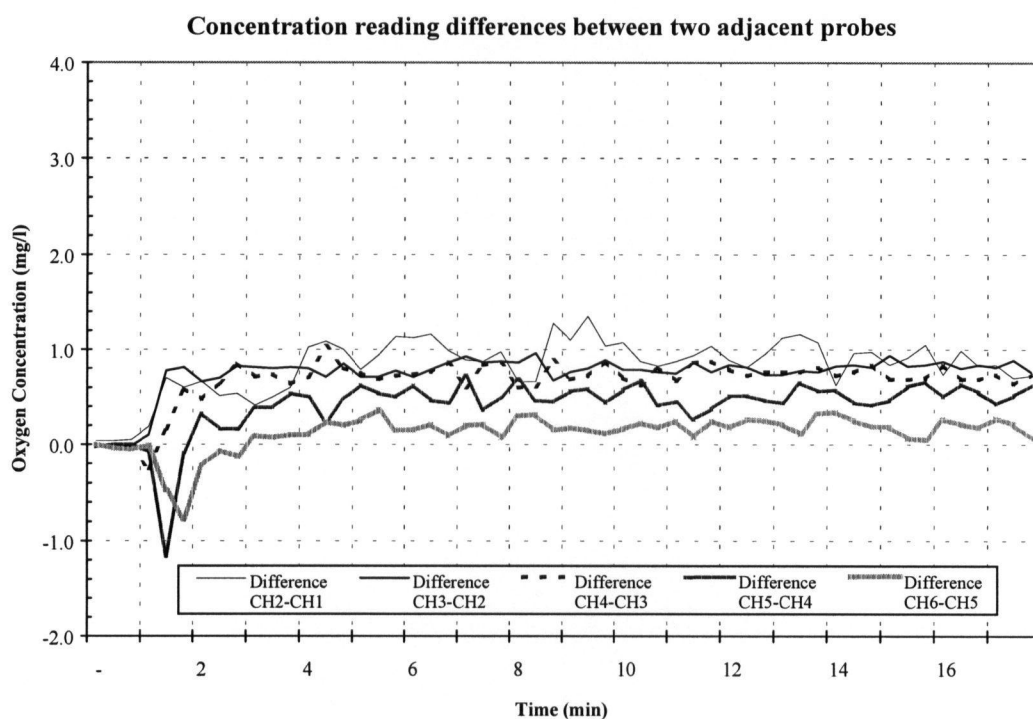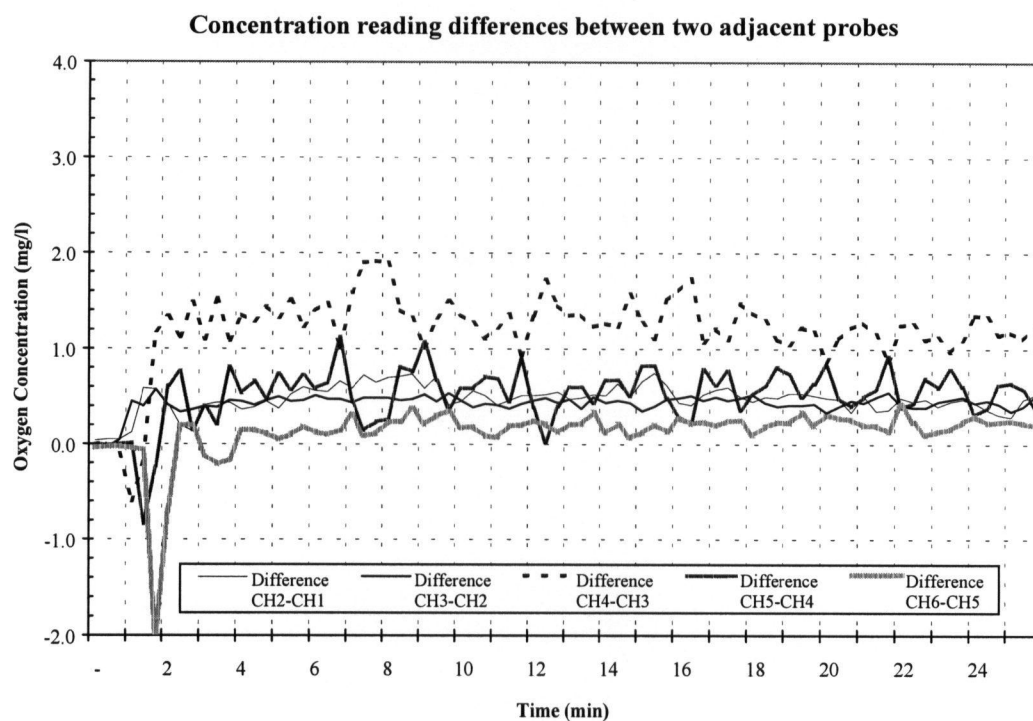
Figure 4.56a-d Oxygen differentials in full lift aerator on PSA O_2 at 2.9 m with 800 μ diffuser and DBCA at 10 l min^{-1} (a), 20 l min^{-1} (b), 30 l min^{-1} (c), 40 l min^{-1} (d).

Figure 4.56 continued

Concentration reading differences between two adjacent probes

Concentration reading differences between two adjacent probes
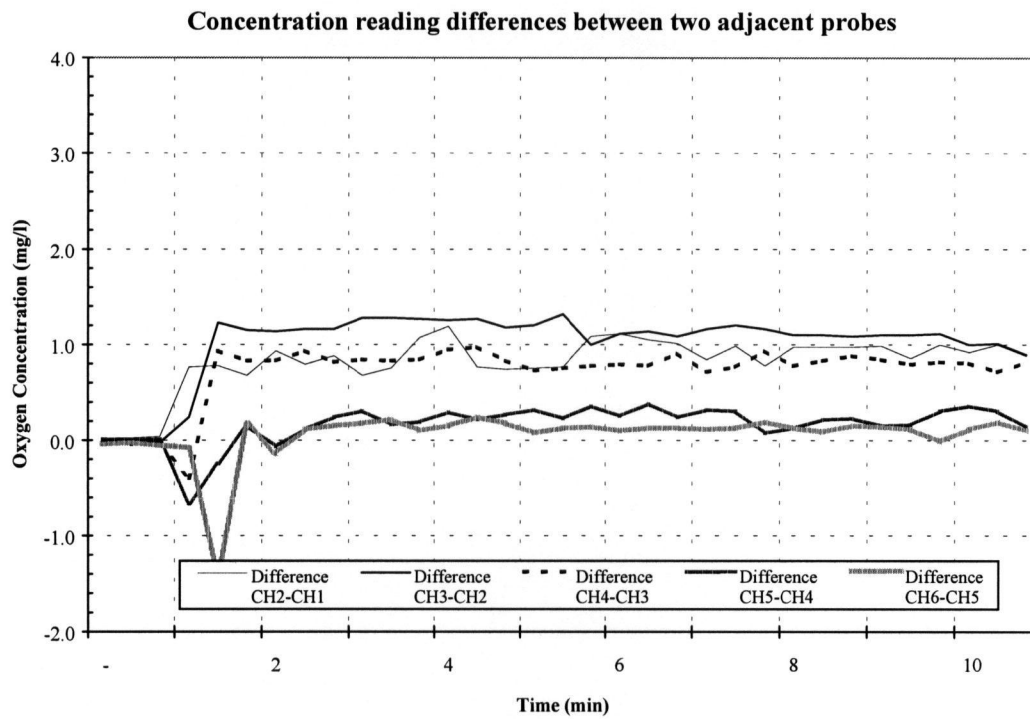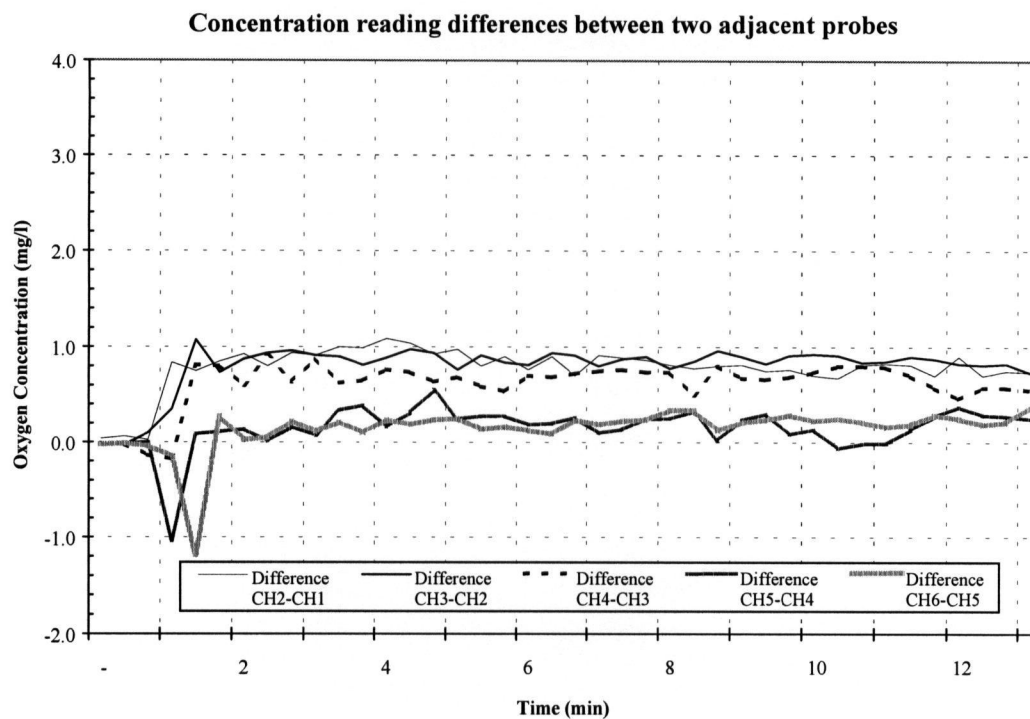
together with a neutral slope, and Zones 4 and 5 behaved similarly, and remained positive. For the 27/3 min^{-1} treatment, Zones 1, 2 and 3 remained grouped, but the oxygen differential in Zone 5 decreased. The pattern of the oxygen differentials were similar at the highest flows of 37/3 min^{-1} with the exception of increased oxygen differentials in Zone 2.

4.4.23   Screen x 140 μ x O_2

The oxygen differential was greatest in Zones 1 and 2, followed by 3, and negative in Zones 4 and 5 (Figure 4.57 a-d). Minimal change in slope was observed over the duration of the test in all zones. There were minimal changes in the general pattern as gas flows increased.

4.4.24   Screen x 800 μ x O_2

The oxygen differential was greatest in Zones 2, followed by Zone 1 and 3, and negative in Zones 4 and 5 (Figure 4.58 a-d). Minimal downward trend was observed over the duration of the test in all zones. The general trend with increasing gas flows was an increase in the oxygen differential in Zones 2 and 1.

4.4.25   Surface cover x 140 μ x O_2

The oxygen differential was greatest in Zone 1, followed by Zones 2 and Zone 3 (Figure 4.59 a-d). The oxygen differential was slightly negative in Zones 4 and 5; indicating oxygen concentrations were decreasing in these zones. Minimal change in slope was observed over the duration of the test in all zones 1. The general trend with increasing gas flows was an increase in the oxygen differential in Zone 1.

Concentration reading differences between two adjacent probes

Concentration reading differences between two adjacent probes
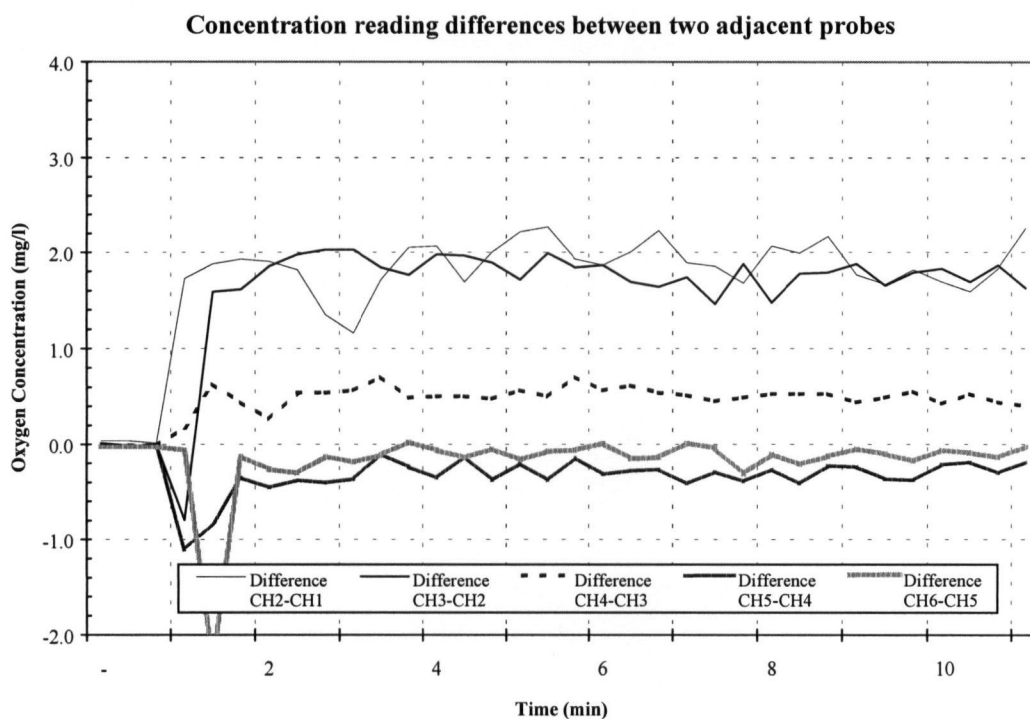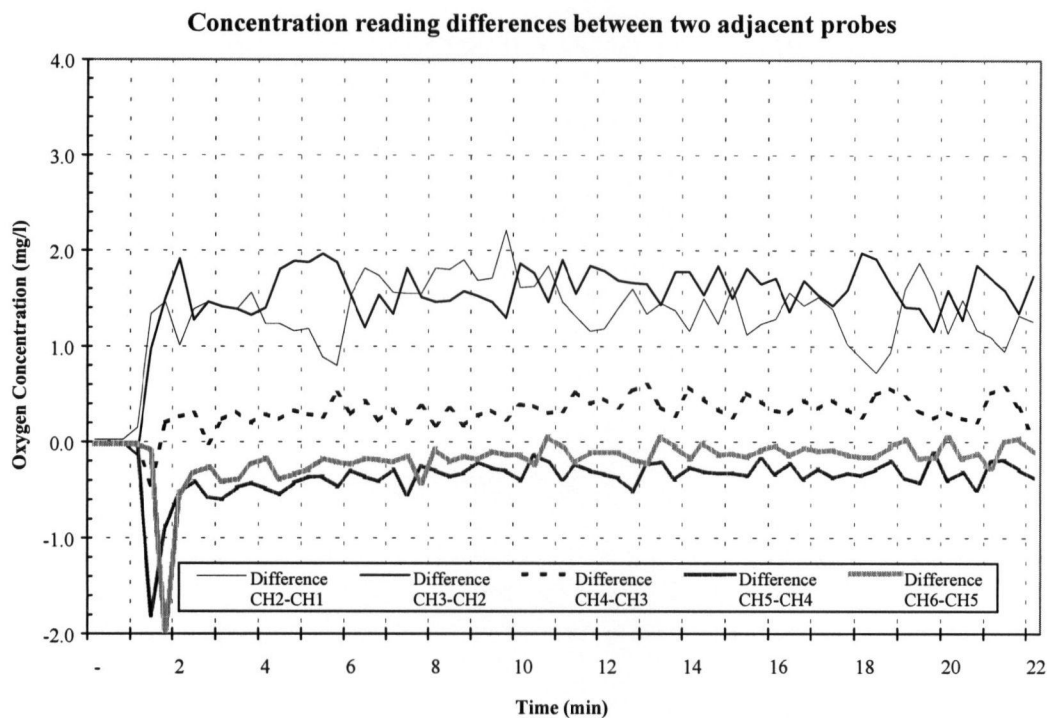
Figure 4.57a-d Oxygen differentials in full lift aerator on PSA O$_2$ at 2.9 m with 140 μ diffuser and Bubble screen at 10 l min^{-1} (a), 20 l min^{-1} (b), 30 l min^{-1} (c), 40 l min^{-1} (d).

Figure 4.57 continued

Concentration reading differences between two adjacent probes

Concentration reading differences between two adjacent probes

Concentration reading differences between two adjacent probes

Concentration reading differences between two adjacent probes
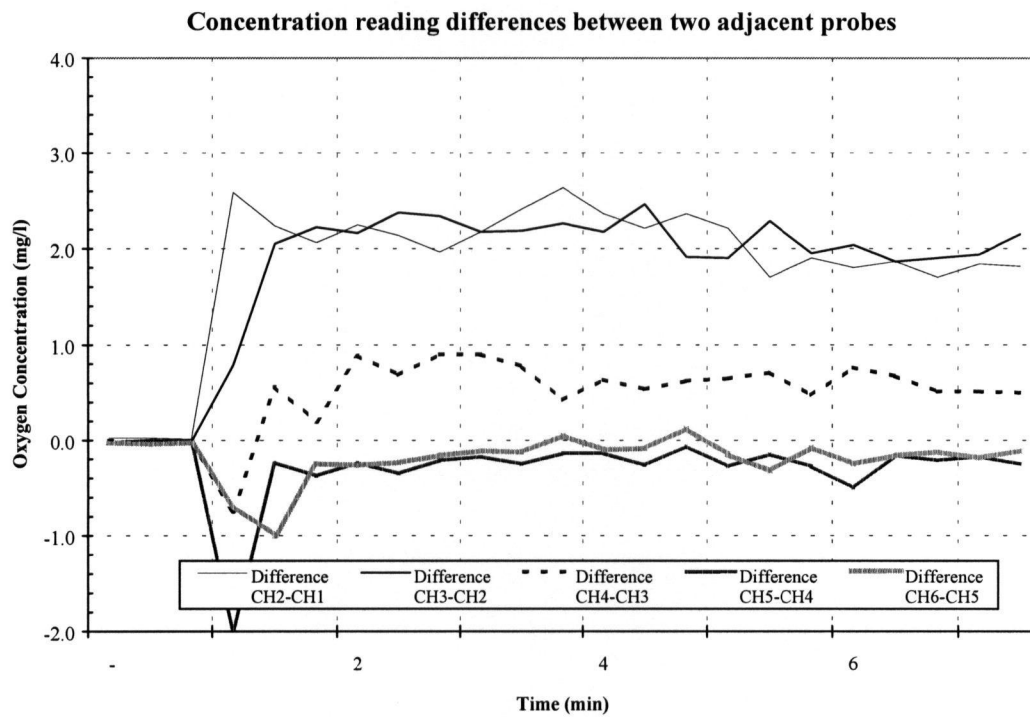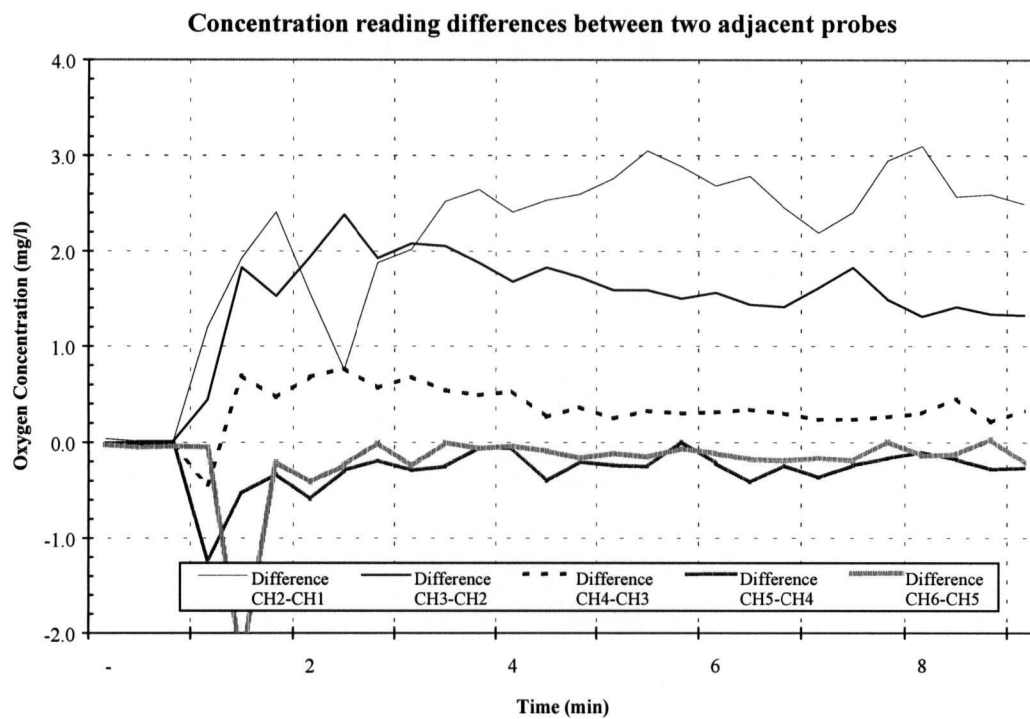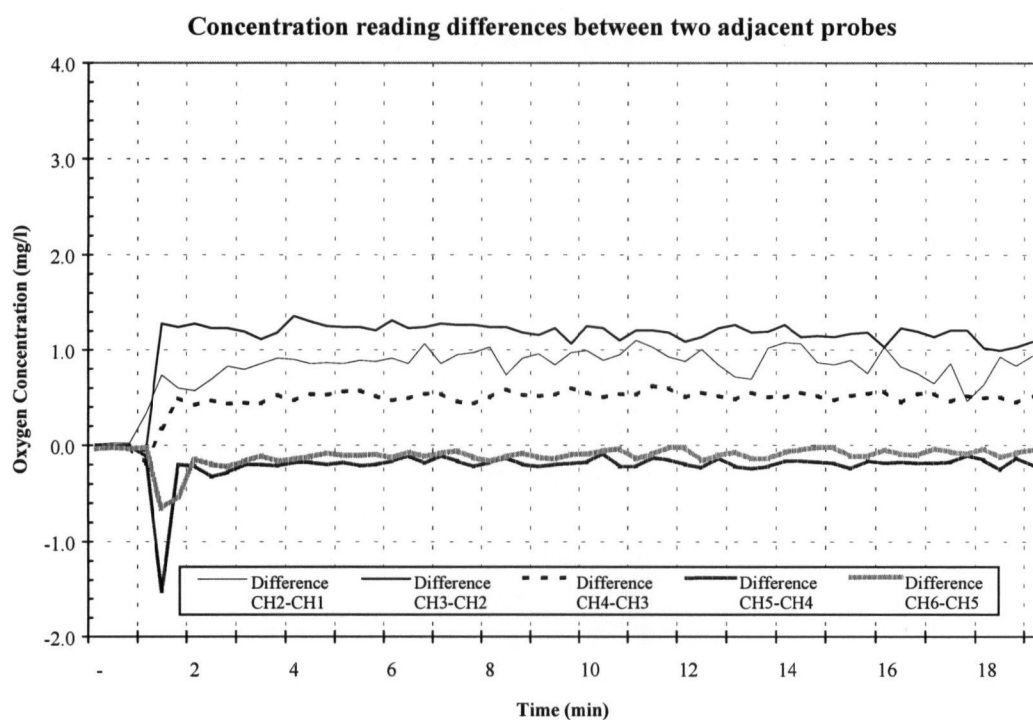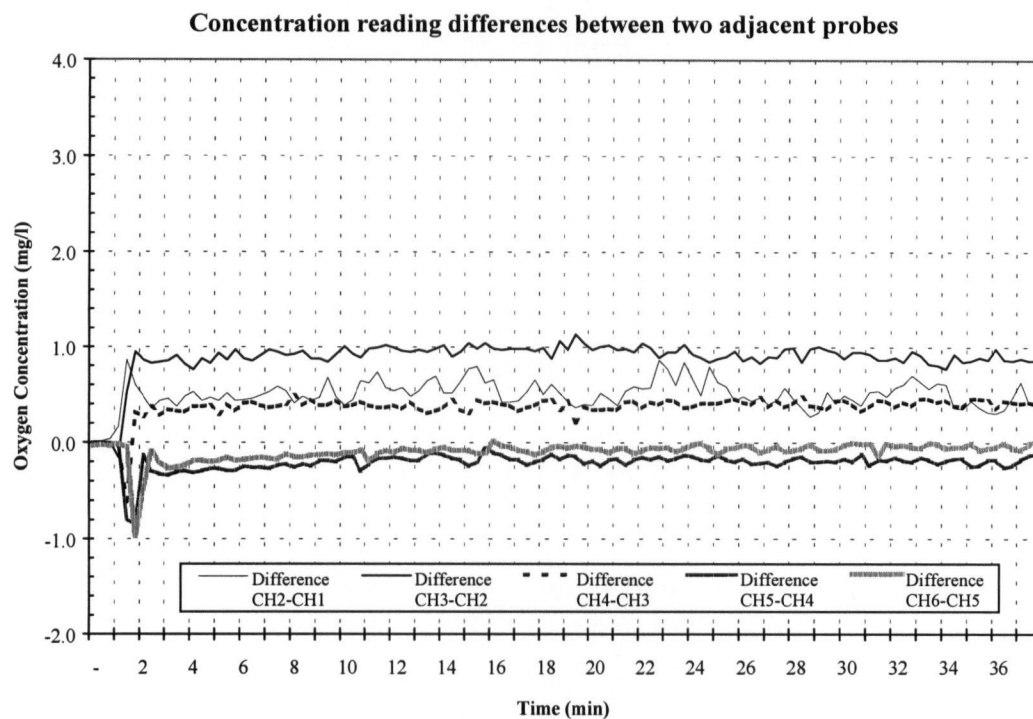
Figure 4.58a-d Oxygen differentials in full lift aerator on PSA O_2 at 2.9 m with 800 μ diffuser and Bubble screen at 10 l min^{-1} (a), 20 l min^{-1} (b), 30 l min^{-1} (c), 40 l min^{-1} (d).

Figure 4.58 continued

Concentration reading differences between two adjacent probes

Concentration reading differences between two adjacent probes

Concentration reading differences between two adjacent probes

Concentration reading differences between two adjacent probes
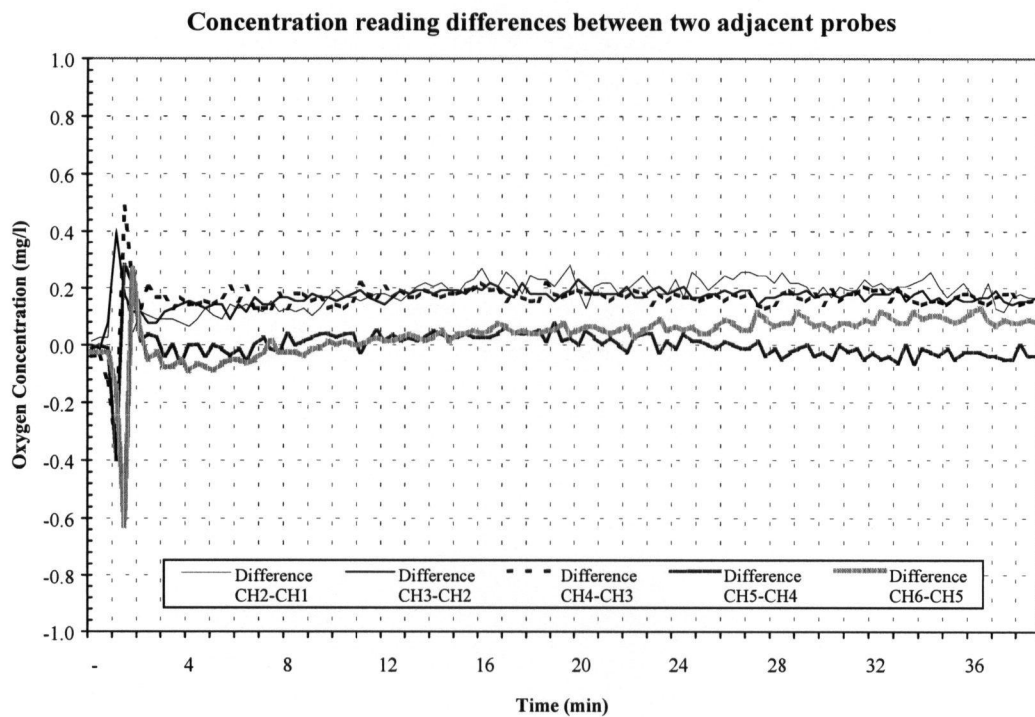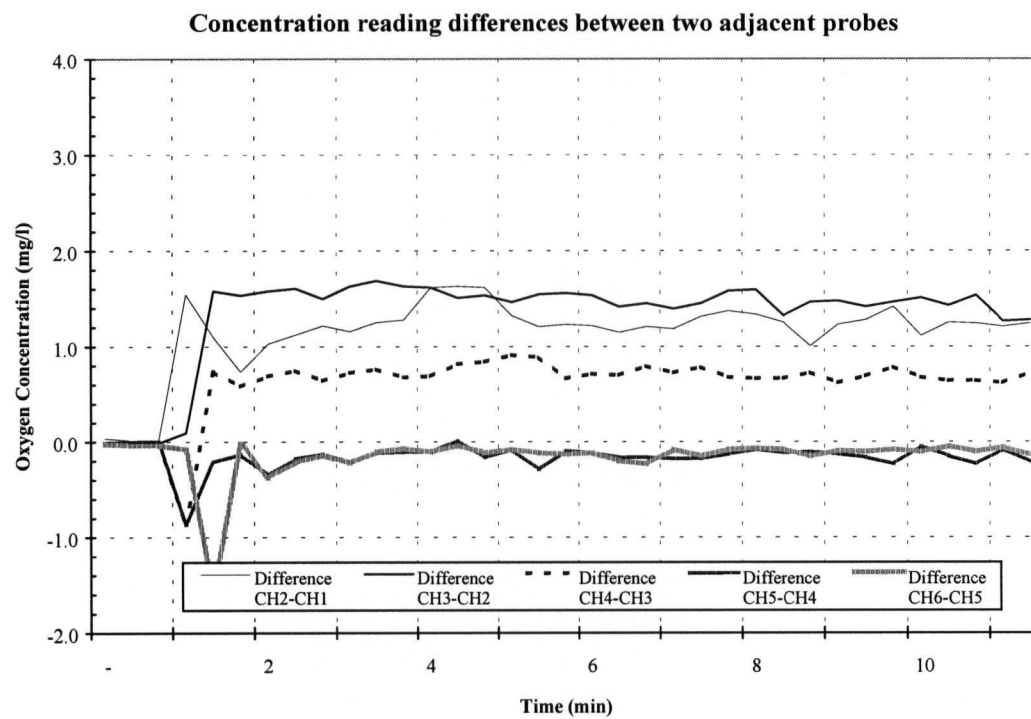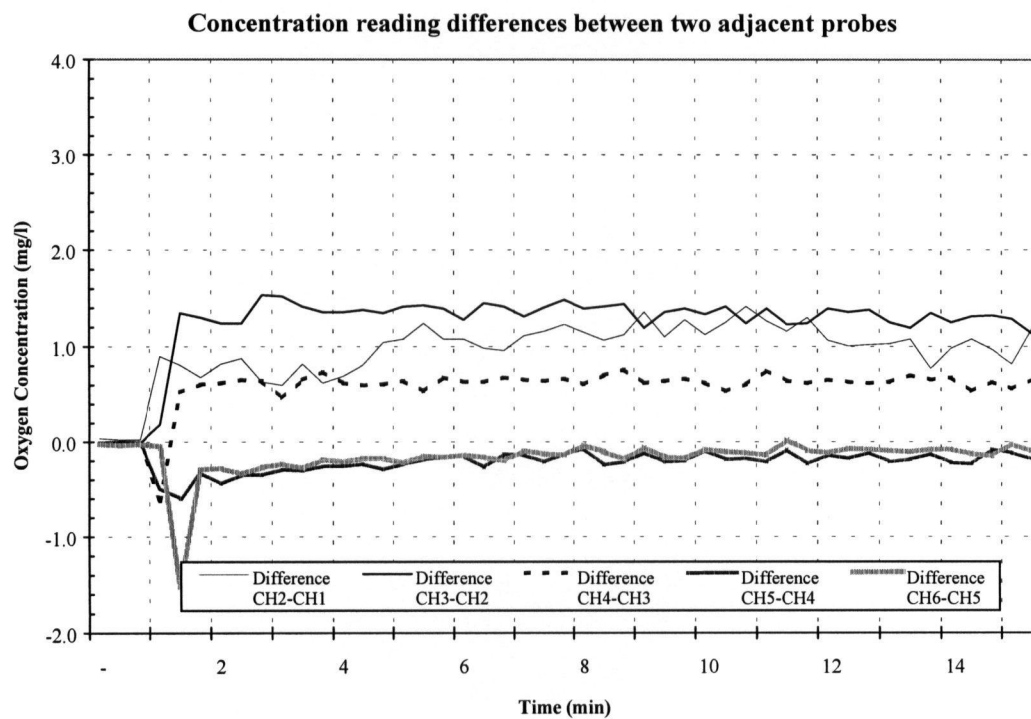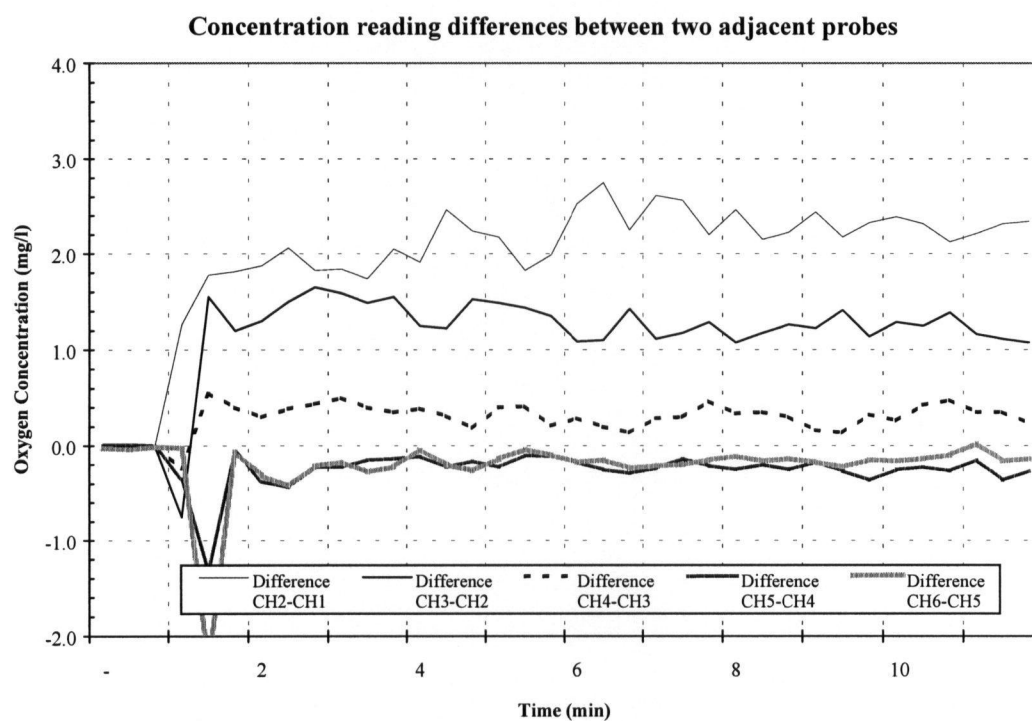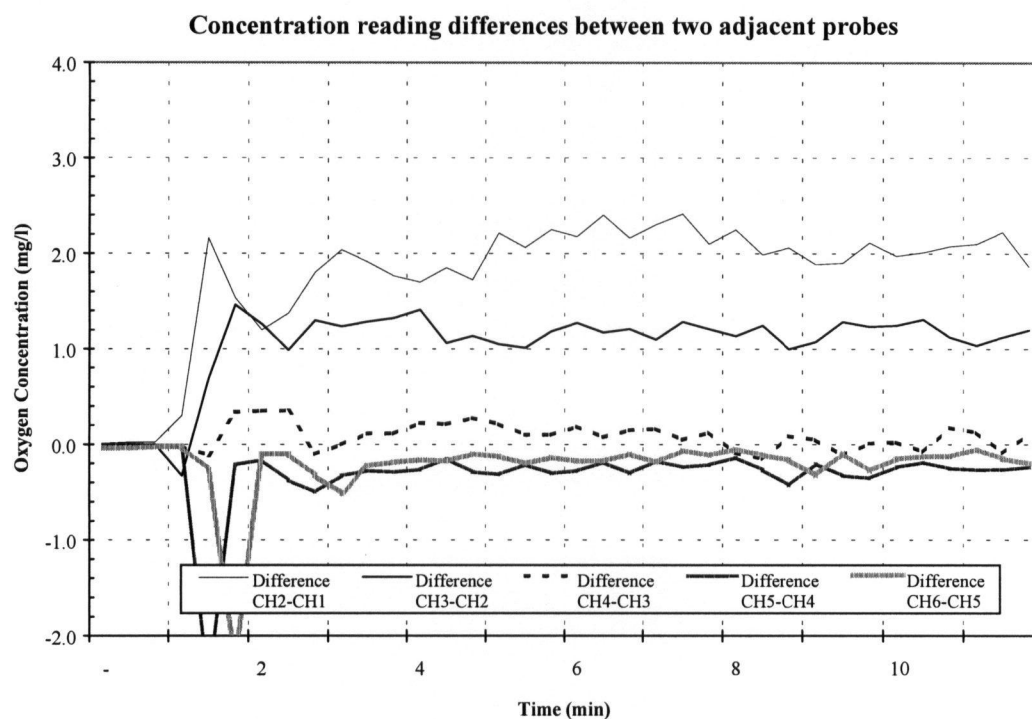

Figure 4.59a-d Oxygen differentials in full lift aerator on PSA O_2 at 2.9 m with 140 µ diffuser and Surface cover at 10 l min^{-1} (a), 20 l min^{-1} (b), 30 l min^{-1} (c), 40 l min^{-1} (d).

Figure 4.59 continued

Concentration reading differences between two adjacent probes

Concentration reading differences between two adjacent probes

196
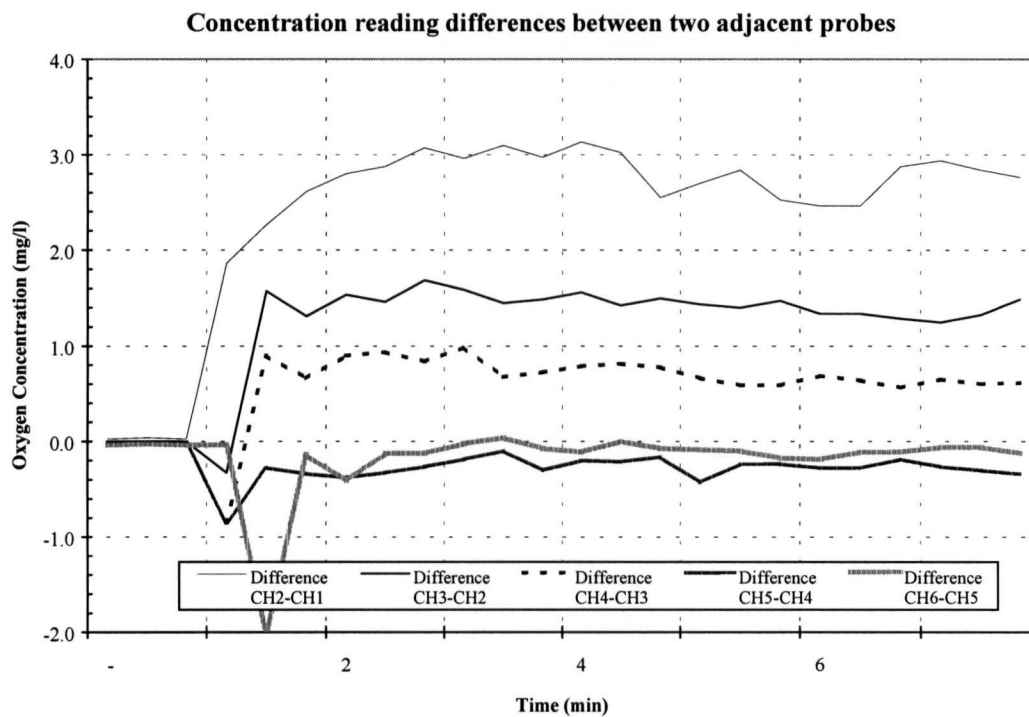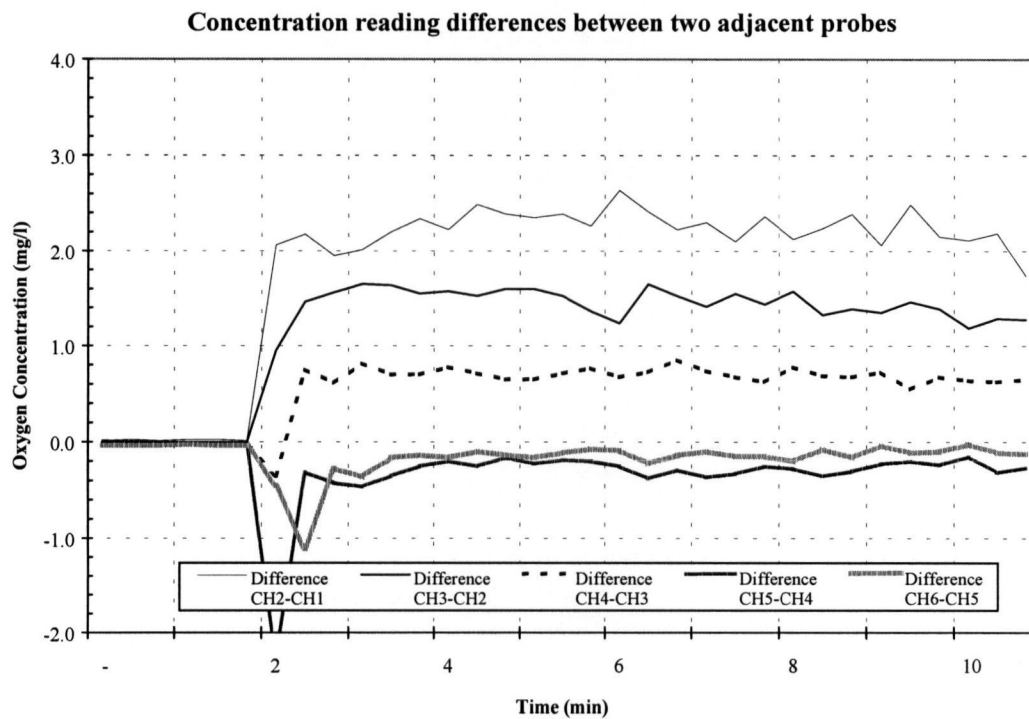
4.4.26   Surface cover x 800 μ x O$_2$

The oxygen differentials were similar in Zones 1and 2, followed by Zone 3, and similar, but

negative, in Zones 4 and 5 (Figure 4.60 a-d). As gas flow increased, the differentials in Zones 1

and 2 increased but remained tightly grouped.

4.4.27   Vanes x 140 μ x O$_2$

Initially, at the lowest gas flow rates, the oxygen differential was highest in Zone 2. However,

in all other flow rates, the oxygen differential was greatest in Zone 1, followed by Zones 2 and

Zone 3, and slightly negative in Zones 4 and 5 (Figure 4.61 a-d). Minimal change in slope was

observed over the duration of the test in all zones, and no major trends were apparent with

increasing gas flows, other than the above noted change as gas flow rates increased above 10 l

min^{-1}.

4.4.28   Vanes x 800 μ x O$_2$

The oxygen differentials were similar in Zones 1, 2 with Zone 3 being lower, while Zones 4

and 5 were similar, but negative (Figure 4.62 a-d). As gas flow increased, the differentials and

neutral slope in Zones 1 and 2 remained similar and tightly grouped; while Zones 4 and 5

remained negative with minimal change in slope. A summary of the qualitative observations of

the *in situ* modifications oxygen differentials, on PSA oxygen, are shown in Table 4.70.

4.5   Speece Cone Hypolimnetic Aeration – Oxygen Transfer

4.5.1   PSA O$_2$ Experiments

The results for the analysis of covariance for the Speece Cone hypolimnetic aerator are shown in

Table 4.70. Unlike the full lift experiments, the Speece Cone was operated at a single depth on

Concentration reading differences between two adjacent probes

Concentration reading differences between two adjacent probes
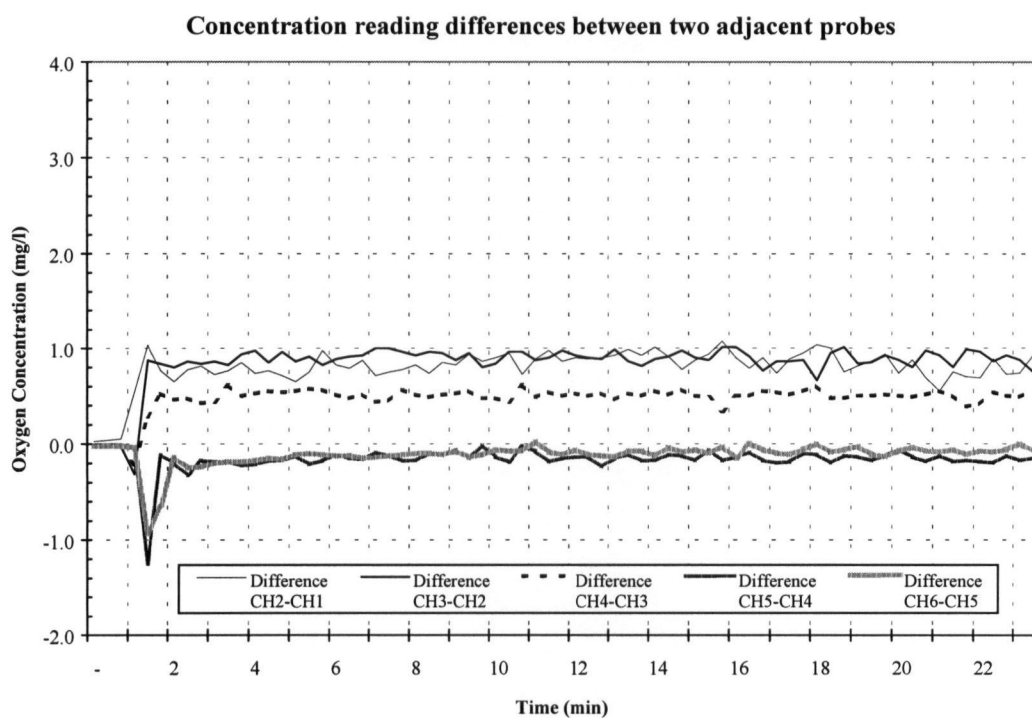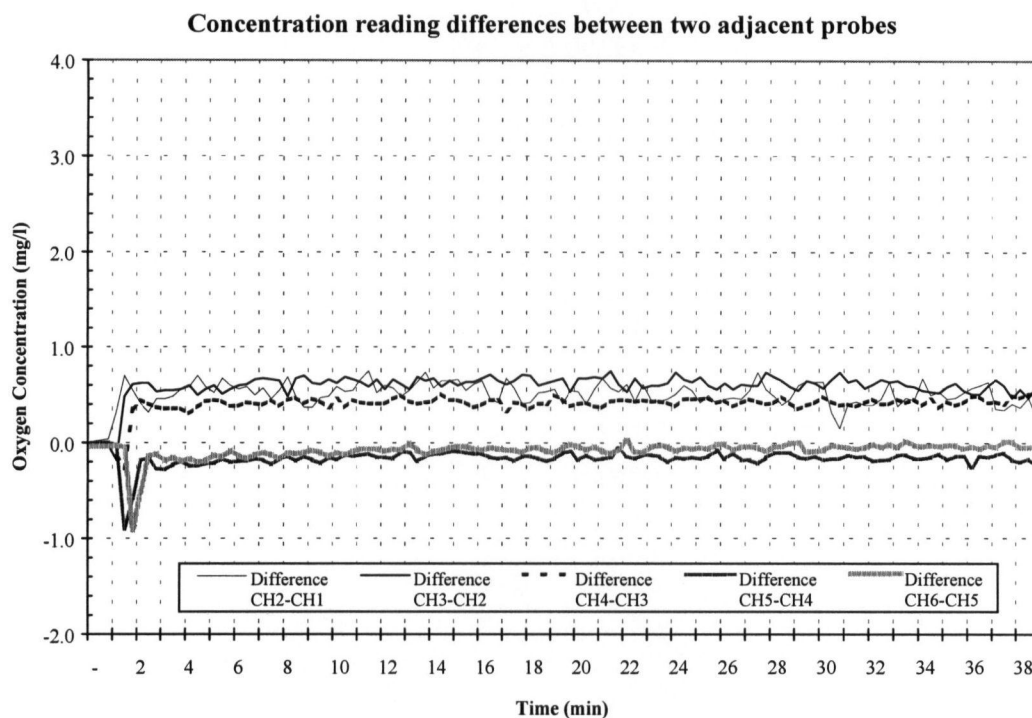
Figure 4.60a-d Oxygen differentials in full lift aerator on PSA O_2 at 2.9 m with 800 μ diffuser and Surface cover at 10 l min^{-1} (a), 20 l min^{-1} (b), 30 l min^{-1} (c), 40 l min^{-1} (d).

Figure 4.60 continued

Concentration reading differences between two adjacent probes

Concentration reading differences between two adjacent probes
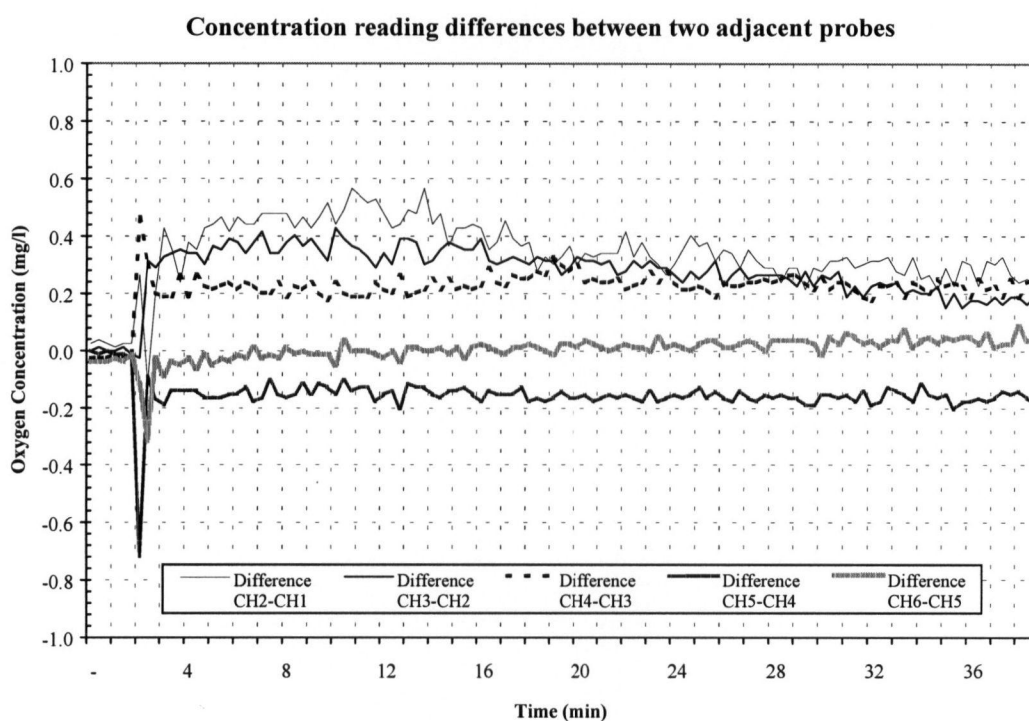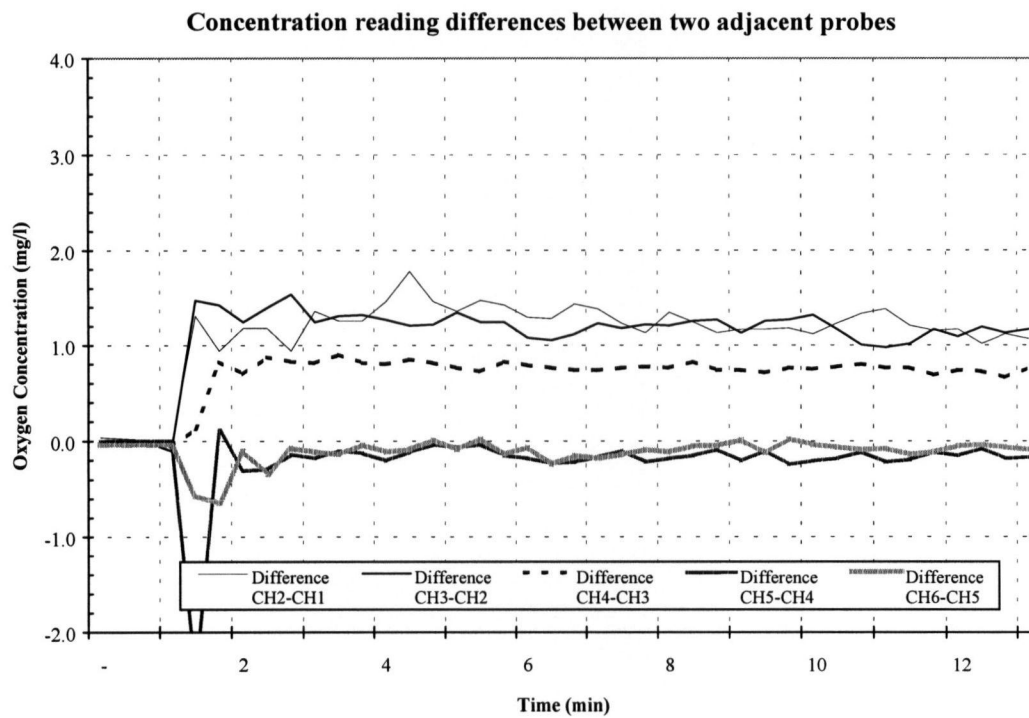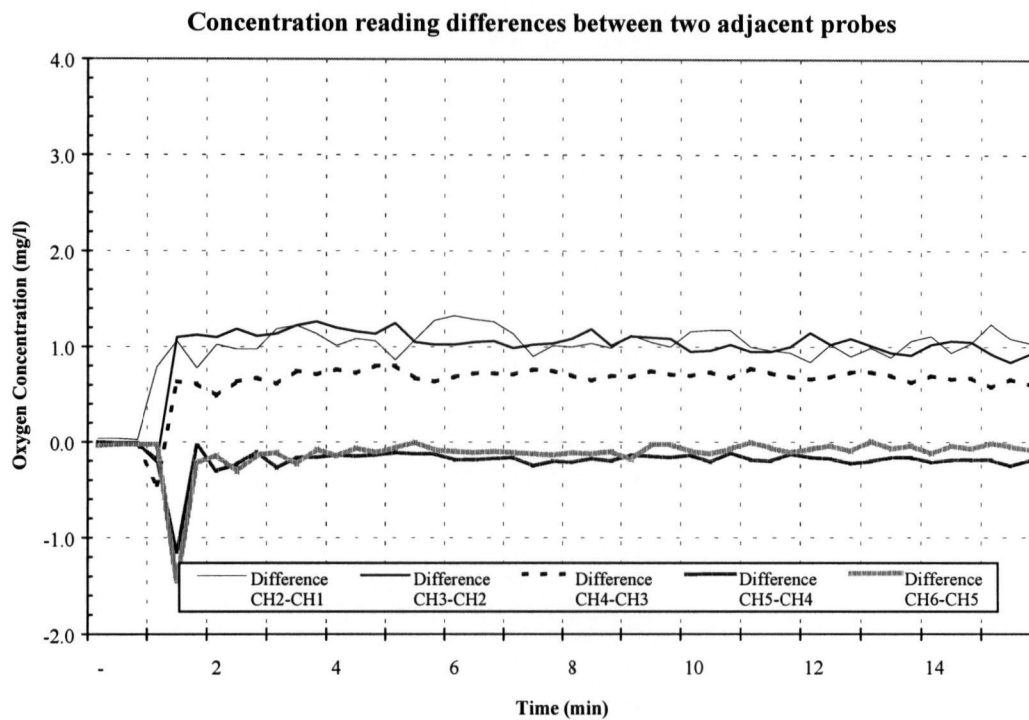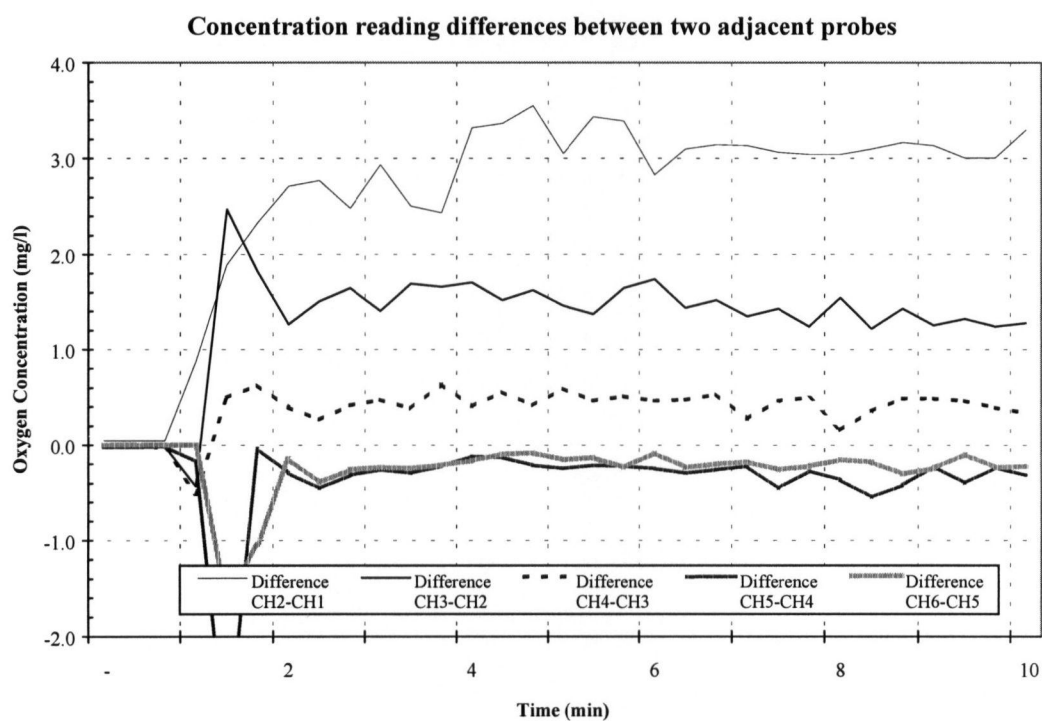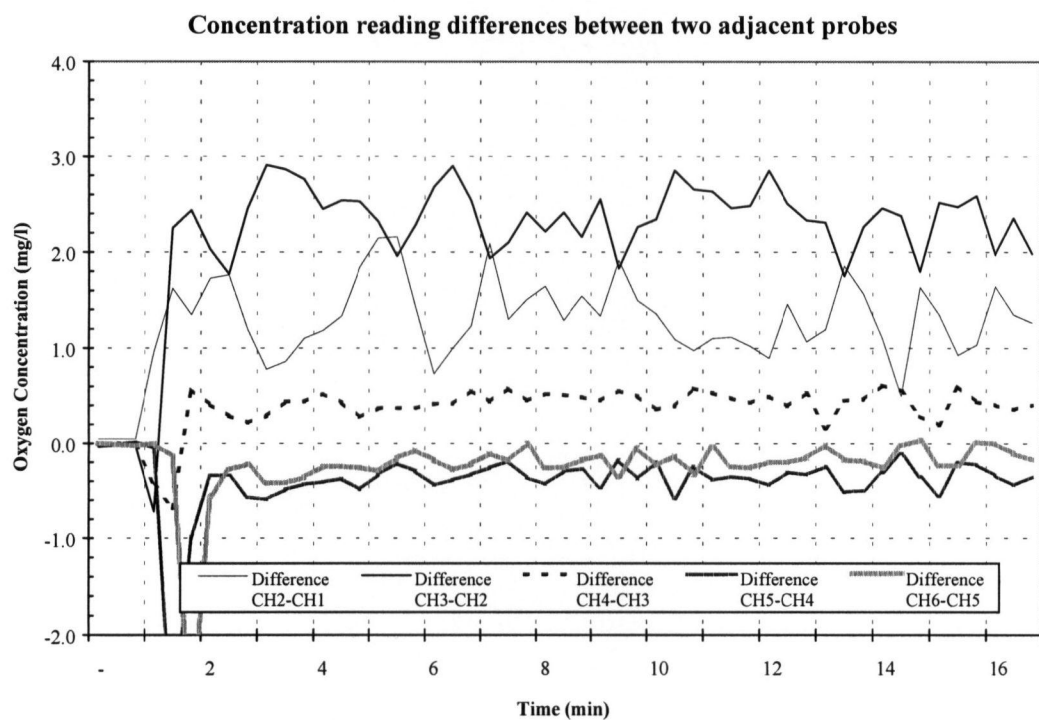
Figure 4.61a-d Oxygen differentials in full lift aerator on PSA O_2 at 2.9 m with 140 μ diffuser and Counter-rotating blades at 10 l min^{-1} (a), 20 l min^{-1} (b), 30 l min^{-1} (c), 40 l min^{-1} (d).

Figure 4.61 continued

Concentration reading differences between two adjacent probes

Concentration reading differences between two adjacent probes

Concentration reading differences between two adjacent probes

Concentration reading differences between two adjacent probes
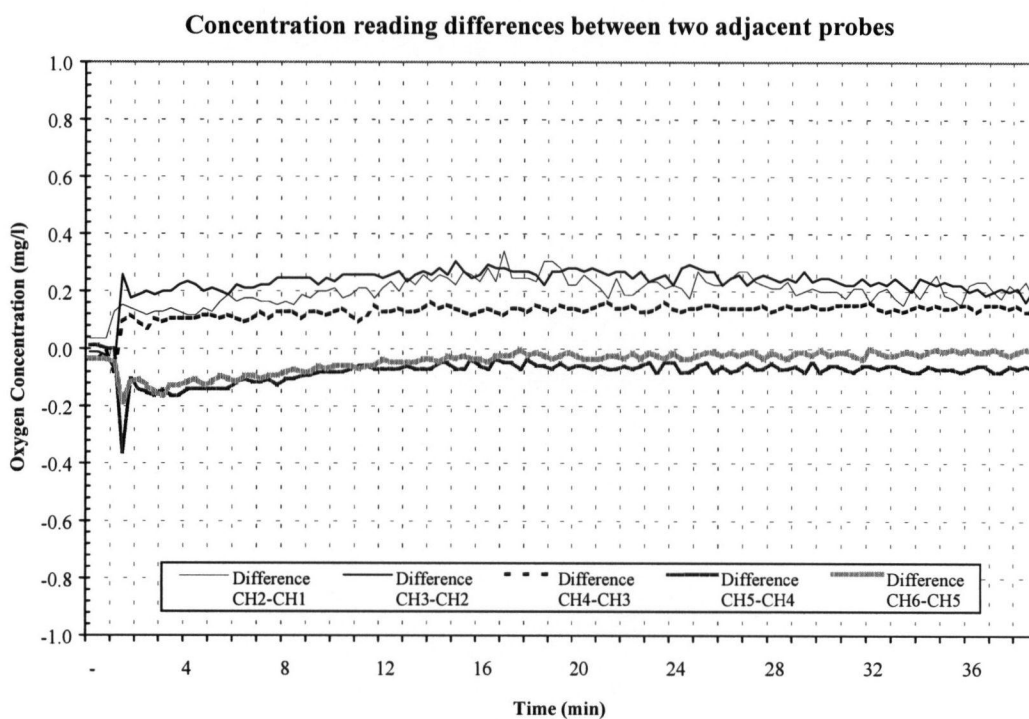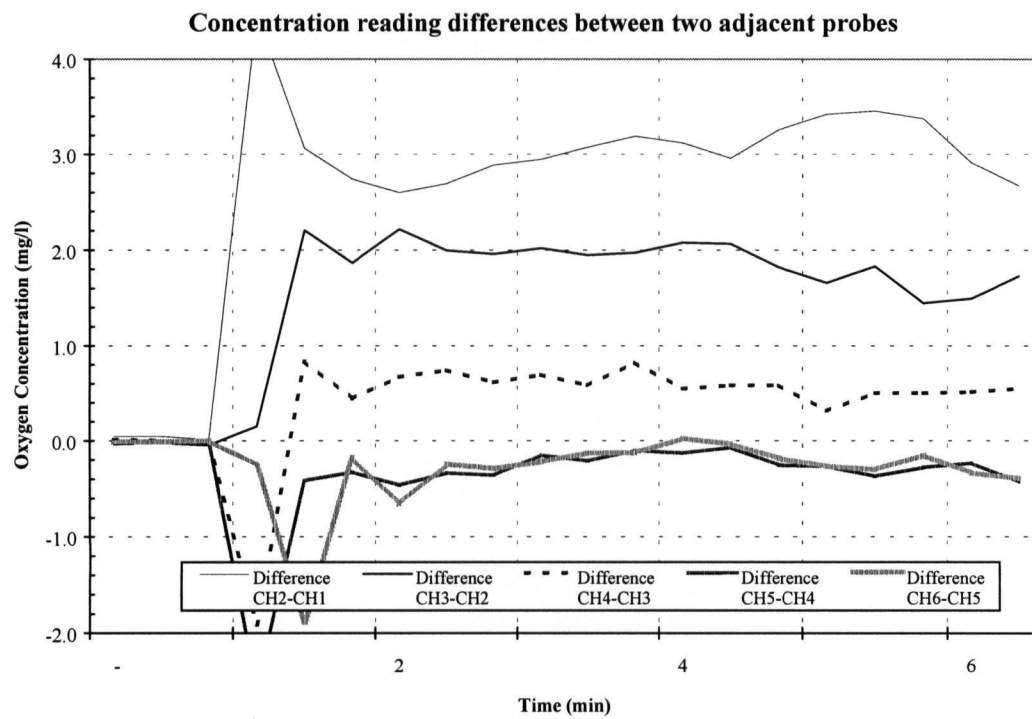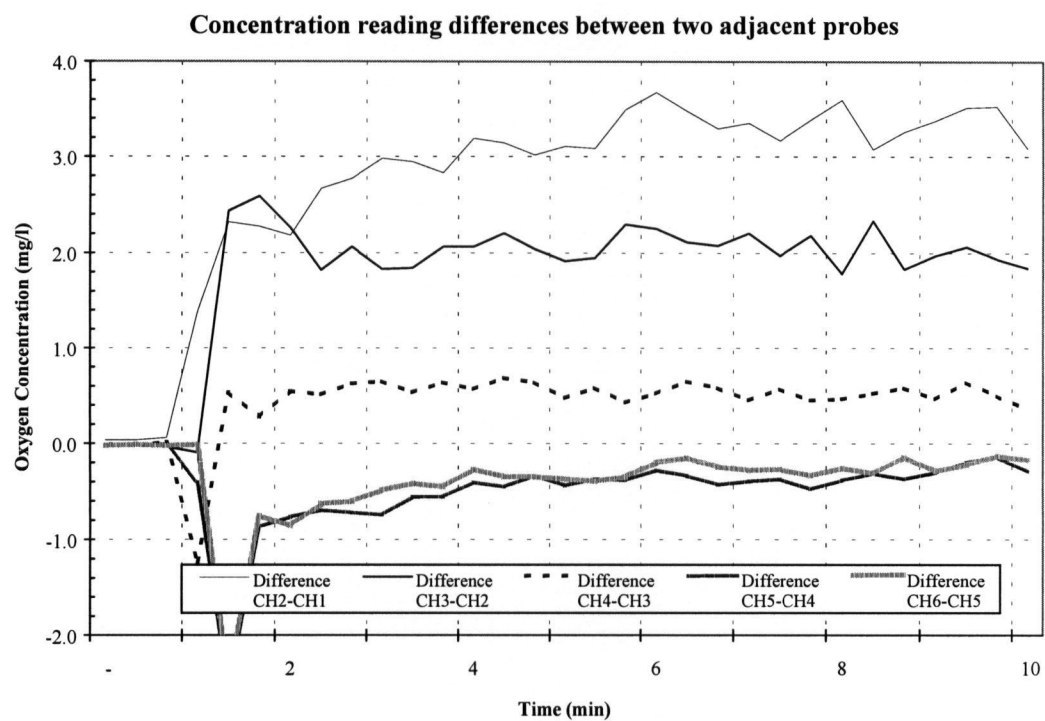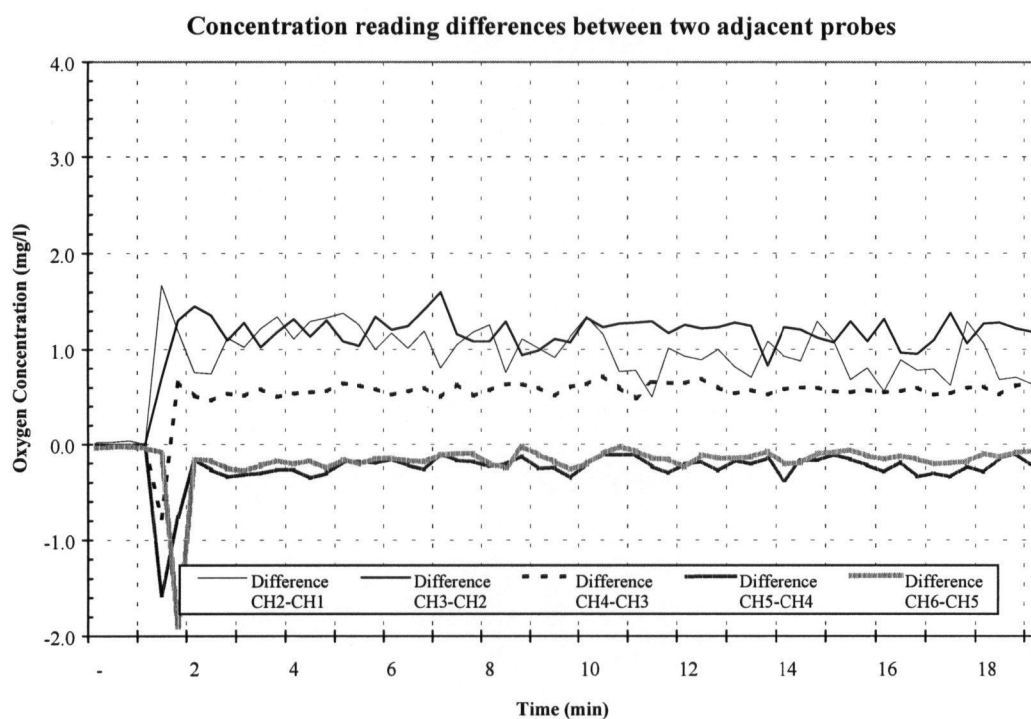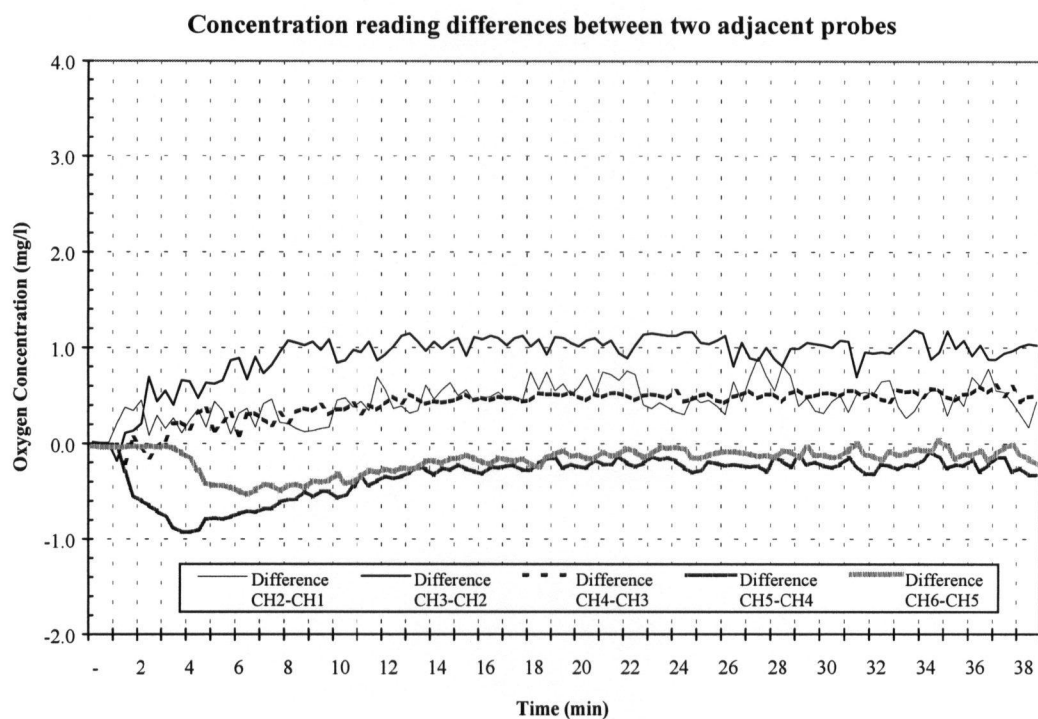

Figure 4.62a-d Oxygen differentials in full lift aerator on PSA O$_2$ at 2.9 m with 800 μ diffuser and Counter-rotating blades at 10 l min^{-1} (a), 20 l min^{-1} (b), 30 l min^{-1} (c), 40 l min^{-1} (d).

Figure 4.62 continued

Concentration reading differences between two adjacent probes

Concentration reading differences between two adjacent probes
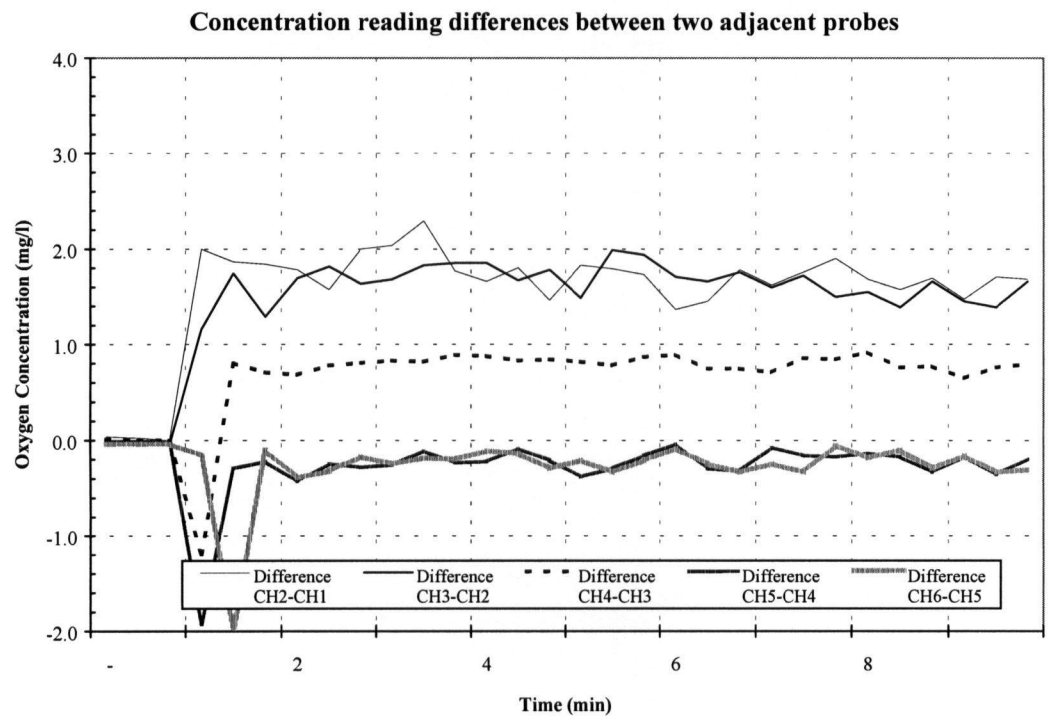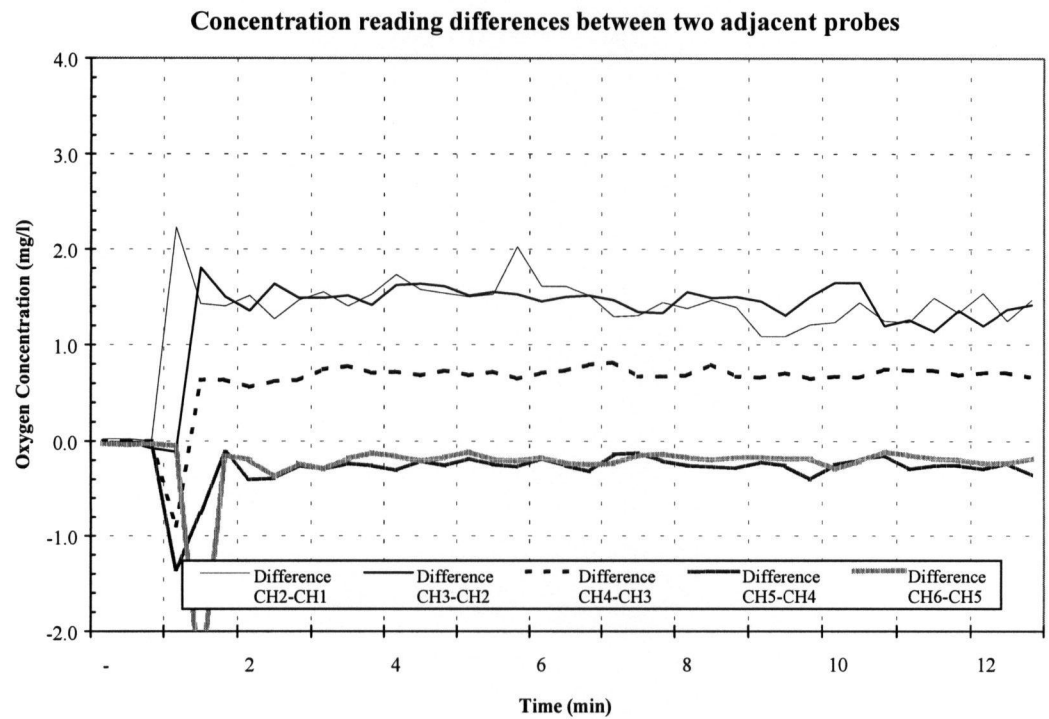
Table 4.70. Summary of qualitative observations of the relative magnitude, slope and response to increasing PSA O_2 flows for oxygen differentials in Zones 1-5 for *in situ* modifications.

Treatment	Zone 1 Ch. 2-1	Zone 2 Ch. 3-2	Zone 3 Ch. 4-3	Zone 4 Ch. 5-4	Zone 5 Ch. 6-5	$10 \rightarrow 40$ l min^{-1}
DBCA x 140 μ x O_2	Highest differential, Neutral slope	2nd highest differential, neutral slope	3rd highest differential, neutral slope	Positive differential, neutral slope	Negative differential, neutral slope	Increase in slope for Zones 1, 2 and 3, decrease in positive differential in Zone 4
DBCA x 800 μ x O_2	Highest differential, Neutral slope	Highest differential, neutral slope	Highest differential, neutral slope	Positive differential, neutral slope	Positive differential, neutral slope	Minimal change, increase in differential for Zones 2
Screen x 140 μ x O_2	Highest differential, Neutral slope	Highest differential, neutral slope	2nd highest differential, neutral slope	Negative differential, neutral slope	Neutral differential, neutral slope	Minimal change
Screen x 800 μ x O_2	2nd highest differential, Neutral slope	Highest differential, neutral slope	3rd highest differential, neutral slope	Negative differential, neutral slope	Negative differential, neutral slope	Increase in oxygen differential and slope for Zones 2 and 1
Surface cover x 140 μ x O_2	Highest differential, neutral slope	2nd highest differential, Neutral slope	3rd highest differential, neutral slope	Negative differential, neutral slope	Negative differential, neutral slope	Increase in Zone 1 differential
Surface cover x 800 μ x O_2	Highest differential, neutral slope	Highest differential, neutral slope	2nd highest differential, Neutral slope	Negative differential, neutral slope	Negative differential, neutral slope	Increase in Zone 1 and 2 differential
Vanes x 140 μ x O_2	Highest differential, Minimal slope	2nd highest differential, less slope	3rd highest differential, neutral slope	Negative differential, neutral slope	Negative differential, neutral slope	Minimal change
Vanes x 800 μ x O_2	Highest differential, Minimal slope	Highest differential, less slope	2nd highest differential, neutral slope	Negative differential, neutral slope	Negative differential, neutral slope	Increase in differential in Zones 1 and 2.

PSA oxygen (except for a single test on air); hence the only treatment effect is oxygen flow rate, and discharge water velocity is the covariate. The initial box and whisker plots of K_La_{20}, SOTR, SAE and SOTE, as a function of oxygen flow rate and discharge water velocity, showed an unusual pattern of increased variance for the 1 l min^{-1} oxygen flow rate (Figure 4.63) and discharge velocities of 60 and 70 cm sec^{-1} (Figure 4.64). The untransformed plots of K_La_{20}, SOTR, SAE and SOTE show a distinct non-linear "break function" type response for the 1 min^{-1} treatment (Figure 4.65 a-d). The log-transformed data showed the same response (Figure 4.66 a-d); hence the analysis was re-run in two separate methods.

The first approach (Analysis I) was to analyse the untransformed data set without the two highest discharge velocities (i.e., 60 and 70 cm sec^{-1}) in an attempt to determine homogeneity of slopes. The analysis indicated a significant interaction effect (Figure 4.67 a-d); hence the data was log transformed, and re-analyzed (Figure 4.68 a-d). A significant result ($\alpha \leq 0.01$) was obtained for the discharge velocity covariate effect for K_La_{20}, SOTR, SAE and SOTE, and the oxygen gas flow rate for K_La_{20}, SOTR and SOTE (Table 4.71). SAE was not significantly influenced by oxygen gas flow rate. A significant oxygen flow rate x discharge velocity interaction effect was observed for K_La_{20}, SOTR, SAE and SOTE (Table 4.71).

Since this approach was unable to linearize the oxygen flow rate x discharge velocity interaction effect, a second analytical approach (Analysis II) was used in which the 1 l min^{-1} gas flow rate treatment was removed from the data set, and the log transformed data re-analysed (Figure 4.69 a-d). Significant results ($\alpha \leq 0.01$) were obtained for the discharge velocity covariate effect for K_La_{20}, SOTR and SOTE, and oxygen flow rate for K_La_{20}, SOTR, SAE and SOTE (Table 4.72). SAE was only significant for oxygen flow rate. A significant oxygen flow rate x discharge
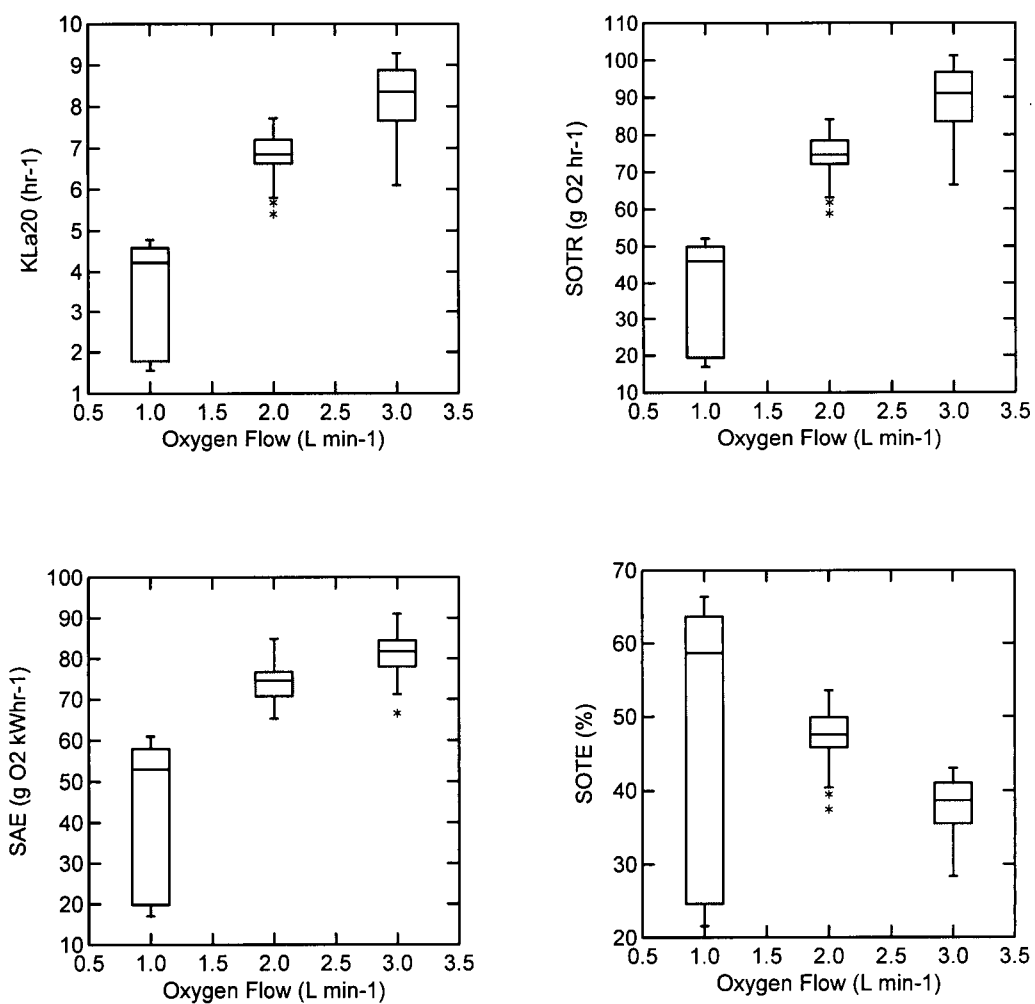
Figure 4.63a-d Box and whisker plots showing effect of PSA O_2 flowrate on K_La_{20} (a), SOTR (b), SAE (c) and SOTE (d).
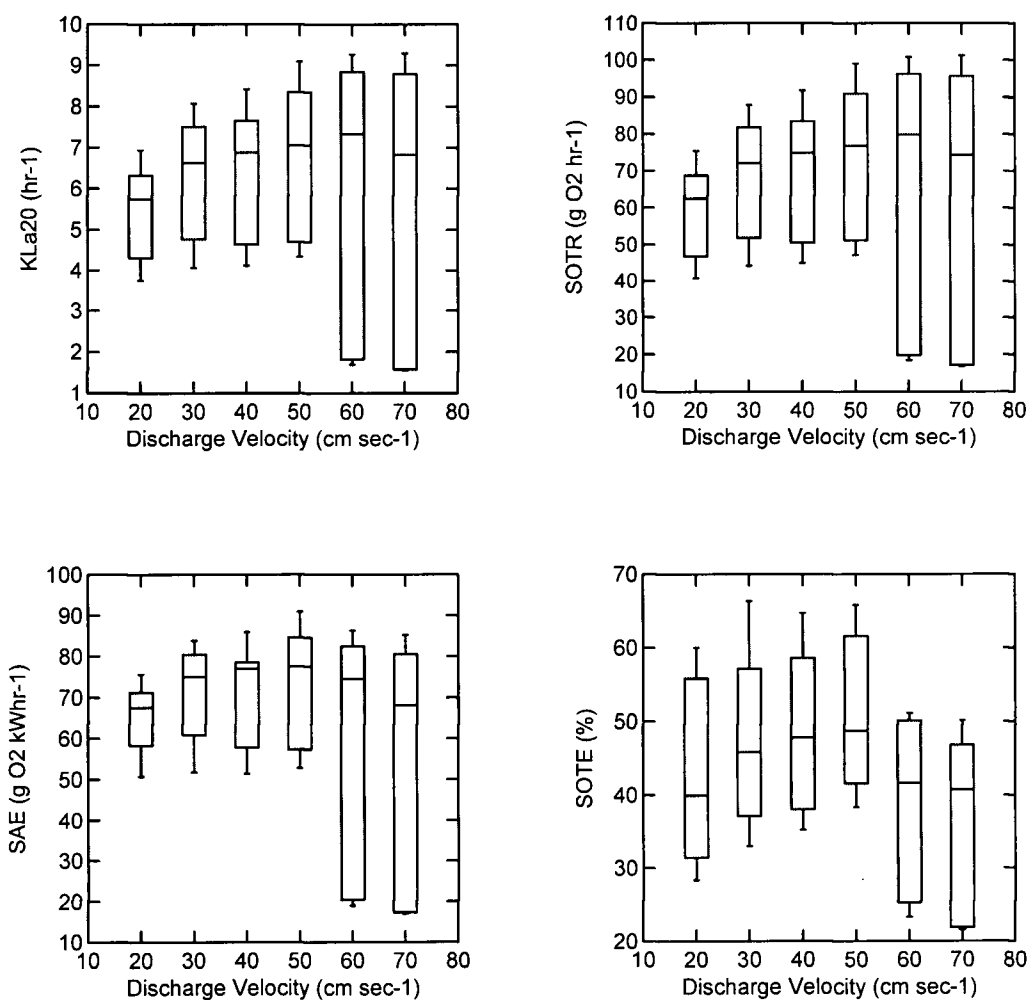
Figure 4.64a-d Box and whisker plots showing effect of water discharge velocity on K_La_{20} (a), SOTR (b), SAE (c) and SOTE (d).
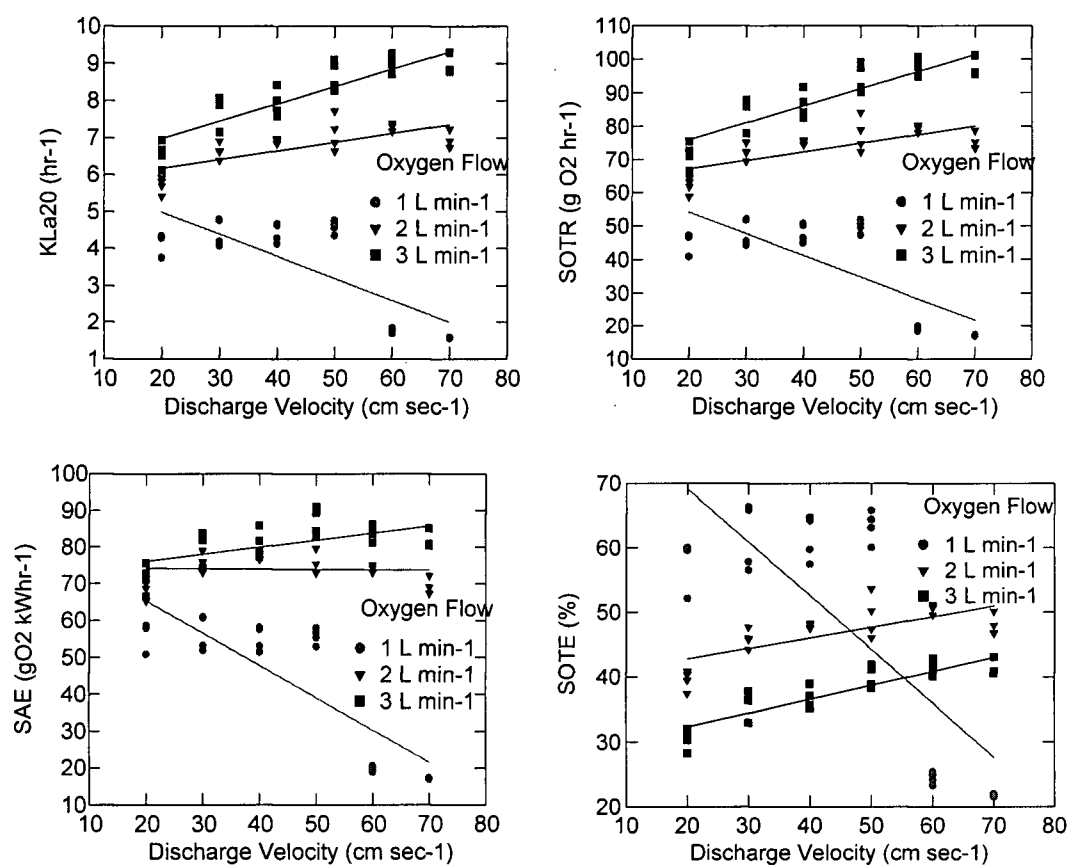
Figure 4.65a-d Effect of PSA O_2 flow rate and water discharge velocity on K_La_{20} (a), SOTR (b), SAE (c) and SOTE (d).
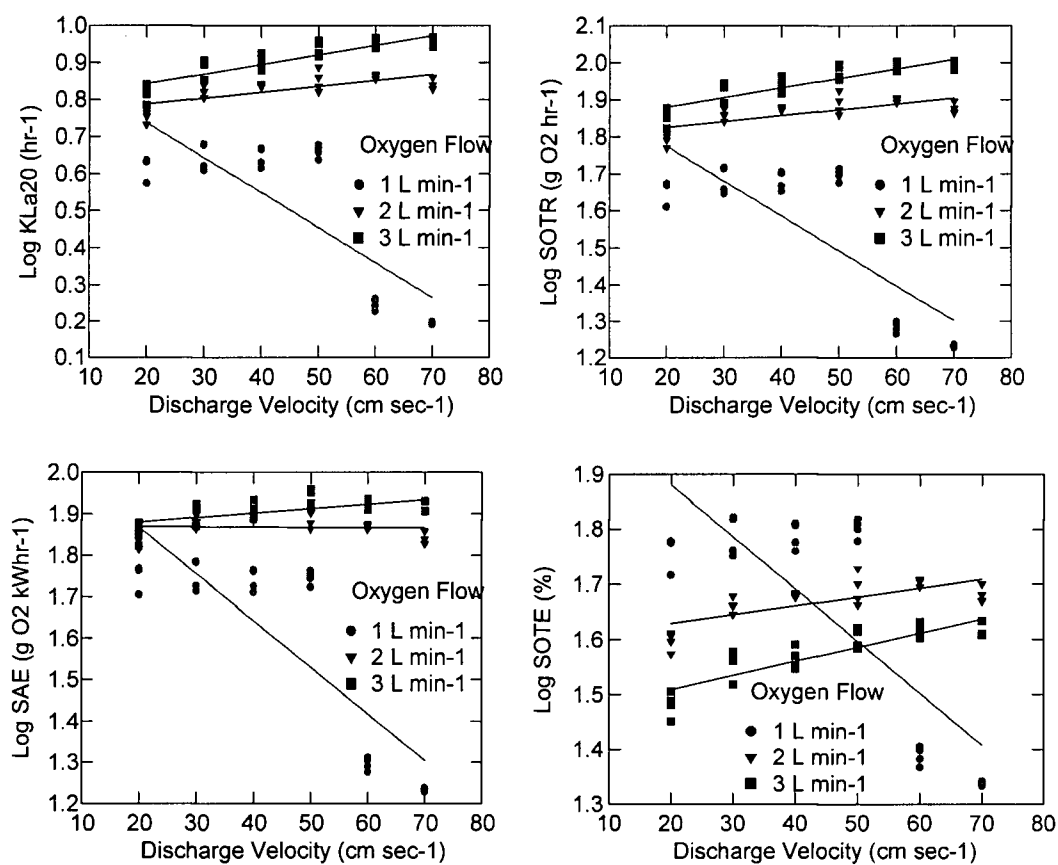
Figure 4.66a-d Effect of PSA O_2 flow rate and water discharge velocity on K_La_{20} (a), SOTR (b), SAE (c) and SOTE (d) using log transformed data.
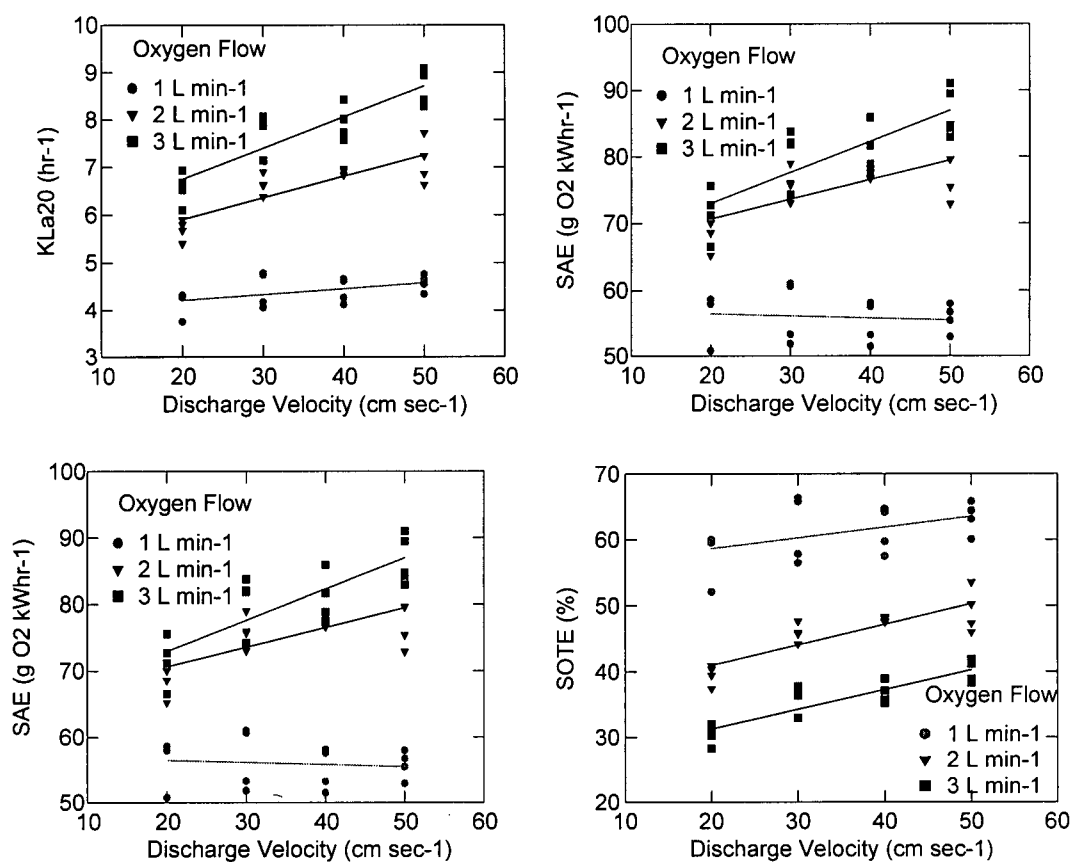
Figure 4.67a-d Effect of PSA O_2 flow rate (1, 2 and 3 l min^{-1}) and water discharge velocity (20-50 cm sec^{-1}) on K_La_{20} (a), SOTR (b), SAE (c) and SOTE (d).
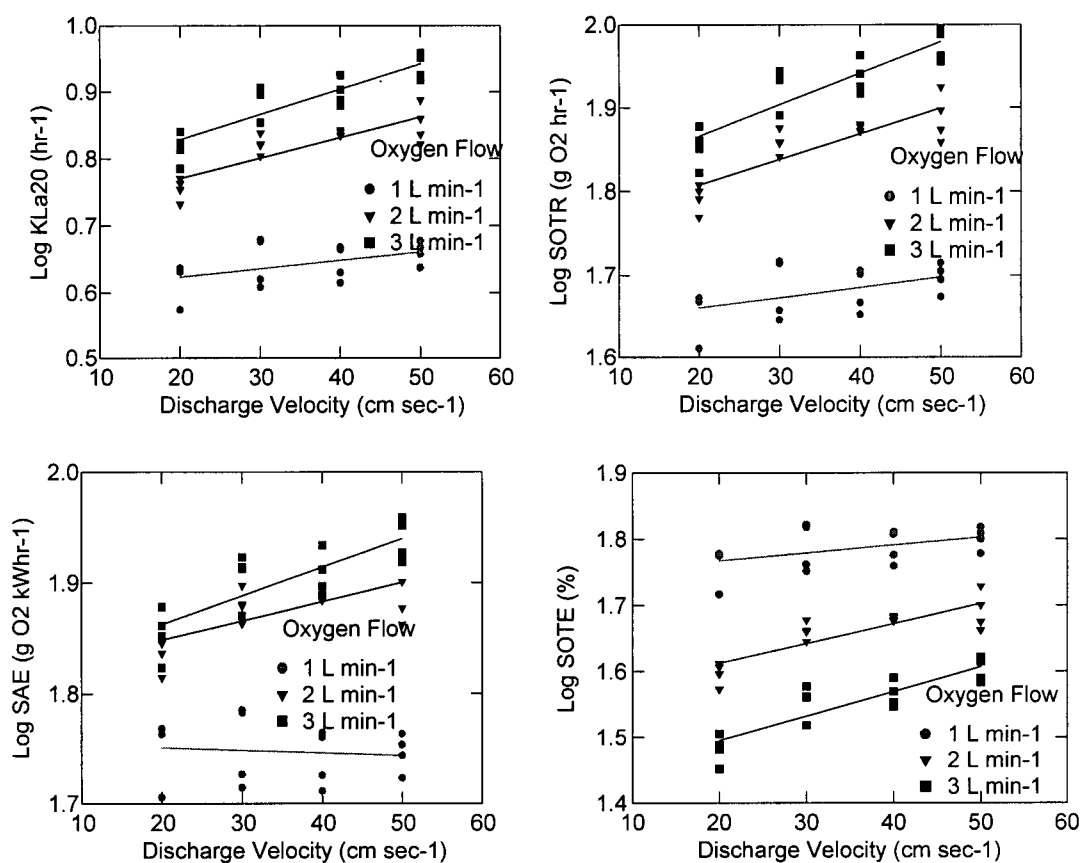
Figure 4.68a-d Effect of PSA O_2 flow rate (1, 2 and 3 l min^{-1}) and water discharge velocity (20-50 cm sec^{-1}) on K_La_{20} (a), SOTR (b), SAE (c) and SOTE (d) using log transformed data.

Table 4.71. Adjusted least squares means (± SE), treatment and interaction effects for various PSA oxygen flow rates with the Speece Cone without the 60 cm sec^{-1} and 70 cm sec^{-1} water discharge velocities.

Treatment	K_La_{20} (hr^{-1})	SOTR (g O_2 hr^{-1})	SAE (g O_2 kWhr^{-1})	SOTE (%)	n
1 l min^{-1}	4.4 (0.09)	47.9 (0.94)	55.9 (0.92)	61.1 (0.69)	16
2 l min^{-1}	6.6 (0.09)	71.7 (0.94)	75.1 (0.92)	45.6 (0.69)	16
3 l min^{-1}	7.7 (0.09)	84.2 (0.94)	80.0 (0.92)	35.8 (0.69)	16
Interaction	Yes	Yes	Yes	Yes	
O_2 flow effect	sig, p = 0.000	sig, p = 0.000	sig, p = 0.000	sig, p = 0.000	
Discharge velocity effect	sig, p = 0.000	sig, p = 0.000	sig, p = 0.000	sig, p = 0.000	
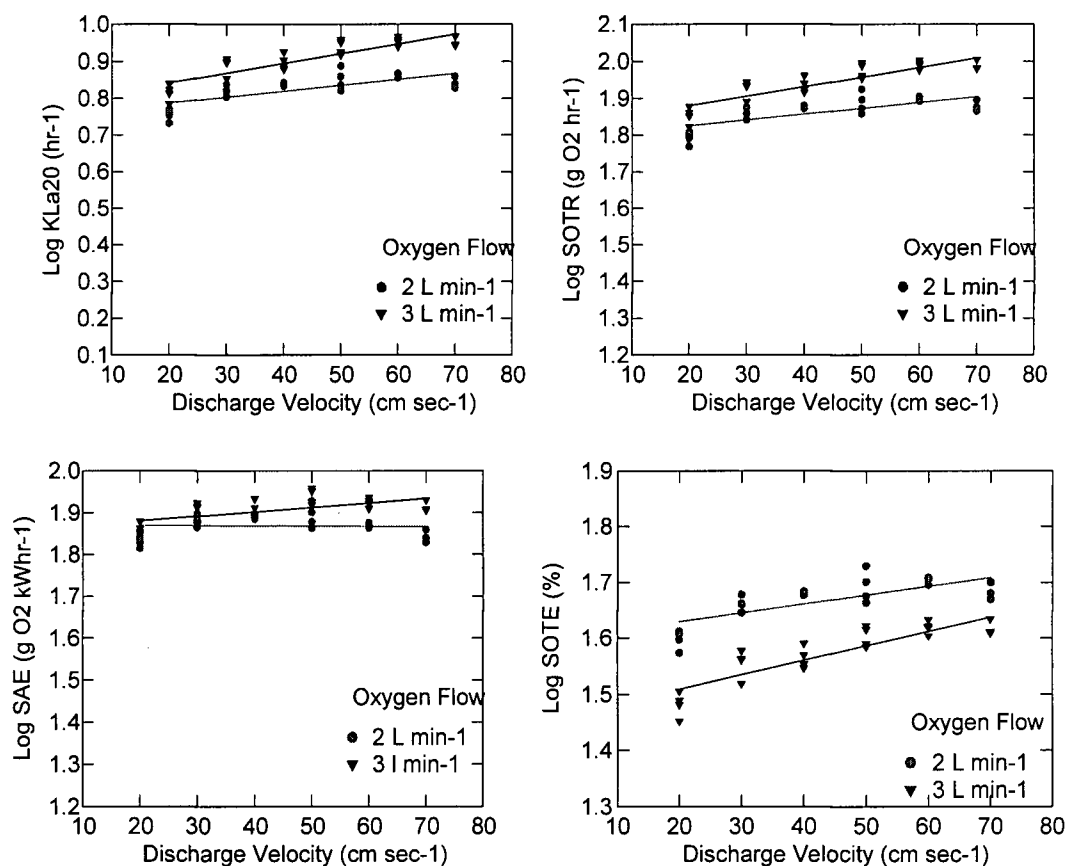
Figure 4.69a-d Effect of PSA O_2 flow rate (2 and 3 l min^{-1}) and water discharge velocity (20-70 cm sec^{-1}) on K_La_{20} (a), SOTR (b), SAE (c) and SOTE (d) using log transformed data.

velocity interaction effect was observed for K_La_{20} and SOTR (Table 4.72). The significant oxygen flow rate x discharge velocity interaction effect indicates that K_La_{20} and SOTR increased 1.2 fold, at 3 l min^{-1}, with increasing discharge velocity as compared to the 2 l min-1 oxygen flow rate (Figure 4.69 a-b).

Of the two analytical approaches, neither is technically correct as some of the actual test data is deleted; however, the latter method appears more useful as the log transformation of the interaction effects allows some initial quantification of the performance of the Speece Cone under two different experimental gas flow rate treatments.

Table 4.72. Adjusted least squares means (± SE), treatment and interaction effects for various PSA oxygen flow rates with the Speece Cone without the l min^{-1} oxygen flow rate treatment.

Treatment	K_La_{20} (hr^{-1})	SOTR (g O_2 hr^{-1})	SAE (g O_2 $kWhr^{-1}$)	SOTE (%)	n
2 l min^{-1}	6.8 (0.087)	73.6 (0.94)	73.9 (0.96)	46.8 (0.50)	24
3 l min^{-1}	8.1 (0.087)	88.7 (0.94)	80.9 (0.96)	37.7 (0.50)	24
Interaction	Yes, 1.20	Yes, 1.20	No	No	
O_2 flow effect	sig, p = 0.000	sig, p = 0.000	sig, p = 0.000	sig, p = 0.000	
Discharge velocity effect	sig, p = 0.000	sig, p = 0.000	sig, p = 0.000	sig, p = 0.000	

An effective non-statistical technique to visualise the entire performance envelope of the Speece Cone is to use three-dimensional graphing to examine the behaviour of $K_La_{20,}$ SOTR, SAE and SOTE under the full range of experimental treatments. This visualization approach clearly shows the "break function" response as well as smaller change in slope between the 2 and 3 l min^{-1} oxygen flow rates. K_La_{20} and SOTR (Figure 4.70 and Figure 4.71) increased as oxygen flow rates increased from 1 l min^{-1} to 2 l min^{-1}, over the range of velocities from 20 cm sec^{-1} to 50 cm sec^{-1}, then exhibited reduced slope as oxygen flow increased to 3 l min^{-1}. However, at
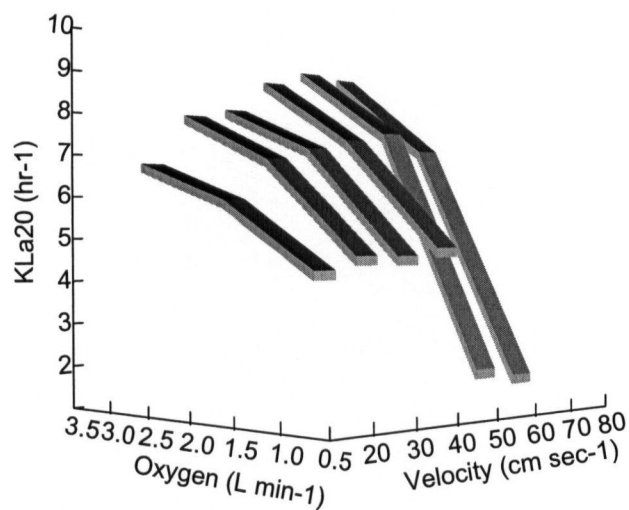
Figure 4.70 **Effect of PSA O$_2$ flow rate (1, 2 and 3 l min^{-1}) and water discharge velocity (20-70 cm sec^{-1}) on K$_L$a$_{20}$.**
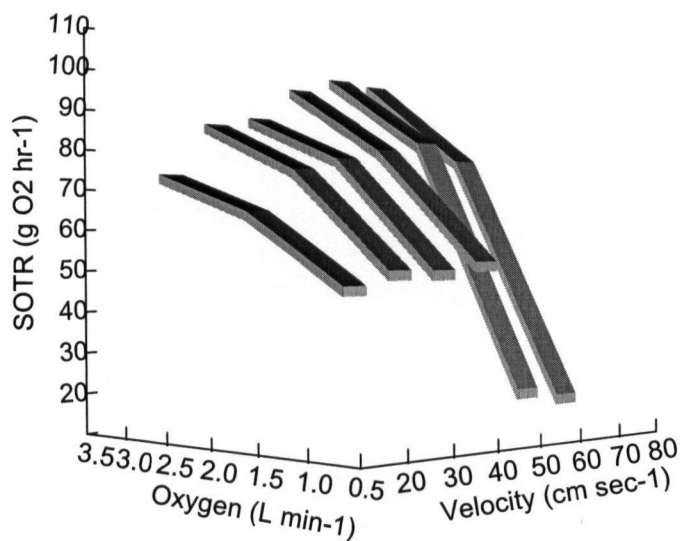
Figure 4.71 **Effect of PSA O$_2$ flow rate (1, 2 and 3 l min^{-1}) and water discharge velocity (20-70 cm sec^{-1}) on SOTR.**

oxygen flow rates < 2 l min^{-1} and discharge velocities > 50 cm sec^{-1}, $K_L a_{20}$ and SOTR decreased

precipitously. The SAE response manifold was similar to $K_L a_{20}$ and SOTR response (Fig-

ure 4.72).

The most dramatic response was for SOTE, which shows increasing oxygen transfer efficiency

as oxygen flow rate decreases from 3 l min^{-1} to 1 l min^{-1} over the range of discharge velocities

of 20 cm sec^{-1} to 50 cm sec^{-1} (Figure 4.73). However, at oxygen flow rates < 2 l min^{-1} and

velocities > 50 cm sec^{-1}, SOTE decreases abruptly, indicating a collapse of the high oxygen

transfer efficiencies normally associated with Speece Cone aerators.

4.5.2   Air Experiments

The results of the air only tests with the Speece Cone were considerably different from the

performance on PSA generated oxygen. The tests were conducted at 3 l min^{-1} air at 50 cm sec^{-1},

as this was among the most efficient oxygen flow rate x discharge velocity combinations for the

Speece Cone. However, the mean values obtained for $K_L a_{20}$, SOTR, SAE and SOTE at this

setting, on air, were lower than any recorded on PSA oxygen (Table 4.73). For comparative

purposes, the air results are shown alongside the 3 l min^{-1} x 50 cm sec^{-1} data for PSA oxygen

from Table 4.71.

Table 4.73.   **Mean (± SE) $K_L a_{20}$, SOTR, SAE and SOTE values for Speece Cone hypolimnetic aerator operating on air at 3 l min^{-1} and 50 cm sec^{-1} compared to PSA oxygen at 3 l min^{-1} and 50 cm sec^{-1}.**

Treatment	$K_L a_{20}$ (hr^{-1})	SOTR (g O$_2$ hr^{-1})	SAE (g O$_2$ kWhr^{-1})	SOTE (%)	N
3 l min^{-1} air at 50 cm sec^{-1}	1.2 (0.01)	13.4 (0.04)	16.9 (0.05)	24.5 (0.08)	3
3 l min^{-1} PSA O$_2$ at 50 cm sec^{-1}	7.7 (0.09)	84.2 (0.94)	80.0 (0.92)	35.8 (0.69)	16
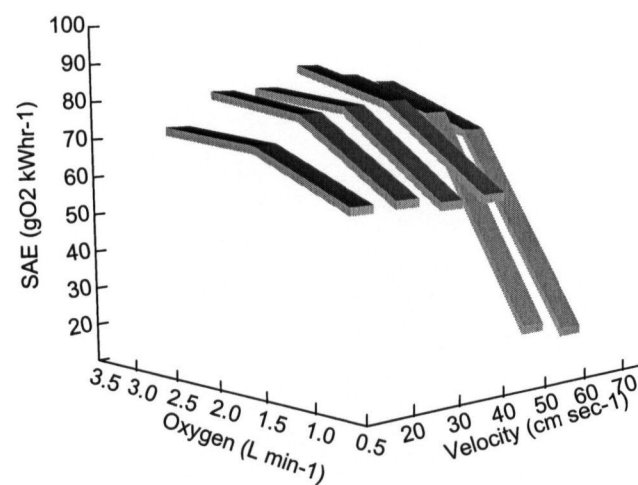
Figure 4.72   **Effect of PSA O$_2$ flow rate (1, 2 and 3 l min^{-1}) and water discharge velocity (20-70 cm sec^{-1}) on SAE.**
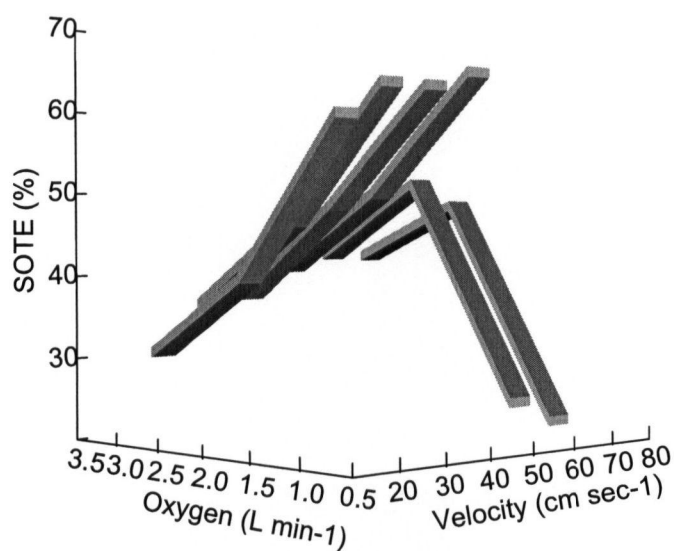
Figure 4.73   **Effect of PSA O$_2$ flow rate (1, 2 and 3 l min^{-1}) and water discharge velocity (20-70 cm sec^{-1}) on SOTE.**

CHAPTER 5: DISCUSSION

5.1   Review of Gas Transfer Theory

It is useful to briefly review gas transfer theory prior to discussing the experimental results, as it will assist in interpreting the data. Several theories have been proposed to describe the mass transfer of a sparingly soluble gas, such as oxygen, to water (Krenkel and Orlob, 1962). These include the Two-Film theory (Lewis and Whitman, 1924) which envisioned a thin film of gas and a film of liquid at the gas-liquid interface; the Film Penetration theory (Higbie, 1935) which postulated that gas transfer occurs during alternate cycles of gas adsorption and mixing; and the Surface Renewal theory (Danckwerts, 1951) which extended the Film Penetration theory by stressing the idea of surface renewal. Although these theories are approximations of the actual physical process, Dobbins (1964) proposed the theory that best appears to describe the gas transfer process. This theory is a combination of the classic Two-Film theory (Lewis and Whitman, 1924) and the Surface Renewal theory (Danckwertz, 1951).

According to Dobbins (1964), a gas such as oxygen passes through two films of gas and liquid, respectively, by molecular diffusion, and the mass transfer is driven by a partial pressure gradient in the gas phase and a concentration gradient in the liquid phase. Initially, oxygen molecules from the gas phase are transported to the liquid film surface, resulting in saturation conditions at the interface. For slightly soluble gases such as oxygen, the gas film offers very little resistance and this phase proceeds rapidly. The liquid interface has a finite thickness with unique properties. This layer is estimated to be at least three molecules thick and composed of water molecules (i.e., H_2O) oriented with their negative sides (i.e., oxygen) facing the gas phase (Eckenfelder and Ford, 1968).

In the second phase, oxygen molecules pass slowly through this film by molecular diffusion. It is presumed that the concentration of oxygen in solution at the interface is at saturation, hence all of the resistance to the passage of oxygen into the water is due to molecular diffusion across the liquid film (Eckenfelder, 1959). In the final stage, oxygen is mixed into the water by diffusion and convection currents. At low energy mixing levels (i.e., laminar flow conditions), the rate of oxygen absorption is regulated by the rate of molecular diffusion through the undis-turbed liquid film, and the Two-Film theory holds true. However, as turbulence levels increase, the surface film is disrupted and renewal of the film becomes responsible for transferring oxygen to the liquid (Eckenfelder, 1969). Thus, renewal of the surface film can be envisioned as the frequency with which fluid with a solute concentration of the bulk liquid (i.e., C_L) is replacing fluid from the interface with a concentration (i.e., C_i) derived from its contact with the gas phase. Turbulent eddies from the bulk liquid move to the interface and undergo a brief interval nonsteady-state molecular diffusion before being displaced from the surface film by subsequent eddies. Therefore, mass transfer becomes a function of the eddy exposure time, and the molecular diffusion during the time interval (Eckenfelder and Ford, 1969). This process is graphically depicted in Figure 5.1 (from Eckenfelder and Ford, 1969).
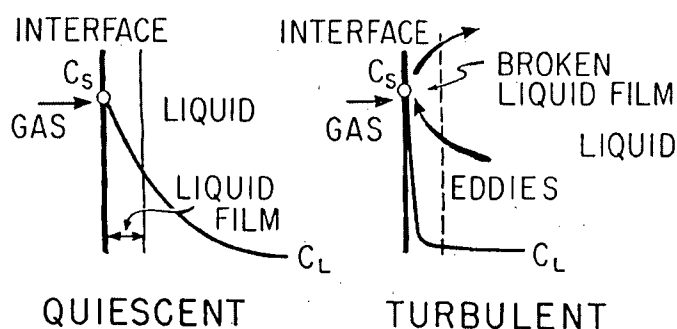
Figure 5.1   **Schematic of Two Film Theory gas transfer process (from Eckenfelder and Ford, 1969).**

Dobbins (1964) resolved the dilemma between the Two-Film theory, Penetration theory and Surface Renewal theory by developing the following equation to describe the liquid film coefficient (K_L) (King, 1970):

$$(5.1) \qquad K_L = \sqrt{D_L r} \; \coth \sqrt{\frac{r l^2}{D_L}}$$

where:

K_L = liquid film coefficient (m hr^{-1});

D_L = diffusion coefficient for oxygen (m^2 hr^{-1});

r = rate of renewal of liquid film (hr^{-1});

l^2 = liquid film thickness (m^2).

When the rate of surface renewal (r) is near zero (i.e., laminar flow conditions), equation (5.1) reduces to:

$$(5.2) \qquad K_L = D_L / l$$

and gas transfer is controlled by molecular diffusion through the liquid film as envisioned by the Two-Film theory.

However, as the rate of renewal (i.e., r) increases equation (5.1) reduces to:

$$(5.3) \qquad K_L = \sqrt{D_L r}$$

and the mass transfer becomes a function of the rate of surface renewal as described by the Danckwertz Surface Rejuvenation theory. In essence, both theories were correct, and these two models may be regarded as the limits between which both gas transfer mechanisms contribute to

the overall oxygen transfer process. In the transitional zone between molecular diffusion and turbulent mixing, the process may be visualized as a transfer, in series, through the diffusional sublayer, at the interface whose boundary layer is subjected to turbulence and subsequent surface renewal (O'Connor, 1982).

Mathematically, this theory can be expressed as follows (Mavinic and Bewtra, 1974):

(5.4) $$dm/dt = K_L A (C_i - C_L)$$

where:

dm/dt = time rate of mass transfer (g hr^{-1});

K_L = liquid film coefficient (m hr^{-1});

A = interfacial or absorbing surface area of air (m^2);

C_i = saturation value of dissolved oxygen at the interface between liquid and air bubble (mg l^{-1});

C_L = average concentration of dissolved oxygen in the bulk liquid (mg l^{-1}).

This mass equation may be expressed in concentration units by introducing the volume of the liquid (V):

(5.5) $$dc/dt = 1/V \, dm/dt = K_L A/V (C_i - C_L) = K_L a (C_i - C_L)$$

where:

dc/dt = rate of oxygen transfer (g L^{-1} hr^{-1});

V = volume of the liquid (m^3);

$A/V = a$ = the interfacial surface area of the air through which diffusion can occur generated by the particular aeration system per unit volume of water (m^2 m^{-3});

$K_L a$ = overall oxygen transfer coefficient (hr^{-1}).

In practice, it is very difficult to measure K_L and "a" directly due to the hypothetical nature of the liquid film thickness in K_L (according to the Two-Film theory), and the technical difficulties of measuring the interfacial surface area "a" (i.e., A/V). Therefore, it has become standard practice to consider the aeration process in terms of the overall oxygen transfer coefficient ($K_L a$), when characterizing the performance of aeration systems (Nienow, 1980).

5.2 Practical Applications of Gas Transfer Theory

The next step to understanding the experimental results is to review the practical applications of the aforementioned gas transfer theory. As previously indicated, mass transfer is driven by (1) a partial pressure gradient in the gas phase and (2) a concentration gradient in the liquid phase, and oxygen absorption is regulated by (3) the rate of molecular diffusion through the undisturbed liquid film at low energy mixing levels, and (4) the rate of renewal of the liquid film at high energy mixing levels. These four fundamental tenants are the underlying principles of gas transfer, mathematically summarized in Equation 5.5: $K_L a$ (C_i - C_L). Therefore, all aspects of gas transfer design must consider the effect of various engineering modifications on the liquid film coefficient (K_L), the interfacial area for gas transfer (a), the saturation value of dissolved oxygen at the interface between liquid and air bubble (C_i) and the average concentration of dissolved oxygen in the bulk liquid (C_L) (Mavinic and Bewtra, 1976).

In total, there are at least sixteen environmental and design factors that influence the rate of oxygen transfer into water in diffused aeration systems, all of which must be considered when designing efficient aeration systems (Mavinic and Bewtra, 1974). These include:

    (1) water temperature;

    (2) depth of gas release;

(3) contact time of the gas bubble in the water;

(4) size of the gas bubble;

(5) rate of gas flow;

(6) type of diffuser;

(7) orifice diameter;

(8) oxygen concentration gradient;

(9) turbulence in and around the gas-liquid interface

(10) position of the diffuser;

(11) geometry of the mixing tank

(12) concentration of dissolved solids;

(13) elevation

(14) barometric pressure;

(15) presence of surface active agents (i.e., surfactants)

(16) presence of oil contaminants in air supply.

From an operational perspective, some factors can be reduced or eliminated through proper

design and maintenance (e.g., geometry of the mixing tank, oil contamination in the air supply),

and several factors are beyond the immediate control of the practicing engineer (i.e., water

temperature, concentration of dissolved solids, elevation, barometric pressure and presence of

surfactants). The remaining nine factors (i.e., depth of release, bubble contact time, bubble

size, gas flow rate, diffuser type, orifice diameter, oxygen concentration gradient, turbulence in

and around the gas-liquid interface and position of the diffuser) define the range of criteria

which must be considered when designing gas transfer systems as they individually, or collec-

tively, influence:

(1) the hydrodynamics of the system which influence (K_L);

(2) the area of contact between the gas and liquid (a);

(3) the concentration gradient between the gas and liquid phase (C_i-C_L) (Bewtra and Mavinic, 1978; Nienow, 1980).

In this set of experiments, one parameter (i.e., the lateral position of the diffuser) was not examined due to the size constraints of the experimental system, thus leaving the remaining eight factors to be considered in the experimental design.

At this stage of the discussion, it is useful to review the relationship between Equation 5.5: K_La (C_i - C_L), the eight remaining operational factors, and the experimental variables selected for this series of experiments (Table 5.1). This demonstrates the interconnectedness and complexity of optimizing gas transfer, as altering one variable can have multiple implications. The rationale for selecting the experimental variables to examine in the full lift and Speece Cone hypolimnetic aerators should now be apparent.

An important fact to note is that the four standard units of measure used to quantify oxygen transfer, i.e., (1) K_La_{20} (hr^{-1}), the oxygen transfer coefficient at 20 °C; (2) SOTR (g O_2 hr^{-1}), the Standard Oxygen Transfer Rate; (3) SAE (g O_2 kWhr^{-1}), the Standard Aeration Efficiency and (4) SOTE (%), the Standard Oxygen Transfer Efficiency; do not necessarily respond similarly to design modifications. By definition, K_La_{20} and SOTR will respond proportionally (see Section 3.9); however, SAE and SOTE are not directly computationally linked to K_La_{20} and SOTR. Therefore, it is possible to cause an increase in K_La_{20} and SOTR in response to a design modification, while causing a simultaneous decrease in SAE and SOTE. Thus, the practising engineer must consider all of the design criteria when attempting to design an optimal gas transfer system. Alternatively, one or more units of measure can be intentionally sacrificed in exchange for improved gas transfer performance in the remaining unit(s) of measure in order to achieve a

Table 5.1. Relationship between $K_L a$ (C_i - C_L), the eight operational factors, and the experimental variables.

Full lift experimental variables	Effect on $K_L a$ (C_i - C_L)	Operational design factors
Diffuser orifice pore diameter (140 μ, 400 μ and 800 μ)	K_L, a	Bubble size, contact time, diffuser type, orifice diameter
Depth of gas release (1.5 and 2.9 m)	K_L, a, C_i-C_L	Depth of release, bubble contact time, bubble size, oxygen concentration gradient
Gas flow rate (10, 20, 30 and 40 l min^{-1})	K_L, a	Bubble contact time, gas flow rate, turbulence in and around the gas-liquid interface
Oxygen partial pressure (air and PSA generated oxygen)	C_i-C_L	Oxygen concentration gradient
Floating surface cover	a	Oxygen concentration gradient
Bubble screen	K_L	Bubble contact time, bubble size, turbulence in and around the gas-liquid interface
Counter-rotating blades	K_L	Bubble contact time, bubble size, turbulence in and around the gas-liquid interface
DBCA	K_L, a, C_i-C_L	Bubble contact time, bubble size, turbulence in and around the gas-liquid interface, type of diffuser, orifice size, oxygen concentration gradient
Speece Cone design factors	**$K_L a$ (C_i – C_L)**	**Operational criteria**
Oxygen flow rate (1, 2 and 3 l min^{-1})	K_L, a, C_i – C_L	Bubble contact time, gas flow rate, oxygen concentration gradient, turbulence in and around the gas-liquid interface
Outlet port discharge water velocity (20-70 cm sec^{-1})	K_L, a C_i – C_L	Bubble contact time, Turbulence in and around the gas-liquid interface

desired level of system performance. This contradictory behaviour is the paradox of gas transfer system design.

5.3   Full Lift Hypolimnetic Aeration - Groups 1 to 6

The rationale of the laboratory experiments in Groups 1 to 6 was to examine the effects of diffuser depth (1.5 and 2.9 m), orifice diameter (140 μ, 400 μ and 800 μ), and oxygen partial pressure (air and PSA O_2) on K_La_{20}, SOTR, SAE and SOTE, with gas flow rate (10, 20, 30 and 40 l min^{-1}) as the covariate. Water velocity and bubble size were additional data collected to assist in the interpretation, recognising that the bubble size data may be of limited use due to the small sample size relative to the number of bubbles in the system. Although K_La_{20} and SOTR are the units of measure which provide basic information on the characteristics of each experimental configuration, the two most relevant units of measure for comparing aeration systems are SAE and SOTE (Beak, 1977, Bewtra and Mavinic, 1978). The effect of varying the experimental treatments on K_La_{20}, SOTR, SAE and SOTE, water velocity and bubble size is discussed below.

5.3.1   Diffuser Depth

The diffuser depth treatment exerted a significant effect on K_La_{20}, SOTR, SAE and SOTE, with all units of measure showing positive increases in response to an increase in diffuser submergence. The magnitude of the responses were all quite large, ranging from 30 to 57% (Table 4.7). The depth of gas release influenced K_La_{20}, SOTR and SOTE, mainly by an increase in bubble contact time due to the longer path length the bubbles must take to reach the surface, and a larger deficit or driving force (C_i-C_L); this resulted in more oxygen transfer (Mavinic and Bewtra, 1974; Mavinic and Bewtra, 1976). The increase in SAE was unexpected, as similar

studies with an upward, co-current, air-water flow observed a decrease in SAE with increased diffuser submergence (i.e., System II; Mavinic and Bewtra, 1976).

SAE increased in these experiments, as there was an increase in the bubble-travel distance, an increase in driving force (C_i-C_L), as well as an increase in water velocity that increased turbulence at the liquid interface, and influenced K_L. The water velocity data (Table 4.47) clearly demonstrate that velocity increased with depth in each experimental treatment combination, thus supporting this conclusion. The fact that SAE increased with diffuser submergence in this case indicates that, despite the additional air power energy required to deliver air or PSA O_2 to greater depths, the energy cost was more than offset by the increased oxygen transfer resulting from the longer bubble contact times, greater turbulence and increased hydrostatic pressure. Unlike the Mavinic and Bewtra (1976) study, there were no water power energy costs in this system, which was a significant energy cost in their Systems II, III and IV. In addition, the outlet tube water from the full lift aerator discharged into the bulk liquid, hence water velocities increased with diffuser submergence, but not to the same extent as the circulating closed-loop system design of Mavinc and Bewtra (1976). This resulted in greater initial turbulence in the inlet tube, as the water entering the inlet tube possessed minimal velocity; hence high shear forces were present as the rising air bubbles mixed with the slower moving water mass entering the inlet tube from the bulk liquid reservoir.

Gas flow rate significantly influenced K_La_{20}, SOTR, SAE and SOTE in all of the experimental combinations. K_La_{20} and SOTR responded positively to increased gas flow rates, a response noted in numerous gas transfer studies (e.g., Bewtra et al., 1970; Schmidt et al., 1978). At least two mechanisms are responsible for this effect. Firstly, higher gas flow rates generate increased

turbulence at the liquid interface. Under highly turbulent conditions, mass transfer is regulated by disruption and the rate of renewal of the liquid film as described by the Danckwertz Surface Rejuvenation theory (Dobbins, 1964) (5.3): $K_L = \sqrt{D_L r}$. As r (the rate of surface renewal) increases, K_L increases. Therefore, one mechanism by which higher gas flow rates increase $K_L a_{20}$ and SOTR is via their positive effect on K_L. Secondly, increased gas flow rates increase the number of bubbles present in the water column per unit time. This increases the total interfacial area available for gas transfer to the surrounding medium (Bewtra and Mavinc, 1974). Therefore, increased gas flow rates positively influence $K_L a_{20}$ and SOTR via their effect on "a".

SAE and SOTE responded negatively to increased gas flow rates, a common observation in diffused aeration systems (Bewtra and Nicholas, 1964; Ellis and Stansbury, 1980; Mavinc and Bewtra, 1976). The general explanation for this response is that air bubbles become larger with an increase in gas flow rates. This results in less oxygen transfer due to the reduced ratio of interfacial area to bubble volume. Secondly, as air bubbles become larger, their terminal rise velocities increase, thus reducing the contact time between air bubbles and the surrounding liquid, even though there is a corresponding increase in turbulence at the liquid film. Finally, increased gas flow rates incur additional energy costs for gas compression, both air and PSA O_2, which penalises SAE. This is an example of how competing factors interact to determine overall gas transfer rates.

As previously indicated, bubble velocity increased significantly with increased diffuser submergence, as the longer path length allows bubbles to increase to their terminal rise velocity. Bubble velocity also increased significantly with increased gas flow rate, as the additional

volume of air in the inlet tube further decreases the density of the air-water mixture in the inlet tube by increasing the gas volume void fraction; this increases the water velocity in air-lift pumps (Andeen, 1974). Higher gas flow rates also create larger bubbles, and larger bubbles exhibit higher rise velocities (Andeen, 1974).

The bubble size data did not show any relationship to gas flow rates. The coefficient of variation (CV) was so large that the broad range in the EQD data hid any significant effect. The bubble size data indicated the size range between the 2.9/0.5 m and 1.5/0.5 m treatments was only 0.4 mm for the 140 μ and 400 μ treatments (Tables 4.58 and 4.59), and 0.8 mm for the 800 μ treatment (Table 4.60). In general, all of the EQD values were within ~2 mm in each orifice size class, hence it appears the technique was not sufficiently accurate to detect an effect of depth on EQD. The r^2 for the depth x gas flow rate regression only ranged from 0.28 to 0.34, even with the log transformed data; hence the utility of the EQD data is minimal.

5.3.2   Oxygen Partial Pressure

The oxygen partial pressure treatment exerted a very significant effect on K_La_{20} and SOTR, with both units of measure showing positive increases in response to an increase in oxygen concentration from the 21% O_2 content of air to the ~95% O_2 content of the PSA gas. The magnitude of the responses were substantial, ranging from 430 to 542% for K_La_{20}, and 432 to 532% for SOTR (Table 4.14). The increase in oxygen partial pressure influenced K_La_{20} and SOTR by substantially increasing the driving force (C_i-C_L), resulting in more oxygen transfer per unit bubble contact time. Since there was no effect of oxygen partial pressure on water velocity (Table 4.46), the increased concentration gradient accounts for all of the observed effect. Interestingly, the ratio of the observed increase in K_La_{20} and SOTR exceeded the PSA gas:air

oxygen ratio (i.e., 95%/21% = 4.5) in most cases, suggesting a non-linear effect may be occurring at the liquid film; this enhances the diffusion of oxygen molecules above what would be expected on O_2:air ratios alone.

SOTE was also positively influenced by oxygen partial pressure, and although the increases were not as large as for K_La_{20} and SOTR, they ranged from 33 to 54%, which is a significant effect. The fact that SOTE did not increase by a ratio of 4.5:1 indicates that a significant fraction of PSA O_2 gas was not being utilised, and was escaping to the atmosphere, essentially as waste gas. A logical design modification would be to capture the unused PSA O_2 in the separator box, and re-introduce it to the downflowing water in the outlet tube by a venturi arrangement, in order to scavenge the oxygen without incurring any additional energy costs. The SAE response was strongly negative, and quite uniform, ranging from a 72 to 76% decrease when operating on PSA O_2. This indicates that, despite the large increase in $(C_i\text{-}C_L)$, resulting in more oxygen transfer per unit bubble contact time, the energy costs to produce 95% oxygen via PSA technology more than offset any gains. A detailed discussion of the efficiency of PSA oxygen generation technology and the explanation for the high energy costs is included later in this chapter.

Gas flow rate significantly influenced K_La_{20}, SOTR, SAE and SOTE in all of the experimental combinations, with K_La_{20} and SOTR responding positively to increased gas flow rates. As before, higher gas flow rates means an increase in the number of bubbles in the system, thus increasing the total interfacial area available for gas transfer to the surrounding medium and the amount of oxygen transfer to the liquid (Bewtra and Mavinic, 1974). In addition, higher gas flows generate increased turbulence, thus increasing turbulence at the liquid interface and the

rate of renewal of the liquid film. Even though bubble contact time is reduced by the higher velocities, the tradeoff favors increased gas transfer.

SAE and SOTE responded negatively to increased gas flow, as air bubbles become larger with an increase in gas flow rates, resulting in less oxygen transfer due to the reduced ratio of interfacial area to bubble volume. The terminal rise velocities of the bubbles also increases, thus reducing the contact time between air bubbles and the surrounding liquid, even though turbulence is increased at the liquid film. The increased energy costs required to compress additional air and PSA O_2 penalised the SAE unit of measure.

There was no effect of gas composition on bubble velocity in any of the experimental combinations (Table 4.46). Bubble size was not measured for PSA O_2; hence there is no basis for comparison of EQD as a function of air or PSA O_2.

5.3.3   Orifice Diameter

Orifice diameter exerted a significant effect on K_La_{20}, SOTR, SAE and SOTE. Each unit of measure increased with a decrease in orifice size (Table 4.19). Smaller orifices produce smaller bubbles, and a reduction in bubble size influences gas transfer in at least four ways:

1.   An increase in surface area per unit bubble volume (Eckenfelder, 1969);

2.   A decrease in terminal rise velocity (Stenstrom and Gilbert, 1981);

3.   A decrease in the liquid film coefficient (Bewtra and Nicholas, 1964);

4.   An increase in the total number of bubbles in the water column per unit gas discharge.

An increase in bubble surface area per unit volume increases the "a" in K_La, and acts to increase K_La_{20} and SOTR. A decrease in terminal rise velocity increases the bubble contact time, which acts to increase K_La_{20} and SOTR and SOTE, and SAE as no additional energy costs are incurred. However, the competing response is that a decrease in terminal rise velocity decreases the liquid film coefficient (K_L) and turbulence at the liquid interface, which decreases K_La_{20}, SOTR, SAE and SOTE. Increased number of bubbles in the water column per unit time can saturate the interstitial spaces between the bubbles with oxygen more quickly, if the bubbles are in a confined column, and reduce the concentration gradient across the liquid film (Mavinic and Bewtra, 1974).

The interaction of these opposing factors determines the net effect on K_La_{20}, SOTR, SAE and SOTE. In these experiments, the overall effect was an increase in all units of measure, indicating that the effect of increased surface area and contact time more than compensated for the reduction in K_L due to slower rise velocities and increased bubble density in the inlet tube. Since the reduction in orifice diameters did not require an increase in energy, SAE responded positively for the same reasons. If orifice diameter were reduced below a critical minimum diameter (e.g., < 2 μ), then additional energy would be required to force gas through the diffuser and overcome surface tension at the orifice-water interface, and SAE would decline accordingly. The 2 μ diffusers used in the DBCA experiments were in the 2 μ size range, and required considerable back pressure before any gas could be seen emerging from the diffuser. In contrast, the 140 μ, 400 μ and 800 μ diffusers showed minimal backpressure, and responded instantly to fluctuations in gas flow rate.

A number of researchers have reported a similar effect of increased SOTE with decreased bubble diameter. For example, Morgan and Bewtra (1960) and Bewtra and Nicholas (1964) both observed increased SOTE with fine bubble (Saran tubes) as compared to coarse bubble diffusers (Spargers). Barnhart (1969) also demonstrated a decrease in K_La_{20} with bubbles diameters of 2 mm and larger.

Scheffé's test indicated each orifice size was significantly different from each other for the four units of measure. Since Scheffé's test is conservative by design and the most rigorous *a posteriori* test for performing comparison among means (Larkin, 1975), there is little doubt the observed results were real, and not statistical artifacts.

Gas flow rate significantly influenced K_La_{20}, SOTR, SAE and SOTE in all of the experimental combinations, with K_La_{20} and SOTR responding positively to increased gas flow rates, and SAE and SOTE decreasing with increased gas flow rate. The reasons are as before, with higher gas flow rates increasing in the number of bubbles and total interfacial area available for gas transfer to the surrounding medium, increased turbulence at the liquid interface and higher renewal rates of the liquid film. Again, even though the higher velocities reduce bubble contact time, the tradeoff increased K_La_{20} and SOTR, thus demonstrating the importance of interfacial area relative to contact time.

SAE and SOTE responded negatively to increased gas flow rates. Air bubbles become larger with an increase in gas flow rates, resulting in less oxygen transfer due to the reduced ratio of interfacial area to bubble volume. The terminal rise velocities of the bubbles also increases, thus reducing the contact time between air bubbles and the surrounding liquid even though turbu-

lence is increased at the liquid film. The additional energy costs required to increase air or PSA O_2 flow also act to penalise the SAE, hence the net result is a decrease in SAE.

The effect of orifice size on water velocity was limited to the 1.5 m submergence treatment, in which the 140 μ and 400 μ diameter orifices generated higher velocities than the 800 μ orifice (Table 4.48). The author believes this result was caused by the larger bubbles released by the 800 μ at 1.5 m rising in a rocking motion, then fragmenting into a variety of bubble sizes and shapes. The bubbles generated by the 140 μ and 400 μ diffuser appeared more uniform in shape and diameter, and rose more quickly through the water column. The coefficient of variation (CV) for the 140 μ bubbles at 1.5 m was the lowest observed (Table 4.53), while the CV for the 800 μ bubbles at 1.5 m was the largest, with some CV's exceeding 100% (Table 4.55). There was no statistical difference in water velocity at the 2.9 m submergence depth (Table 4.53). It is believed this was caused by an averaging effect that takes place during bubble ascent in the inlet tube, in which fragmentation and coalescing of bubbles, under decreasing hydrostatic pressure, tends to "average out" the bubble size, and hence velocity.

The bubble size data was contradictory. At the 1.5/0.5 m test, the 140 μ orifice generated the largest bubbles, with 400 μ and 800 μ being smaller and statistically indistinguishable from each other. At 2.9/0.5 (i.e., same photo depth, increased diffuser submergence), a similar trend was observed, i.e., the 140 μ and 400 μ bubbles were larger than the 800 μ, but not statistically different from each other. This was reversed for the 2.9/2.7 m treatment, as 140 μ were the smallest, and the 400 μ and 800 μ similar to each other. As before, the r^2 of the relationship only ranged from 0.28 to 0.38, hence the relationship is of minimal value. About the only credible information on EQD is the CV data, which increases with orifice diameter.

5.3.4   Group 1 to 6 Summary

The Group 1 to 6 experiments illustrated a number of key aspects of gas transfer. Increased

depth of submergence and decreased orifice diameter, within the ranges explored in these tests,

are design variables that are beneficial to all units of measure. This demonstrates the impor-

tance of contact time, concentration gradient, and increased interfacial bubble area on oxygen

transfer. Increased oxygen partial pressure created significant increases in K_La_{20} and SOTR,

moderate increases in SOTE, but moderate losses in SAE. This indicates the importance of

concentration gradient on some aspects of gas transfer, but the additional energy costs to

generate the oxygen incurred an energy penalty for SAE. In this case, the design engineer is

presented with the option of enhancing some aspects of gas transfer, while sacrificing others. A

more detailed discussion on the practical implications of these findings will follow in a later

section.

The effect of increasing gas flow rate was similar across all depths, orifice diameters, and

oxygen partial pressures. This clearly demonstrates the overriding importance of higher turbu-

lence and interfacial areas for increasing K_La_{20} and SOTR, and the negative implications on

SAE and SOTE resulting from greater energy costs of gas delivery (air and PSA O_2). Again,

the balancing act between K_La and SOTR, and SAE and SOTE is readily apparent. Water

velocity in the full lift aerator, not surprisingly, was directly related to diffuser depth, and gas

flow rate, and was independent of orifice diameter, except at the 1.5 m submergence depth. The

bubble size data, expressed as equivalent bubble diameter, was of minimal use due to the

significant scatter in the data, and the small sample size relative to the population of bubbles in

the system. An improved procedure for measuring bubble size is required using a more sophis-

ticated technique such as an optical image analyzer. The most credible data emerging from the

EQD data set is that CV increases with orifice diameter. This was caused by the larger bubbles from the 800 μ orifices fragmenting into a range of bubbles from very large to very small, whereas most of the bubbles emitted from the 140 μ orifice were quite uniform in size. The 400 μ diffuser, being mid-way between fine and coarse bubble diffuser classification, exhibited CV's mid-way between the 140 μ and 800 μ diffusers

5.4 Full Lift Hypolimnetic Aeration - Groups 7 to14

The Group 7 to14 experiments examined the influence of four *in situ* modifications (DBCA, bubble screen, counter-rotating vanes and surface cover), orifice diameter (140 μ and 800 μ), and oxygen partial pressure (air and PSA O_2) at a single diffuser depth (2.9 m) on K_La_{20}, SOTR, SAE and SOTE, with gas flow rate (10, 20, 30 and 40 l min^{-1}) as the covariate. Water velocity and bubble size data were collected to assist in the interpretation. The effect of varying the experimental treatments on K_La_{20}, SOTR, SAE and SOTE, water velocity and bubble size is discussed below.

5.4.1 *In situ* Modifications

The *in situ* modifications treatment exerted a significant effect on K_La_{20}, SOTR, SAE and SOTE, with all units of measure showing a negative response to the various *in situ* treatments. The magnitude of the responses were all quite large, ranging from 22 to 50% on air (Table 4.31), and 22 to 48% on PSA O_2 (Table 4.42). The general trend was that the No Treatment option generated the highest values of K_La_{20}, SOTR, SAE and SOTE (1st ranking), the Screen and Cover treatments the lowest values (4th and 5th ranking), and the Vanes and DBCA treatments were in the middle range (2nd and 3rd ranking).

There are at least two reasons for this effect, the first being that the various *in situ* modifications

caused a reduction in water velocity in the full lift aerator (Table 4.49, and Table 5.2). It is

known from earlier discussions that orifice diameter had no effect on water velocity at the 2.9 m

submergence depth (5.3.3), and that gas composition had no effect on water velocity, regardless

of depth (5.3.2). Diffuser submergence did influence water velocity (5.3.1), but since all of the

in situ tests were carried out at 2.9 m depth, the only remaining treatment that can explain the

reduction in water velocity is the *in situ* treatments. It was quite obvious when the tests were

being conducted that the *in situ* treatments were causing a reduction in water velocity by

restricting flow either in the inlet tube, the separator box, or the outlet tube.

Table 5.2. **Summary of various full lift *in situ* modification treatments on water velocity with the 140 μ and 800 μ diffuser, on air, showing percentage increase/decrease relative to No Treatment.**

Treatment	Velocity (cm sec^{-1})
None x 140 μ	33.2
Cover x 140 μ	30.4 (-8%)
Screen x 140 μ	29.0 (-13%)
DBCA x 140 μ	26.7 (-20%)
Vanes x 140 μ	23.9 (-28%)
None x 800 μ	31.2
DBCA x 800 μ	24.5 (-21%)
Screen x 800 μ	23.8 (-24%)
Cover x 800 μ	23.2 (-26%)
Vanes x 800 μ	19.6 (-37%)

The two treatments that were located inside the inlet tubes (screen mesh, counter-rotating vanes)

restricted flow by their physical presence, as the gas:bubble mixture had to pass through the

various physical constrictions. The small screen mesh size openings (0.64 cm square) presented

considerable resistance to the bubble:water mixture, and elongated bubbles could be seen

streaming upwards from the upper surface of the screen. The counter-rotating vanes acquired mechanical energy to turn the blades from the flowing water, in addition to possessing significant cross-sectional area (which caused drag resistance). The counter-rotating design of the vanes forced the directional rotation of the bubble: water mixture to change rapidly between the two vanes. Therefore, it is not surprising that the Vanes treatment exhibited the lowest water velocity.

The *in situ* treatments located outside the inlet tube (DBCA) and separator box (Surface Cover) also reduced water velocity. The Surface Cover treatment restricted the height of the bubble:water plume exiting into the separator box. The head differential created by the air:bubble plume is the driving force in air lift pumps (Andeen, 1974). By restricting the height of the air:bubble plume, the surface cover effectively reduced the head differential, hence velocity. The DBCA modification reduced velocity by filling the outlet tube with bubbles, mainly very small (Table 4.56 and 4.57), but some larger bubbles were formed by coalescence in the turbulent mixing zone at the entrance to the outlet tube. The presence of a significant number of bubbles in the outlet tube reduced the density of the air:water mixture and caused an upward buoyant force, as the outlet tube attempted to function as a co-current upflow air lift pump. Since the gas flow rate to the DBCA diffuser was fixed at 3 l min^{-1}, the co-current air lift pump in the inlet tube dominated the direction of the flow pattern, but the DBCA configuration exacted a price by reducing the net velocity. In addition, since the total gas flow in each treatment was fixed at 10, 20, 30 or 40 l min^{-1}, the 3 l min^{-1} portion allocated to the DBCA diffuser in the separator box reduced the gas flow rate, hence energy input, to the inlet tube. Since water velocity is related to gas flow rate in air lift pumps (Andeen, 1974), this contributed to a reduction in water velocity with the DBCA configuration.

If water velocity was the single factor by which the *in situ* treatments influenced K_La_{20}, SOTR, SAE and SOTE, then their expected ranking, and % change relative to No Treatment, should be approximately similar to the velocity rankings in Table 5.2. (i.e., No Treatment 1st, Screen and Cover 4th and 5th, and Vanes and DBCA treatments 2nd and 3rd ranking). If one assumes a +/- 5% leeway around the % differences, then it appears the % relative reduction in water velocity more or less accounts for the % reduction in K_La_{20}, SOTR, SAE and SOTE as a result of the Vanes treatment (Table 5.3). The % reduction in K_La_{20}, SOTR, SAE and SOTE from the DBCA treatment seems to be slightly greater than the expected % reduction from water velocity alone. However, since 3 l min^{-1} of the gas flow rate was re-directed to the diffuser in the separator box with the DBCA treatment, this would partially explain the additional variance.

The two treatments that greatly exceeded the reduction in K_La_{20}, SOTR, SAE and SOTE, expected solely as a result of reduced water velocity, are the Screen and Cover treatments. In

Table 5.3. Summary of various *in situ* full lift hypolimnetic aerator treatments on air with the 140 μ and 800 μ diffuser showing percentage increase/decrease relative to No Treatment for K_La_{20}, SOTR, SAE and SOTE and water velocity.

Treatment	Water velocity and % change relative to No Treatment	K_La_{20} (hr^{-1})	SOTR (g O_2 hr^{-1})	SAE (g O_2 kWhr^{-1})	SOTE (%)
None x 140 μ	33.2 cm sec^{-1}	3.3	35.4	324.5	7.9
Vanes x 140 μ	23.9 (-28%)	2.4 (-27%)	26.5 (-25%)	248.1 (-24%)	6.0 (-24%)
DBCA x 140 μ	26.7 (-20%)	2.3 (-30%)	24.9 (-30%)	241.3 (-26%)	5.9 (-25%)
Screen x 140 μ	29.0 (-13%)	2.1 (-36%)	22.5 (-36%)	209.6 (-35%)	5.1 (-35%)
Cover x 140 μ	30.4 (-8%)	1.9 (-42%)	20.6 (-42%)	192.7 (-41%)	4.7 (-41%)
None x 800 μ	31.2 cm sec^{-1}	2.2	22.1	197.1	4.8
DBCA x 800 μ	24.5 (-21%)	1.5 (-32%)	16.0 (-28%)	154.2 (-22%)	3.7 (-23%)
Vanes x 800 μ	19.6 (-37%)	1.2 (-45%)	13.5 (-39%)	121.0 (-39%)	2.9 (-40%)
Screen x 800 μ	23.8 (-24%)	1.2 (-45%)	13.4 (-39%)	121.9(-38%)	3.0 (-38%)
Cover x 800 μ	23.2 (-26%)	1.1 (-50%)	12.1 (-45%)	107.6 (-45%)	2.6 (-46%)

these treatments, K_La_{20}, SOTR, SAE and SOTE were typically 35 to 50% less than the No Treatment, whereas the reduction in water velocity, as a result of these treatments, only ranged from 8 to 26%. This suggests additional factors negatively influenced gas transfer in these treatments. For the Screen treatment, the observations of elongated bubbles streaming upwards from the wire mesh likely de-gassed oxygen, which had been absorbed during the initial rise from the release depth (2.9 m). As will be discussed in a later section, most of the gas transfer occurred in the lower ½ of the inlet tube. If turbulence and low pressure zones around the mesh screen caused oxygen to de-gas, this could explain the additional negative effect of the Screen treatment on K_La_{20}, SOTR, SAE and SOTE, above what would have be expected solely on the basis of reduced water velocity. The Cover treatment likely caused a reduction in gas transfer by decreasing the transfer of atmospheric oxygen at the turbulent air-water interface generated by the bursting air bubbles. Neilson (1974) observed reduced rates of oxygenation in similar laboratory experiments using a floating stryrene cover. Therefore, the *in situ* Cover treatment negatively influenced K_La_{20}, SOTR, SAE and SOTE by reducing water velocity and likely decreased oxygen transfer in the separator box.

As seen in the Group 1 to 6 experiments, gas flow rate significantly influenced K_La_{20}, SOTR, SAE and SOTE in all of the experimental combinations. K_La_{20} and SOTR responded positively to increased gas flow rates, and SAE and SOTE responded negatively. As before, K_La_{20} and SOTR responded as higher gas flow rates increased the number of bubbles in the system and increased the total interfacial area available for gas transfer to the surrounding medium (Bewtra and Mavinc, 1974). The higher gas flows generate increased turbulence at the liquid interface and enhance the rate of renewal of the liquid film. Even though the higher velocities reduce bubble contact time, the tradeoff favored K_La_{20} and SOTR. As expected, SAE and SOTE

responded negatively to increased gas flow. High gas flow rates increased bubble sizes, result-

ing in less oxygen transfer due to the reduced ratio of interfacial area to bubble volume. The

terminal rise velocities of the bubbles also increased, thus reducing the contact time between air

bubbles and the surrounding liquid, even though turbulence was increased at the liquid film.

Finally, the incremental energy costs required to compress additional air and PSA O_2 penalised

the SAE unit of measure.

A significant gas flow rate x *in situ* modification interaction was observed for all of the K_La_{20},

SOTR, SAE and SOTE measurements with the 800 μ diffuser, and for the K_La_{20} and SOTR

with the 140 μ diffuser. The K_La_{20} and SOTR interaction is the additive effect of gas flow rate

on oxygen transfer, caused by increasing turbulence and interfacial area with each increase in

gas flow rate. Statistically, this means that the effect of a particular treatment is partially

explained by the covariate gas flow rate, and is not solely a function of the treatment being

examined. The most interesting interaction was the gas flow rate x DBCA treatment with the

800 μ diffuser on SAE and SOTE (Figures 4.18 c and d; 4.20 c and d). A similar, but not

statistically significant response, occurred with the 140 μ diffuser treatment (Figures 4.17 c and

d; 4.20 c and d).

The data indicates the DBCA treatment exhibited quite high SAE and SOTE values at the

lowest gas flow rate (i.e., 10 l min^{-1}); however, SAE and SOTE plummeted with increasing gas

flow, more so than the other *in situ* treatments, hence the significant interaction effect. This

response was caused by destabilisation of the DBCA effect occurring in the outlet tube at the

lowest gas flow rate. At the lowest gas flow, the downward water velocity in the outlet tube

closely matched the upward rise velocity of the DBCA bubble swarm in the outlet tube, signifi-

cantly increasing contact time and turbulence at the liquid interface, and generating high values

for SAE and SOTE. The data indicates that with the 800 μ orifice diffuser on air, the outlet tube

water velocity at 10 l min^{-1} was ~15 cm sec^{-1} (Figure 4.25 b). The bubble size for the DBCA

treatment with the 800 μ diffuser on air at 10 l min^{-1} air flow was approx. 2.8 mm EQD (Table

4.57). The rise velocity of bubbles in this size range is described by (Haberman and Morton,

1954):

(5.1) $$u = 1.02\sqrt{gr_e}$$

where:

u = terminal rise velocity (cm sec^{-1});

g = acceleration due to gravity (980 cm sec^{-2});

r_e = equivalent bubble radius (cm)

Therefore, 2.8 mm EQD bubbles would have an upward velocity of ~12 cm sec^{-1} using Eqn.

(5.1), and closely match the downward water velocity in the outlet tube. As gas flow rates

exceeded 10 l min-1, water velocity increased to >20 cm sec^{-1}, while bubble size decreased to

~1.7 mm EQD due to additional turbulence and bubble fragmentation in the separator box

(Table 4.57); bubble rise velocity would have decreased to ~ 9 cm sec^{-1}. The net result was a

destabilization of the DBCA effect as the bubbles were washed out of the outlet tube into the

bulk water in the tank. The loss of the counter-current bubble exchange conditions in the outlet

tube, combined with increasing energy costs associated with the higher gas flow rates, resulted

in the precipitous decline of SOTE and SAE with gas flow rates >10 l min^{-1}. A similar, but not

as dramatic, effect occurred with the 140 μ diffuser on air. The water velocities in the outlet

tube at 10 l min^{-1} were slightly greater than those recorded with the 800 μ diffuser (Figure 4.25 a) and the bubble size was smaller (~1.7 mm EQD), hence the DBCA effect did not establish itself as strongly as with the 800 μ diffuser, nor was the collapse in SAE and SOTE as dramatic, although it did occur. Mavinic and Bewtra (1974) experienced similar responses with their experiments, and designated Q_{min} air flow rates for their counter-current design (i.e., System III) and Q_{max} air flow rates for their co-current downflow design (i.e., System IV) to prevent destabilization of their systems.

5.4.2   Water Velocity

Much of the effect of the *in situ* modifications on water velocity has been discussed in the previous section. One remaining point to discuss is the observed reduction in water velocity with the 800 μ diffuser relative to the 140 μ diffuser (see Table 5.2). Orifice diameter has been previously shown to have no effect on water velocity at the 2.9 m submergence depth (5.3.3). This conclusion is supported by the No Treatment velocity data in Table 4.49, which shows similar water velocities for the 140 μ and 800 μ diffusers at 2.9 m diffuser submergence. However, as shown in Table 5.2, some of the *in situ* modifications with the 800 μ diffuser showed lower velocities than with the 140 μ diffuser. The magnitude of the reduction in velocity with the 800 μ diffuser treatment, relative to the 140 μ diffuser treatment, is shown in Table 5.4. Given the standard error of the velocity data Table 4.49, the DBCA treatment showed the least difference. As previously discussed, the larger bubble size generated by the 800 μ diffusers would cause increased upward velocity in the DBCA zone in the outlet tube, which decreased water velocity relative to the 140 u diffuser treatment.

Table 5.4. Decrease in water velocity with the 800 μ diffusers as compared to 140 μ diffusers on air for the full lift *in situ* modification treatments (from Table 5.2).

Full lift treatment	Decrease in velocity with 800 μ diffuser relative to 140 μ diffuser (cm sec^{-1})
None	2.0
Cover	7.2
Screen	5.2
DBCA	2.2
Vanes	4.3

The reduction in velocity caused by the Vanes and Screen treatments with the 800 μ diffuser was likely a result of some of the smaller bubbles generated by the 140 μ diffuser passing through the screen or rotating blades without striking the mesh screen or blades and fragmenting. Many large bubbles could be seen colliding with the mesh screen and vanes with the 800 μ diffuser, and this likely slowed velocity relative to the 140 μ treatment, both of which were slower than No Treatment. The explanation for the greater decrease in velocity caused by the 800 μ diffuser with the Cover treatment is not apparent.

5.4.3 Bubble Size

The effect of the various *in situ* treatments on bubble size has already been discussed in detail. The bubble size data shows a clear distinction between DBCA bubble size, and bubble sizes generated by the Screen and Vane treatments (bubble size was not collected for the Cover treatment) (Table 4.64 and 4.65). The EQD was significantly smaller with the DBCA treatment, as the fine pore diffuser in the separator box used to create the DBCA effect had a rated pore diameter of 2 μ. Scanning Electron Microscope (SEM) imaging of this diffuser confirmed the pore size was considerably smaller than the 140 μ diameter diffuser, and it was effective at

generating demonstrably smaller bubbles when operated within the gas flow range recommended by the manufacturer.

The size of a bubble formed at low gas flow rates, as they emerge from a single orifice, is the result of a balance between the buoyant force of the bubble and the surface tension attracting the bubble to the diffuser orifice. An individual bubble increases in size until its buoyancy exceeds the surface tension forces, and it then detaches itself (Bowers, 1955). At low gas flow rates, bubbles tend to emerge in single formation, with a relatively constant diameter of approx. eleven times the orifice diameter (Haney, 1954). However, as gas flow rates increase, single bubbles cannot carry the gas away quickly enough so the bubbles become larger and leave the orifice in the form of a chain, with adjacent bubbles just touching (Bowers, 1955). The gas flow rate at which chain formation occurs is known as the critical point, above which bubble size becomes dependent on gas flow rate and independent of orifice diameter. Bowers (1955) describes the mathematical derivation of the critical gas flow point for various sized bubbles. The mean bubble diameter produced within the range of gas flow rates typically used in aeration practice is an exponential function of the gas flow rate, with the exponent n varying from 0.10 to 0.44 (Eckenfelder, 1959):

(5.6) $$d_b \sim G_s^n$$

where:

d_b = mean bubble diameter;

G_s^n = gas flow rate.

Visual observations of bubble formation for the diffusers used in these experiments indicated bubbles emerged in chain formation, so the gas flow rate per orifice was above the critical flow

rate for single bubble formation. As a result, bubble size was dependent on gas flow rate, and

the resulting bubble sizes were not markedly different for the 140 μ, 400 μ and 800 μ diffusers.

Bubble size was smaller, statistically and visually, with the DBCA configuration, because of the

extremely small orifice diameter of the Point Four diffuser (i.e., 2 μ), and the nature of the

counter-current effect (which tended to maintain the original bubble size and reduce bubble

coalescence relative to the co-current flow pattern). Markofsky (1976) observed a similar effect

with 90 μ and 180 μ porous diffusers, and concluded at the experimental gas flow rates he was

using, there was no significant difference in oxygen transfer efficiency between the two orifice

diameters.

Given the competing effects of large and small bubbles on rise velocity, contact time, K_L and

interfacial area, is there an optimum bubble size which provides the highest overall oxygen

transfer coefficient? An examination of a bubble rise velocity vs. equivalent bubble diameter

curve (Figure 5.2, from Barnhart, 1969) reveals a distinct pattern and the answer to this ques-

tion. Initially, bubble velocity increases linearly with increasing size, to a local maximum

VELOCITY OF AIR BUBBLES IN WATER AT 20° C
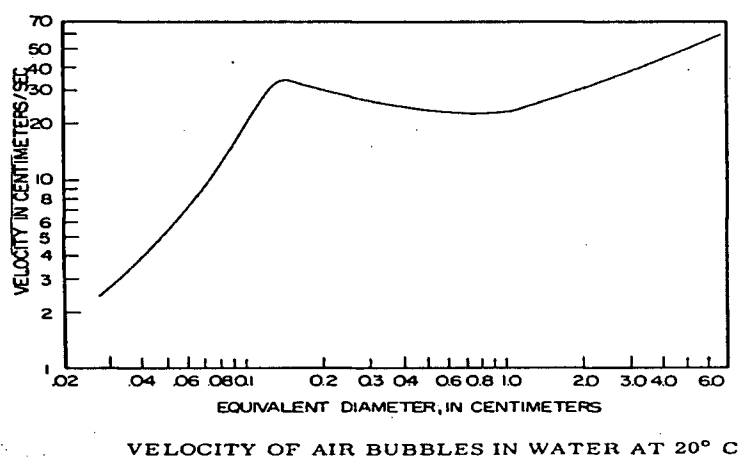
Figure 5.2   **Graph of bubble rise velocity vs. radius of equivalent spherical bubble (from Barnhart, 1969).**

velocity, in water, of ~35 cm sec^{-1} for single bubbles of 1.2-1.4 mm diameter (Haney, 1954). Bubble velocity then decreases from 1.4 mm to 6 mm before increasing again with bubble diameter. The characteristic shape of the curve is due to interactions between hydrodynamic, viscous and interfacial forces acting on the bubbles (Haberman, and Morton, 1954). Small bubbles assume a spherical shape, as surface tension reduces the surface area to a minimum for a given volume. This spherical shape dictates that small bubbles rise according to Stoke's Law, and the viscosity of the liquid is the most important parameter influencing their rise velocity.

As bubble size increase, the viscous and hydrodynamic forces acting on the bubble become more dominant, and flattening of the bubble occurs. This results in an oblate spheroid shape, which has a higher drag coefficient than a sphere of the same volume. The rise velocity decreases accordingly, and the bubbles rise with a rectilinear rocking motion (Eckenfelder, 1959). As bubble size continues to increase, the viscous and surface tension forces become small relative to hydrodynamic forces and the bubble assumes a spheroid cap shape. The upper surface of these bubbles is essentially spherical, and they rise independently of the properties of the liquid (Haberman and Morton, 1954).

An examination of a liquid film coefficient (i.e., K_L) vs. bubble diameter graph reveals that K_L increases rapidly to a peak at 2-2.5 mm diameter, then gradual declines with increasing bubble size (Figure 5.3, from Barnhart, 1969). A plot of surface area vs. bubble volume results in an exponential decay type of curve (Figure 5.4). The net result of these interacting effects is a $K_L a$ response curve similar to the K_L vs. bubble diameter relationship. The $K_L a$ increases sharply to a peak at 2.0-2.5 mm diameter, then declines exponentially with increasing bubble diameter
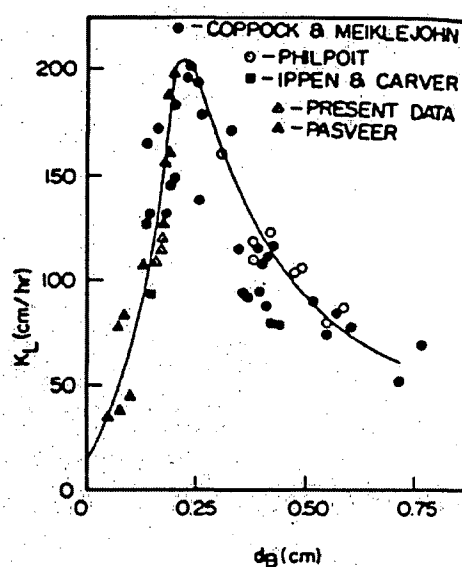
RELATIONSHIP
BETWEEN LIQUID
FILM COEFFICIENT
AND BUBBLE DIAME-
TER

Figure 5.3   Graph of K_L vs. bubble diameter (all data and graph from Barnhart, 1969).
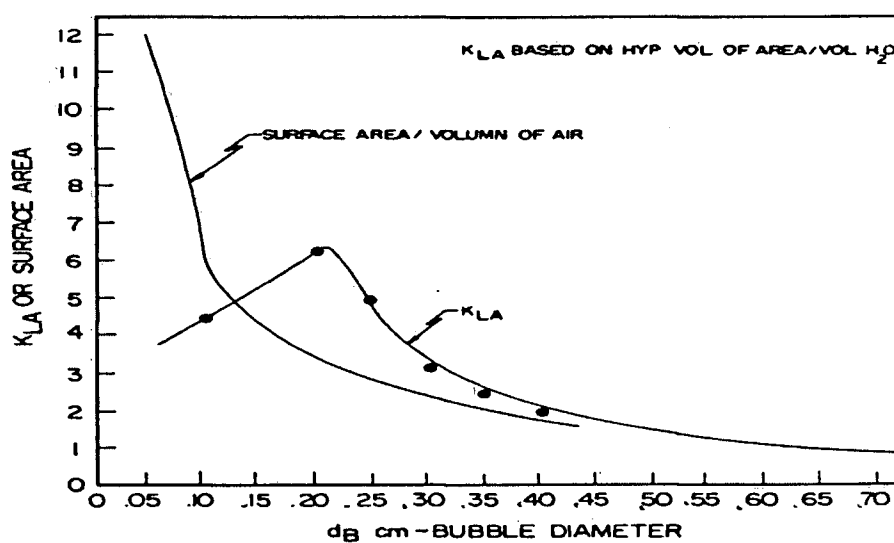
EFFECT OF BUBBLE SIZE ON MASS TRANSFER

Figure 5.4   Graph of $K_L a$ vs. bubble diameter (from Barnhart, 1969).

(Figure 5.5, from Barnhart, 1969). Therefore, the optimum bubble size required to maximize $K_L a$ is 2.0-2.5 mm diameter.

This confirms that the bubble sizes generated by the 140 μ, 400 μ and 800 μ diffuser were slightly larger than the optimum size (see Tables 4.53, 4.54 and 4.55); however, the DBCA configuration generated bubbles in the correct size range (see Tables 4.56 and 4.57). Eckenfelder and Ford (1968) state that silicon dioxide, aluminum oxide and Saran diffusers generally produce bubble in the 2.0-2.5 mm ranges when operated at optimal gas flow rates, which explains why these diffusers are consider so efficient at oxygen transfer. However, Downing (1966) states ".... That practical difficulties, such as the clogging of orifices of air diffusers, limit the smallest size of bubble that it is feasible to produce by air diffusers alone, to a diameter of about 2-3 mm." Therefore, the lower limit of practical bubble size formation from ceramic diffusers with appropriate gas flow rates is also the optimum size for oxygen transfer.

5.4.4   Orifice Diameter and Oxygen Partial Pressure

The effect of orifice diameter and oxygen partial pressure (Table 4.31 and 4.32) on $K_L a_{20}$, SOTR, SAE and SOTE were similar to the effects observed in the Group 1 to 6 results, and will not be discussed further.

5.4.5   Group 7 to 14 Summary

The Group 7 to 14 tests illustrated several additional aspects of gas transfer. All of the *in situ* modifications treatment exerted a negative effect on $K_L a_{20}$, SOTR, SAE and SOTE. The general trend was that the No Treatment showed the highest values of $K_L a_{20}$, SOTR, SAE and SOTE (1st ranking), the Vanes and DBCA treatments were in the middle range (2nd and 3rd

ranking) and the Screen and Cover treatments had the lowest values (4th and 5th ranking). This was caused by a reduction in water velocity in the full lift aerator due to physical flow restrictions in the inlet tubes (screen mesh, counter-rotating vanes); this restricted the height of the bubble:water plume exiting into the separator box (Cover treatment) and caused an upward buoyant force in the outlet tube (DBCA treatment). The reduction in water velocity by the Vane and DBCA treatments largely accounted for the observed reduction in K_La_{20}, SOTR, SAE and SOTE. In addition to reducing water velocity, the Screen and Cover treatments exerted additional negative effects on K_La_{20}, SOTR, SAE and SOTE, likely by degassing oxygen from the mesh screen and decreasing the transfer of oxygen in the separator box.

As seen in the Group 1 to 6 experiments, K_La_{20} and SOTR responded positively to increased gas flow rates, due to increased interfacial area and turbulence at the liquid interface. SAE and SOTE responded negatively due the reduced ratio of interfacial area and bubble contact time, and the additional energy costs required to compress additional air and PSA O_2. A significant gas flow rate x *in situ* modification interaction was observed for K_La_{20} and SOTR with the 140 μ and 800 μ diffusers, due to the additive effect of gas flow rate on oxygen transfer resulting from additional turbulence and interfacial area. A very noticeable gas flow rate x DBCA treatment interaction effect occurred on SAE and SOTE with the 800 μ diffuser, and marginally with the 140 μ diffuser, due to velocity related destabilisation of the DBCA zone in the outlet tube and increasing energy costs associated with the higher gas flow rates.

Water velocity with the 800 μ diffuser was slower than with the 140 μ diffuser, due to increased upward velocity in the DBCA zone in the outlet tube (DBCA treatment) and increased collisions with the mesh screen and vanes (Screen and Vane treatments). Bubble sizes created by the

DBCA configuration were significantly smaller than the Screen and Vane treatments, due to the 2 μ fine pore diffuser used to create the DBCA effect. The effect of reduced orifice diameter, and increased oxygen partial pressure, exerted similar effects on K_La_{20}, SOTR, SAE and SOTE, as seen in the Group 1 to 6 experiments.

5.5   Miscellaneous Tests

5.5.1   Pump Only Tests

The Pump Only full lift tests in DBCA mode were conducted as curiosity driven research, to determine if there was any advantage to operating a full lift hypolimnetic aerator using circulating water pumps as the prime mover of the system, rather than air lift pumps. The results were quite interesting as the mean values for K_La_{20}, SOTR and SAE were among the lowest recorded for any of the full lift tests; whereas, the mean SOTE values were among the highest recorded (Table 4.43). The low values of K_La_{20} and SOTR were related to the low gas flow rate (i.e., 3 l min^{-1}) used in these experiments, which were ~1/3 of the gas flow rates used in the lowest gas flow setting for the Group 7 DBCA tests (i.e., 7/3 l min-1) or the Group 1 tests (i.e., 10 l min^{-1}).

If one multiplies the K_La_{20}, SOTR and SAE values from the Pump Only tests by 3.3 (i.e., 10/3) to standardize the gas flow rates, the hypothetical results, for K_La_{20} and SOTR on air or PSA O_2, appear more efficient per unit gas flow than the DBCA values from the Group 7 tests (Table 4.44) or the Group 1 tests (Table 5.5).

However, when one considers the SAE comparison in Table 5.5, the hypothetical Pump Only SAE values on air were only ~7-8% of those recorded during the Group 7 and Group 1 tests.

Table 5.5. **Hypothetical comparison of Pump only, Group 7 and Group 1 values.**

Parameter	Pump only value	Pump only x 3.3	Group 7:7/3 l min^{-1} DBCA Mode	Group 1: 10 l min^{-1}
K_La_{20} Air (hr^{-1})	0.6	2.0	1.5	1.5
SOTR Air (g O_2 hr^{-1})	6.2	20.7	15.8	16.0
SAE Air (g O_2 kWhr^{-1})	8.0	26.7	359.3	349.4
K_La_{20} PSA O_2 (hr^{-1})	2.7	9.0	7.1	8.4
SOTR PSA O_2 (g O_2 hr^{-1})	29.6	98.7	77.3	91.6
SAE PSA O_2 (g O_2 kWhr^{-1})	28.4	94.7	77.1	89.1

The hypothetical SAE values on PSA O_2 were greater than those recorded during the Group1 and Group 7 tests. The explanation for this discrepancy is that the actual SAE values obtained during the Group1 and 7 tests, on air, used considerably less energy to compress and deliver the air, than was required to operate the circulating pumps in the hypothetical standardized Pump Only SAE comparison. In contrast, due to the higher energy requirements of PSA O_2 generation, the hypothetical SAE values for the Pump Only tests, on PSA O_2, were greater than the actual values recorded during the Group 1 and 7 tests, as the circulating pumps used less energy than PSA generated oxygen.

This hypothetical comparison, and the fact that the SOTE values recorded during the Pump Only tests were quite high, indicate that a Pump Only configuration may be a reasonable option if one wishes to design a system that is high in SOTE at the expense of reduced SAE performance. As will be discussed in the next section, a Pump Only configuration, with low oxygen flow rates, high pump energy requirements, and a co-current downflow pattern, is the basis of a DBCA system, and is analogous to a rudimentary Speece Cone, which is discussed in Section 5.6.

5.5.2   Extended Aeration Tests

The extended aeration tests were conducted to determine if the calculated oxygen saturation for each test day bore any relation to an actual oxygen saturation value obtained after an extended period of operation. The results from these two tests, admittedly a small sample size, indicate the oxygen saturation achieved after 247 to 270 minutes of operation on air was within 3% of the calculated value (Table 4.45). This indicates that the procedure used to determine the oxygen saturation for each test day (3.2.2) provided a reasonably accurate estimate of oxygen saturation for this series of tests.

The extended aeration on PSA O_2 was primarily curiosity driven research, to determine how much oxygen could be dissolved into the test water using PSA O_2. The highest oxygen concentration achieved on PSA oxygen was 50.4 mg l^{-1} or 446% saturation after 206 minutes of operation, thus exceeding the C^*_s for the day for air (i.e., 103.2 %) by a ratio of 4.33 (Table 4.45). At this concentration the water appeared milky and the entire surface of the tank was effervescing, as oxygen was degassing from the surface, and no further tests were run.

5.6   Speece Cone

Note: since the Speece Cone in these experiments was improperly designed, the following statements apply only to the experimental system. Due to the interrelation between oxygen flow rates and discharge velocity, and the use of different statistical approaches to analyze the data (i.e., Analysis I and II), both oxygen flow rate and water discharge velocity treatments are discussed together, rather than separately as in the Full Lift discussion sections.

5.6.1   Oxygen Flow Rate and Discharge Velocity

The oxygen flow rate and discharge velocity treatments exerted a significant effect on K_La_{20} and SOTR, with both units of measure showing positive responses to increased oxygen flow rate and discharge velocity. K_La_{20} and SOTR increased with oxygen flow rate, as more oxygen was being introduced into the Speece Cone; hence, a larger deficit of driving force (C_i-C_L) was available, resulting in more oxygen transfer. In addition, the higher oxygen flow rates created more bubbles in the Speece Cone and more interfacial area was available for oxygen transfer, and K_La_{20} and SOTR responded accordingly. The increased discharge velocity influenced K_La_{20} and SOTR by creating more turbulence inside the Speece Cone, thereby increasing K_L.

The effect of oxygen flow rate and discharge velocity on SAE depended on which analytical method was used. Analysis I indicated there was no effect of oxygen flow rate on SAE. This result was caused by the differential response of the 1 l min^{-1} flow rate, which was independent of flow, whereas SAE responded positively with the 2 and 3 l min^{-1} flow rates (Figure 4.68c). Analysis II indicated SAE increased with oxygen flow rates, as the 1 l min-1 treatment was deleted, and the 60 and 70 cm sec^{-1} discharge velocities were included. It is at these two higher velocities that the effect of the gas flow rates starts to diverge, hence the treatment effect becomes statistically significant.

The effect of discharge velocity on SAE also differed according to which analytical approach was used. Analysis I indicated SAE increased with discharge velocity, whereas Analysis II indicated discharge velocity had no effect of SAE. Since Analysis II linearized the gas flow rate by discharge velocity interaction effect, it has more credibility. The explanation for the response is that the additional water pump energy required to provide the higher discharge veloci-

ties offset the additional dissolved oxygen gained by the greater turbulence inside the Speece Cone. In addition, since increased discharge rates would act to decrease residence time in the Speece Cone, bubble:water contact time would decrease, which would also act to nullify any gains in SAE resulting from increased discharge velocity.

SOTE increased with water discharge velocity regardless of which analytical method was used. This indicates the additional turbulence caused by the increased discharge velocities more than compensated for the reduced bubble:water contact time in the Speece Cone, and the net result was an increase in SOTE. The additional turbulence likely acted in concert with the higher gas flow rates to increase bubble interfacial area, which would also act to increase SOTE. Analysis I indicated a significant oxygen flow rate by discharge velocity interaction, whereas Analysis II did not, hence the effect is not dominant and depends on which data set is analysed.

SOTE responded negatively to increasing oxygen flow rates in both analyses. The highest SOTE values were recorded with the lowest oxygen flow rates (except at discharge velocities > 50 cm sec^{-1}), and the effect was consistent at all discharge velocities. The highest SOTE value recorded was 63% with the 1 l min^{-1} oxygen flow rate at 50 cm sec^{-1}. This suggests that oxygen flow rates > 1 l min^{-1} were not being fully dissolved inside the Speece Cone, and thus oxygen gas was being wasted. Oxygen bubbles could been seen leaving the discharge port of the Speece Cone under higher gas flow rates. This is another example of the difficulty in optimising gas transfer with competing units of measure. The highest SOTE of 63% was an artifact of inadequate inlet velocity which could not prevent the bubble swarm from collapsing. Properly designed Speece Cones should achieve > 98% oxygen absorption efficiency (pers. Comm, Dr. Richard Speece, Vanderbuilt University).

The explanation for the precipitous decline in SOTE at low oxygen flow rates and discharge velocities > 50 cm sec^{-1} (Figure 4.73) is the same effect that was observed with the DBCA configuration in 5.4.1. Discharge velocities > 50 cm sec^{-1} destabilised the bubble swarm in the Speece Cone, and forced the oxygen bubbles out the discharge port, thus collapsing the DBCA effect and triggering the precipitous decline in SOTE (and K_La_{20}, SOTR and SAE). At oxygen flow rates > 1 l min^{-1}, there was sufficient positive buoyancy inside the Speece Cone from the additional oxygen bubbles such that discharge velocities > 50 cm sec^{-1} were not able to purge the bubble swarm. Therefore, the DBCA effect was not destabilised and was able to exchange oxygen, with SOTE values exceeding those recorded at lower discharge velocities (even though many excess oxygen bubbles were purged from the Speece Cone by the higher discharge velocities). The additional turbulence, increased C_i-C_L and greater interfacial bubble area created by the higher discharge velocities more than compensated for the increased wasting of the air bubbles, and continued to increase SOTE. Operationally, this would present a problem as the mass wasting of bubbles may destratify a lake or reservoir. For this reason, full size Speece Cones must have bubble collector hoods located downstream of the main cone, to collect stray bubbles and vent them to the surface through a discharge pipe, to avoid unintentional destratification. Properly designed Speece Cones should discharge very few excess bubbles.

5.6.2 Speece Cone on Air

The single test of the Speece Cone on air was curiosity motivated research, basically to see what type of performance was possible on air, with an oxygenation system designed to operate on oxygen. The results of the air test were lower than any recorded on PSA oxygen for K_La_{20}, SOTR, SAE and SOTE (see Table 4.73). It is not possible to directly compare the performance

of the Speece Cone on air with the full lift tests, as the maximum air flow rate to the Speece

Cone was ~1/3 of the minimum air flow rate to the full lift aerator. However, it is instructive to

compare the relative performance of the Speece Cone on air at 3 l min^{-1} and 50 cm sec^{-1}, with

the nearest analogue in the full lift configuration to demonstrate the relative difference in

performance. In this case, the full lift treatment which crudely approximated a Speece Cone

was the Group 8 configuration (i.e., 800 μ diffuser, 2.9 m diffuser submergence) full lift DBCA

test, running on air with a 7/3 l min^{-1} split between the main diffuser and the separator box

diffuser (Table 5.6)

Table 5.6. Adjusted least square treatment means ($\pm$ SE) comparison between Speece Cone on air at 3 l min^{-1} and 50 cm sec^{-1}, with the Group 8 (i.e., 800 μ diffuser, 2.9 m diffuser submergence) full lift DBCA test, running on air with a 7/3 l min^{-1} allocation between main and separator box diffuser.

Treatment	K_La_{20} (hr^{-1})	SOTR (g O_2 hr^{-1})	SAE (g O_2 kWhr^{-1})	SOTE (%)	N
3 l min^{-1} air at 50 cm sec^{-1} Speece	1.2 (0.01)	13.4 (0.04)	16.9 (0.05)	24.5 (0.08)	4
7/3 l min^{-1} air Full Lift	0.88 (0.06)	9.6 (0.66)	210.2 (14.49)	5.10 (0.35)	3

The comparison indicates that even at the 1/3 the air flow rate being delivered to the full lift

aerator, the Speece Cone on air delivered superior performance for K_La_{20}, SOTR, and particu-

larly SOTE. The SAE performance was very low, as the higher energy cost required to operate

the water pump penalized this key energy related unit of measure. The relative performance of

the Speece Cone on air was therefore similar to its performance on oxygen: good K_La_{20} and

SOTR response, low SAE performance, and very good SOTE. For this aeration system, the two

most important units of measure for comparing aeration systems (SAE and SOTE) were in

contrast to each other, demonstrating the paradox of optimizing oxygen transfer. In practice, a

Speece Cone would rarely be operated on air as this would forfeit the higher performance available on oxygen; there would also be concerns about nitrogen supersaturation causing fish mortalities, particularly in salmonids (Rucker, 1972).

5.6.3   Speece Cone Summary

K_La_{20} and SOTR responded positively to increased oxygen flow rate and discharge velocity, due to a larger deficit of driving force (C_i-C_L), greater interfacial area and more turbulence inside the Speece Cone. The SAE response depended on which analytical approach was used; however, the general conclusion was that oxygen flow rates > 1 l min^{-1} increased SAE.

SAE appeared to be independent of discharge velocity as the higher pump energy costs nullified any gain in SAE. SOTE was positively influenced by discharge velocity, as the additional internal turbulence and interfacial area compensated for the reduced bubble:water contact time. SOTE was negatively influenced by oxygen flow rates, as the highest SOTE values were recorded with the lowest oxygen flow rates (except at discharge velocities > 50 cm sec^{-1}). SOTE declined precipitously at oxygen flow rates < 1 l min^{-1} and discharge velocities > 50 cm sec^{-1}, as the DBCA bubble swarm in the Speece Cone was destabilised, and forced out the discharge port. Full size Speece Cones must have bubble harvesters to collect stray bubbles and prevent unintentional destratification. A single test on air revealed significantly reduced performance relative to an equivalent flow rate of oxygen. However, even on air, the Speece Cone delivered superior K_La_{20}, SOTR, and particularly SOTE performance, when compared with a full lift aerator operating on 10 l min^{-1} air at the same diffuser depth. In practice, a Speece Cone would rarely be operated on air, for reasons outlined previously.

5.7 Comparison of Relative Performance of Full Lift vs. Speece Cone

As previously stated, direct comparisons between the performance of the Full Lift and Speece

Cone systems are not possible, as they were not operated at comparable gas flow rates or

oxygen partial pressures. In addition, the Speece Cone was not properly scaled-down; hence the

performance of the experimental Speece Cone was less than optimal. The design principle of a

Speece Cone is to provide a downward water velocity of ~305 cm sec^{-1} at the top of the cone.

This high velocity prevents bubbles from escaping out the top of the cone, and the high velocity

inlet stream provides the turbulence to maintain the bubble swarm in a dynamically regenerated

state, with an exceptionally high gas surface to water volume ratio; this favors high oxygen

transfer rates (Speece, 1992). As the cross sectional area of the Speece Cone increases, the net

downward velocity of the water decreases to a design velocity of ~ 9 cm sec^{-1} near the outlet of

the cone. Since the buoyant velocity of smaller bubbles is ~ 35 cm sec^{-1} (see Figure 5.2), the

oxygen bubbles are maintained in contact with the water inside the Speece Cone indefinitely. In

addition, the relative volumetric flow ratio of oxygen to water should be about 3%, to efficiently

dissolve oxygen (Speece, 1992).

The Speece Cone used in these experiments did not have sufficient velocity at the top of the

cone, and the cross sectional velocity at the base of the cone was too low (Table 5.7). As a

result, the dynamic bubble swarm never properly developed inside the cone, but remained as a

gas pocket at the top of the cone that the inlet water dropped through, resulting in a drastically

reduced gas surface area to water ratio. Therefore, all of the performance measures from this

experimental Speece Cone are much lower than would be expected with the correct inlet

velocity of 305 cm sec^{-1} and correct cross sectional velocity at the base of the cone.

Table 5.7.   Comparison of experimental Speece Cone inlet water velocities and oxygen water ratios to design specifications.

Inlet water velocity (cm sec^{-1})	Water flow (l min^{-1})	Oxygen flow (l min^{-1})	Base cross-sectional velocity (cm sec^{-1})	O_2:water ratio (%)
20	38	1 to 3	0.7	2.6 - 7.9
30	57	1 to 3	1.0	1.8 – 5.3
40	76	1 to 3	1.4	1.3 – 3.9
50	95	1 to 3	1.7	1.1 – 3.2
60	114	1 to 3	2.1	0.9 – 2.6
70	133	1 to 3	2.4	0.8 – 2.3
305 (design velocity			9 (design velocity)	3 (design ratio)

However, relative comparisons, qualitative in nature, are instructive for examining the oxygenation performance of the two systems; it must be realized that the oxygenation performance of the Speece Cone was much lower than expected, due to inlet water velocities that were too low. In these experiments, the most comparable data sets are those of the Speece Cone on PSA oxygen at 1 or 3 l min^{-1} and a discharge velocity of 50 cm sec^{-1}, with the Group 2 full lift tests, on air or PSA oxygen at 10 l min^{-1} with an 800 µ diffuser (Table 5.8). (Note: the inlet velocity in the Speece Cone is equivalent to the discharge velocity, as the diameter of the inlet and outlet piping was similar, i.e., 6.35 cm).

Table 5.8.   Adjusted least square treatment means (± SE) comparison between Speece Cone on PSA O_2 at 1 and 3 l min^{-1} and 50 cm sec^{-1}, with the Group 2 (i.e., 800 µ diffuser, 2.9 m diffuser submergence) full lift test, on air or PSA O_2.

Treatment	K_La_{20} (hr^{-1})	SOTR (g O_2 hr^{-1})	SAE (g O_2 kWhr^{-1})	SOTE (%)	N
1 l min^{-1} O_2 at 50 cm sec^{-1} Speece	4.6 (0.09)	49.8 (0.98)	55.7 (1.09)	63.4 (1.23)	4
3 l min^{-1} O_2 at 50 cm sec^{-1} Speece	8.7 (0.20)	94.6 (2.14)	86.9 (1.96)	40.1 (0.87)	4
10 l min^{-1} Full Lift on O_2	6.4 (0.55)	69.7 (5.97)	70.63 (6.04)	8.97 (0.67)	3
10 l min^{-1} Full Lift on Air	1.0 (0.03)	11.3 (0.34)	262.2 (7.88)	5.98 (0.18)	3

The data clearly show the different oxygenation capabilities of the two systems. The Speece Cone, at 1 l min^{-1}, delivered K_La_{20}, SOTR and SAE values that were ~70-79% of the Full Lift system operating on oxygen, and 460-480% of the K_La_{20} and SOTR values of the Full Lift system operating on air, but using only 1/10 of the gas flow rate. The Speece Cone response is not linear, as the values at 3 l min^{-1} are not three times that recorded at 1 l min^{-1}. The SAE of the Speece Cone is considerably less then the Full Lift system on air, whereas the SOTE of the Speece Cone is very high at the lowest gas flow rate. The Speece Cone SOTE was still > 40% at the highest gas flow rates, even though it was obvious that considerable oxygen gas was being wasted from the discharge port at the higher gas flow rates.

Therefore, in relative terms, the Speece Cone, at oxygen flow rates between 1 and 3 l min^{-1}, delivered K_La_{20} and SOTR performance comparable to the Full Lift system at 10 l min^{-1} on oxygen, and superior performance to the Full Lift system on air. This indicates the Speece Cone design provides increased interfacial area (i.e., a) and a highly turbulent gas exchange environment (K_L) that facilitate oxygen transfer. The Speece Cone also has the benefit of increasing the oxygen differential (C_i-C_L), as the units are typically located at the lake or reservoir bottom, hence utilizing the ambient hydrostatic pressure to maximize oxygen differential. The most outstanding feature of the Speece Cone design is the SOTE performance, as values > 60% have not been achieved with the full lift design on air or oxygen. This supports the previous conclusion that the DBCA counter-current flow principle of the Speece Cone provides a superior gas transfer environment by enhancing the fundamental aspects of gas transfer (i.e., a, K_L and C_i-C_L).

In these experiments, with an incorrect scale-down, the Achilles heel of the Speece Cone was its SAE performance. Although, the SAE performance of the Speece Cone was comparable to the SAE of the Full Lift system on oxygen, the SAE performance was considerably less than the Full lift design on air. The SAE performance increased significantly as gas flow rate increased from 1 to 3 l min^{-1}; however, the SOTE declined from > 60% to 40% as the gas flow rate exceeded the dissolution rate in the Speece Cone, thus offsetting the improved SAE performance. However, as previously mentioned, the low SAE performance of this Speece Cone was a reflection of this particular design. Given this, two factors contributed to the low SAE performance: (1) the energy cost of PSA oxygen, and (2) the energy cost of pumping water. Since the Speece Cone is designed to operate on oxygen, the energy costs of delivering oxygen to the unit are considerably higher than delivering compressed air. This topic will be discussed in Section 5.10, entitled "PSA Engineering Design Factors Influencing SAE".

The other reason for the reduced SAE performance is the energy costs related to pumping large volumes of water. Unlike the air-lift pump principle of the Full Lift design, which provides oxygen *and* circulates the water, the Speece Cone requires an additional energy input to circulate the water though the mixing chamber and out the diffuser. The combination of the additional energy required for oxygen generation and water circulation result in reduced SAE performance, relative to the Full Lift design on air. Since the systems were not operated at comparable gas flow rates, and the Speece Cone was incorrectly scaled-down, any further comparison of the oxygenation performance of these two designs from this data set becomes hypothetical. This indicates the need for direct experimental evaluation of both designs under equivalent gas flow rates. Nonetheless, even an incorrectly sized Speece Cone delivered

superior oxygenation performance to the full lift design, in most of the performance comparisons.

5.8   Comparison with Civil Engineering Studies

Although numerous engineering studies have examined various aspects of oxygen transfer, relatively few have systematically examined the effect of diffuser depth, orifice diameter, gas flow rate, and oxygen partial pressure on the four standard unit of measure in an experimental system that is comparable in scale to the present study. Fortunately, the Ph.D. work of Mavinic (1973) and subsequent publications (Mavinic and Bewtra, 1974; Mavinic and Bewtra, 1976) show reasonable similarity, such that performance comparisons can be made. Their study examined the effect of diffuser depth, air flow rate, and circulation pattern on K_La_{20}, SOTR, SAE and SOTE (Table 5.9).

The configuration, which was most similar to the present study, was System II, the co-current upflow with no water pump. The Mavinic (1973) study used a coarse bubble diffuser (1,600 μ diameter) at a similar maximum depth (2.7 vs. 2.9 m), with a smaller diameter tube (10 vs. 19.5 cm) and lower air flow rates (2.8-10.7 vs. 10.5-42.1 l min^{-1}). By coincidence, the unit air flow rate was almost identical in both systems. The K_La_{20} and SOTE values obtained from each experimental system were quite similar; indicating the performance of the current system is comparable to other designs. However, the SAE performance obtained from the current study was considerably lower than the Mavinic (1973) study. The explanation is likely related to the compression ratio in the adiabatic compression formula (ASCE, 1992) used to calculate the energy requirements of the system. This current study operated at a higher pressure than would

Table 5.9. Comparison of experimental system of Mavinic (1973) and this study, Full Lift only on air, Groups 1-6.

Parameter	Mavinic System I	Mavinic System II	Mavinic System III	Mavinic System IV	Full lift – Present Study
Diffuser depth (m)	0.6-2.7	0.6-2.7	0.6-2.7	0.6-2.7	1.5, 2.9
Riser diameter (cm)	10	10	10	10	19.5
Orifice diameter (μ)	1,600	1,600	1,600	1,600	140, 400, 800
Air flow rate (l min^{-1})	2.8-10.7	2.8-10.7	2.8-10.7	2.8-10.7	10.5-42.1
Unit air flow rate (l min^{-1} cm^{-2})	0.036-0.136	0.036-0.136	0.036-0.136	0.036-0.136	0.035-0.141
Circulation pattern	Single column	Air, co-current upflow	Air and water pump, counter current flow	Air and water pump, co-current downflow	Air, co-current upflow
Water pump capacity (l sec^{-1})	n/a	6.3	6.3	6.3	n/a
$K_L a_{20}$ (hr^{-1})	7.8-25.3	0.8-2.4	3.2-7.8	3.0-9.9	0.6-4.8
SOTR (g O$_2$ hr^{-1})	n/a	n/a	n/a	n/a	6.8-51.9
SAE (g O$_2$ kWhr^{-1})	1,202-1,655	1,275-2,971	1,759-2,766	861-1,520	125-349
SOTE (%)	0.7-4.0	2.0-4.9	5.8-17.6	7.4-19.0	2.9-8.5

be required to overcome frictional line losses and hydrostatic pressure, hence this penalized the SAE performance of the system. The sensitivity of SAE performance to compression ratios will be discussed in more detail in Section 5.10.

5.9 Linkage to Hypolimnetic Aeration Studies

As best as can be determined, this is the first experimental evaluation of a bench-scale, Full Lift and Speece Cone hypolimnetic aerator; hence there is no published data available on similar

263

bench-scale systems for performance comparison. K_La_{20} and SOTR data for full-scale systems are not obtainable, as lakes or reservoirs have variable hypolimnetic oxygen concentrations and biochemical oxygen demands, and it is not feasible to conduct non steady-state reaeration tests in a lake or reservoir. However, it is possible to use data collected from field measurements to derive preliminary estimates of oxygen transfer and energy efficiency that are analogous to SOTE and SAE.

The data available from the literature show a wide range in aeration efficiency (AE) and transfer efficiency (TE) for full lift and partial lift systems (Table 5.10), although published performance data on the Speece Cone was non-existent. The highest value obtained for a full lift system was from the Wahnbach II system (Bernhardt, 1974), which had an AE of 1.1 kg O_2 kWhr^{-1} and TE

Table 5.10. Estimates of AE and TE from full scale hypolimnetic aeration systems. (Note: AE and TE are not derived from the non steady-state procedure). Speece Cone[1] operated at 22.9 m, and Speece Cone[2] surcharged to equivalent depth of 39.6 m.

Hypolimnetic aerator design	AE (kg O_2 kWhr^{-1})	TE (%)	Influent O_2 concentration (mg l^{-1})	Gas	Reference
Full Lift	0.95	50	< 4	Air	Bernhardt, 1967
Full Lift	0.77	46	0	Air	Fast, 1971
Full Lift	1.10	50	<4	Air	Bernhardt, 1974
Full Lift	0.25	10	0	Air	Hess, 1975
Full Lift	0.32	21	0	Air	Smith et al., 1975
Full Lift	0.32	10	2-7.5	Air	Smith et al., 1975
Full Lift	0.43-0.52	24-28	n/a	Air	Wirth et al., 1975
Full Lift	0.05-0.41	10-49	0.3-4.7	Air	Taggart and McQueen, 1981
Full Lift	0.09	6	0.4-6.7	Air	Ashley, 1983
Full Lift	0.50-0.56	15-17	0.8	Air	Ashley et al., 1987
Partial Lift	0.54	10.6	4	Air	Fast et al., 1975
Speece Cone[1]	3.2	86	n/a	O_2	Speece, 1992
Speece Cone[2]	3.1	100	n/a	O_2	Speece, 1992

of 50%, whereas the lowest performance was an AE of 0.09 kg O_2 kWhr^{-1} and TE of 6% for the Black Lake system (Ashley, 1983). (Note AE and TE indicate units of measure that have not been derived from non steady-state oxygen transfer tests. AE is kg oxygen delivered per hour divided by the nameplate power in kW). One data set was available on a Partial Lift system, which had an AE of 0.54 kg O_2 kWhr^{-1} and TE of 10.6 % (Fast et al., 1975). The information on the Speece Cone was taken from an internal report on the proposed Camanche Reservoir system (Speece, 1992). The design AE of this system is 3.1-3.2 kg O_2 kWhr^{-1} and the TE is 86 to 100%. These values exceed any reported oxygenation values for full lift and partial lift systems by a very wide margin, and illustrate the superior oxygen transfer capabilities of the Speece Cone design.

However, it soon becomes evident that relative comparisons between different studies are of limited value, due to the wide range in environmental and engineering variables capable of influencing oxygen transfer. For example, the concentration of influent oxygen ranged from 0 to 6.7 mg l^{-1}, diffuser submergence varied from 4.6 to 42 m, and some systems were degassing H_2S, which would impart an immediate chemical oxygen demand and negatively influence AE and TE performance. As discussed earlier, the concentration gradient (C_i-C_L) exerts a significant influence on oxygen transfer, as does hydrostatic pressure. Therefore, in order to derive meaningful comparisons between systems, the different designs need to be studied at a bench-scale in a laboratory setting, as in the current study, or examined in the same body of water under similar conditions.

A useful observation from the field studies is that oxygen transfer did not occur uniformly in the full lift systems during ascent through the water column, but the majority of oxygen transfer

occurred in the lower portion of the inlet tubes. The same effect was noted in this study (Section 4.4) as the majority of the oxygen transfer occurred in Zone 1 when diffuser submergence was at 2.9 m, and in Zone 2 when diffuser submergence was at 1.5 m. For example, Bernhardt (1967) noted most oxygen transfer took place in the first 7.3-20.1 m of a 35.9 m bubble rise distance (Table 5.11).

Table 5.11. **Decrease of the oxygen content in influent air at various depths during bubble rise to the surface (from Bernhardt, 1967).**

Test dates	O$_2$ volume in influent air (%)	O$_2$ volume at 36.6 m	O$_2$ volume at 15.2-20.1 m	O$_2$ volume at 0.9 m
8/6/62	20.8	20.4	16.8	16.8
9/3/62	20.8	20.2	16.5	15.8
10/21/62	20.8	20.4	15.5	15.2
Average value	20.8	20.3	16.3	15.9

Smith et al. (1975) observed a similar trend in Mirror Lake, where they measured inlet tube dissolved oxygen concentrations of 0.7 mg l^{-1} at 3.0 m, 2.3 mg l^{-1} at 6.1 m, but no further increase during the remaining 6.1 m ascent to the surface. These observations suggest that although hydrostatic pressure increases the driving force (i.e., C$_i$-C$_L$) for oxygen transfer, additional factors modify the magnitude of the effect of hydrostatic pressure. Speece (1975) suggests that declining hydrostatic pressure, decreasing oxygen content of the rising oxygen bubbles and the additive effect of bubble and water velocity in a co-current upflow system are responsible for this effect. Downing (1966) and Mavinic and Bewtra (1974) indicate that the interstitial liquid rising in a confined column with dense bubble clouds becomes saturated with dissolved oxygen very quickly. This reduces the concentration gradient across the liquid film and increases the resistance to lateral diffusion of oxygen, thus negatively influencing K$_L$. This suggests that for Full Lift designs, a key factor for increasing oxygen transfer performance is to

optimize diffuser design, as the conditions for gas transfer become progressively less favorable once the bubbles detach from the surface of the diffuser and ascend through the water column.

An examination of bubble formation behavior, in which there are three distinct phases with three different rates of gas transfer, lends support to this conclusion. The first phase occurs during bubble formation at the interstitial space or orifice openings of the diffuser. During formation and growth of the bubble, the liquid-gas interface surrounding the bubble is continually expanding and the concentration gradient in the liquid film remains high, resulting in an unusually high rate of oxygen transfer (Ippen and Carver, 1954). In the second stage, known as the intermediate steady-state, the concentration gradients in the surrounding liquid film attain lower values, hence a reduced transfer of oxygen occurs during the bubble's ascent through the water column. This phase is subject to deviations from the steady-sate, depending on shear and turbulence in the water column (Mancy and Okun, 1960). In the final phase, the bubble bursts when it reaches the surface and releases its gas contents to the surface. The liquid film that surrounded the bubble and contained relatively high concentrations of dissolved oxygen is left behind, and the disturbance of the interface by the bursting bubbles tends to enhance oxygen exchange with the atmosphere at this stage. Therefore, the increase in transfer efficiency arising from smaller orifices occurs during the bubble formation stage, prior to the bubbles coalescing into a heterogeneous mixture. Although the period of bubble formation is quite brief, it is sufficient to allow for increased oxygen transfer. Pasveer (1955) states that the liquid film becomes saturated with oxygen in a time span of 1×10^{-7} seconds, which is considerably faster than the time required for bubble formation. As noted in Section 5.5.3, the overall effect of a decrease in orifice diameter was an increase in all units of measure. Therefore, as demonstrated

in these experiments, one area by which full lift hypolimnetic aeration systems can increase

their oxygenation performance is by using diffusers with pore diameters of ~140 μ.

Since oxygen transfer in co-current full lift designs is limited by declining hydrostatic pressure,

decreasing oxygen content of the rising oxygen bubbles and the additive effect of bubble and

water velocity, a highly efficient diffuser is an important design consideration for full lift

systems.

5.10   PSA Engineering Design Factors Influencing SAE

The effect of PSA oxygen on full lift K_La_{20} and SOTR performance, relative to air, was quite

spectacular (Section 5.3.2); however, SAE performance was penalized by the additional energy

requirements of the PSA process. As previously indicated, a variety of factors in addition to

oxygen partial pressure influenced the standard aeration efficiency (SAE) of the experimental

full lift system (gas flow rate, diffuser depth and orifice size). However, there are at least two

engineering design factors external to the oxygen transfer process which are key to improving

the SAE of aeration systems using PSA generated oxygen. These include (1) PSA oxygen

recovery efficiency and (2) the feed air pressure requirements of the PSA system.

If one examines the air input/oxygen output ratios and resulting oxygen recovery efficiencies of

PSA units manufactured by Oxygen Generating Systems Inc. (Niagara Falls, New York), a clear

trend emerges. The air input/oxygen output ratio decreases and the oxygen recovery efficiency

increases from 31.1% to 46% as the units increase in capacity from their Model OG 25 to the

OG 1000 (Table 5.12).

Table 5.12. Air input/oxygen output ratio and oxygen recovery efficiencies of selected OGSI Inc. PSA units.

Model No.	Feed air	O_2 output	Air input/O_2 Output ratio	O_2 recovery efficiency
	$Nm^3\ hr^{-1}$	$Nm^3\ hr^{-1}$		%
OG 25	10.2	0.7	15.5	31.3
OG 50	19.2	1.3	14.8	32.7
OG 75	27.0	2.0	13.5	35.8
OG 100	34.8	2.6	13.4	36.1
OG 175	50.4	4.6	11.0	44.1
OG 250	70.8	6.6	10.7	45.0
OG 500	138.6	13.1	10.6	45.7
OG 750	210.0	19.7	10.7	45.3
OG 1000	276.0	26.3	10.5	46.0

PSA systems cannot be 100% efficient, as every nitrogen molecule in the feed air does not contact with a molecular sieve particle, and pressurized dry oxygen generated via the PSA process is required to purge saturated nitrogen from the sieves on each depressurization cycle. This oxygen is lost from the process, which places a theoretical, and practical upper limit on the oxygen recovery efficiency of PSA technology.

The efficiency of the PSA units increases with unit capacity, as smaller PSA units are not designed solely for optimum oxygen recovery efficiency. The most important aspect of small units is that they produce oxygen for a given application within a cost effective design package. Since their energy use is small, less design attention is focused on optimizing oxygen recovery efficiency. However, when unit capacity increases, energy costs and oxygen recovery efficiency become significant operational concerns and the design of the PSA systems is modified to recover as much oxygen as possible (pers. comm., Joe McMahon, OGSI, Chief Engineer, Niagara Falls, NY). For example, the small OGSI system (OG 25) is 31% efficient at recovering oxygen, whereas the largest unit (OG 1000) is 46% efficient (Table 5.12). This is achieved

by increasing the density of the molecular sieve beds, optimizing the sieve surface area to air

contact ratio, and other proprietary design features.

An example of the importance of proprietary design features can be seen by comparing the air

input/oxygen output ratio and oxygen recovery efficiency of similar sized PSA units from

different manufacturers. Both systems shown in Table 5.13 deliver identical amounts of oxygen

at similar purity and air feed pressure (i.e., 90-95% O_2 @ 6.3 kg cm^{-2}); however, air in-

put/oxygen output ratio and oxygen recovery efficiency differ by 19%.

Table 5.13. **Performance comparison of equivalent capacity PSA systems.**

Model No.	Feed air	O_2 output	Air input/O_2 Output ratio	O_2 recovery efficiency
	Nm^3/hr	Nm^3/hr		%
AirSep 1000	328.2	26.29	12.5	38.7
OGSI 1000	276.0	26.30	10.5	46.0

One can then examine the effect of variable PSA oxygen recovery efficiency on the SAE of a

given aeration system. The calculated improvement is a direct result of the reduced weight of

air used in the standard adiabatic compression formula, which determines the energy component

of SAE. For example, the mean SAE from each gas flow rate in the Group 1 PSA oxygen full

lift experiments was re-calculated using the range of oxygen recovery efficiencies listed in

Table 5.12. The results illustrate that the SAE increases in direct proportion to the oxygen

recovery efficiency, and that significant improvements (i.e., 46%) in SAE can be expected when

using larger capacity PSA systems (Table 5.14).

Table 5.14.   Calculated effect of variable PSA oxygen recovery efficiency on Group 1 Full Lift SAE performance.

Air input/O_2 Output ratio	O_2 recovery efficiency	SAE (g O_2 kWh^{-1})	SAE (g O_2 kWh^{-1})	SAE (g O_2kWh^{-1})	SAE (g O_2 kWh^{-1})
	%	@ 10 l min^{-1}	@ 20 l min^{-1}	@ 30 l min^{-1}	@ 40 l min^{-1}
15.5	31.3	91.3	89.1	79.6	65.1
14.8	32.7	95.6	93.3	83.3	68.2
13.5	35.8	104.6	102.2	91.3	74.8
13.4	36.1	105.4	103.0	91.9	75.3
11.0	44.1	127.8	125.1	111.8	91.7
10.7	45.0	131.3	128.6	115.0	94.2
10.6	45.7	132.5	129.8	116.0	95.1
10.7	45.3	131.3	128.6	115.0	94.2
10.5	46.0	133.8	131.0	117.1	96.0

The pressure requirements of the PSA generator also significantly influences the SAE of a hypolimnetic aeration system as a result of the energy required for feed air compression. One can use this information to examine the theoretical effect of reduced PSA feed air compression ratios on the SAE of a given aeration system. The calculated improvement is a direct result of the reduced compression ratio energy used in the standard adiabatic compression formula (Metcalf and Eddy Inc., 1991). To illustrate, the mean SAE from each flow rate in the Group 1 PSA full lift experiments were re-calculated with compression ratios varying from 6.33 to 0.78 kg cm^{-2}, using three oxygen recovery efficiencies (i.e., 31.3, 36.1 and 46.0%) listed in Table 5.12. The results illustrate that SAE increases dramatically in relation to the feed air compression ratio, and that major improvements in SAE could be achieved by using lower pressure PSA generators (Table 5.15). As discussed in Section 5.8, unnecessarily high compression ratios were likely responsible for the lower SAE performance, on air, of this study relative to the SAE values reported by Mavinic and Bewtra (1976) for their System II co-current upflow configuration.

Table 5.15. Calculated effect of variable PSA feed air compression ratios on Group 1 full lift SAE results using three ranges of PSA oxygen recovery efficiency.

O₂ recovery efficiency %	Feed air pressure kg cm⁻²	SAE (g O₂ kWh⁻¹) @ 10 l min⁻¹	SAE (g O₂ kWh⁻¹) @ 20 l min⁻¹	SAE (g O₂ kWh⁻¹) @ 30 l min⁻¹	SAE (g O₂ kWh⁻¹) @ 40 l min⁻¹
31.3	6.33	91.3	89.1	79.6	65.1
31.3	4.92	104.1	101.7	90.8	74.4
31.3	3.52	124.7	122.1	109.1	89.4
31.3	2.11	166.1	163.1	146.0	119.8
31.3	0.70	309.9	308.5	277.3	228.0
36.1	6.33	105.4	103.0	91.9	75.3
36.1	4.92	120.0	117.4	104.9	86.0
36.1	3.52	143.8	141.0	126.0	103.3
36.1	2.11	191.2	188.3	168.6	138.3
36.1	0.70	355.4	355.2	319.8	263.1
46.0	6.33	133.8	131.0	117.1	96.0
46.0	4.92	152.3	149.4	133.6	109.6
46.0	3.52	182.2	179.2	160.5	131.6
46.0	2.11	241.7	239.1	214.5	176.1
46.0	0.70	445.7	449.2	405.7	334.2

In recognition of these potential efficiency gains, AirSep Corp. manufactures a low pressure PSA system, optimized for energy use, which generates oxygen at 1.05 kg cm⁻². This model is more energy efficient than their standard pressure units, which generate oxygen at 3.16 kg cm⁻², essentially by saving energy during the compression cycle.

A relatively recent development in oxygen generation technology which takes this concept even further is the Vacuum Swing Adsorption process (i.e., VSA), which generates oxygen at 1.55 kg cm⁻² and regenerates the molecular sieve in a mild vacuum (0.52 kg cm⁻²). The rationale for adopting this approach was recognition that the majority of energy costs in standard PSA generators arise from the need to compress large volumes of air at high pressure. By lowering the operating pressure, the entire process becomes more energy efficient. The oxygen recovery efficiency of the molecular sieve is identical to higher pressure units. VSA generating systems

(without pressure boosters) are restricted to low pressure applications; however, this development emphasizes the importance of minimizing energy requirements for the energy efficient oxygenation of water. Therefore, the lower SAE performance on PSA generated oxygen, relative to air, can be substantially improved by utilizing PSA generators with higher recovery efficiencies and lower operating pressures, this enables hypolimnetic aeration systems to provide the highest possible oxygenation performance, without being unnecessarily penalized with reduced Aeration Efficiency (i.e., AE). As will be discussed in the following section, aeration systems are not selected on AE performance alone. The ability to deliver greatly enhanced oxygenation performance on PSA generated oxygen, using full lift or Speece Cone designs, will likely emerge as the key technological advancement in the field of hypolimnetic aeration.

5.11   Comments on Full Scale Application of Full Lift and Speece Cone Systems

One of the most challenging aspects of engineering is the successful transition from bench-scale study to full-scale application. The proper design, installation and operation of hypolimnetic aeration systems are no exception. Given the robustness and consistency of the results obtained in this study, the relative magnitude of the effects should be transferable to full-scale application, within reasonable limits. For example, the relative effects of diffuser orifice diameter, gas flow rate, oxygen partial pressure and diffuser submergence depth on oxygen transfer should be similar in a full-scale full lift system. Similarly, the excellent oxygenation performance of the Speece Cone will occur in full-scale systems, provided that the inlet and outlet water velocities meet realistic design specifications. However, factors that could not be examined at the bench-scale, such as extreme depth, will change the absolute magnitude of some units of measure (i.e., SAE) as a result of the additional energy require to deliver air to greater depths.

A more difficult issue is how to select the most appropriate design of a hypolimnetic aerator for a particular installation. A general guide on destratification and hypolimnetic aeration techniques was published in the ecological literature in the mid 1970's (Lorenzen and Fast, 1977); however, it requires updating given the recent technological developments (e.g., PSA generators and Speece Cone). In addition, there is no counterpart in the civil engineering literature; hence, civil engineers have a minimal amount of information from which to compare and select systems. Companies who actively market hypolimnetic aeration systems, some with more enthusiasm than scientific credibility or engineering expertise, compound this paucity of information. The author has personally adjudicated, on more than one occasion, grievances between suppliers and various levels of government, when commercially purchased hypolimnetic aeration systems failed to deliver their advertised level of oxygenation performance.

How then, given the paucity of comparative information on the subject, does one select an appropriate hypolimnetic aeration system for a particular project? The short answer is that there is no simple answer. Each installation will have different priorities, different infrastructure requirements, and variable amounts of pre-existing data from which to design a system. As has been noted throughout this study, some factors (e.g., orifice diameter) positively influenced all units of measure, while other design factors (e.g., gas flow rate) positively influenced K_La_{20} and SOTR, while negatively influencing SAE and SOTE. Therefore, in each installation, one unit of measure will likely be de-emphasized in order to achieve specified performance targets in another unit of measure. In reality, there are many factors unrelated to gas transfer that play a critical role in system selection. These include obvious factors such as noise level, delivery dates, capital and operating costs, to less quantifiable issues such as esthetics, liability concerns and local politics.

There are at least five steps required to assist in resolving the engineering aspects of system selection:

1. Lab Testing – comparative testing of different designs under similar laboratory conditions (as per this study);

2. Field testing – comparative testing of different designs under actual field conditions with similar conditions of depth, gas flow rate etc.;

3. Developing predictive models – once sufficient comparative laboratory and field information has been collected, the data can be used to quantify the underlying physical processes and develop predictive models that can be evaluated against systems that were not part of the original data set (to avoid circularity of modeling);

4. Reporting the results in engineering journals and conferences – obvious, but necessary to educate engineers unfamiliar with the process, and the extent to which lake and reservoir pre-treatment with hypolimnetic aeration can be a viable alternative to conventional in-plant unit processes to improve raw water quality;

5. Case study reviews of specific installations – although some systems may have gone through an initial screening process, very few installations have been reviewed after a few years of operation to examine the systems' actual performance, and the appropriateness of the original decision. For obvious reasons this will be a difficult task; however, performance audits are particularly useful in reviewing the quality of the original performance specifications and decision making process, and would be beneficial in resolving the engineering aspects of system selection, regardless of successes or failures.

As discussed in Section 2.2, progress is occurring in some of the aforementioned areas, albeit in an uncoordinated fashion. Nonetheless, based on this study, and existing information, a tentative guide to the engineering and limnological suitability of various hypolimnetic aeration designs would be as follows (subject to change with additional information) (Table 5.16).

As expected, there is considerable overlap among the various designs in the selection table, demonstrating that the engineering and limnological selection criteria are quite flexible. In practice, non-engineering and non-limnological site-specific selection criteria will generally determine which system is selected. For example, the City of New York examined the potential for hypolimnetic aeration to improve raw drinking water quality in the Croton Water System,

Table 5.16. General guide to hypolimnetic aeration system selection.

Engineering and limnological scenario	Full Lift hypolimnetic aeration	Partial Lift hypolimnetic aeration	Speece Cone hypolimnetic aeration
Cold water fisheries management	Acceptable on air or oxygen	Acceptable on oxygen	Acceptable on oxygen
Improvement of raw potable water quality	Acceptable on air or oxygen	Acceptable on air or oxygen	Acceptable on oxygen
Hypolimnetic dam discharges from eutrophic reservoirs	Acceptable on air or oxygen	Acceptable on oxygen	Acceptable on oxygen
Hypolimnetic oxygen in lakes < 7 m max. depth	Acceptable on oxygen	Acceptable on oxygen	Acceptable on oxygen
Hypolimnetic aeration in ice-prone areas	Acceptable if submerged or removed during winter	Acceptable on air or oxygen	Acceptable on oxygen
Hypolimnetic aeration in high boat traffic areas	Not recommended due to liability concerns	Acceptable on air or oxygen	Acceptable on oxygen
Hypolimnetic aeration in reservoirs with significant bird populations	Not recommended	Acceptable on air or oxygen	Acceptable on oxygen
Hypolimnetic aeration in esthetically strategic areas	Acceptable depending on esthetic concerns	Acceptable on air or oxygen	Acceptable on oxygen

which is one of three systems (Croton, Catskill and Delaware) that provide drinking water to New York City and upstate communities. The City did not want any floating objects in the reservoir, as it may attract roosting birds, and swimmers, neither of which is desirable in a potable water reservoir. Therefore, a full lift design was not acceptable, and three partial lift hypolimnetic aerators operating on air were selected, based on an assumed daily oxygen input of 1,500 kg. Field testing in the second year of the program revealed the combined input from the

three aerators was 900 kg O_2 day^{-1}, hence the system was undersized, and the reservoir continued to experience significant oxygen depletion and water quality problems. The estimate to oxygenate the entire reservoir with partial lift systems, on air, required an additional 18 aerators, at a cost of $7.2 million (New York City Department of Environmental Protection, 2000). Although not considered, the existing three aerators, on oxygen, likely could have met the required oxygen demand, at a fraction of the cost of the 18 aerator option. Due to liability concerns about oxygen storage, cryogenic oxygen was not acceptable; however, PSA generated oxygen was acceptable, and compatible with the existing infrastructure. Also, a single large Speece Cone, similar to the Camanche Reservoir system, would have easily been able to supply the daily oxygen demand of the reservoir. The various options to improve water quality, including upgrading water treatment plants, are currently under review.

5.12   Future Research Requirements

Future research requirements to advance the field of hypolimnetic aeration should focus on comparative testing of bench-scale and full-scale systems as per the five steps outlined in the preceding section. At this stage, most of the bench-scale research has been completed on full lift hypolimnetic aerators; hence, the laboratory research should focus on examining partial lift systems, and exploring the performance envelope of the Speece Cone. Based on observations from this study, varying the height to width ratio of the Speece Cone should influence the behavior of the bubble swarm inside the cone, and may significantly influence the oxygenation performance. In addition, minimal attention has been directed at optimizing diffuser design in Speece Cones, as oxygen is introduced through a pipe connection near the top of the cone. Given the known effect of diffuser orifice diameter, it may be possible to improve the oxygen transfer within the Speece Cone by using more efficient diffusers. However, since bubble size

in properly designed Speece Cones is a function of the inlet turbulence and is not related to bubble size when injected, this idea may be of marginal use.

In terms of full-scale testing, there is considerable need for additional research. Full-scale comparative testing of the oxygenation performance of full lift, partial lift and Speece Cones in the same body of water under similar conditions (e.g., diffuser depth, gas flow rates, diffuser orifice diameter) would be very informative. As previously indicated, it is not possible to extract comparative performance data from the existing literature due to the wide variation in environmental variables known to influence oxygen transfer. Given the energy requirements of the Speece Cone, a relevant research topic would involve testing of extremely efficient low head pumps to minimize the energy consumption of the main water pump, and further improve the already strong performance of the Speece Cone. Also, as indicated for the bench-scale studies, additional gains in Speece Cone oxygenation performance may be possible by examining the use of fine pore diffusers in the inlet pipe, and considering the use of different aspect ratios to determine if an optimal hydraulic design exists which would enhance oxygen transfer inside the Speece Cone.

Given the energy impact on SAE from standard pressure PSA oxygen generators, a useful area of research to pursue would be processes that reduced the energy costs of generating oxygen. This would include the testing of low pressure PSA generators, including the new Vacuum Swing Adsorption process. In addition, a comparative study of PSA generated oxygen and liquid oxygen (LOX) would be useful, although the high rental cost of cryogenic storage facilities, liability concerns and limited availability in rural areas would likely favor PSA oxygen generation.

Once sufficient laboratory and comparative field data becomes available, it would be useful to develop mathematical models to predict oxygen transfer rates and aerator performance. This process is already underway (Little, 1995); however, it has been hampered by a lack of published experimental data (McGinnis and Little, 1998).

CHAPTER 6: SUMMARY AND CONCLUSIONS

6.1   Full Lift Experiments

6.1.1   Depth Treatment

1.   The diffuser depth treatment exerted a significant effect on KLa_{20}, SOTR, SAE and SOTE, with all units of measure showing positive increases in response to an increase in diffuser submergence;

2.   The depth of gas release influenced KLa_{20}, SOTR and SOTE mainly by an increase in bubble contact time due to the longer path length the bubbles must take to reach the surface, and a larger deficit of driving force (C_i-C_L), resulting in more oxygen transfer;

3.   SAE increased with diffuser submergence, indicating that despite the additional energy required to deliver air or PSA O_2 to greater depths, the energy cost was more than offset by the increased oxygen transfer resulting from the longer bubble contact times, greater turbulence and increased hydrostatic pressure;

4.   Water velocity increased with depth in each experimental treatment;

5. KLa_{20} and SOTR responded positively to increased gas flow rates due to increased turbulence at the liquid interface and interfacial area available for gas transfer to the surrounding medium;

6.   SAE and SOTE responded negatively to increased gas flow rates due to the reduced ratio of interfacial area to bubble volume, reduced contact time between air bubbles in the surrounding liquid and additional energy costs for gas compression;

7.   Water velocity increased significantly with gas flow rate;

8.   The bubble size data did not show any relationship to gas flow rates. The coefficient of variation (CV) was so large that the variance in the data hid any significant effect;

6.1.2   Oxygen Partial Pressure Treatment

9.   Oxygen partial pressure treatment exerted a significant effect on K_La_{20} and SOTR by substantially increasing the driving force (C_i-C_L), resulting in more oxygen transfer per unit bubble contact time;

10.   SOTE was positively influenced by oxygen partial pressure;

11.   SAE response decreased on PSA oxygen, indicating that the energy costs to produce 95% oxygen via PSA technology offset the gains in oxygen transfer;

12. K_La_{20} and SOTR responded positively to increased gas flow rates (see 5);

13.   SAE and SOTE responded negatively to increased gas flow (see 6);

14.   Gas composition had no effect on bubble velocity;

6.1.3   Orifice Diameter Treatment

15.   Orifice diameter exerted a significant effect on K_La_{20}, SOTR, SAE and SOTE. Each unit of measure increased with a decrease in orifice size due to an increase in surface area per unit bubble volume, a decrease in terminal rise velocity, a decrease in the liquid film coefficient and an increase in the total number of bubbles in the water column per unit gas discharge;

16.   Gas flow rate significantly influenced K_La_{20}, SOTR, SAE and SOTE in all of the experimental combinations, with K_La_{20} and SOTR responding positively to increased gas flow rates, and SAE and SOTE decreasing with increased gas flow rate;

17. K_La_{20} and SOTR increased with higher gas flow rates (see 5);

18.   SAE and SOTE responded negatively to increased gas flow rates (see 6);

6.1.4   *In situ* Modifications Treatment

19.   The *in situ* modifications treatment exerted a significant effect on K_La_{20}, SOTR, SAE and SOTE, with all units of measure showing a negative response to the treatments;

20.   The general trend was that the No Treatment option generated the highest values of K_La_{20}, SOTR, SAE and SOTE (1st ranking), the Screen and Cover treatments the lowest values (4th and 5th ranking), and the Vanes and DBCA treatments were in the middle range (2nd and 3rd ranking);

21.   The various *in situ* modifications caused a reduction in water velocity in the full lift aerator by restricting flow either in the inlet tube, the separator box, or the outlet tube;

22.   The Screen and Cover treatments exerted an additional negative effect on K_La_{20}, SOTR, SAE and SOTE. Further analysis is required to determine the factors responsible;

23.   A significant gas flow rate x *in situ* modification interaction was observed for all of the K_La_{20}, SOTR, SAE and SOTE measurements with the 800 μ diffuser, and for the K_La_{20} and SOTR with the 140 μ diffuser;

24.   The K_La_{20} and SOTR interaction is the additive effect of gas flow rate on oxygen transfer, caused by increasing turbulence and interfacial area with each increase in gas flow rate;

25.   The DBCA treatment exhibited quite high SAE and SOTE values at the lowest gas flow rate (i.e., 10 l min^{-1}) but plummeted with increasing gas flow due to destabilisation of the DBCA effect in the outlet tube;

26.   The DBCA treatment generated the smallest bubble sizes;

6.2   Speece Cone

27.   The oxygen flow rate and discharge velocity treatments exerted a significant effect on K_La_{20} and SOTR, with both units of measure showing positive responses to increased oxygen flow rate and discharge velocity;

28. K_La_{20} and SOTR increased with oxygen flow rate due to a larger deficit of driving force (C_i-C_L) and more interfacial area was available for gas inside the Speece Cone;

29.   SAE increased with oxygen flow rates but discharge velocity had no effect of SAE as the additional water pump energy required to provide the higher discharge velocities offset the additional dissolved oxygen gained by the greater turbulence inside the Speece Cone and decreased hydraulic residence time;

30.   SOTE increased with water discharge velocity as additional turbulence caused by the increased discharge velocities compensated for the reduced bubble:water contact time in the Speece Cone;

31.   SOTE responded negatively to increasing oxygen flow, suggesting that oxygen flow rates > 1 l min^{-1} were not being fully dissolved inside the Speece Cone;

32.   A precipitous decline in SOTE at low oxygen flow rates and discharge velocities > 50 cm sec^{-1} was due to a destabilisation of the bubble swarm in the Speece Cone;

33.   The results of an air test were lower than any recorded on PSA oxygen for K_La_{20}, SOTR, SAE and SOTE; however, even at the 1/3 the air flow rate being delivered to the full lift aerator, the Speece Cone delivered superior performance for K_La_{20}, SOTR, and particularly SOTE;

34.   The SAE performance was very low due to the energy cost of PSA oxygen and pumping water, and an incorrectly designed Speece Cone, preventing an efficient counter-current bubble swarm from developing in the cone;

35.   Direct comparisons between the performance of the Full Lift and Speece Cone systems are not possible as they were not operated at comparable gas flow rates or oxygen partial pressures;

36.   Relative comparisons, qualitative in nature, indicate the Speece Cone, at oxygen flow rates between 1 and 3 l min^{-1}, delivered K_La_{20} and SOTR performance comparable to the Full Lift system at 10 l min^{-1} on oxygen, and superior performance to the Full Lift system on air;

37.   Even with the unit tested, the Speece Cone delivered outstanding SOTE performance, as values > 60% are unattainable with the full lift design on air or oxygen;

38. The DBCA counter-current flow principle of the Speece Cone provides a superior gas transfer environment to the full lift design by enhancing the fundamental aspects of gas transfer (i.e., a, K_L and C_i-C_L);

39. The Speece Cone SAE performance, on oxygen, is comparable to the SAE of the Full Lift system on oxygen;

40. The Speece Cone SAE performance, on air, is considerably less than the Full lift design on air;

41. The relatively low SAE performance of the Speece Cone was due to three factors: (1) the inlet water velocities were considerably less than the design requirement of ~305 cm sec^{-1}, (2) the additional energy cost to generate PSA oxygen, and (3) the energy cost of pumping water;

6.3   Comparison with Civil Engineering Studies

42. The $K_L a_{20}$ and SOTE values obtained from the full lift experiments were quite similar to literature values, indicating the performance of the current system is comparable to other designs;

43. The SAE performance obtained from the full lift design was considerably lower than reported literature values, likely due to the higher compression ratio in the adiabatic compression formula used to calculate the energy requirements of the system;

6.4   Linkage to Hypolimnetic Aeration Studies

44. The data available from the literature show a wide range in AE and TE, and relative comparisons between different studies are of limited value due to the wide range in environmental and engineering variables capable of influencing oxygen transfer;

45. The majority of oxygen transfer occurred in the lower portion of the inlet tubes in the full lift designs, and same effect was noted in this study;

46. Declining hydrostatic pressure, decreasing oxygen content of the rising oxygen bubbles and the additive effect of bubble and water velocity in a co-current upflow limit the efficiency of full lift designs;

6.5   PSA Engineering Design Factors Influencing SAE

47. The efficiency of the PSA units increases with unit capacity, as smaller PSA units are not designed solely for optimum oxygen recovery efficiency;

48. Significant improvements (i.e., 46%) in SAE can be expected when using larger capacity PSA systems;

49. The pressure requirements of the PSA generator significantly influences the SAE of a hypolimnetic aeration system as a result of the energy required for feed air compression;

50. Major improvements in SAE could be achieved by using lower pressure PSA generators;

6.6 Comments on Full Scale Application of Full Lift and Speece Cone Systems

51. The relative magnitude of the effects from this study should be transferable to full-scale application, within reasonable limits;

52. In each hypolimnetic aerator installation, one unit of measure will likely be de-emphasized in order to achieve specified performance targets in another unit of measure;

53. There are many factors unrelated to gas transfer that play a critical role in system selection;

54. Lab testing, comparative field studies, development of predictive models, reporting in engineering journals and case study reviews of specific installations will assist in resolving the engineering aspects of system selection;

6.7 Future Research Requirements

55. Laboratory research should focus on examining partial lift systems, and various designs of Speece Cones;

56. Varying the height to width ratio of the Speece Cone and optimizing diffuser design may improve the oxygen transfer within the Speece Cone;

57. Comparative full-scale testing of the oxygenation performance of full lift, partial lift and Speece Cones in the same body of water under similar conditions (e.g., diffuser depth, gas flow rates, diffuser orifice diameter) would be very informative;

58. Speece Cone oxygenation performance may be improved by using extremely efficient low head pumps, using fine pore diffusers in the inlet pipe, and investigating different aspect ratios to determine if an optimal hydraulic design exists which would enhance oxygen transfer inside the Speece Cone;

59. Once sufficient laboratory and comparative field data becomes available, it would be useful to develop mathematical models to predict oxygen transfer rates and aerator performance. This process is already underway; however, it has been hampered by a lack of published experimental data.

6.8   Conclusions

In the 21st century, hypolimnetic aeration will become more accepted within the engineering community as a technique for improving raw water quality in eutrophic lakes and reservoirs that receive significant amounts of nutrients from internal loading and uncontrollable external sources. The most widely used designs will likely be (1) Downflow Bubble Contact Aeration using the Speece Cone design and (2) full lift hypolimnetic aerators equipped with high efficiency diffusers using compressed air or oxygen. The Speece Cone, with its relatively compact size, exceptional oxygenation performance, and shallow water capability, represents one of the most significant advances in the design of hypolimnetic aeration since their inception over half a century ago. Equally important is the recent development of on-site PSA oxygen generating systems, which eliminates concerns surrounding the use/storage of pure oxygen and allows for the development of smaller and more efficient designs of hypolimnetic aeration systems. Civil engineers should consider hypolimnetic aeration as a proven technique, which can significantly improve raw water quality, and serve as an integral component of an overall watershed management program.

BIBLIOGRAPHY

[1] Andeen, G.B. 1974. Bubble pumps. Compressed Air Magazine 79:16-19.

[2] American Public Health Association, American Water Works Association and Water Pollution Control Federation. 1980. Standard methods for the examination of water and wastewater, 15th edition. American Public Health Association, Washington, D.C.

[3] ASCE. 1992. Measurement of oxygen transfer in clean water. ANSI/SSCE 2-91, 2nd edition, June, 1992. American Society of Civil Engineers, New York, New York, USA.

[4] Ashley, K.I. 1983. Hypolimnetic aeration of a naturally eutrophic lake: physical and chemical effects. Can. J. Fish. Aquat. Sci. 40(9):1343-1359.

[5] Ashley, K.I. 1985. Hypolimnetic aeration: practical design and application. Water Research 19(6):735-740.

[6] Ashley, K.I., S. Hay and G.H. Scholten. 1987. Hypolimnetic aeration: field test of the empirical sizing method. Water Research 21(2):223-227.

[7] Ashley, K.I. 1988. Hypolimnetic aeration research in British Columbia. Verh. Internat. Verein. Limnol. 23:215-219.

[8] Ashley, K.I. 1989. Factors influencing oxygen transfer in diffused aeration systems and their application to hypolimnetic aeration. M.A.Sc. thesis, Dept. of Civil Engineering, University of British Columbia.

[9] Ashley, K.I. and K.J. Hall. 1990. Factors influencing oxygen transfer in hypolimnetic aeration systems. Verh. Internat. Verein. Limnol. 24:179-183.

[10] Ashley, K.I., D.S. Mavinic and K.J. Hall. 1990. Oxygen transfer in full lift hypolimnetic aeration systems. pp. 648-659 in Air-Water Mass Transfer: Selected Papers from the Second International Symposium on Gas Transfer at Water Surfaces. S.C. Wilhelms and J.S. Gulliver (Eds.). American Society of Civil Engineers, New York, USA.

[11] Ashley, K.I., K.J. Hall and D.S. Mavinic. 1991. Factors influencing oxygen transfer in fine pore diffuser aeration. Water Research 25(12):1479-1486.

[12] Ashley, K.I., T. Tsumura and B.M. Chan. 1992. Fisheries management of winterkill lakes in Southern Interior British Columbia. pp. 287-297 in Aquatic Ecosystems in Semi-Arid Regions: Implications for Resource Management. R.D. Robarts and M.L. Bothwell (Eds.). N.H.R.I. Symposium Series 7, Environment Canada, Saskatoon, Canada.

[13] Ashley, K.I. and R. Nordin. 1999. Lake aeration in British Columbia: Applications and experiences. pp. 87-108 in Aquatic Restoration in Canada. T. Murphy and M. Munawar (Eds.). Ecovisoon World Monogrpah Series. Backhuys Publishers, Leiden, The Netherlands.

[14] Barnhardt, E.L. 1969. Transfer of oxygen in aqueous solutions. J. Sanit. Eng. Div.Proc. ASCE 95 No. SA3:645-661.

[15] Beak Consultants Ltd. 1977. CPAR Project Report 542-1. State of the art review: Aeration. Beak Consultants Ltd., Montreal, Quebec. July, 1977.

[16] Bernhardt, H. 1967. Aeration of Wahnbach Reservoir without changing the temperature profile. J. American Water Works Assoc. 59:943-964.

[17] Bernhardt, H. 1974: Tens years experience of reservoir aeration. Prog. Water Technol. 7:483-495.

[18] Bewtra, J.K. and W.R. Nicholas. 1964. Oxygenation from diffused air in aeration tanks. J. Water. Poll. Control Fed. 36(10):1195-1224.

[19] Bewtra, J.K., R.W. Nicholas and L.B. Polkowski. 1970. Effect of temperature on oxygen transfer in water. Water Research 4(1):115-122.

[20] Bewtra, J.K. and D.S. Mavinic. 1978. Diffused aeration systems from theory to design. Can. J. Civil Eng. 5(1):32-41.

[21] Bowers, R.H. 1955. The mechanics of bubble formation. J. Applied Chemistry 5:542-548.

[22] Boyd, C.E. 1986. A method for testing aerators for fish tanks. Prog. Fish Cult. 48:68-70.

[23] Boyd, C.E. and B.J. Watten. 1989. Aeration systems in Aquaculture. Reviews in Aquatic Sciences 1(3):425-472.

[24] Colt, J. 1984. Computation of dissolved gas concentrations in water as functions of temperature, salinity and pressure. American Fisheries Society Special Publication No. 14. Bethesda, Maryland, USA.

[25] Danckwerts, P.V. 1951. Significance of liquid film coefficient in gas absorption. Industrial and Engineering Chemistry 43(6):1460.

[26] Dinsmore, W.P. and E.E. Prepas. 1994a. Impact of hypolimnetic oxygenation on profundal macroinvertebrates in a eutrophic lake in central Alberta. I. Changes in macroinvertebarte abundance and diversity. Can. J. Fish. Aquat. Sci. 54:2157-2169.

[27] Dinsmore, W.P. and E.E. Prepas. 1994b. Impact of hypolimnetic oxygenation on profundal macroinvertebrates in a eutrophic lake in central Alberta. II. Changes in Chironomus spp. abundance and biomass. Can. J. Fish. Aquat. Sci. 54:2170-2181.

[28] Dobbins, W.E. 1964. Mechanisms of gas absorption by turbulent liquids. Advances in Water Research Proc. 1st International Conf. Water Pollution Research. Pergamon Press Ltd., London, England. Vol. 2, p. 61.

[29] Doke, J.L., W.H. Funk, S.T.J. Jull, and B.C. Moore. 1995. Habitat availability and benthic invertebrate population changes following alum treatment and hypolimnetic oxygenation in Newman Lake, Washington. J. Freshwater Biol. 10:87-102.

[30] Downing, A. L. and G. A. Truesdale. 1955. Some factors affecting the rate of solution of oxygen in water. J. Applied Chemistry 5:570-581.

[31] Dunst, R.C., S.M. Born, S.A. Smith, S.A. Nichols, J.0. Peterson, D.R. Knauer, S.L. Serns, D.R. Winter and T.L. Wirth. 1974. Survey of lake rehabilitation techniques and experiences. Tech. Bull. No. 75. Wisconsin Dept. Natural Resources, Madison, Wisconsin. 179 pp.

[32] Eckenfelder, W.W. 1959. Absorption of oxygen from air bubbles in water. J. Sanit. Eng. Div. Proc. ASCE 85 No. SA4:89-99.

[33] Eckenfelder, W.W. and D.L. Ford. 1968. New concepts in oxygen transfer and aeration. In Advances in Water Quality Improvement. E.F. Gloyna and W.W. Eckenfelder (Eds.). Water Resource Symposium No.1.

[34] Eckenfelder, W.W. (Ed.) 1969. Oxygen transfer and aeration. In Manual of Treatment Processes, Vol. 1. Environmental Sciences Services Corp., USA.

[35] Ellis, S.E. and R. Stanbury. 1980. The scale-up of aerators. Paper No.3 Symposium on The Profitable Aeration of Waste Water, (London, April, 1980). BHRA Fluid Engineering, Cranfield, Bedford. U .K.

[36] Fast, A.W. 1971. The effects of artificial aeration on lake ecology. EPA Water Pollution Control Research Series 16010 EXE 12/71.

[37] Fast, A.W. 1973. Effects of artificial hypolimnion aeration on rainbow trout (*Salmo gairdneri* Richardson) depth distribution. Trans. Am. Fish. Soc. 73(4):715-722.

[38] Fast, A.W., B. Moss and R.G. Wetzel. 1973. Effects of artifical aeration on the chemistry and algae of two Michigan lakes. Water Resources Research 9:624-647.

[39] Fast, A.W. 1975. Artificial aeration and oxygenation of lakes as a restoration technique. pp. 135-165 in Recovery and Restoration of Damaged Ecosystems. Cairnes et al. (Eds.). The University Press of Virginia, Charlottesville, USA.

[40] Fast, A.W., W.J. Overholtz and R.A. Tubb. 1975. Hypolimnetic oxygenation using liquid oxygen. Water Resources Research 11:294-299.

[41] Fast, A.W. and M.W. Lorenzen. 1976. Synoptic survey of hypolimnetic aeration. J. Environ. Eng. Div., Proc. Amer. Soc. Civil Eng. 106 (EE6):1161-1173.

[42] Fast, A.W., M.W. Lorenzen and J.H. Glenn. 1976. Comparative study with costs of hypolimnetic aeration. J. Environ. Eng. Div., Proc. Amer. Soc. Civil Eng. 106 (EE6):1175-1187.

[43] Fast, A.W., Overholtz, W.J. and R.A. Tubb. 1977: Hyperoxygen concentrations in the hypolimnion produced by injection of liquid oxygen. Water Resources Res. 13:474-476.

[44] Fast, A.W. 1981. Some applications of lake aeration technology and artificial thermal upwelling on fish culture. pp 574-606 in Destratification of Lakes and Reservoirs to Improve Water Quality. Proceedings of a joint United States/Australia Seminar and Workshop, Melbourne, Australia, Feb 19-24, 1979. A.J. Burns and I.J. Powling (Eds.). Australian Government Publishing Service, Canberra, Australia.

[45] Field, K.M. and E.E. Prepas. 1997. Increased abundance and depth distribution of pelagic crustacean zooplankton during hypolimnetic oxygenation in a deep, eutrophic Alberta lake. Can. J. Fish. Aquat. Sci. 54: 2146-2156.

[46] Garrell, M.H., J.C. Confer and D. Kirschner. 1977. Effects of hypolimnetic aeration on nitrogen and phosphorus in a eutrophic lake. Water Resources Res. 13:343-347.

[47] Gemza, A.F. 1997. Water quality improvements during hypolimnetic oxygenation in two Ontario lakes. Water Qual. Res. J. Canada 32:365-390.

[48] Haberman, W.L. and R.K. Morton. 1954. An experimental study of bubbles moving in liquids. Proc. Amer. Soc. Civil. Eng. 80:379-429.

[49] Halsey, T.G. 1968. Autumnal and overwinter limnology of three small eutrophic lakes with particular reference to experimental circulation and trout mortality. J. Fish. Res. Bd. Can. 25:81-89.

[50] Haney, P.D. 1954. Theoretical principles of aeration. J. American Water Works Assoc. 46(4):353-376.

[51] Higbie, R. 1935. The rate of absorption of a pure gas into a still liquid during periods of short exposure. Amer. I. Chem. Eng. Trans. 31:365-390.

[52] Hess, L. 1975. The effect of the first year of artificial hypolimnetic aeration on oxygen, temperature and depth distribution of rainbow trout (*Salmo gairdneri*) in Spruce Knob Lake. West Virginia Dept. of Natural Resources Report F-19-R-3.

[53] Ippen, A.T. and C.E. Carver. 1954. Basic factors of oxygen transfer in aeration systems. Sewage and Industrial Wastes 26(7):813-829.

[54] Jaeger, D. 1990. TIBEAN - a new hypolimnetic water aeration plant. Verh. Internat. Verein. Limnol. 24:184-187.

[55] King, D.L. 1970. Reaeration of Streams and Reservoirs; Analysis and Bibliography. Engineering and Research Center, U. S. Bureau of Reclamation REC-OCE- 70-55. 131 pp.

[56] Krenkel, P.A. and G.T. Orlob. 1962. Turbulent diffusion and the reaeration coefficient. J. Sanit. Eng. Div., Proc. Amer. Soc. Civril Eng. 88 (SA2):53-83.

[57] LaBaugh, J.W. 1980. Water chemistry changes during artificial aeration of Spruce Knob Lake, West Virginia. Hydrobiologia 70: 201-216.

[58] Lappalainen, K.M. 1994. Positive changes in oxygen and nutrient contents in two Finnish lakes induced by Mirox hypolimnetic oxygenation method. Verh. Internat. Verein. Limnol. 25:2510-2513.

[59] Larkin, P.A. 1975. Biometrics. Biology 300 Course Book. Fall Term, 1975. University of British Columbia, 206 p.

[60] Lawrence, G.A., J.M Burke, T.P. Murphy and E.E. Prepas. Exchange of water and oxygen between the two basins of Amisk lake. Can. J. Fish. Aquat. Sci. 54:2121-2132.

[61] Little, J.C., 1995. Hypolimnetic aerators: predicting oxygen transfer and hydrodynamics. Water Research 29:2475-248.

[62] Lee, G.F. 1970. Eutrophication. University of Wisconsin Water Resources Center, Eutrophication Information Program. Occasional paper No. 2, Madison, Wisconsin, USA.

[63] Lewis, W.K. and W.G. Whitman. 1924. Principles of gas absorption. Ind. Eng. Chem.16:1215-1220.

[64] Lind, 0.T. 1979. Handbook of Common Methods in Limnology. Second Ed. C.V. Mosby. St. Louis, 199 p.

[65] Lorenzen, M. and A.W. Fast. 1977. A guide to Aeration/Circulation techniques for lake management. U. S. Environmental Protection Agency 600/3-77-004.

[66] Mancy, K.H. and D.A. Okun. 1960. Effects of surface active agents on bubble aeration. J. Water Poll. Control Fed. 32(4):351-364.

[67] Markofsky, M. 1979. On the reoxygenation efficiency of diffused air aeration. Water Research 13:1339-1346.

[68] Mavinic, D.S. 1973. Optimization of oxygen transfer into water in a coarse-bubble, diffused aeration system. Ph.D. thesis, University of Windsor, Windsor, Ontario, Canada.

[69] Mavinic, D.S. and J.K. Bewtra. 1974. Mass transfer of oxygen in diffused aeration systems. Can. J. Civil. Eng. 1:71-84.

[70] Mavinic, D.S. and J.K. Bewtra. 1976. Efficiency of diffused aeration systems in waste-water treatment. J. Water Poll. Control Fed. 48(10):2273-2283.

[71] McGinnis, D.F. and J.C. Little. 1998. Bubble dynamics and oxygen transfer in a Speece Cone. Water Sci. Tech. 37(2):285-292.

[72] McQueen, D.J. and D.R.S. Lean. 1983. Hypolimnetic aeration and dissolved gas concentrations: Enclosure experiments. Water Research 17:1781-1790.

[73] McQueen, D.J., S.S. Rao and D.R.S. Lean. 1984. Hypolimnetic aeration:changes in bacterial populations and oxygen demand. Arch. Hydrobiol. 99(4):498-514.

[74] McQueen, D.J. and D.R.S. Lean. 1986. Hypolimnetic aeration: An overview. Water Poll. Res. J. Canada 21(2):205-217.

[75] Mercier, P. and J. Perret. 1949: Aeration station of Lake Bret, Monastbull, Schweiz. Ver Gas. Wasser-Fachm 29:25.

[76] Metcalf and Eddy Ltd. 1991. Waterwater Engineering: Treatment, Disposal and Reuse, Third Edition. Revised by G. Tchobanoglous and F.L. Burton. McGraw-Hill, Inc., New York, New York, USA.

[77] Morgan, P.F. and J.K. Bewtra. 1960. Air diffuser efficiencies. J. Water Poll. Control Fed. 32(10):1047-1059.

[78] Neilson, B.J. 1974. Reaeration dynamics of reservoir destratification. J. Amer. Water Works Assoc. 66:617-620.

[79] New York Department of Environmental Protection. 2000. Hypolimnetic Aeration Pilot Project: Final Report. New York City Department of Environmental Protection. Prepared by the Division of Drinking Water Quality Control, Valhalla, New York.

[80] Nienow, A.W. 1980. The aeration of waste water: Basic physical factors. Paper No. 1. Symp. on the Profitable Aeration of Waste Water, (London, April, 1980). BHRA Fluid Engineering, Cranfield, Bedford, U .K.

[81] O'Connor, D.J. 1982. Wind effects on gas-liquid transfer coefficients. J. Environ. Eng., Proc. ASCE 109(3):731-753.

[82] Pasveer, A. 1955. Research on activated sludge VI. Oxygenation of water with air bubbles. Sewage and Industrial Wastes 27(10):1130-1146.

[83] Perrin, C.J., K.I. Ashley and G.A. Larkin. 2000. Effect of drawdown on ammonium and iron concentrations in a coastal mountain reservoir. Water Qual. Res. J. Canada 35(2):231-244.

[84] Point Four Systems, 1997. PT4 Users Manual UBC Civil Engineering Dept. Point Four Systems, Inc., Richmond, B.C. Canada.

[85] Prepas, E.E., D.J. Webb, C.L.K. Robinson and T.P. Murphy. 1990. Impact of liquid oxygen injection on a deep, naturally eutrophic lake: Amisk Lake, Alberta, year one. Verh. Internat. Verein. Limnol. 24:320.

[86] Prepas, E.E. and J.M. Burke. 1997. Effects of hypolimnetic oxygenation on water quality in Amisk Lake, Alberta, a deep eutrophic lake with high internal phosphorus loading rates. Can. J. Fish. Aquat. Sci. 54:2111-2120.

[87] Prepas, E.E., K.M. Field, T.P. Murphy., W.L. Johnson., J.M. Burke and W.M. Tonn. 1977: Introduction to the Amisk Lake Project: oxygenation of a deep, eutrophic lake. Can. J. Fish. Aquat. Sci. 54:2105-2110.

[88] Rohlf, F.J. and R.R. Sokal. 1969. Statistical Tables. W.H. Freeman and Co. San Francisco, Ca. 253 p.

[89] Rucker, R. 1972. Gas bubble disease of salmonids: a critical review. U.S. Fish and Wildlife Service. Tech. Paper 58.

[90] Schmit, F.L., J.D. Wren and D.T. Redmon. 1978. The effect of tank dimensions and diffuser placement on oxygen transfer. J. Water Poll. Control Fed. 50(7):1750-1767.

[91] Smith, S.A., D.R. Knauer and T.Wirth. 1975. Aeration as a lake management technique. Wisconsin Dept. Natural Res., Tech. Bull. No.87.

[92] Soltero, R.A., L.M. Sexton, K.I. Ashley and K.O. McKee. 1994. Partial and full lift hypolimnetic aeration of Medical Lake, Wa to improve water quality. Water Research 28:2297-2308.

[93] Speece, R.E. 1971. Hypolimnion Aeration. J. Amer. Water Works Assoc. 64(1):6-9.

[94] Speece, R.E. 1975. Ten Year's experience of reservoir aeration. Reply to H. Bernhardt. Prog. Water Technol. 7:489-494.

[95] Speece, R.E., N. Nirmalakhandan and G. Tchobanoglous. 1990. Commercial oxygen use in water-quality management. Water Environment and Technology 2(7):54-61.

[96] Speece, R.E. 1992. Pilot Scale demonstration of Speece Cone for oxygenation of Camanche Reservoir. Internal Report (Revised), Vanderbuilt University. 11 pp.

[97] Steinberg, C. and K. Arzet. 1984. Impact of hypolimnetic aeration on abiotic and biotic conditions in a small kettle lake. Environ. Technol. Letters. 5: 151-162.

[98] Stenstrom, M.K. and R.G. Gilbert. 1981. Effects of alpha, beta and theta factor upon the design, specification and operation of aeration systems. Water Research 15:643-654.

[99] Taggart, C.T. and D.J. McQueen. 1981. Hypolimnetic aeration of a small eutrophic kettle lake: physical and chemical changes. Arch. Hydrobiol. 91(2) 150-180.

[100] Taggart, C.T. and D.J. McQueen. 1982. A model for the design of hypolimnetic aerators. Water Research 16:643-654.

[101] Taggart, C.T. 1984. Hypolimnetic aeration and zooplankton distribution: a possible limitation to the restoration of cold water fish production. Can. J. Fish. Aquat. Sci. 41:191-198.

[102] Thomas, J.A., W.H. Funk, B.C. Moore and W.W. Budd. 1994: Short term changes in Newman Lake following hypolimnetic aeration with the Speece Cone. Lake and Res. Manage. 9:111-113.

[103] Verner, B. 1974. Long term effect of hypolimnetic aeration of lakes and reservoirs, with special considerations of drinking water quality and preparation costs. In J. Taggart and L. Moore (Eds.) Lake and Reservoir Management:134-138. Proc. 3rd Annual Conf. North Amer. Lake Management Soc., October 18-20, 1983, Knoxville, Tenn., USA. U. S. EPA 440/5- 84-001. 604 p.

[104] Webb, D.J., R.D. Robarts and E.E. Prepas. 1997. Influence of extended water column mixing during the first 2 years of hypolimnetic oxygenation on the phytoplankton community of Amisk lake, Alberta. Can. J. Fish. Aquat. Sci. 54:2133-2145.

[105] Weisberg, S. 1980. Applied Linear Regression. John Wiley and Sons, New York, New York, USA.

[106] Wetzel, R.G. 1975. Limnology. W. B. Saunders Co., Philadelphia, Pa. 743 p.

[107] Wilkinson, L. and M. Coward. 2000. Linear Models II: Analysis of Variance. Chapter 15 in SYSTAT 10, Statistics 1. SPSS Inc., Chicago, USA.

[108] Wirth, T.L., D.R. Knauer and S.A. Smith. 1975. Total and hypolimnetic aeration of lakes in Wisconsin. Verh. Internat. Verien. Limnol. 19:1960-1970.

LIST OF APPENDICES

APPENDIX 1:

RE-AERATION TEST PROCEDURE – FULL LIFT HYPOLIMNETIC AERATOR

1. Turn on main power bar (on control panel);

2. Fill tank with water (~ 1200 L);

3. Turn on secondary power bar (at top of stairs and activate pump mixers when tank is full);

4. Turn on PT4 data logger/oxygen-temperature probes;

5. Insert YSI probe into tank and turn meter on (zero meter initially);

6. Insert current meter probe into outlet tube and turn meter on;

7. Turn on electronic balance;

8. Let system mix for 5 minutes;

9. Take water sample in 2 x 300 ml BOD bottles and measure temperature of tank water;

10. Do Winkler titration in Civil Lab within 5 minutes;

11. Calculate % saturation from Winkler, tank water temperature and barometric pressure;

12. Calibrate data logger using single point manual calibration to % saturation value for Chs. 1-6;

13. Check Ch. 7 temperature against YSI temp and thermometer;

14. Calibrate YSI in mg/L from Winkler test;

15. Put on safety glasses and gloves;

16. Calibrate Ch. 7 to 100% for certified oxygen from compressed oxygen cylinder;

17. Attach compressed air line and pressurize manifold;

18. Cycle AirSep unit to full pressure;

19. Calculate amount of cobalt chloride required, and add only once per 5-6 tests dissolved in test water;

20. Calculate amount of sodium sulfite required (+10%), dissolved in flask and add to test water;

21.   Mix for 6 minutes, confirm all probes are below 0.5% saturation;

22.   Review data logger setting for calibration settings, time stamp and data capture frequency;

23.   Set up Laptop with data link, power cord and mouse, open Hyperterminal;

24.   Record experimental parameters, setting and conditions on record sheet;

25.   Confirm YSI is < 0.5 mg/L;

26.   Configure data logger to start data collection;

27.   Configure manifold to deliver desired (1) gas mixture and (2) gas flow rate and (3) pressure from random number generated treatment schedule;

28.   Start data logger after 6 minutes of mixing;

29.   Turn mixers off at start of test run;

30.   Start air or oxygen flow (If oxygen > 10 SLPM then AirSep on Auto, if > 10 SLPM then AirSep on manual);

31.   Adjust regulators to 45 psig;

32.   Monitor data logger;

33.   Monitor current velocity and record;

34.   Terminate test at _% sat;

35.   Stop data logger;

36.   Prepare computer for data capture;

37.   Transfer data to Lap Top;

38.   Find file in Excel as .csv file;

39.   Save data as unique Excel file;

40.   Repeat procedure from Step 20 according to treatment table (Note : max 6 tests per batch of water);

41.   Drain tank after 5-6 tests and refill as soon as possible to avoid stressing tank joints at start on new set of 5-6 experiments.

APPENDIX 2:

RE-AERATION TEST PROCEDURE – SPEECE HYPOLIMNETIC AERATOR

1.   Turn on main power bar (on control panel);

2.   Fill tank with water (~ 1200 L);

3.   Turn on secondary power bar (at top of stairs and activate pump mixers only when tank is full);

4.   Turn on PT4 data logger/oxygen-temperature probes;

5.   Insert YSI probe into tank and turn meter on (zero meter initially);

6.   Check current meter probe on discharge tube and turn meter on;

7.   Turn on electronic balance;

8.   Let system mix for 5 minutes;

9.   Take water sample in 2 x 300 ml BOD bottles and measure temperature of tank water;

10.   Do Winkler titration in Civil Lab within 5 minutes;

11.   Calculate % saturation from Winkler, tank water temperature and barometric pressure;

12.   Calibrate data logger using single point manual calibration to % saturation value for Chs. 1-6;

13.   Check Ch. 7 temperature against YSI temp and thermometer;

14.   Calibrate YSI in mg/L from Winkler test;

15.   Put on safety glasses and gloves;

16.   Calibrate Ch. 7 to 100% for certified oxygen from compressed oxygen cylinder;

17.   Attach compressed air line and pressurize manifold;

18.   Cycle AirSep unit to full pressure;

19.   Calculate amount of cobalt chloride required, and add only once per 5-6 tests dissolved in test water;

20.   Calculate amount of sodium sulfite required (+10%), dissolved in flask and add to test water;

21. Mix for 8 minutes, confirm all probes are below 0.5% saturation;

22. Review data logger setting for calibration settings, time stamp and data capture frequency;

23. Set up Laptop with data link, power cord and mouse, open Hyperterminal;

24. Record experimental parameters, setting and conditions on record sheet;

25. Confirm YSI is < 0.5 mg/L;

26. Configure data logger to start data collection;

27. Configure manifold to deliver desired (1) gas mixture and (2) gas flow rate and (3) pressure from random number generated treatment schedule;

28. Leave mixers on throughout test run;

29. Select current velocity, and adjust rheostat to desired current velocity;

30. Start data logger after 8 minutes of mixing;

31. Start air or oxygen flow (If oxygen > 10 SLPM then AirSep on Auto, if > 10 SLPM then AirSep on manual);

32. Adjust regulators to 45 psig;

33. Monitor data logger;

34. Monitor current velocity and record;

35. Terminate test at _% sat;

36. Turn off gas flow and turn off main pump to allow system to degas for 5 seconds through vent tube;

37. Turn main mixer back on and let mix for 2 minutes without any gas flow to obtain complete mixing in tank;

38. Stop data logger;

39. Prepare computer for data capture;

40. Transfer data to Lap Top;

41. Find file in Excel as .csv file;

42. Save data as unique Excel file;

43.   Repeat procedure from Step 20 according to treatment table (Note : max 6 tests per batch of water);

44.   Drain tank after 5-6 tests and refill as soon as possible to avoid stressing tank joints at start on new set of 5-6 experiments.